DISSERTATION / DOCTORAL THESIS

Titel der Dissertation /Title of the Doctoral Thesis

Novel Shoe Inserts for Adult-acquired Flatfoot Deformity—Design, Fabrication, and Biomechanical Assessment

verfasst von / submitted by

Che-Wei Hu, MSc

angestrebter akademischer Grad / in partial fulfilment of the requirements for the degree of

Doctor of Philosophy (PhD)

Wien, 2022 / Vienna 2022

Studienkennzahl lt. Studienblatt / degree programme code as it appears on the student record sheet:	UA 794 680 481
Dissertationsgebiet lt. Studienblatt / field of study as it appears on the student record sheet:	Sportwissenschaft
Betreut von / Supervisor:	Univ.-Prof. Dipl.-Ing. Dr. Arnold Baca
Betreut von / Supervisor:	Prof. Dr. Peter Dabnichki

Acknowledgement

Throughout the PhD program, I have received the great deal of support and assistance. I don't think I can get my PhD degree without them.

Firstly, I would like to thank my senior supervisor, Professor Peter Dabnichki, who spends a great amount of time and effort to help me to bring my work to the higher level. He is also a caring supervisor who sometimes gives me suggestion on my life and work. I would also like to acknowledge the other supervisors, Professor Arnold Baca and Dr. Toh Yen Pang, for their patient support and their feedback to sharpen my thinking on my thesis. I would also like to thank my colleagues, Dominik Hoelbling, Rance Brennan Tino, Soh Kam Huah, and Canh Toan Nguyen, for their collaboration and their help in my research.

In addition, I would like to thank my parents, my wife, my pastor and my brothers and sisters from Melbourne Glory City Church. They are always there to encourage and empower me during the last few years. I also want to give thanks to God who always gives me love and strength in my life.

Table of Contents

Chapter 1. Introduction

Human foot arch is a curved skeletal structure supported passively by the bone-ligament juncture and actively by the respective muscle and tendon groups. Flatfoot (i.e. flatfoot) is a term used for a foot deformity with little or no space between the plantar surface and the ground. Flatfoot compromises foot's normal mechanism in weightbearing conditions including deteriorating postural stability (Puszczalowska-Lizis et al., 2017), limiting the joint's motion of foot and changing the muscle activation level (Buldt et al., 2015). Most importantly, it compromises the compression and recoil of foot arch in locomotion and reduces the movement efficiency (Stearne et al., 2016). People with flatfoot are considered at a higher risk of foot and/or knee injury and musculoskeletal problems especially for children, the elderly, and athletes (Puszczalowska-Lizis et al., 2017; Michelson et al., 2002; Kothari et al., 2016). Shoe insert, a common intervention for low arch and flatfoot (Chen et al., 2010; Murley et al., 2010), is designed to support the fallen medial longitudinal arch by the solid filling underneath the foot arch. It has been proved that current shoe insert can reduce the excessive foot pronation in walking and standing (Leung et al., 1998; Genova and Gross, 2000), increase the static and dynamic stability (Aboutorabi et al., 2015), bring towards the muscle activation pattern observed from normal-arched people (Murley et al. 2010). However, Stearne et al. (2016) found the solid filling of current shoe insert restricts the motion of midfoot and compromises the compression and recoil of foot arch and decrease the movement efficiency in gait. As the motion of human body is a chain reaction, midfoot restriction can affect the motion in knee, hip and spine in gait.

Our study has successfully developed the novel inserts to address such limitations. Three novel inserts—Honeycomb, Bubble and Gyroid, were developed and they were proved to support the fallen arch as well as facilitate the arch's compression and recoil through motion analysis. Through finite element analysis, novel inserts were proved to reduce the plantar pressure and internal joint's stress compared to current solid inserts. In addition, the integrated non-invasive diagnostics to production method for low arch identification and automated customized shoe insert design and manufacturing are developed in current study. The foot arch assessment through 3D subject-specific foot imaging set the thresholds for low arch identification established as a part of the database development for the current study reduced the type 1 and type 2 errors to below 10.7% in comparison to previously reported above 55% (Swedler et al, 2010). For shoe insert design, an automated algorithm is developed in current study to translating scanned foot data into insert geometry, which decreases the required time of insert computer-aided design from over 3 hours to less than 2 minutes.

Chapter 2. Literature review

Adult-acquired flatfoot deformity (i.e. flatfoot) is identified when there is little or no space between foot arch and ground while subject is standing. It is considered to increase an individual's risk of injury or the cause of musculoskeletal issues. Therefore, establishing a simple, repeatable and accurate protocols for early-stage assessment are necessary to obtain meaningful measurements that can provide insights into injury risk and prescribe the appropriate interventions (e.g. shoe inserts). From section 2.1 to 2.3, the anatomy and function of foot and most importantly the foot arch assessment are reviewed. Section 2.4 to 2.6 reviewed current traditional and additive manufacturing of shoe insert and the analysis specifically used in foot biomechanics. Finally, the knowledge gaps and the aims and research questions are elaborated in section 2.7 and 2.8.

2.1. Foot arch

2.1.1. Bones and joints

Human foot is a complex structure consisting of 26 bones, 33 joints and more than hundred muscles, tendons, and ligaments (Franco, 1987). As the segmented structure can best hold up weight and dynamic loads if it is built in the form of arches, human foot forms a curved structure of arches supported by the bone and ligament (i.e. passive structure), and muscles and tendons (i.e. active structure) serve as an adaptable and supportive base of the entire body. The human foot is normally divided into three regions: the forefoot, midfoot and rearfoot (Fig 2.1). These regions are clearly partitioned by the bones of the foot and function as a unit during gait. Forefoot is made up by cuneiforms, metatarsals, and phalanges. Midfoot is made up by navicular and cuboid that articulates to forefoot by Lisfranc's joint. Rearfoot is made up by talus and calcaneus that articulate to midfoot by midtarsal joint. The rearfoot includes the calcaneus and the talus, the midfoot includes the cuneiforms, cuboid, and the navicular while the forefoot is composed of all the metatarsals and the phalanges (Hamill and Knutzen, 2006). The foot arches are divided in two longitudinal arches, i.e. medial longitudinal arch (MLA), lateral longitudinal arch (LLA), and transverse arch (TA). The orientation and articulations of skeletal components provide mechanical support under load, attachment sites for connective tissue and rigid points for leverage. The cover area and the bones of the foot arches are shown in Table 2.1 (Hamill and Knutzen, 2006).

Table 2.1. The cover area of medial longitudinal arch, lateral longitudinal arch and transverse arch

	MLA	LLA	TA
Cover area	Medial two-third of foot arch from metatarsal head to calcaneus (blue area in Fig. 2.1)	Lateral one-third of foot arch from metatarsal head to calcaneus (green area in Fig. 2.1)	Middle-third of foot arch from metatarsal head to cuboid and cuneiform (red area in Fig. 2.1)
Bones	calcaneus, talus, navicular, cuneiforms, and 1st to 3rd metatarsal bone	calcaneus, cuboid, and 4th and 5th metatarsal bone	1st to 5th metatarsal bone, cuboid, and lateral, middle and medial cuneiform

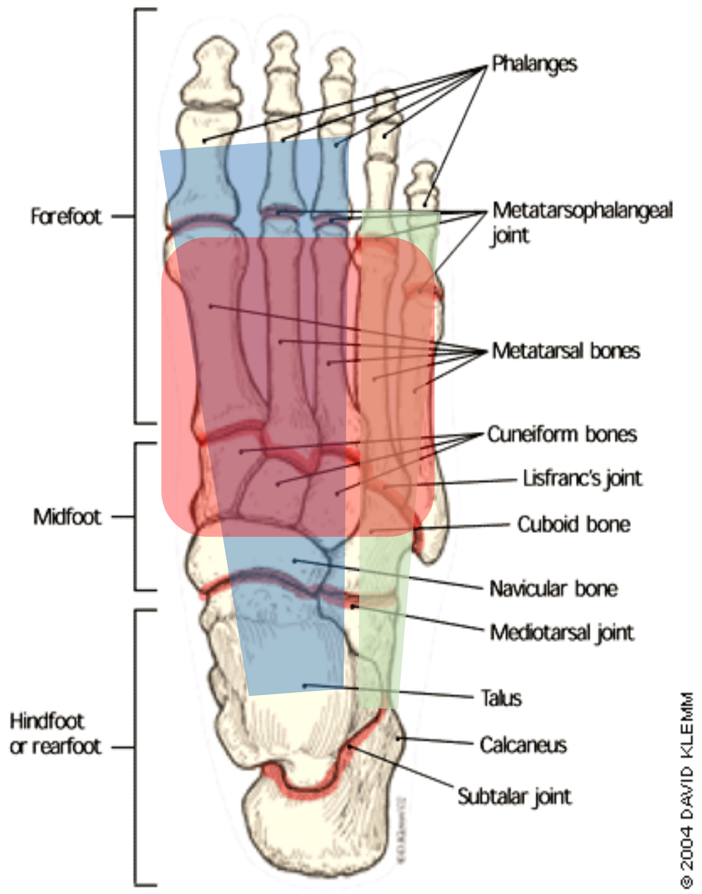

Figure 2.1. The bones of foot and the different regions of foot arch (David Klemm, 2004)

2.1.2. Connective tissue

Foot bones are supported by a connective tissue. The shapes of arches allow the foot the flexibly to counteract both expansion and contraction. And, bearing the external force from different directions in position or locomotion. The main connective tissue for supporting

MLA is posterior tibial tendon (PTT), the spring ligament complex (SLC), the plantar fascia and the plantar ligaments. The main connective tissue accounting for 37% of foot stiffness (Huang et al., 1993).

PTT is a major contributor to the foot arch support and originates from the posterior tibialis. PTT dysfunction is a common problem of the foot and ankle in adulthood. It occurs when the PTT becomes inflamed or torn that often results in adult-acquired flatfoot deformities.

The SLC consists of three ligaments— superomedial ligament, medioplantar oblique ligament and inferoplantar longitudinal ligament that connects the calcaneus and the navicular bone The SLC contributes as the primary stabilizer of MLA in static conditions, together with posterior tibialis tendon (Taniguchi et al., 2003). Failure of the SLC cannot be sufficiently compensated by other structures that can easily cause the instability of rearfoot (Jennings and Christensen, 2008). Orr and Nunley (2013) and Deland et al. (2005) also found that adult-acquired flatfoot deformities manifest in cases where there is an isolated failure of the SLC.

The plantar fascia is a fibrous aponeurosis originates from the calcaneus and inserts at the metatarsophalangeal articulations that plays a major role in MLA maintenance (Huang et al., 1993). Moreover, together with the plantar ligaments, the plantar fascia is identified by the finite element simulation as the primary ligament in arch maintenance (Tao et al., 2010).

Apart from major connective tissues mentioned above, the intrinsic and extrinsic foot muscles contribute 63% of foot stiffness to maintain the MLA (Huang et al., 1993). The extrinsic foot muscles originate from the lower leg and cross the ankle joint. The intrinsic foot muscles are those found within the foot (Hamill and Knutzen, 2006).

McKeon et al. (2014) has recently proposed ‘foot-core paradigm’ to explain the functional anatomy of the foot. This theory explained that muscles with larger cross-section areas can produce relatively large lever arms, which are used for gross global movements. For the relatively smaller muscles with the shorter intersegmental lever arms, they act primarily as local stabilizer. This theory elaborates that the extrinsic muscles of the foot for the gross global movement of the foot and the intrinsic foot muscles mainly act to stabilize the foot and maintain the form of MLA. According to McKeon et al. (2014), the foot form is mainly maintained by the intrinsic foot muscles. Flexor digitum brevis and the abductor hallucis are the primary intrinsic muscles to stiffen the form of MLA and shortens the foot arch to prevent collapse. (Wong, 2007; Kelikian and Sarrafian, 2011). The decrease in navicular height is found when the nerves pathway of intrinsic foot muscle is hindered (Fiolkowski et al. 2003), which shows the direct connection between the activation of intrinsic foot muscle and foot arch form.

The intrinsic foot muscles are oriented in four overlapping plantar layers and one layer on the dorsal aspect of the foot (Fig 2.2) (McKeon et al., 2014). Because of the complexity of the intrinsic foot muscle, it is difficult to quantify fatigue and activation of individual muscles through electromyography (EMG). Therefore, investigations into the relative contributions of each foot intrinsic muscle have not been conducted. The conditions and properties of connective tissues can affect the form of foot arch and consequently the function of foot. For instance, the injury of ligament would be directly reflected as a skeletal deformity, the fatigue of foot muscles may result in temporary changes in arch height or excessive external loads can result in temporary change the support of connective tissue that might affect the form of MLA (Cowley & Marsden, 2013; Headlee et al., 2008; Okamura et al., 2017).

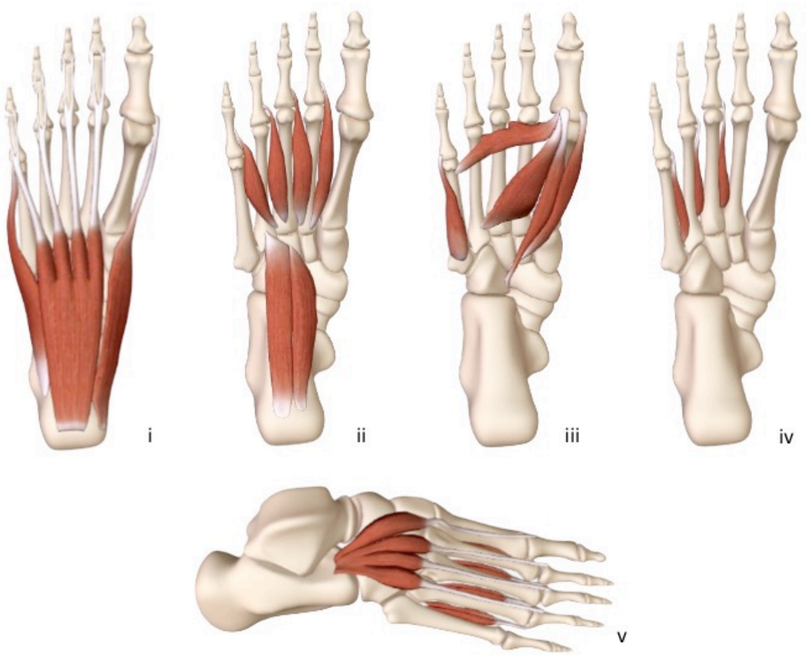

Figure 2.2: Foot core system paradigm: four layers of plantar intrinsic muscles are shown in (i) to (iv) from the most superficial layer to the deepest (McKeon et al., 2014).

Foot arch is maintained by bones and connective tissues according to the shape of bone, the strength of ligament like the staple, and the tension of muscle as the tie beam and suspension (Hansen, 2000). Some foot bones are wedge-shaped with the thin edge lying inferiorly like navicular and talus bone. They are like the keystone that is the central stone at the apex of an arc. The ligaments connect each bone and act like staples tie the inferior edges of bones together to form the foot arch. The intrinsic muscles and tendons resemble tie beam and suspension of the bridge or arch. The tie beam connects the two ends of the arch. For example, the flexor hallucis longus— its origin is from the distal two-thirds of the posterior surfaces of the fibula and inserts to the plantar aspect of the great toe after traveling between the first metatarsal head (Hansen, 2000). The action of flexor hallucis longus is the flexion of the great toe that pulls two ends of the arch together and supports the foot arch. The suspension is to lift the whole structure from above, which is also important for the foot arch support. For example, the peroneus longus— its origin is from the proximal two-thirds of the lateral surface of the fibula and inserts to the base of the first metatarsal bone. It works as the suspending bridge to supports the arches of the foot (Hansen, 2000).

Table 2.2. The mechanisms that the muscles, tendons, and ligaments support foot arch (Hansen, 2000).

		MLA	LLA	TA
Main muscles and ligaments	Staple	plantar calcaneonavicular ligament (spring ligament), tibialis posterior	long & short plantar ligaments	deep transverse head of adductor hallucis, dorsal interossei
	Tie beam	medial part of flexor digitorum longus and brevis, flexor hallucis longus & brevis, abductor hallucis	lateral part of flexor digitorum longus & brevis, abductor digiti minimi, flexor digiti minimi	peroneus longus
	Suspend	tibialis anterior, tibialis posterior, medial ligament of ankle	peroneus longus & brevis	peroneus longus

2.1.3. Foot/ankle motion

Three main joints contribute the movement of the foot and ankle— talocrural, subtalar and midtarsal joints. The motion of talocrural joints includes dorsiflexion and plantarflexion of the foot. The axis of motion is 20-30˚ from frontal plane at top view and 8˚ from transverse plane at back view. The passive range of motion (ROM) of dorsiflexion and plantarflexion are 20˚ and 50˚, respectively (Manter, 1941). The motion of subtalar joint includes the eversion and inversion of rearfoot. The axis of motion is 42˚ from transverse plane at side view. The passive ROM of rearfoot eversion and inversion are 10˚ and 20˚, respectively. The midtarsal joint provides the rotational movement between forefoot and rearfoot. The motion at midtarsal joints is two axes— the longitudinal and oblique midtarsal joint axis. Longitudinal midtarsal joint axis slopes upward and medial that provides the eversion and inversion for forefoot (Manter, 1941). Both passive motion of forefoot eversion and inversion are 25˚. Inversion and eversion at midfoot can provide the rise and drop of the medial arch, respectively. The oblique midtarsal joint axis inclines 52˚ from horizontal and 57˚ from the frontal plane (Manter, 1941). The motion at oblique axis is the combination of plantarflexion and adduction, and dorsiflexion and abduction. The passive ROM of forefoot abduction and adduction are 15˚ and 30˚. The pronation of foot is the combination of dorsiflexion, eversion, and abduction. The supination of foot is the combination of plantarflexion, inversion, and adduction.

2.1.4. Events of gait cycle

Gait cycle is the period between initial contact of one foot with the ground and subsequent contact of the same foot that consist of stance phase and swing phase (Burnfield, 2010). Stance and swing phase make up about 60% and 40% of a gait cycle, respectively (Burnfield, 2010). The classic division of stance phase include four events: heel-strike, foot-flat, heel-off, and toe-off occurs at 0%, 10%, 45%, and 60% of the gait cycle respectively (Burnfield, 2010). However, Harris & Wertsch (1994) argued the common classification may not be appropriate to some disabilities such as there is no heel-strike or heel-off for a person with neuromuscular impairment. Observational gait analysis was proposed by Perry (1992) to analyse both normal and pathological gait function. Stance phase is divided into five events: initial contact, load response, mid-stance, terminal stance, and pre-swing (Figure 2.3). As flatfoot deformity is considered as a foot pathology, observational gait analysis may be more appropriate. The swing phase is made up by three sub-phases— initial swing (i.e. accelerate phase), midswing, and terminal swing (i.e. deceleration phase). Perry (1992) also proposed the three rockers of gait— heel rocker, ankle rocker, and forefoot rocker, due to different rotational centres in loading response, mid-stance, and terminal stance, respectively (Figure 2.4). In heel rocker, foot rotates (i.e. ankle plantarflexion) around the heel during loading response after initial contact (Figure 2.4.A-B). In ankle rocker, lower leg (i.e. tibial) rotates around the ankle (i.e. ankle dorsiflexion, subtalar eversion) during midstance and brings the whole body travel over the stance foot (Figure 2.4.B-C). In forefoot rocker, the foot rotates around metatarsophalangeal joint (MPJ) (i.e. ankle plantar flexion, subtalar inversion) during terminal stance (Figure 2.4.C-D) followed by the pre-swing and ending by toe-off.

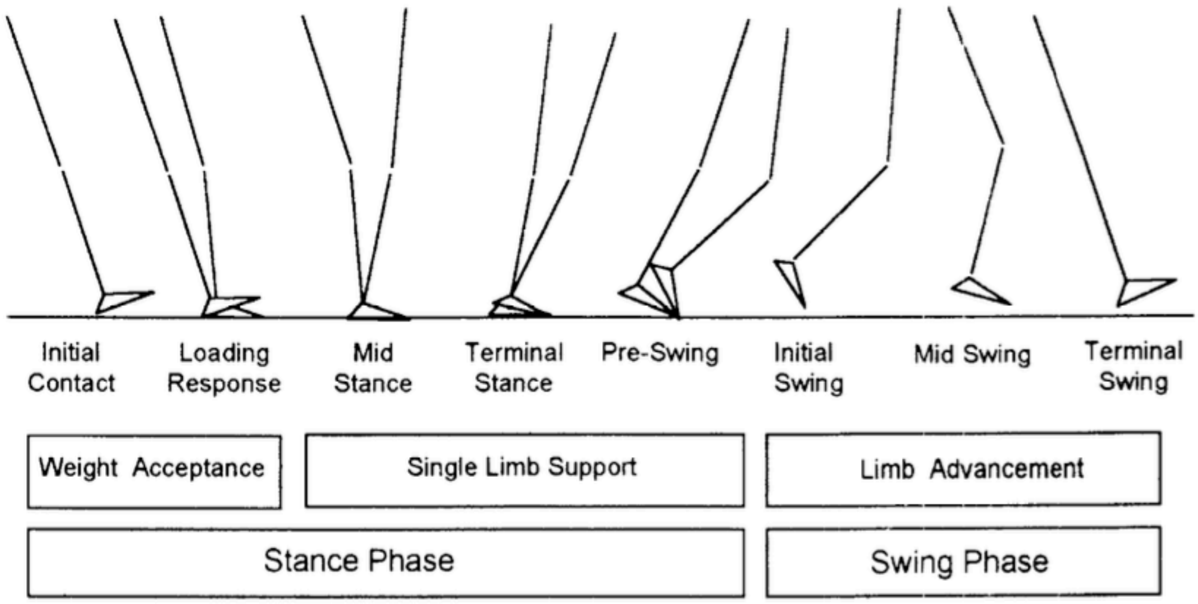

Figure 2.3. Observational gait analysis proposed by Perry (1992) for normal and pathological gait analysis

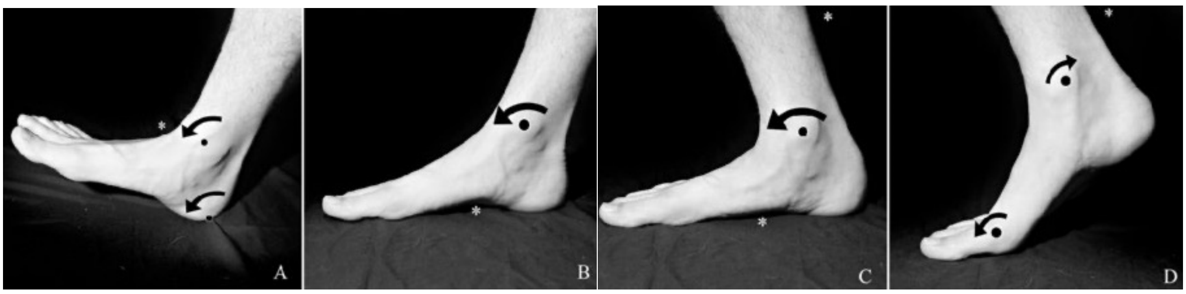

Figure 2.4. The 3 rockers of gait. (A-B) Heel rocker. Foot rotates around the heel during loading response. (B-C) Ankle rocker. Tibia rotates around the ankle during mid-stance. (C-D) Forefoot rocker. Foot rotates around the metatarsophalangeal joint (Mayich et al., 2014)

MLA plays important role for weight absorption in early stance phase to attenuate the impact (e.g. gravity, ground reaction, momentum) by lowering the arch height (i.e. arch compression). The arch is lifted (i.e. arch recoil) in the late stance phase to generate forward. Arch compression occurs from initial contact to mid-stance at early stance phase and arch recoil occurs from midstance to pre-swing at late stance phase. The dynamic change of MLA in stance phase is described as:

(a) Initial contact (foot contact) (Fig. 2.5.a): When the foot contacts to the ground, the MLA angle starts to increase as the plantar muscles start lengthening by the external load. The extended muscles actively generate the tension that increases the strain of plantar muscles. This action is to restore the potential energy of the body.

(b) Mid-stance (peak) (Fig. 2.5.b): The MLA reaches the maximum angle as the plantar muscles reach the maximum length at the midpoint of the stance phase. Meanwhile, the strain of the plantar muscle reaches its peak.

(c) Pre-swing (toe-off) (Fig. 2.5.c): After the peak, the MLA angle starts to decrease as the plantar muscles start shortening. As the external load starts to remove, the plantar muscles return the elastic strain energy that stored in the earlier phase, which provides the propulsion that pushes the entire body to move forward.

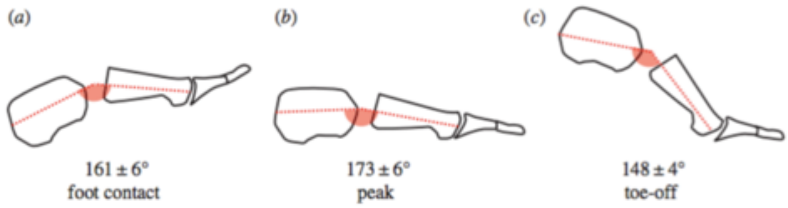

Figure 2.5. The arch angle in stance phase: (a) foot contact (b) at peak (c) toe-off (Kelly et al., 2015)

As shown in Table 2.3, three-dimensional joint motions are presented for early and late stance phase divided by arch compression and arch recoil. Arch compression (i.e. decrease the height of navicular) is initiated by subtalar joint eversion and the relative midtarsal joint inversion to extend the plantar muscle groups and connective tissue to absorb the impact. Subtalar eversion followed by medial rotation of the tibia and femur results in the hip internal rotation and adduction, which eccentrically contract glute muscle for deceleration of gait. Moreover, ankle dorsiflexion also extends the surrounded muscle groups such as claves and plantar and the connective tissue to absorb the impact. Arch recoil occurs when swing leg travels beyond the stance leg followed by the pelvis forward rotation. This initiates the external rotation of the femur and tibia results in the inversion of subtalar joint and relative eversion of midtarsal joint, which lifts the foot arch (i.e. increase the height of navicular). The hip motion is still internal rotation at arch recoil is because the forward rotation of the pelvis is faster than the external rotation of femur results in a relatively hip internal rotation and so does the femur to the tibial as knee internal rotation.

Table 2.3. Three-dimensional joint kinematic in stance phase (Harris & Wertsch, 1994)

	Arch compression	**Arch recoil**
	Initial contact to midstance	**Midstance to pre-swing**

	Sagittal	Frontal	Transverse	Sagittal	Frontal	Transverse
Midtarsal	Dorsiflexion	Inversion	Abduction	Plantar flexion	Eversion	Adduction
Subtalar	Plantar flexion	Eversion	Abduction	Dorsiflexion	Inversion	Adduction
Ankle	Plantar flexion to dorsiflexion	N/A	N/A	Plantar flexion	N/A	N/A
Knee	Flexion	Abduction	Internal rotation	Extension	Adduction	Internal rotation
Hip	Flexion	Adduction	Internal rotation	Extension	Abduction	Internal rotation

2.1.5. Elastic energy in gait

In human gait, metabolic energy must be consumed when muscles have action that generates work (Alexander, 1991). Muscles generate work if they lengthen or shorten while exerting tension and the mechanical energy degrades to generate heat (Alexander, 1991). However, some muscles can act as Hookean spring to provide the elastic mechanism in gait with the same mechanical effect but no metabolic cost. In Hooke's law, since the force has the form

$$F = -kx \qquad [2.1]$$

the work done by the compression/stretch of the spring a distance x is,

$$Work = \Delta PE = \frac{1}{2}kx^2 \qquad [2.2]$$

Where PE is the potential energy and k is the constant of the spring.

The Hookean spring is able to store the potential energy while exerting force and return it when the force is removed. The foot arch is like a spring that can be deformed and absorb partial impact as the potential energy when the force is applied, and it returns the potential energy when the foot is unloaded (Fig. 2.6). Therefore, foot arch's muscles play the important role in human gait to provide the energy-saving mechanism. During the period of foot contact with the ground, the vertical force exerts rise and fall. In the study of Kelly et al. (2015), the elastic mechanism is described by the dynamic change of MLA in stance phase. The angle in sagittal plane between calcaneus and metatarsal is recorded by motion capture system to explain the compression and recoil of MLA for energy-saving mechanism.

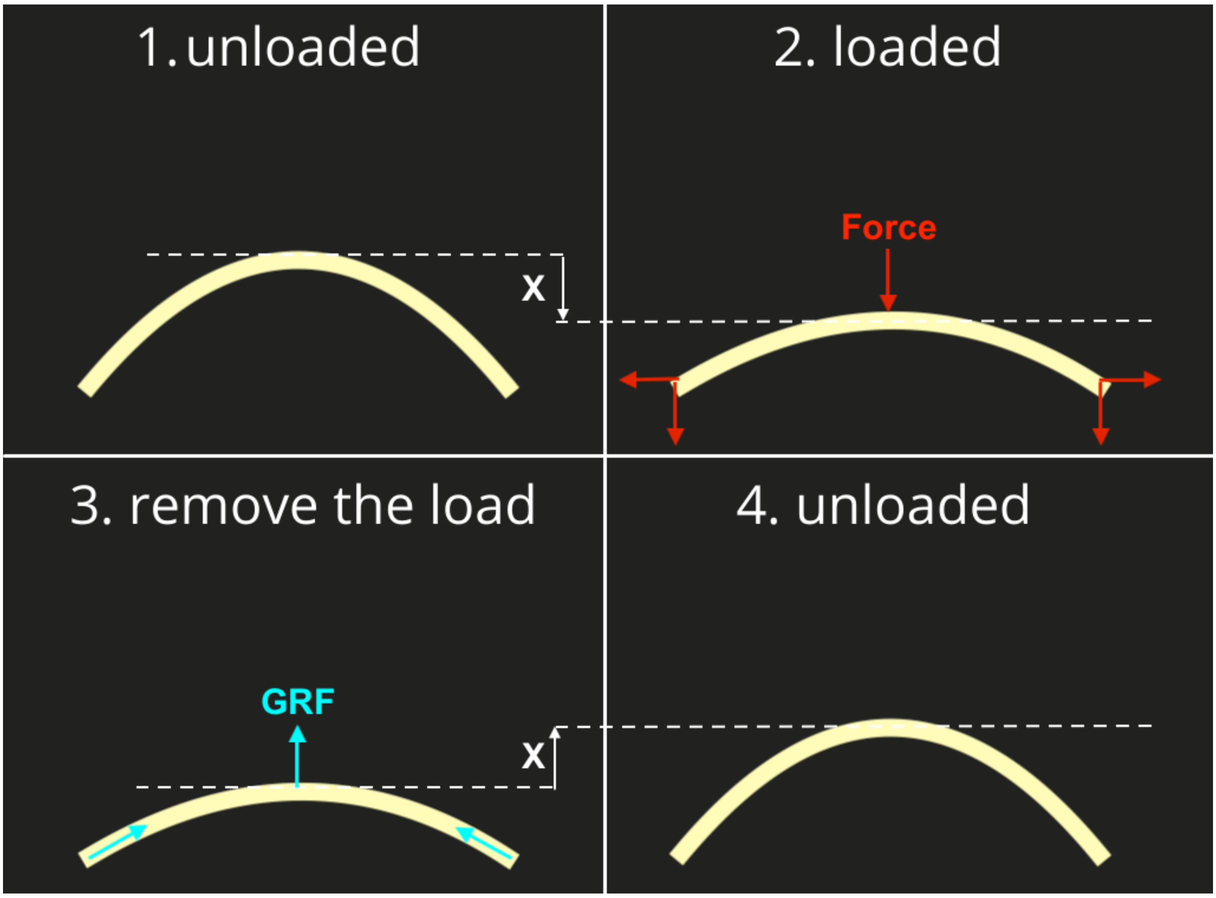

Figure 2.6. (1) The original shape of foot arch (2) When the load applies to the arch (3) The ground reaction force from the ground (4) Return to its original shape when unloaded.

2.2. Adult-acquired flatfoot deformity

2.2.1. Functional changes of flatfoot

Flatfoot deformity (also known as Flatfoot) is divided into congenital (if present at birth) and acquired (occurring after the completion of foot development) (Kuhn et al., 1999). Adult-acquired flatfoot deformity is found when the foot arch is collapsed and lost its original arched structure (Franco, 1987). The collapsed foot arch disrupts the normal process of weight bearing and causes functional changes in the foot. Flatfoot is reported to alter the skeletal alignment (Younger et al., 2005), muscle electromyographic (EMG) activation (Murley et al., 2009c) and lower limbs biomechanics. The altered biomechanics includes the ROM in foot (Buldt et al., 2013; Buldt et al., 2015, Hunt and Smith, 2004) or knee joints (Williams et al., 2001), foot joint moments (Hunt and Smith, 2004), plantar pressure distribution (Franco, 1987, Ledoux and Hillstrom, 2002), static balance and stability (Hertel et al., 2002) and ground reaction force in gait (Bertani et al., 1999). The functional changes of flatfoot are as the following:

• Skeletal alignment

Flatfoot causes the talar head medially and anteriorly displace from the navicular (Franco, 1987). From the antero-posterior view on sagittal plane of the foot (Fig. 2.7), flatfoot increases the talonavicular coverage angle— between the lines connect two ends of articular surface of the talus head and navicular (Younger et al., 2005). The talar head displacement can also cause the eversion of the calcaneus. From the posterior aspect on frontal plane (Fig. 2.8), the increased suptal-inftal angle is found in flatfooted people (Cody et al., 2016). And, from the lateral aspect (Fig. 2.9), the talar-first metatarsal angle is convex downward indicating collapsed MLA for flatfoot deformity (Cody et al., 2016).

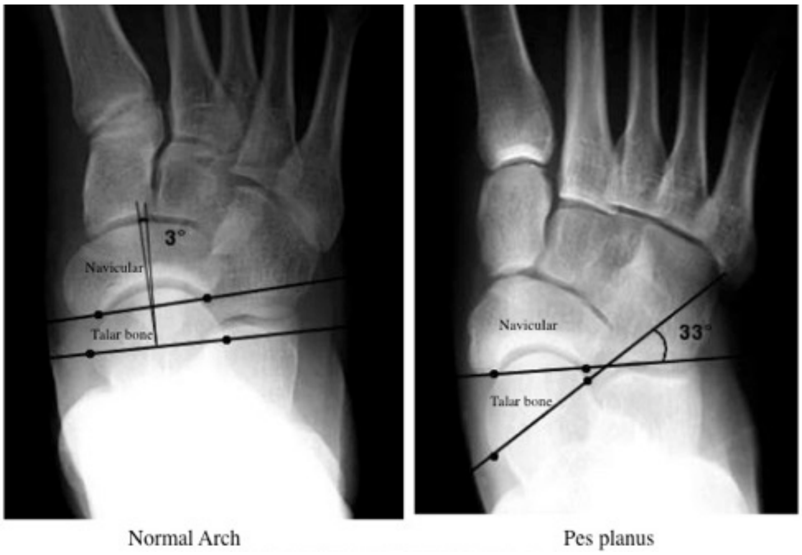

Figure 2.7. Compare normal arch and flatfoot from antero-posterior view (Cody et al., 2016).

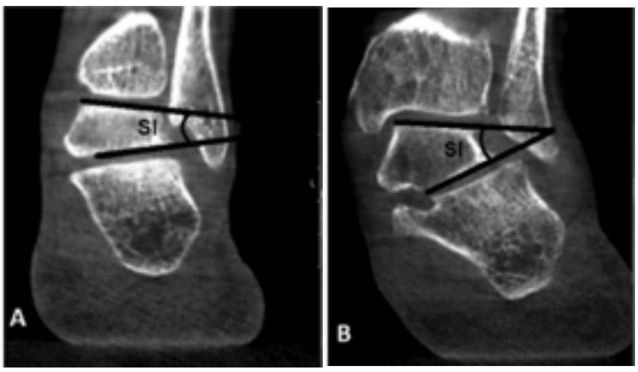

Figure 2.8. Compare normal arch and flatfoot from posterior view of frontal plane (Cody et al., 2016).

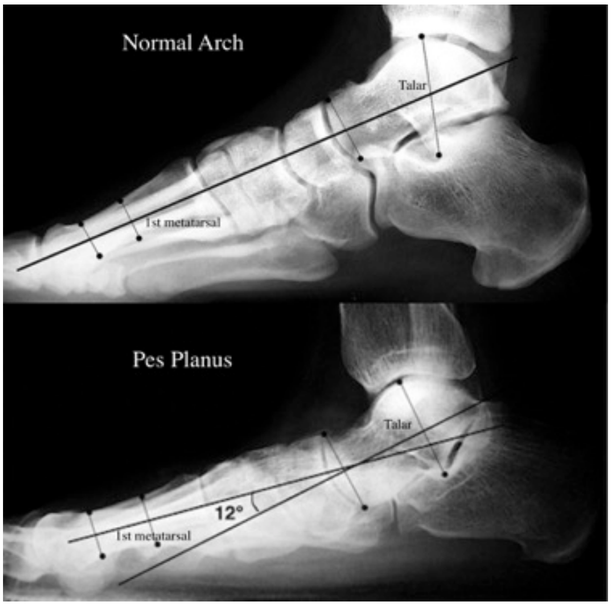

Figure 2.9. Comparison of normal arch and flatfoot from lateral view (Cody et al., 2016).

- EMG activation

In a systematic review, Murley et al. (2009c) reported foot invertor muscle demonstrated increased EMG activation and foot evertor muscle demonstrated decreased EMG activation for flatfoot compare to normal developed foot. The significantly greater EMG amplitude was found in tibialis anterior and tibialis posterior during stance phase for flatfoot (Murley et al., 2009c). The significantly lower EMG amplitude was found in peroneus longus during stance phase (Murley et al., 2009c). As shown in Fig. 2.10, tibialis anterior and tibialis posterior are both attached on the medial side of MLA, and peroneus longus attaches on the lateral side. They are the antagonists to control pronation and supination of the foot (Myers, 2014). As the over-pronated is reported in flatfooted people's gait (Franco, 1987), the finding of Murley et al. (2009c) may reflect on tibialis anterior and tibialis posterior undergoes the greater loading and a compensatory lack of activity in peroneus longus. Tibialis anterior and Tibialis posterior is an inventor of subtalar joint and it is activated (i.e. lengthen) when subtalar joint everts at early stance phase. Flatfoot increases subtalar joint eversion in both joint's motion and moment could contribute to the increased EMG activation in tibialis anterior and tibialis posterior. Peroneus longus is an evertor of subtalar joint and it is activated when subtalar joint inverts at late stance phase. Flatfoot deceased subtalar joint inversion in both joint's motion and moment, and it could contribute to the decreased EMG activation in Peroneus longus.

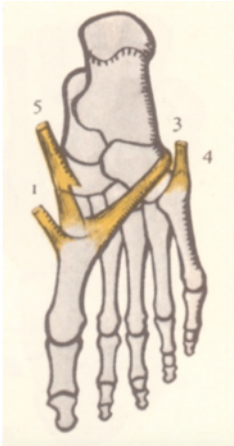

Figure 2.10. The muscle attachment of (1) tibialis anterior (3) peroneus longus (5) tibialis posterior

- Plantar Pressure distribution

In the static weight-bearing condition, the external loads can distribute evenly on the calcaneus to the fifth metatarsal head for normal-arched people (Fig. 2.11) (Franco 1987). However, when the MLA collapses, larger pressure was measured on the medial side of the foot— calcaneus and first and second metatarsal heads (Fig. 2.11) (Franco 1987). Ledoux and Hillstrom (2002) also reported that flatfooted people had greater pressure in hallux area during gait, which explained that the collapse of MLA causes more pressure on the medial side of the foot. In gait analysis, flatfooted participants were found to significantly increase the contact area beneath the medial midfoot when compared to normal-arched participants during both walking and running (Chuckpaiwong et al., 2008). Moreover, the maximum force and peak pressure beneath the lateral forefoot is significantly decreased for the flatfoot (Chuckpaiwong et al., 2008).

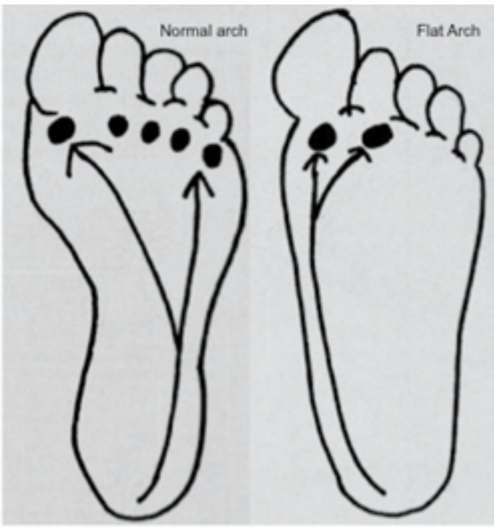

Figure 2.11. The pressure distribution between normal arch and flat arch (Franco 1987)

- COP trajectory

The trajectory of the centre of pressure (COP) in the foot during gait is illustrated in Figure 2.11.1, and COP excursion is normally described as the medial-and-lateral excursion from the foot axis along with X axis (Fuchioka et al., 2015; Wong et al., 2008). Studies demonstrate that people with flatfoot have a significant medial deviation of COP during walking, which the increased COP medial excursion and decreased COP lateral excursion (Aboutorabi et al., 2015). The COP trajectory in standing is used to indicate the level of postural control (i.e. static balance). Hertel et al. (2002) reported flatfooted people have greater COP excursion area in single-leg standing indicating poorer balance.

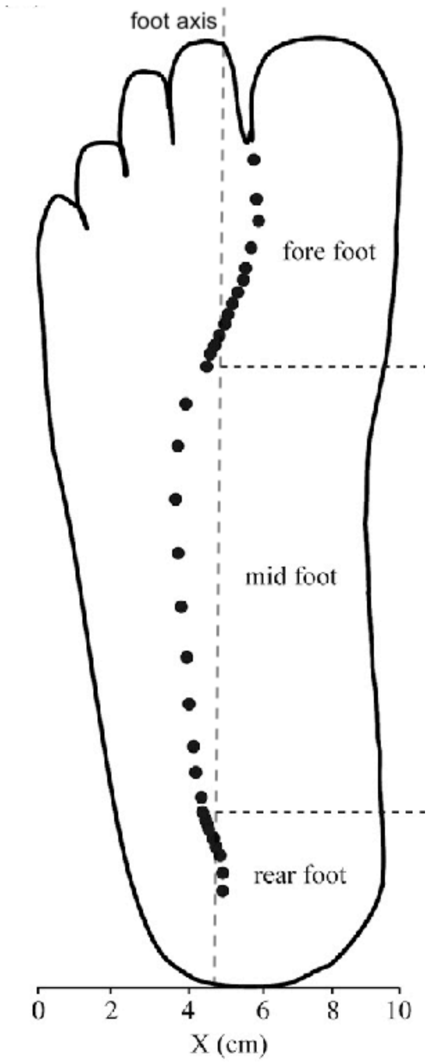

Figure 2.11.1. The trajectory of centre of pressure in the foot during stance phase in gait (Fuchioka et al., 2015).

- Joint kinematic in gait

Hösl et al. (2014) measured foot kinematic during gait cycle for asymptomatic and symptomatic flexible flatfeet and normal feet in thirty-five children and adolescents as figure 2.12.1. Although no statistically significant difference was observed between asymptomatic and symptomatic flexible flatfeet, a large discriminatory is reported between flatfoot and normal developing foot in sagittal, frontal, and transverse plane. As shown in Figure 2.12.1, for hindfoot/tibia (i.e. subtalar, ankle) kinematic in sagittal plane, a significantly larger peak plantarflexion in loading response and smaller peak dorsiflexion in stance phase were found in flatfoot (Hösl et al., 2014; Prachgosin et al., 2015). Flatfoot showed considerably restricted dorsiflexion during stance phase, and plantarflexion during push-off. In frontal plane, the flatfoot was in a greater everted position at initial contact. Although the larger peak eversion was presented by flatfoot, the total eversion ROM was smaller than normal foot in stance phase (Hösl et al., 2014). Flatfoot was also observed to have prolonged hindfoot eversion as they converted to inversion at 58.31% of stance, which is later than normal foot at 56.64% of stance (Prachgosin et al., 2015). Moreover, smaller peak inversion and range were found in flatfoot (Hösl et al., 2014). In the transverse plane, significant increase in the peak internal rotation angle of hindfoot was observed in flatfoot during stance phase (Prachgosin et al., 2015). Moreover, external rotation at toe off was increased in flatfoot with respect to normal foot (Hösl et al., 2014).

For the kinematic of knee joint, Kim et al. (2017) found flatfoot was in a more flexed position (5 to 6 degrees) throughout the gait cycle compared to normal developed foot in the sagittal plane (Figure 2.12.2B). In frontal plane, the significantly larger peak knee valgus was found in flatfoot during stance phase (Figure 2.12.2A). In transverse plane, flatfoot was found in a more externally rotated position and less motion of internal rotation during stance phase (Figure 2.12.2C).

For the hip kinematic, Shih et al. (2012) was found less hip internal rotation excursion for flatfoot children in stance phase (Figure 2.12.3C). Flatfoot children was also found in a more flexed and adducted position for hip in sagittal and frontal plane during stance phase (Figure 2.12.3A & 3B).

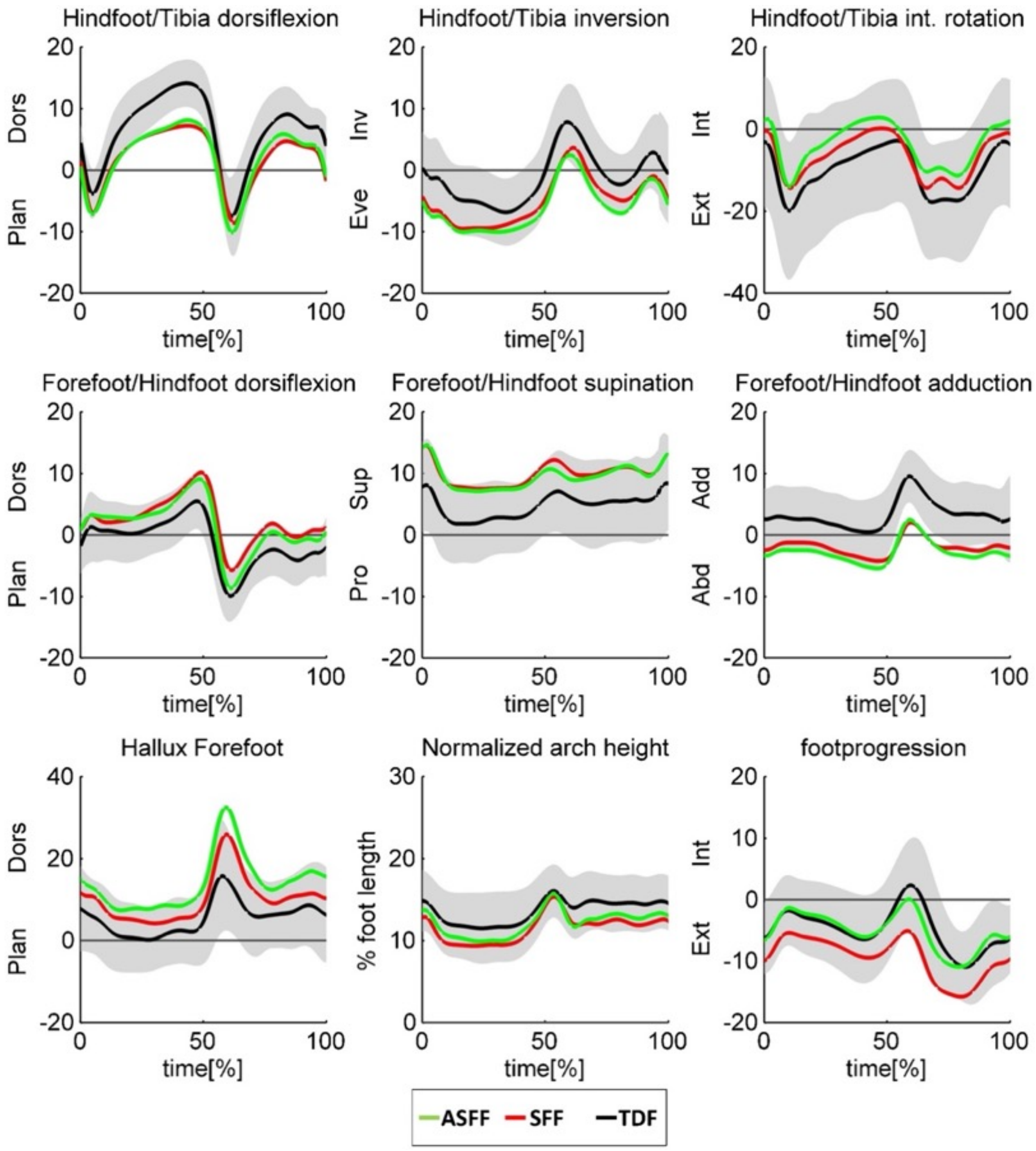

Figure 2.12.1. Foot kinematics (°) during the gait cycle for asymptomatic (ASFF) and symptomatic (SFF) flexible flatfoot and typically developing foot (TDF) (Hösl et al., 2014)

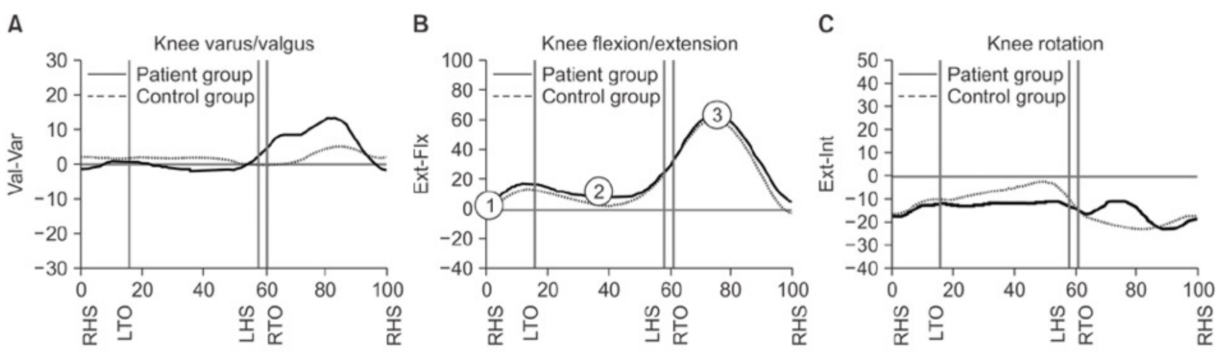

Figure 2.12.2. Knee kinematics (°) during the gait cycle for flatfoot (patient group) and normal developed foot (control group) (Kim et al., 2017)

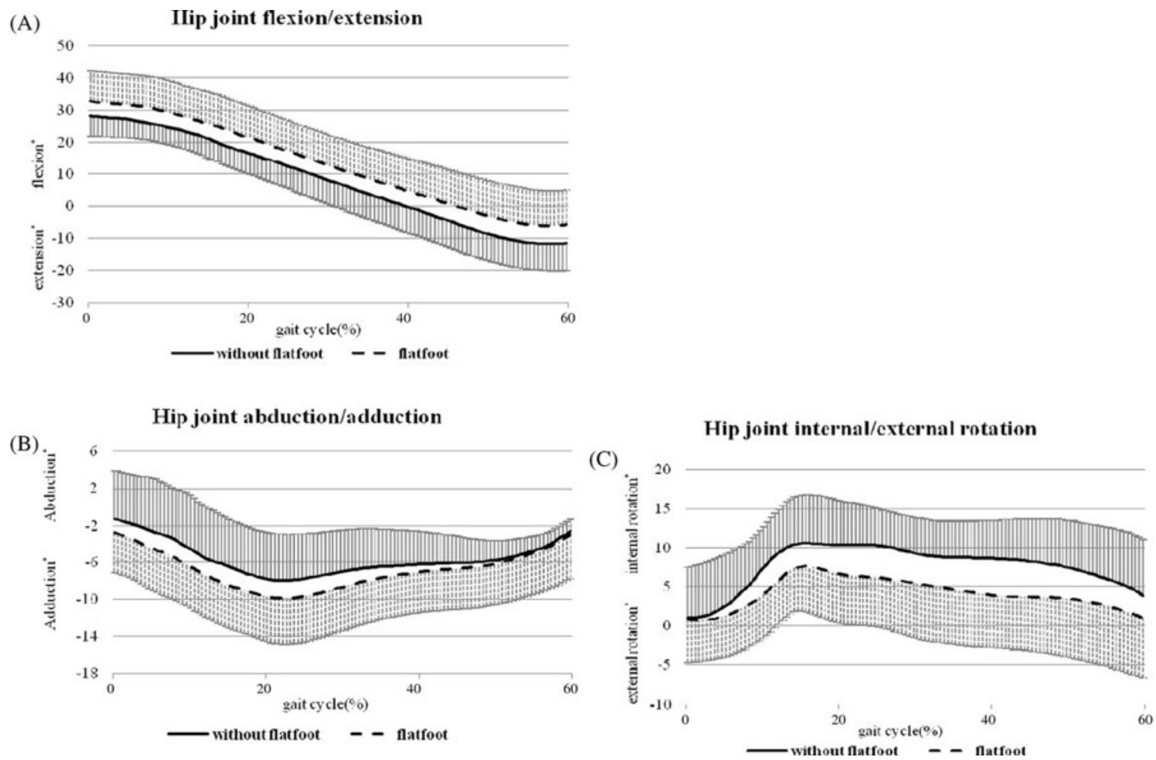

Figure 2.12.3. Hip kinematics (°) during the stance phase for flatfoot and normal developed foot (Shih et al., 2012)

Other studies also reported joint kinematic regards to the ROM during gait as Hunt and Smith (2004) reported flatfooted people exhibit higher plantarflexion angle during the stance phase and less forefoot adduction at propulsion phase of walking. Moreover, the finding of Buldt et al. (2013) displayed a strong positive relationship was found between decreasing arch height and increasing peak rearfoot (subtalar joint) eversion. Buldt et al. (2013) also reported less midfoot eversion during pre-swing phase. In several cases of flatfoot, the forefoot is dorsiflexed and adducted on the rearfoot that result in anteromedial displacement of navicular and talar bone (Manter, 1941). Flatfoot can cause foot over-pronation in weight-bearing condition. Over-pronation is coupled with increased tibial internal rotation, femoral internal rotation and knee flexion in walking or running (Stacoff et al. 2000a; Williams et al., 2001). Together those could bring the knee joint to a valgus position. Knee valgus describes an outwards angle from the mid-line from the distal to the proximal end of a segment (Haines et al. 2011). Thus, the change of foot and ankle motion can further affect the knee joint.

- Joint kinetic in gait

For ankle moment in sagittal plane shown as Figure 2.12.4A, flatfoot group has lower peak dorsiflexion moment at the loading response and the lower peak plantar flexion moment (approximately 30% less) at the later stance phase (i.e. push-off) than the normal foot (Kim et al., 2017). For ankle power in sagittal plane shown as Figure 2.12.4B, the downward peak (A1Spw) represents the power absorption corresponding to the eccentric contraction of plantar flexor at the ankle during the midstance, and the upward peak (A2Spw) represents the power generation corresponding to the concentric contraction of plantar flexor during pre-swing (Kim et al., 2017). Flatfoot group displayed the significantly smaller power absorption and generation (45% less) compared to normal foot (Figure 2.12.4B). The reduction of ankle moment presented by flatfoot group indicates the inefficiency of the leverage system during gait, which results in the reduced power generation in concentric propulsive activity providing the forward momentum (Kim et al., 2017). Prachgosin et al. (2015) observed the significantly larger peak MLA moment on in the frontal plane during mid stance in flatfoot compared to normal foot, which indicates the significant increase of eversion moment in flatfoot. However, statistically significant differences of the MLA moment were in the sagittal and transverse planes during stance between the two groups (Prachgosin et al., 2015).

Other studies reported that flatfoot showed greater in peak plantarflexion moment at toe-off (Hunt and Smith, 2004). After heel strike, the peak dorsiflexion moment was reached later than normal-arched people (Hunt and Smith, 2004). Moreover, at 10% of stance phase, a significant midfoot inversion moment was found in flatfooted people, while a significant midfoot eversion moment was found in normal-arched people (Hunt and Smith, 2004).

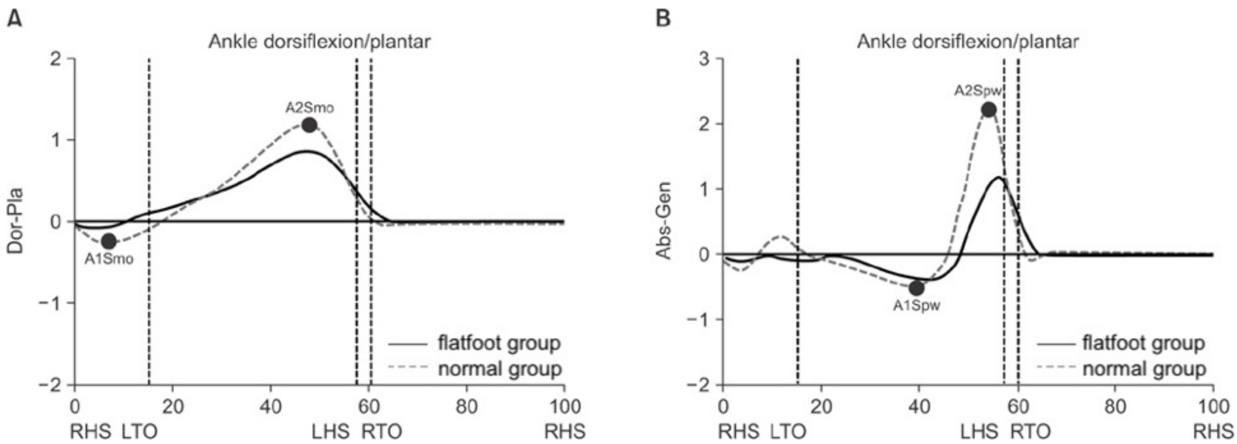

Figure 2.12.4. Ankle kinetic during gait for flatfoot and normal developed foot. (A) Ankle moment (B) Ankle power in sagittal plane (Kim et al., 2017)

The ground reaction force (GRF) vector in three planes during stance phase was measured by Kim et al. (2017) as shown in Figure 2.13. For the vertical vector shown in Figure 2.13A, flatfoot groups significantly reduced in GRF at the push-off ($F_{LOAD}{}^3$). For fore-and-aft vector shown in Figure 2.13B, both peak braking force ($F_{AP}{}^1$) and peak pushing force ($F_{AP}{}^2$) reduced in flatfoot group. For medial-and-lateral vector shown in Figure 2.13C, F_{ML}^1 and F_{ML}^2 significantly increased in flatfoot groups, which was attributed to a subtalar everted (hindfoot valgus) alignment.

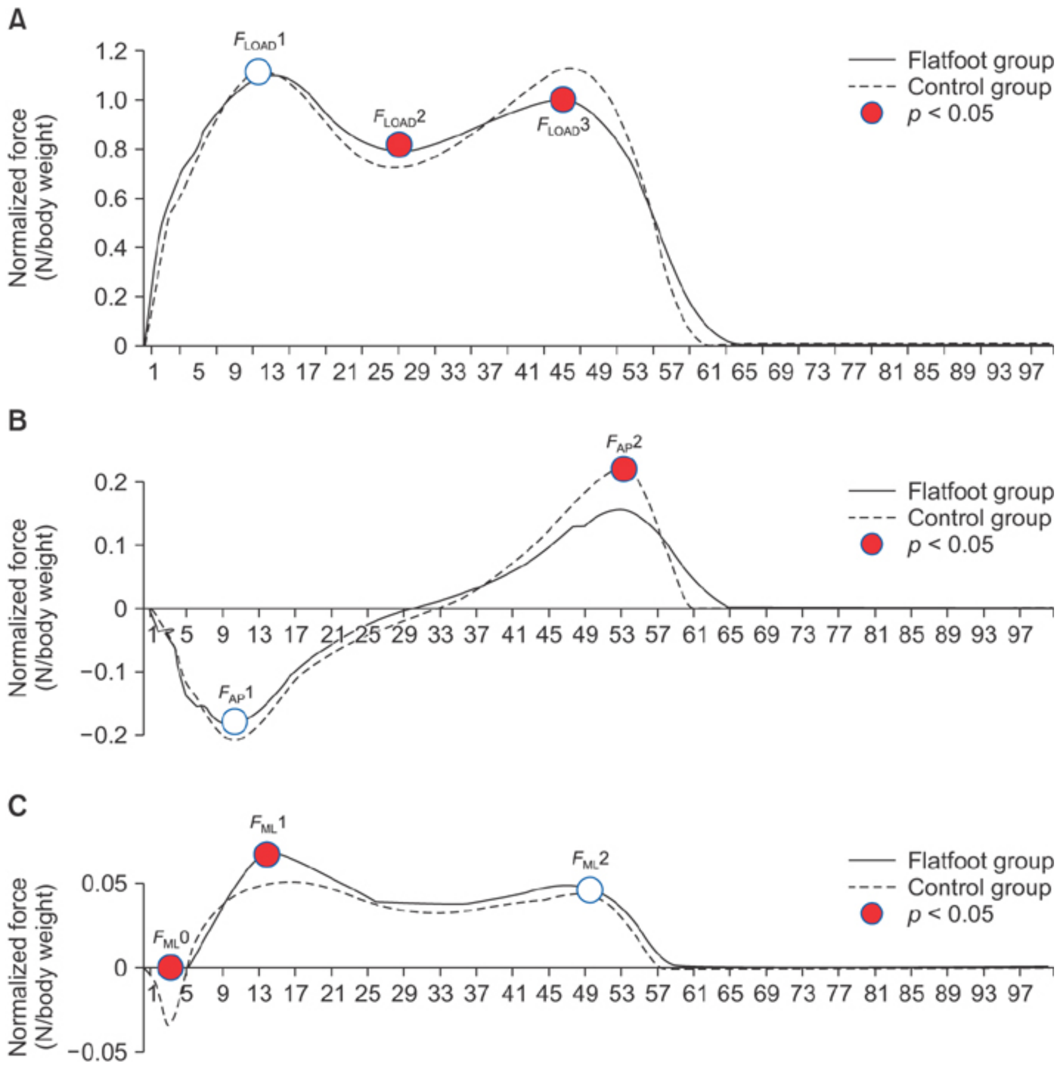

Figure 2.13. Ground reaction force in three dimensions: (A) vertical vector (B) fore-and-aft vector (C) medial-and-lateral vector, reported by Kim et al. (2017).

Other studies also reported that GRF has significant differences during running in different between low, normal, and high arch (Nachbauer and Nigg 1992). The change of the GRF can alter running cadence, step length, and lower-extremity joint kinematics and affect the muscle capacity (Giddings et al., 2000). Queen et al. (2009) found flatfooted athletes are difficult to dampen the GRF compare to normal-arched ones in locomotion. Moreover, Chang et al. (2012) found that flatfoot had a larger peak GRF than normal arch in the drop jump testing

2.2.2. Flatfoot and injury

There is a broad range of risk factors that may contribute to injury include muscle fatigue or weakness, excessive loading, malalignments in the skeletal system and sarcopenia (Dixon, 2016). As shown in Fig. 2.13, the injury threshold is displayed in the inverse relationship between the amount of load applied and the number of cycles describes (Hamill and Knutzen, 2006). Injuries can occur in biological tissue when a single large impact force is applied or when loads are repeatedly applied until the biological capacity of the tissue is exceeded (Hamill and Knutzen, 2006). Therefore, for people or athletes with flatfoot, the functional change could make them more susceptible to injuries or musculoskeletal symptoms. Low-arched individuals suffer a higher incidence of knee, soft tissue, and medial side injuries due to the lower extremity structural deviations lead to mechanical deviations (Williams et al., 2001a). This could compromise the ability to manage GRFs may lead to higher force being transmitted through the kinetic chain; subsequently increasing the risk of injury (Queen et al. 2009; Giddings et al., 2000; Chang et al. 2012). The increased peak GRF found in flatfoot the medial vector during stance phase (figure 2.13C) shows significantly larger evertor moment. This may subsequently add the abnormal load on the surround tissue such as plantar fascia, Achilles tendon, posterior tibial tendon, or other joints (e.g. knee) and further result in musculoskeletal problems. Williams et al. (2001a) reported runners with flatfoot are prone to suffer plantar fasciitis, posterior tibialis tendinitis, patellar tendinitis, and knee pain (Table 2.4). Williams et al. (2001a) claimed it could be caused by the over-pronated foot followed by excessive eversion of hindfoot during running, which increases the stress on the medial side of the foot/ankle.

Table 2.4. Flatfoot runners and musculoskeletal problems (Williams et al., 2001a)

Flatfoot	Plantar fasciitis	Posterior tibialis tendinitis	General knee pain	Patellar tendinitis
Incidences (%)	25%	15%	35%	25%

The over-pronated foot led to knee valgus in weight-bearing condition that is linked to anterior knee pain (Rodrigues et al., 2015). Regarding the injury risk in flatfoot, Michelson et al. (2002) reported 15.3% of lower extremity injured athletes in different sport is flatfoot. Riskowski et al. (2013) studied 1856 participants aged over 50 years and found widespread lower extremity symptoms especially knee pain for flatfoot. Kosashvili et al. (2008) identified 16% of 97229 militaries are flatfoot and found the flatfoot was associated with nearly twofold increase in the rate of knee pain and intermittent low back than normal arch. Musculoskeletal problems include stress fractures, Achilles tendinitis, iliotibial band syndrome, patellofemoral syndrome, plantar fasciitis is considered to have connection with flatfoot. Kaufman et al. (1999) identified 31% of flatfoot from 449 naval seal trainees. As they assumed the risk ratio of normal arch is 1 in musculoskeletal injury (i.e. stress fractures, Achilles tendinitis, and iliotibial band syndrome), they obtained the risk ratio of flatfoot is from 1.39 to 2.45 times greater than normal-arched group (Table 2.5).

Table 2.5. Flatfoot naval seal trainees and their incidence of musculoskeletal problems (Kaufman et al., 1999).

Flatfoot	Stress fractures	Achilles tendinitis	Iliotibial band syndrome	Patellofemoral syndrome
Incidence (%)	11.5	7.4	11.5	7.8
Risk ratio	2.45	1.93	1.76	1.39

MacAuley and Best (2008) reported that flatfoot could be the most common reasons for the contribution of stress fractures and plantar fasciitis. Roxas (2005) found 81% to 86% of individuals suffered plantar fasciitis are flatfoot and have excessively pronated foot position. Chuckpaiwong et al. (2007) found 12.1% of runners and other athletes who experienced second metatarsal stress fracture are flatfoot. In Tong and Kong's (2013) meta-analysis review study, flatfoot is significantly associated with lower extremity injuries and musculoskeletal symptoms. As flatfoot is strongly related to injury, clinicians need to take a proactive step in prevention and potentially administer orthopaedic aids before injury occurs. Before providing the interventions to improve compromised biomechanics caused by flatfoot, proper and accurate assessment method is important for identifying individuals with abnormal arches. Therefore, the quality of life or sport performance of flatfoot could be improved.

2.3. Foot arch assessment

2.3.1. Visual assessment

The accurate flatfoot screening is crucial at early stage to develop and implement appropriate interventions to provide structural support, prevent injuries, and alleviate discomfort. As a common practice, medical clinicians use visual assessments to identify foot types (Dahle et al., 1991) based on their professional judgement. Visual assessment is a reliable examination procedure for foot morphology since it bases its conclusion on the judgment of clinical professionals (e.g. general practitioner, podiatric surgeon, and physiotherapist). The visual assessments review by an expert health professional on commonly based on three planes—mediolateral, back and bottom view.

- Mediolateral view

The angle formed by the lines connecting the first metatarsal head, the navicular tuberosity, and the medial malleolus is visually assessed (Fig. 2.14) (Çilli et al. 2009). When this angle close to 90˚a low arch is declared, whereas if it is close to 180˚ then is high arch (Dahle et al. 1991).

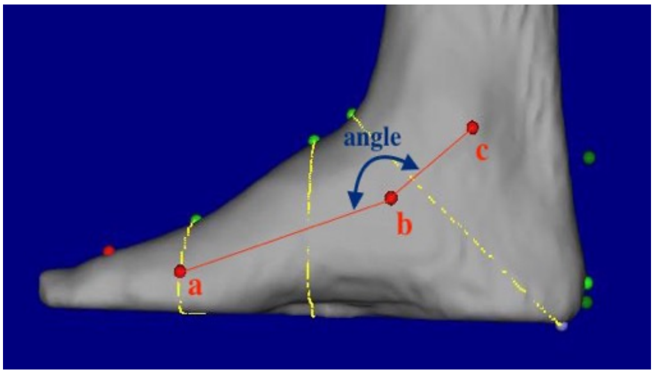

Figure 2.14. Mediolateral view. Use the angle form by the lines connecting a (first metatarsal head), b (navicular tuberosity), and c (medial malleolus) to visualize foot type

- Back view

The deviated angle between the bisecting line of the calcaneus and the perpendicular line to the ground is visually assessed (Fig. 2.15) (Tenenbaum et al. 2013). The larger positive angle represents the severer low arch (Dahle et al. 1991).

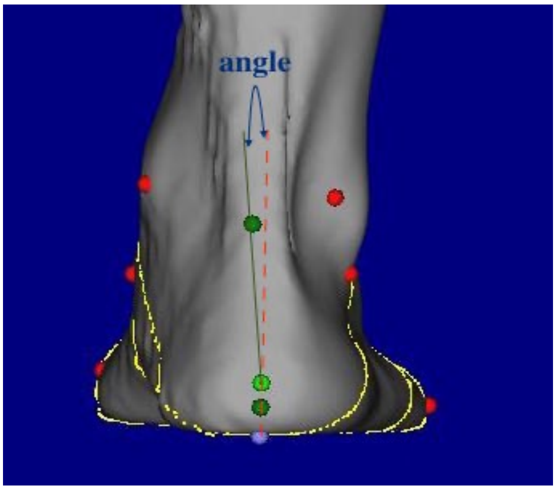

Figure 2.15. Back view. Use the angle between the bisecting line of the calcaneus (green line) and the perpendicular line to the ground (red line) to visualize foot type

- Bottom view

The bottom view of foot image or foot imprint is normally employed to determine foot types according to the foot contact area. Image with more foot contact area in the middle third (Fig. 2.16), the lower the foot arch. The less the foot contact area, the higher the foot arch (Swedler et al. 2010). However, Swedler et al. (2010) reported high percentage type 1 and 2 errors of using bottom view to determine foot types.

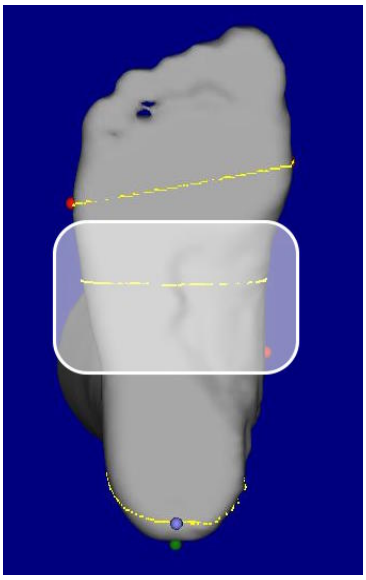

Figure 2.16. Bottom view. Use the foot contact area (white area) of middle third to visualize the foot type

Although visual assessments identifying foot types based on the professional judgement, it is deemed inevitably subjective because it is lack of the cliff-edge transition (i.e. cut-off value) from one foot type to another (e.g. from normal arch to low arch). For the major studies that used visual assessment for flatfoot classification (Table 2.6), the reported flatfoot prevalence varies from 0.7% to 14% indicating inconsistency of visual assessment in flatfoot identification. McCrory et al (1997) claim that the 2D index of foot arch on transverse plane and sagittal plane are not strongly correlated. Abdel et al. (2006), Sachithanandam and Joseph (1995) and Swedler et al. (2010) all used the footprint to visually assess the foot types but reported flatfoot prevalence varies from 2.9% to 10.9%. This variation could explain the existence of inconsistency in visual assessment due to subjective perception. In addition, visual assessment could be time-consuming if the foot should be observed and assessed in different aspects and postures to ensure accurate classification. Moreover, another further issue is that people are less likely to seek an assessment in a hospital until they are injured or have symptoms of some severity. Such reluctance leads to delay in the diagnosis and makes it more difficult to prevent injuries and/or associated musculoskeletal problems caused by foot deformity in the early stage.

Table 2.6. The flatfoot prevalence using visual assessment in different studies

Study	Flatfoot prevalence	Total subjects	Visually assess point
Tenenbaum et al. (2013)	14%	825964	Hindfoot valgus
Çilli et al. (2009)	0.7%	3169	Absence of medial longitudinal arch
Abdel et al. (2006)	5.0%	2100	Footprint
Sachithanandam and Joseph (1995)	2.9%	1846	
Swedler et al. (2010)	10.9%	3968	

2.3.2. Quantitative assessment

For other health professionals and non-clinically trained allied health practitioners, there are three major quantitative measurements— radiography, anthropometric values and footprint parameters, to assess foot shape and more importantly to diagnose flatfeet by comparing the values to known population norms.

- Radiographic measurement

Radiographic measurement is the current gold standard for assessing foot arch type, which could more precisely to identify flatfoot by the displacement of foot skeleton (Cody et al., 2016; Pavlov, 1990; Younger et al., 2005). Three characteristics are evident in flatfoot: forefoot adduction, fallen longitudinal arch, and rearfoot valgus (Younger et al., 2005). There are several features that the clinicians normally use to identify flatfoot.

i. Forefoot adduction (on the anteroposterior view) (Fig. 2.17):

(a) Talonavicular coverage angle (F): the angle between the two lines that one is connected of the edges of the articular surface of the talus head and the other is connected the edges of the articular surface of the navicular. The angle greater 7° is considered flatfoot

(b) Talar-first metatarsal angle (G-E): the angle between the axis of the talar bone (G) and the axis of the first metatarsal (E).

Figure 2.17. The antero-posterior radiographic view of foot (Cody et al., 2016)

ii. Fallen longitudinal arch (on the mediolateral view) (Fig. 2.18):

(a) Lateral talar-first metatarsal angle (B-C): the angle between the axis of the talar bone (B) and the axis of the first metatarsal (C). For angle greater than 4° convex downward, it is diagnosed as flatfoot. Angle between 15° and 30° is considered as moderate flatfoot and the angle greater than 30° is considered as severe flatfoot.

(b) Calcaneal inclination: the angle between horizontal and the line from the plantar-most surface of the calcaneus to the inferior border of the distal articular surface. The decreased angle could indicate flatfoot, which less than 17°

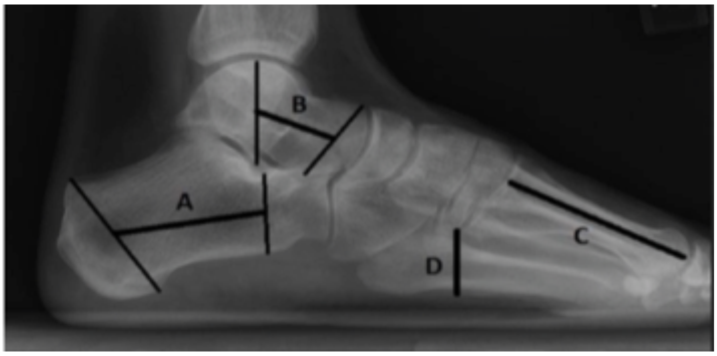

Figure 2.18. Lateral radiographic view of foot (Cody et al., 2016)

iii. Rearfoot valgus (on the back view) (Fig. 2.19)

The SI angle, which is the angle between the inferior and superior facets of the talus. The larger SI angle at the static position represents the larger calcaneus eversion which is more likely to acquire flatfoot.

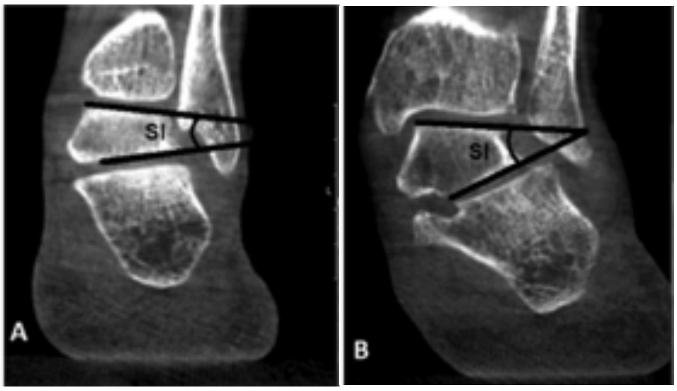

Figure 2.19. The back radiographic view of foot (Cody et al., 2016)

- Anthropometric and footprint index measurement

Different measurements are introduced to characterise the foot arch and classify the foot types based on its morphology and structure. Since the medial longitudinal arch (MLA) is considered to have clinical significance for flatfoot and pas cavus (Franco 1987), some of direct measurements have studied the parameters provided by MLA on sagittal plane, which includes arch height index (Xiong et al. 2010), longitudinal arch angle (Jonson & Gross, 1997; Nilsson et al. 2012), navicular height (Nilsson et al. 2012), and normalized navicular height (Williams & McClay 2000; Xiong et al. 2010). Except for these measurements listed above, there are still many other measurements were not selected in current study. Such as some other clinical measurements have obtained parameters on transverse plane: arch index (Cavanagh & Rodgers 1987), modified arch index (Riskowski et al. 2013), and frontal plane: rearfoot angle (Jonson & Gross, 1997). In order to more precisely to classify normal arch, low arch and flatfoot, we only selected measurements that have been widely used for foot type classification in the previous studies.

i. Arch index

The arch index (AI) is calculated as the ratio of the midfoot area (B) to the area of the entire foot excluding the toes (A + B + C) (Cavanagh & Rodgers 1987). As Fig. 2.20 shown, the procedure to divide area A, B and C is firstly to take the footprint of subjects and draw the foot axis ($\overline{\iota k}$) from the tip of the second toe to the center of the heel. Then, draw two lines perpendicular the foot axis and tangential to the foot were. The outline of the footprint, excluding the toes then is divided into equal thirds by parallel lines that are perpendicular to the foot axis. Therefore, AI can be calculated as eq. [2.3]

$$\text{Arch index } (AI) = {}^{B}/_{A + B + C} \qquad [2.3]$$

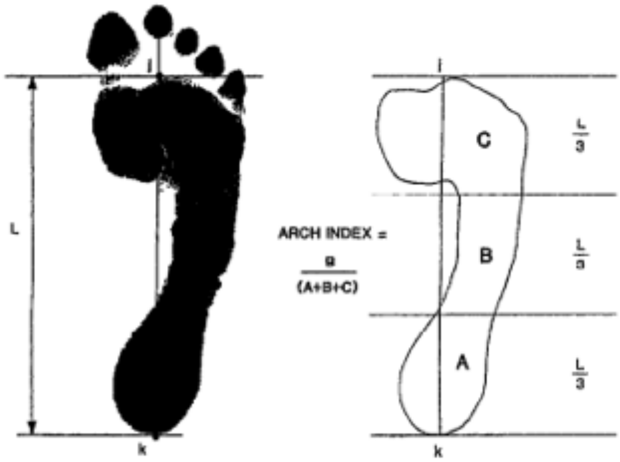

Figure 2.20. The footprint for calculating arch index (Cavanagh & Rodgers 1987)

ii. Modified arch index

Modified arch index (MAI) is a similar concept to AI using the ratio of the middle one-third pressure to the entire foot pressure. The footprint and entire foot pressure and were detected digitally by the pressure device invented by Chu et al. (1995). The foot area is divided by the same procedure as AI in figure 15. MAI can be calculated as eq. [2.4]

$$\text{Modified arch index } (MAI) = {}^{I_B}/_{I_A} + I_B + I_c \qquad [2.4]$$

iii. Rearfoot angle

Rearfoot angle is the angle between two selected lines, as lines were drawn when subject is prone as shown in Fig. 2.21(Jonson & Gross, 1997). Line 1 is longitudinally bisecting the distal one-third of lower leg and Line 2 is longitudinally bisecting the calcaneus. The larger angle caused by the larger eversion of subtalar joint indicating the decreasing of navicular height. It should be noted that the angle of eversion is recorded as positive and the angle inversion as negative.

Figure 2.21. The rearfoot angle

iv. Longitudinal arch angle

Longitudinal arch angle (LAA) is the angle between the two lines as drawn in Fig. 2.22 (Jonson & Gross, 1997; Nilsson et al., 2012). Line 1 is the line from first MPJ to navicular tuberosity, and Line 2 - from the navicular tuberosity to the most medial point of medial malleolus. The angle between Line 1 and 2 is LAA. The greater degree of LAA represents the higher arch and the smaller LAA represents the lower arch.

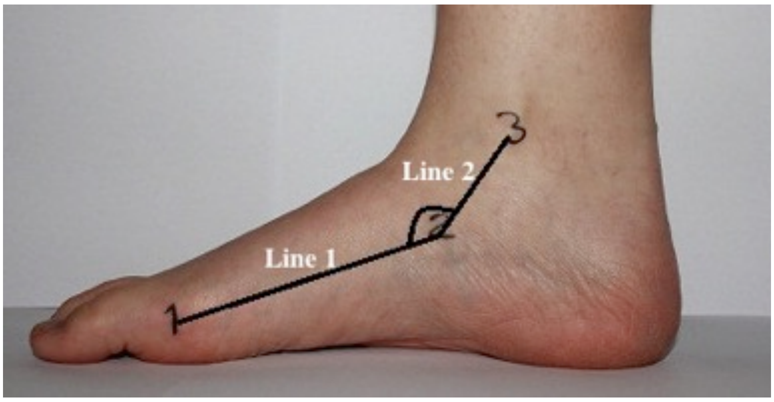

Figure 2.22. The longitudinal arch angle is obtained by line 1 (from first MPJ to navicular tuberosity) and line 2 (from navicular tuberosity to the most medial point of medial malleolus) (Nilsson et al., 2012).

v. Arch height index

Arch height index (AHI) is instep height divided by arch length (Xiong et al. 2010) as shown in Fig. 2.23. Instep height is the dorsal height at 50% of foot length. Arch length is the distance between the first metatarsophalangeal joint (MPJ) to pternion (i.e. heel bone point). AHI can be calculated as eq. [2.5].

$$AHI = {}^{IH}/_{AL}$$ [2.5]

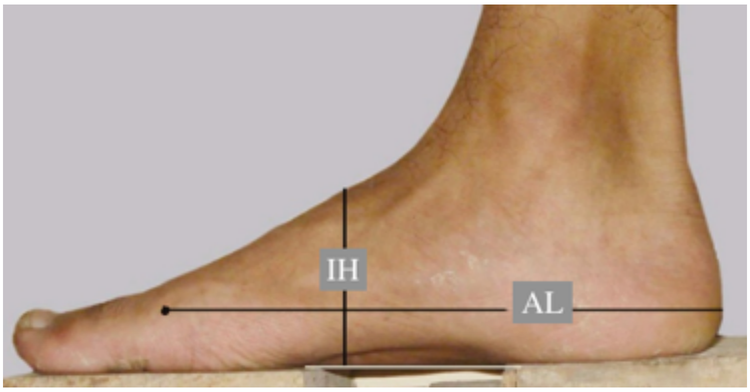

Figure 2.23. Arch height is obtained by the ratio of IH to AL (Nilsson et al., 2012).

vi. Navicular height

Navicular height (NH) is the perpendicular distance between the navicular tuberosity to the floor (Saltzman, Nawoczenski & Talbot 1995) as shown in Fig. 2.24. Normalized navicular height & Truncated normalized navicular height (Fig. 2.24) (Swedler et al., 2010; Murley et al., 2009a)

vii. Normalized navicular height

Normalized navicular height (NNH) is equal to NH divided by total foot length (Swedler et al., 2010; Murley et al., 2009a). Total foot length is from the tip of second toe to the pternion.

viii. Truncated normalized navicular height

Truncated normalized navicular height (NNHt) is NH divided by the truncated foot length (Swedler et al., 2010; Murley et al., 2009a) as shown in Fig 2.24. The truncated foot length is equal to arch length, which is the distance between the first metatarsophalangeal joint (MPJ) to pternion.

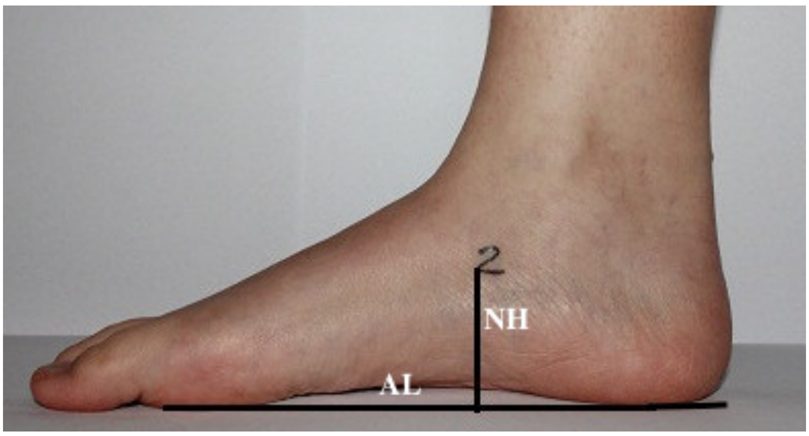

Figure 2.24. Truncated normalized navicular height is NH divided by AL (Nilsson et al., 2012).

The measurements listed above were compared to each other according to the previous studies in complexity, repeatability, and accuracy (Table 2.7). The level of complexity is determined by the complexity and the number of the tool. The repeatability refers to the intercorrelation of measures. The accuracy refers to the agreement between the measurement and the radiography.

Radiography is considered as the gold standard in foot arch assessment but the radiographic is related to radiation exposure. Moreover, the radiography equipment is cumbersome and not necessarily available in small clinics. Normally people only go to a hospital for undertaking radiographic foot arch assessment if they experience intolerable discomfort. The complexity, repeatability and accuracy of above footprint parameters and anthropometric measurements are reviewed in the Table 2.7. Compared to anthropometric measurements, footprint parameters are inevitably more complex. The traditional method of AI needs to use ink to acquire the footprint, which easily to cause stain and mess. Moreover, the calculation process is complex and time-consuming. Chu et al. (1995) introduced a digital image processing approach to improve AI so called MAI. By using foot pressure instead of footprint, MAI improved the time-consuming calculation process. However, foot volume is reported to be significantly changed causing by the change of soft tissue property due to activities (Allen et al., 2008). Although there is no study investigate the repeatability of AI and MAI, we considered the change of foot volume may affect the footprint and also affect the repeatability. Although high agreement between radiography and AI and MAI is reported, only foot length has been assessed (Saltzman et al., 1995). It is apparent that a single parameter is insufficient to represent the accuracy and reliability of the discussed indices - AI and MAI. As a result, AI and MAI are considered high complexity and low repeatability and accuracy compared to other quantitative measurements (Table 2.7).

Anthropometric measurements are normally based on angle or distance between bone's tuberosities, which is less complex than footprint parameters. Rearfoot Angle is measured by the deviation of calcaneus from lower leg. As it is measured by a simple tool such as ruler, pen and goniometer manually (Jonson and Gross, 1997), its repeatability could be low because the result can be easily affected by the drawing or reading bias as the tester's error. For now, there is no study reports the reliability and validity of rearfoot angle. As the index is not widely used, we consider rearfoot angle is low in complexity but also low in repeatability and accuracy (Table 2.7).

Longitudinal arch angle has the similar strengths and drawbacks. The drawing of longitudinal arch angle is simpler than rearfoot angle because the lines are between the prominent bony tuberosity that is more repeatable. Longitudinal arch angle is considered low in complexity and accuracy and medium in repeatability (Table 2.7). Arch height index requires the use of a steel ruler to obtain the dorsal height and arch length (i.e. truncated foot length). As a specific tool called arch height index measurement system (AHIMS) introduced by Robert et al. (2008) was implemented, the repeatability and accuracy have greatly improved (Saltzman et al., 1995). However, the measuring time and complexity has inevitably increased. Therefore, we consider that arch height index medium in complexity and high in repeatability and accuracy (Table 2.7).

Navicular height (NH) measures by the vertical distance from the ground to navicular tuberosity. Navicular height is one of the representative quantitative measurements since navicular bone is consider as the significant bone to determine the curvature of medial longitudinal arch (Franco, 1987). The repeatability is high since the measurement is relatively simple and only one parameter involved (Menz and Munteanu, 2005). The accuracy of NH is also high because it has good agreement with radiography (Saltzman et al., 1995). However, Williams and McClay (2000) pointed out that NH does not provide an accurate representation of the arch curve because it ignore the arch height in different foot lengths. Based on the value of NH, we might be misled because the same navicular height values may correspond to different arch curvature if they have different foot length. Moreover, the significant difference in NH between genders (i.e. male's NH is higher than female) makes it gender specific (Saghazadeh et al., 2015). The finding of gendered differences also support the view of Williams and McClay (2000) that the NH could be the poor representative in arch curvature. Normalized navicular height and truncated normalized navicular height were introduced to overcome the shortcomings of NH (Saghazadeh et al., 2015). By dividing NH by the foot length or truncated foot length, NNH and NNHt are more related to the arch curve. Statistical difference in NNHt between genders is not as significant as NH (Saghazadeh et al., 2015). This finding explained that NNHt could reduce the bias in cross-gender foot type classification.

NNHt could be more accurate than NNH since NNHt measure the truncated foot length that excludes the big toe, negating the bias brought by toe deformities (e.g. Hallux Valgus or Varus) (McPoil et al., 2008). Compared to NH, the repeatability of NNH and NNHt is a bit lower since there are two parameters have involved to the indices. Therefore, we considered that NNH and NNHt are both low in complexity and medium in repeatability but NNHt is considered higher in accuracy than NNH (Table 2.7).

By considering the complexity, repeatability and accuracy of each index, AHI and NNHt are identified as more suitable for the early-stage diagnosis of flatfoot because they are less complex and perform good repeatability and accuracy. NNHt would be even more suitable than AHI to characterize the morphology of MLA because NNHt measure the foot arch curvature of plantar rather than dorsum. Moreover, NNHt involves navicular bone that is the most significant bone of describing MLA from the anatomical point of view (Williams & McClay, 2000)

Table 2.7. Complexity, repeatability and accuracy of common indices for footprint and anthropometric measurement.

Index	Complexity*	Repeatability**	Accuracy+
Arch Index/Modified Arch Index (Chu et al., 1995)	HIGH • Specific tools require • The ink causes staining and may damage garments (only AI) • Time-consuming calculation process	LOW • Plantar volume can be temporarily changed (Allen et al., 2008) that may affect the footprint area. • Different foot pressure and skin property may affect the footprint	LOW • Only footprint length is assessed by radiographic measurement (Saltzman et al., 1995)
Rearfoot Angle (Jonson and Gross, 1997)	LOW • Simple tools include markers, steel ruler, and goniometer	LOW • No prominence bony landmark or quantitative method to define the bisecting lines.	LOW • No study reported its reliability and validity.
Longitudinal Arch Angle (Nilsson et al., 2012)	LOW • Simple tools include markers, steel ruler, and goniometer.	LOW • Prominent bony landmark. • Measuring the angle in 3D uneven surface affects the consistency.	LOW • No study reported its reliability and validity.
Arch Height Index (Robert et al., 2008)	MEDIUM • Specific tool (AHISM) to measure the vertical distance of dorsal highest point (Robert et al., 2008).	MEDIUM • Measure two parameters (i.e. Navicular height and foot length)	MEDIUM • High agreement to radiographic measurement in adult subjects (Saltzman et al., 1995)
Navicular Height (NH)	LOW • Simple tools include markers	HIGH • Prominent bony landmark.	MEDIUM • High agreement to radiographic

(Swedler et al., 2010)	and steel ruler.	• Measure only one parameter (i.e. Navicular height)	measurement in both adult and elder subjects (Saltzman et al., 1995; Menz and Munteanu, 2005) • Cannot give an accurate representation of the arch in different foot size (Williams and McClay, 2000)
Normalized Navicular Height (Swedler et al., 2010)	LOW • Simple tools include markers and steel ruler.	MEDIUM • Prominent bony landmark. • Measure two parameters (i.e. Navicular height and foot length)	• MEDIUM • High agreement to radiographic measurement in both adult and elder subjects (Saltzman et al., 1995; Menz and Munteanu, 2005) • Toe's deformity may affect the result (e.g. Hallux Valgus or Varus) (McPoil et al., 2008)
Truncated Normalized Navicular Height (NNHt) (Swedler et al., 2010; Murley et al., 2009a)	LOW • Simple tools include markers and steel ruler.	MEDIUM • Prominent bony landmark. • Measure two parameters (i.e. Navicular height and truncated foot length)	HIGH • High agreement with radiographic measurement in both adult and elder subjects (Saltzman et al., 1995; Menz and Munteanu, 2005)

*The complexity is considered the required time, test procedure, and tools.

**The repeatability is considered the consistency of different testers; bony landmark identification and the number of parameters has to be measured

+The accuracy is considered the agreement to radiography and other evidence or comments from previous studies.

As 3D foot scanning is considered to assess the foot arch, four quantitative measurements—Arch height index, Navicular height, Normalized navicular height, Normalize navicular height truncated, were selected because the parameters can be extracted by scanner.

Moreover, the selected measurement should be low in complexity but high in repeatability and accuracy. The detail of foot arch assessment is in Chapter 4.

2.3.3. Foot type classification

Foot type classification (quantitative assessment) uses statistical analysis to determine cut-off values between different foot types based on population norms. Three classification methods— quartile, quintile and standard deviation, are commonly used for foot type classification are detailed as following.

i. Quartile: The quantitative data is divided into four groups equally. The middle 50% is defined as normal arch and the top or bottom 25% represents low arch or high arch

ii. Quintile: The quantitative data is divided into five groups equally. The middle 60% is defined as normal arch and the top or bottom 20% represents low arch or high arch

iii. Mean ($\bar{X}$) and standard deviation (SD): Calculate the mean and standard deviation from the quantitative data as eq. [2.6] and [2.7] respectively.

$$\bar{X} = \frac{\sum_{i=1}^{n} x_i}{n} \qquad [2.6]$$

$$SD = \sqrt{\frac{\sum_{i=1}^{n}(X_i - \bar{X})^2}{n}} \qquad [2.7]$$

The values fall in the range of $\bar{X} \pm$ SD (middle 68.2%) were identified as normal arch. The values above $\bar{X} +$ SD (top 15.9%) or below $\bar{X} -$ SD (bottom 15.9%) is identified as low arch. Some studies identify the extreme case when values above $\bar{X} + 2$SD or below $\bar{X} - 2$SD as very low arch or very high arch.

Cowan et al. (1993), Chu et al. (1995) and Riskowski et al. (2013) used quintile, Xiong et al. (2010), Cavanagh and Rodgers (1987) used quartile, Nilsson et al. (2012); Jonson and Gross (1997); Murley et al. (2009a) used mean and standard deviation for foot type classification. Cowan et al. (1993) derived three foot arch indexes AHI, NH and NHH from 246 US military and used quintile method to classify low arch in the first 20% of population, normal arch in the middle 60% and high arch in the last 20%. The low, normal and high arch in AHI are defined as less than 0.21, between 0.21 to 0.27, more than 0.27 respectively, in NH are defined as less than 4.09cm, between 4.09 to 5.08, more than 5.08 respectively, in NNH are define as less than 0.15, between 0.15 and 0.19, more than 0.19 respectively (Table 2.8). Riskowski et al. (2013) used the same classification method in MAI set up the threshold for low, normal and high arch as more than 0.163, between 0.031 and 0.163, less than 0.031 respectively. Chu et al. (1995) used the same classification method in AI and set up the threshold for low, normal and high arch as more than 0.257, between 0.169 and 0.257, less than 0.169 respectively; and, in MAI are identified as more than 0.163, between 0.031 to 0.163, less than 0.031 respectively (Table 2.8). For MAI measurement, it should be noted that the thresholds of low-to-normal arch are similar to between the studies of Riskowski et al. (2013) and Chu et al. (1995) but the threshold of normal-to-high arch were greatly different. Xiong et al. (2010) measures 48 subjects' AHI, NH, NNH, AI and MAI and used quartile to classified low arch in the first 25% of population, normal arch in the middle 50% and high arch in the last 25%. Interestingly, although Xiong et al. (2010) classified higher percentage of population as low arch than Cowan et al. (1993), the thresholds of AHI (less than 0.105) and NH (less than 1.87cm) of Xiong et al. (2010) are much lower than that of Xiong et al. (2010) (Table 2.8). This might indicate that the foot arch in the study of Xiong et al. (2010) derived a lower norm. Such inconsistencies indicate the existing problems in classification's thresholds. Cowan et al. (1993) recruited the subjects in America and Xiong et al. (2010) recruited the subjects in China, i.e. ethnicity could be a factor to affect the height of foot arch. However, when we compare the threshold of low arch of MAI in these two studies, it seems quite reasonable since the threshold from Xiong et al. (2010) was smaller since they classify higher percentage of population into low arch. Again, it not only showed the threshold's inconsistency from different studies but also the inconsistency between anthropometric-based and footprint-based measurements. Another reason for the discrepancy could be the subject number. Cowan et al. (1993) recruited 246 subjects represent medium sample size while Xiong et al. (2010) only recruited 48 subjects. The insufficient sample size might have resulted in the bias when the cut-off values were defined.

Chu et al. (1995), Xiong et al. (2010) and Cavanagh and Rodgers (1987) used AI to classify foot types. Xiong et al. (2010) and Cavanagh and Rodgers (1987) used the same classification method (i.e. quartile) and found the similar cut-off values for low-to-normal arch while the considerable differences in the cut-off point of normal-to-high arch. The subject number of Xiong et al. (2010) is about half of Cavanagh and Rodgers (1987) but displayed a much higher interval of normal arch than Cavanagh and Rodgers (1987). Chu et al. (1995) used quintile that supposed to classify smaller percentage as low and high arch and more percentage in normal arch. However, the percentage of normal arch in Xiong et al. (2010) was higher than that of Cavanagh and Rodgers (1987). Murley et al. (2009a) used mean and standard deviation in AI and found low and normal arch are defined as more than 0.26 and between 0.11 and 0.25 respectively (Table 2.8). Throughout these four studies that used AI as a foot arch measurement, the cut-values of low-to-normal arch seems more similar than that of normal-to-high arch. Such discrepancy in AI could be caused by the skin movement during the measurement or the pressure applied on the plantar surface while acquiring the footprint. It seems that AI is not reliable for foot type classification.

Cowan et al. (1993), Xiong et al. (2010) and Nilsson et al. (2012) used NH as the measurement but classified the foot type by different methods. The cut-off values and class intervals were similar in the studies of Cowan et al. (1993) and Nilsson et al. (2012) but the values in the study of Xiong et al. (2010) are lower. NH can be easily affected by the foot length since a smaller foot tends to have smaller navicular height. It is unclear to as to how the higher NH reported by Cowan et al. (1993) and Nilsson et al. (2012) occurred - due to higher-arched population or just larger feet. NNH and NNHt were introduced to improve NH by displaying a more meaningful value to describe the curve of foot arch (Cowan et al., 1993; Murley et al., 2009a). However, there was only few studies used NNH and NNHt to classify for now, so the firm and consistent cut-off values have not been established for foot type classification. Nilsson et al. (2012) and Jonson and Gross (1997) both used LAA and classified the foot types by the mean and standard deviation. The cut-off values and class intervals were similar for those studies. LAA requires two straight lines from three prominent bone landmarks for obtaining the angle. The repeatability might be easily affected since it is challenging to manually draw a straight line on the uneven foot surface. Since the manual measurement took place of the 3D uneven surface, the reading angle of goniometer could also create bias.

Table 2.8. The foot type classification using 2D index in different studies

Classification method	Literature	Subject number	Measurement	Classification		
				Low arch	Normal	High arch
Quintile	Cowan et al. (1993)	246	AHI	0.14-0.21	0.21-0.27	0.27-0.34
			NH (cm)	2.72-4.08	4.09-5.08	5.09-6.05
			NNH	0.10-0.15	0.15-0.19	0.19-0.24
	Riskowski et al. (2013)	1865	MAI	>0.163	0.031-0.163	<0.031

	Chu et al. (1995)	102	AI	>0.257	0.169-0.257	<0.169
			MAI	>0.178	0.096-0.178	<0.096
Quartile	Xiong et al. (2010)	48	AHI	<0.105	0.105-0.165	>0.165
			NH (cm)	<1.87	1.87-2.81	>2.81
			AI	>0.278	0.127-0.278	<0.127
			MAI	>0.158	0.047-0.158	<0.047
	Cavanagh and Rodgers (1987)	107	AI	>0.250	0.179-0.250	<0.179
Mean and standard deviation	Nilsson et al. (2012)	254	NH (cm)	2.7-3.5	3.6-5.5	5.6-6.4
			LAA (°)	121 - 130	131 - 152	153 - 162
	Jonson and Gross (1997)	63	LAA (°)	127 - 133	134 - 150	151 – 157
			Rearfoot angle (°)	0-2	3-9	10-12
	Murley et al. (2009a)	50	NNHt	0.17-0.21	0.22-0.31	NA
			AI	0.26-0.32	0.11-0.25	NA

As 2D data may be considered insufficient to comprehensively assess or describe the foot arch in 3D, 3D data were explored by several studies aiming to improve the accuracy of foot measurement. There are three methods in 3D foot type classifications —Arch volume index (Chang et al., 2012; Meneses et al., 2002) and mean and Gaussian curvature (Liu et al. 2004).

1. Arch Volume Index

Chang et al. (2012) and Meneses et al. (2002) used 3D foot image for calculating the volume of foot and the space between the foot arch and the ground as the foot arch measurement in 3D perspective. Chang et al. (2012) investigated the dynamic change of the volume between foot arch and the ground from non-weightbearing to weightbearing for evaluating the flexible flatfoot in 3D perspective. Flexible flatfoot by definition is the foot arch is collapse (i.e. excessive pronation) in the weightbearing condition but remains neutral in the non-weightbearing condition. Meneses et al. (2002) defined arch volume index (AVI) as eq. [2.8]

$$AVI = \frac{V_0 - V_x}{V_0} \tag{2.8}$$

Where V_0 is the volume at non-weightbearing and V_x is the volume at weightbearing. When higher AVI is found, the greater foot pronation is occurred from non-weightbearing to weightbearing condition, which indicates the greater collapse of the foot arch when loaded. Foot presents larger collapse showing less ability to maintain the curve of arch under loading and its foot arch is lower. AVI is similar to the 2D index— Navicular drop (Nielsen et al., 2009). Navicular drop measures the dynamic change of navicular height from a non-weightbearing to weightbearing condition to indicate flexible flatfoot (Nielsen et al., 2009). The greater drop of navicular height in weightbearing condition, the higher possibility to acquire flexible flatfoot. AVI is claimed to be a more appropriate to characterise the function and abnormality of MLA than other 2D measurement since MLA encompasses three-dimensional movement and structure (Chang et al., 2012). However, since this method needs to determine the 'volume under foot arch', which is much more complex than determine the navicular height, it is hard to conclude that AVI is better than Navicular drop unless the repeatability of AVI is reported. Moreover, different activities can result in different levels of foot swelling, which changes the volume of foot (Winkel and Jørgensen, 1986). Soft tissue's property can be dynamically changed within a day according to the condition of the human body and such changes can also change the volume of the soft tissue (Avin et al., 2015). These might be another consideration for using AVI because the value might be affected by the soft tissue or human body conditions at measurement. Navicular drop, on the other hand, is less affected by the foot swell or the property change of the soft tissue since the measurement is based on the prominent bony landmark. The anthropometric measurements are reported to reduce the errors resulting from skin displacement and tissue distortion that can occur during measurement (Telfer and Woodburn, 2010). However, the complexity of AVI in calculation may not be appropriate for early-stage screening because it is time consuming. Furthermore, the reliability and repeatability of AVI has not been reported by any study and remain unclear.

2. Gaussian curvature

In order to investigate the shape of a given anatomical region, Liu et al. (2004) applied the curvature map on foot to present the morphology of plantar and dorsal surface. Liu et al. (2004) extracted the curvatures of the foot morphology and evaluated of prominent features on foot surface. Three types of mean and Gaussian curvature— convex, concave and saddle-shaped is be plotted in the study and the Koenderink shape index is applied to separate convexity from concavity. As shown in Fig. 2.29, there are mainly two different surface types— concave (blue) and saddle-shaped (green) at the plantar arch region (the white area is for clear differentiation of different surface types). Moreover, the Gaussian curvature on the dorsal surface consists of convex (red), saddle-shape (green) and concave (blue) areas. They successfully analysed 3D surface with a highly accurate mathematical method that is the map of mean and Gaussian curvature. However, we can clearly see that the curvature of plantar arch region is varied and much more complex in 3D space. Due to the complex limb shape and the uneven skin surface, the Gaussian curvature varies widely across the foot and hard to provide a unique identifier for different foot types (i.e. low, normal and high arch). Curvature map may not be practical for foot type classification unless the foot arch is approximated by a simpler shape. A simpler geometry is required to describe foot arch as a global shape so that a single type of Gaussian curvature shall be applied. Therefore, it is important to identify the geometrical invariant that could be used reliably and objectively for the diagnosis and/or classification of the foot arch.

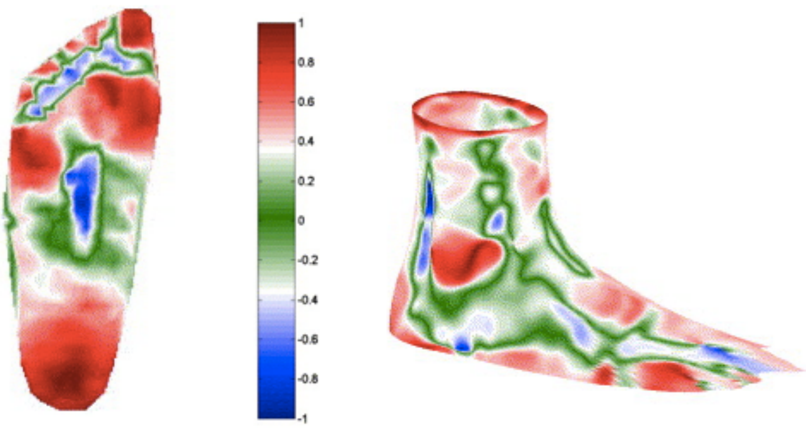

Figure 2.25. Gaussian curvature map of plantar (left) and dorsal (right) surface. Red: convex curvature; Green: saddle-shape; Blue: concave curvature; White: edge of different curvature types. The unit of Gaussian curvature is m^{-1} (Liu et al., 2004).

2.3.4. Correlation between activity levels and foot arch

Beside the measurement itself, the activities prior to the measurement could also potentially affect the outcome. Transient changes in foot have been observed in several studies reporting that prolonged sedentary activity or standing are associated with peripheral edema as volume of the lower extremities is increased (Noddeland and Winkel, 1988; Winkel and Jørgensen, 1991). Few studies reported that foot muscle fatigue affected the arch height, function and behaviour during static or dynamic conditions (Headlee et al., 2008; Cowley and Marsden, 2013). The differences that daily activities cause have effects on the capacity of foot arch support.

1. Interaction between muscle and bone

Since muscle and bone share the same mesodermal origin, the load can be transmitted between muscle and bone (Avin et al., 2015). Muscle fatigue compromises its capacity to attenuate load, which is reasonable to increase the load transmitted to the surrounding bones. Increased bone strain has been also found when the surrounded skeletal muscles are fatigued (Yoshikawa et al., 1994). In addition, the load distribution within the bone changes greatly when the muscle is fatigued (Yoshikawa et al., 1994). Furthermore, muscle fatigue can even lead to the stress fracture once the regional bone strain is excess (Milgrom et al., 2007). Based upon these findings, several studies have reported the significant change in the displacement of navicular bone when the foot and/or lower legs muscle were fatigued (Headlee et al., 2008; Cowley and Marsden, 2013; Okamura et al., 2017).

Headlee et al. (2008) utilized a pulley system to intentionally fatigue the plantar foot intrinsic muscle. After a high repetition of maximal voluntary isometric contractions of the plantar foot intrinsic muscle, the authors found a significant increment in Navicular drop. Navicular drop measures the changes between the navicular height in non-weightbearing and weightbearing condition. The increased navicular drop represents the more foot pronation occurs, which is less capacity in foot arch support.

This finding is supported by the study of Cowley and Marsden (2013), who reported reduced navicular height and change in foot posture index after a half marathon run. The results also indicate that foot has more pronated position in fatigue stage. However, Okamura et al. (2017) observed an increase in navicular height after performing an intrinsic foot muscle fatiguing protocol similar to Headlee et al. (2008). It seems contradictory to the previous two studies, but it can be rationalized by the foot core paradigm (Fig. 2.2) explained by McKeon et al.

(2014). Okamura et al. (2017)'s protocol specifically targeted the abductor hallucis (AH) through isolated flexion of the first metatarsophalangeal joint (MPJ). AH muscle is the largest intrinsic foot muscle and act as a primary mover but is less involved in static foot posture maintenance. Flexion at first MPJ primarily recruits the AH and flexor hallucis brevis (FHB). This may allow other muscles involved in arch maintenance to adequately compensate for the fatigued AH and FHB muscles, which might contribute to an increase of arch height. From these studies, although it remains unclear whether the foot arch height is increased or decreased in the foot muscle fatigue stage, we speculate that different levels of human activities can result in change of foot arch measurements.

2. Creep of Connective tissue

In addition to muscle, collagenous tissue also plays an important role in maintaining MLA. Collagenous tissue is a viscoelastic material prone to creep (Whiting and Zernicke, 2008). Creep describes a temporary short-term elongation of viscoelastic material that occurs under constant or repetitive loading. The constant or repetitive loads applied to viscoelastic materials can cause a decrease in tension and a gradual increase in deformation. Maganaris and Paul (2002) concluded that constant and repetitive load can result in elastic deformation according to their force-elongation data. Lavagnino et al. (2014) investigated patella tendon length before and after cyclic eccentric loading to failure and found that tendon length increased significantly immediately after and 24 hours after exercise. These studies found that the load-depending characteristics of collagenous tissue, its dimensions and stiffness can be affected by weight bearing activities. The collagenous tissues in the feet are also susceptible to creep following constant or high repetition loads is applied (e.g. long standing, walking, running, jumping). This phenomenon may contribute to transient changes in foot morphology. Therefore, this could be the second reason that we suspect that the different activities prior to foot arch assessment can result in different values in MLA measurement.

3. Fluid retention

Different activities may also influence muscle properties such as water content that can contribute to the change of foot volume. An individual's foot volume change over several hours depending on their activity levels (Winkel and Jørgensen, 1986; Noddeland and Winkel, 1988). Winkel and Jørgensen (1986) immobilized one foot and lower leg while the other was allowed to freely move in an 8-hour prolonged sitting condition. They reported that the 8-hour swelling averaged 5.7% and 2.7% in the inactive and the active foot, respectively. The mechanism of foot swelling is explained as an increase in interstitial fluid and vascular distention (Winkel and Jørgensen 1986). For other studies analysing foot and lower leg volume changes in people's work nature, Noddeland and Winkel (1988) reported intermittent activity between static bouts can reduce the amount of swelling compared to the work involving prolonged standing. Bao and Lin (2018) investigated the muscle fatigue and foot swelling in alternative sit and stand for office workers. They found that office workers that spent more time standing than sitting had lesser foot swelling. Evans and Ratchford (2016) explained that there is a drop-in pressure that hinders venous return after blood is actively pumped to the lower extremities. Calf muscle contraction can assist in venous blood return through the calf muscle pump, but this mechanism is underutilized in sedentary individuals (Evans and Ratchford, 2016). Therefore, prolongedly inactive tissue can increase in fluid retention which brings about the increment of foot volume. When the changes in foot volume can be a consideration to MLA measurement since several foot arch assessment indices rely on the area of the foot plantar (i.e. footprint area)— arch index, footprint index, arch (footprint) angle, arch-length index, truncated arch index and Brucken index (Razeghi and Batt, 2002).

4. Muscle temperature

Another main factor contributes to the change of foot morphology and/or posture could be the muscle and skin temperature. The activity level (i.e. sedentary and active) can result in different skin temperature of the foot and lower limbs (Noddeland & Winkel, 1988). The reduction of skin temperature (2 to 3˚C) has been found in the less-active feet (Noddeland & Winkel, 1988). The reduction of the soft tissue's temperature is reported to decrease the nerve-conduction rate and muscle force production (Bishop, 2003). Therefore, nerve conduction and force production are two important temperature-related mechanisms that might occur during transient change in foot morphology and posture.

5. Neuromuscular condition

Since foot arch is actively supported by muscles controlled by the central nervous system, foot morphology and foot posture could be affected if the normal nerve conduction of is impeded. Fiolkowski et al. (2003) reported that the anaesthetically inhibiting nerve signals to the intrinsic foot muscles can result in a significant change in MLA, pi.e. neural control plays an important role for maintaining foot posture in weight-bearing. A reduction of muscle temperature decreases the nerves' transmission speed by increasing the duration of action potential propagating along the muscle fibres (Noddeland & Winkel, 1988). As reduced muscle temperature is reported in less-active individual's feet (Noddeland & Winkel, 1988), this suggests that the individual's feet were less able to maintain the foot morphology and posture resulting in more changes of anthropometric values than more actively individual. In the contrast, the increased muscle temperature is reported to improve central nervous system function and increase the transmission speed of nervous impulses (Karvonen, 1992). It may also mean that individual with higher activity level could result in less change in the foot morphology and foot posture. The above assumption is based upon avoiding any moderate or vigorous-intensity physical activities (e.g. running, jogging, dancing) that could induce muscle fatigue prior to the foot arch measurements.

Secondly, the force production is also an important temperature-related mechanism. The increased isometric and dynamic force production have been found after warm-up routines prior to exercises (Bishop, 2003). It seems that the more-active individuals are able to create more force to maintain the foot posture than the less-active individual. In contrast, reduced muscle temperature is reported to decrease the capacity of muscle fibre in force production (Rome et al. 1984). The reduction of force production caused by the muscle fatiguing exercise is strongly linked to altered MLA height (Headlee et al., 2008; Okamura et al., 2017). From the findings above, it seems that larger changes in MLA would be found in the less active feet since the force production is decreased. However, Okamura et al. (2017) found that the fatigue and less force producing feet muscle has the higher MLA. Okamura et al. (2017) explained that a reduced force output of foot muscle might be compensated for by other muscles to increased MLA in weight-bearing conditions (i.e. standing and walking). In addition, Pohl et al. (2010) also reported other muscles can compensate for the lack of force production of foot muscles to maintain foot kinematic during walking. From the contrary results the studies of Okamura et al. (2017) and Pohl et al. (2010), it is unknown whether the MLA height increases or decreases by reducing the force production. But it still seems that the less force production feet muscle might cause larger transient changes in foot morphology and foot posture maintenance that could further affect the values of the measurement. It could be summarized that the different activities change the mechanism to support foot arch. However, it is unclear whether human activity of daily living could affect the results of the foot arch measurements. If the outcome of measurement could be affected by the activity levels, certain control protocol needs to be implemented.

2.3.5. Assessment limitations

The most commonly used indices of quantitative measurement— arch index, modified arch index, rearfoot angle, longitudinal arch angle, arch height index, navicular height, normalized navicular height and normalized navicular height truncated, have been reviewed in the current study and limitations identified.

1. Low level of agreement between foot type classifications

Swedler et al. (2010) examined the correlation between visual assessment and a quantitative measurement - Navicular Height (NH. They found a poor agreement resulting in a higher proportion of inconsistences when identifying foot types. It is difficult to explain the origin of this discrepancy in the absence of the full data set, but it is likely to be caused by the subjective nature of the visual threshold definition and testing protocols. The foot type classifications determined by NNHt has the potential 54.4% overlap area between low and normal arch, and 77.7% overlap between normal and high arch. This substantial overlap indicates large proportion of type 1 (i.e. wrongly identifying flatfoot as normal arch) and type 2 errors (i.e. wrongly identifying normal arch as flatfoot) in current method.

2. The inconsistency of classification thresholds between studies

For the statistical analysis of continuous variable, quantiles or the mean and standard deviation are commonly used. However, there is no clear statistical approach in previous studies. Some studies used quartile (Cavanagh and Rodgers, 1987; Xiong et al., 2010), some used quintile (Chu et al., 1995; Cowan, Jones and Robinson; 1993), and some used the mean and standard deviation (Murley et al., 2009a; Jonson and Gross; 1997; Nilsson et al., 2012). Therefore, it is hard to have identical cut-off points in each measurement to identify flatfoot (Table 2.9). Thus, an identical statistical method is needed for foot type classification. Furthermore, in the research of flatfoot and injury risk or musculoskeletal problems, adopting different cut-off points could affect the result. Thus, an identical statistical method is needed for foot type classification. We consider that quartiles or quintiles are to divide the population samples into groups regardless their data distribution. The mean and standard deviation is used to provide conjunction and summarize continuous variables for presenting the more representative idea of data distribution which provide the more reliable cut-off values.

Table 2.9. Cut-off values of Truncated Normalized Navicular Height from different studies are different.

	Flatfoot	Normal arch	Pes cavus
Cowan et al. (1993)	< 0.15	0.15 – 0.19	> 0.19

Murley et al. (2009a)	< 0.21	0.21 – 0.31	NA
Xiong et al. (2010)	< 0.33	0.33 – 0.37	> 0.37

3. Inconsistency between different quantitative measurements

Chu et al. (1995) and McCrory et al. (1997) studied the agreement between footprint based (i.e. arch index and modified arch index) and anthropometric based measurements (i.e. navicular height and normalized navicular height). Chu et al. (1995); McCrory et al. (1997) used arch index (AI) and modified arch index (MAI) to indicate normalized navicular height (NNH). The correlation coefficient of AI and NNH, MAI and NNH are both nearly 0.70, which is in between 0.68 to 1.0 that generally is considered strong or high correlation (Taylor 1990). However, Taylor (1990) argues that the correlation coefficient is less meaningful unless it could be interpreted properly. In Fig. 2.26, we still can clearly see that people with the similar AI can be significantly different in NNH values and vice versa. This finding shows an arch could be classified as low arch in one index but normal arch in the other index.

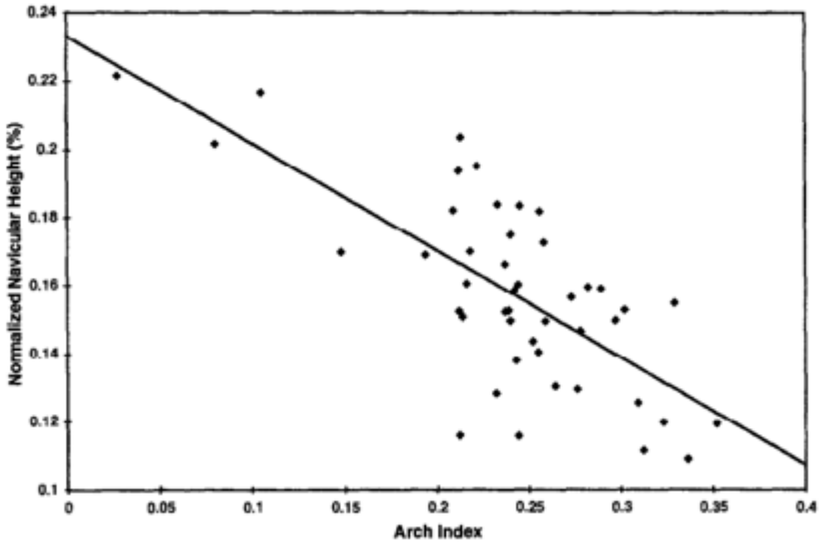

Figure. 2.26. The relationship between arch index and Normalized navicular height (McCrory et al., 1997)

4. By nature, clinical indices are 2D, which does not fully reflect the 3D arch shape and no 3D index is used for low arch/flatfoot diagnosis.

Foot arch consists of medial and lateral longitudinal arch and transverse arch, moves in three planes— sagittal (i.e. dorsiflexion and plantarflexion), frontal (i.e. eversion and inversion) and transverse (i.e. adduction and abduction) plane. Predominantly foot arch assessments utilise 2D information byapplying foot morphology to plane projections (Chang et al., 2012). Literature show a large variation on the estimated flatfoot prevalence from 0.7% to 16% of young adult by 2D projection assessment (Çilli et al. 2009; Tenenbaum et al. 2013). The assessment in these studies (Çilli et al. 2009; Tenenbaum et al. 2013) assessed the 3D objects by partial 2D plane which is not mathematically unique and reversible process leading to the problems outlined above. In a study of Swedler et al. (2010), a low agreement and substantial mismatch was reported between two 2D measurements based on different views of the foot.

The current practices only measure the parameters on a single foot-projected plane, which is hard to represent the whole 3D foot arch shape and structure. For example, normalized navicular height (NNH) considers parameters solely on the medial side of sagittal plane. When two different feet have the same arch length (the distance between the 1st MPJ to pternion) and navicular height that makes them have the same NNH. However, it does not mean they would have exactly same foot breadth or distance between the 2nd, 3rd, 4th, or 5th MPJ to pternion, which make the foot arch structure completely identical. Moreover, arch index (AI) and modified arch index (MAI) rely on the plantar contact area to indicate the foot arch structure. For the non-contact area, we have no way to predict the height of the arch, which cannot present the foot arch structure in 3D. This could be a reason to cause the low correlation between the measurements that based on the different projective plane's parameters (e.g. AI/MAI and NNH). These findings further emphasise that 2D measurement is insufficient to reflect the complexity of the foot morphology in 3D.

The 3D measurements mentioned above provide the methods and ideas to improve current 2D measurements by utilizing the 3D data. Theoretically, 3D measurements should be more precise for describing foot morphology since it recognises that the foot arch is structured in a 3D-plane. However, there is no study confirming that the 3D is more reliable and accurate than 2D measurement.

AVI measures the change of the volume under the arch from non-weightbearing to weightbearing (Chang et al., 2014). By observing the change of volume indicating the foot motion, the foot types could be determined as more excessive in foot pronation represents lower foot arch. The only concern is the foot volume can be easily affected by the activity prior to the measurement or the dynamic change of the soft tissue's conditions. It could be improved if the measurement was based on simpler geometry based on the anatomical landmark of foot arch. In this way, it might reduce the effect brought by the skin of the plantar surface. However, what geometry could be used reliably and objectively for the diagnosis and/or classification of the foot arch is still an open question. Mean and Gaussian curvature map can precisely capture the curvature of the foot arch in 3D space and classify the curvature into three different types— convex, concave and saddle-shaped. Like AVI, curvature map captures the feature on skin that could be easily affect by the changing of foot volume or skin's condition. Moreover, the curvature types were varied across the arch regions of plantar surface that fails to generate a valid identifier for foot types. Therefore, a simpler geometry based on the anatomical landmark of foot arch could be also beneficial in applying the same type of curvature map. And the curvature of the foot arch could be compared by the values of the curvature. Although none of the 3D measurement mentioned above provided a valid identifier for flatfoot, they provide us the initial ideas in measuring foot with 3D data and describe the foot arch more precisely in 3D realms.

4. Other measurement inaccuracy

(A) Tester's experience affects the accuracy

Most of foot arch measurements require palpation for neutralizing the subtalar joint to make sure the foot was measured in a neutral position. Most measurements (except for AI and MAI) also required palpation for identifying the skeletal landmarks. The experience of the tester could bring the effect on the precision of palpation. According to Williams and McClay (2000), the correlation coefficients for two physiotherapists in different experiences (3 vs. 20 years) of five parameters were low. The lowest one was only 0.48, i.e. experience could be a factor to make the result inaccurate. Different testers could result in the inconsistent cut-off values. Some studies had large samples (e.g. 1865 subjects in the study of Riskowski et al. (2013)), it is hard to measure every subject by one tester. If there was more than one tester in such study, the palpation difference could happen to affect the research outcome.

(B) It is unclear whether one foot is sufficient for classify foot type

In foot research, data is usually collected from both feet. Similar to some other study involve bodypart such as knee, hand, shoulder, etc, there is a significant issue that should we each foot as an individual data or choose one foot from a subject to analyse. The former measurea 'foot' as unit that can pool the data from left and right foot. It could be beneficial to the researcher since the data has been double to increase the sample size as well as the statistical power of the study. Williams & McClay (2000) used 'foot' as measurement unit instead of using 'subject'. The later one consider the 'subject' as the unit of mearsurment, which chooses the either right or left foot, dominated foot, or random foot selection to represent a subject.

However, Menz (2004) has reported that analyzing foot as an unit rather than subject as an unit can cause some conceptul and statistical problems in interpreting the results of the study. By measuring foot as a unit, it violates the independence assumption of statistical analysis. It also tends to make the value of 'significant differences' and 'correlation coefficient' unreliable or spurious (Menz, 2004). It has been reported that the correlation coefficient of two sets of data can be increased by measuring five pairs of data from the same subject. Menz (2004) added that in certain situation it might be acceptable analysing foot as a unit. Some symptoms (e.g. arthritic degeneration in the first metatarsophalangeal joint) caused by structural characteristic such as joint's ROM could be specific to the individual body part. In such case, some important characteristic or factors might be missed out if we randomly measure left or right foot to represent an individual.

The current study investigates the foot arch height of individual and the arch height could be different between person's feet. The arch height differences have been reported in right and left foot and the dominate foot tends to be higher than another (Saghazadeh et al., 2015; Zifchock et al., 2006). However, it is unclear whether such difference is sufficient to show statistical differences and left and right foot should be analyzed separately. From the anatomical point of view, human body is not completely symmetric. It is not uncommon for feet to have different size. People might flatfoot in one side but normal arch height in the other. Therefore, it might be inappropriate to randomly measure a foot of a person and to claim his/her is flatfoot or not. Cowan et al. (1993) only used right foot to determine the foot type of the subject and analyzed the relationship between arch types and injury risk. It might not be the best scenario since left foot of the subject might let him to be classified into different foot types and affect the accuracy of the result. Therefore, for most of the cases, it is not a good idea to merely measure the single foot from a random selection or use dominant foot to represent the foot type of an individual

(C) Activities prior to the arch measurement tend to affect the outcome but no further investigation

There is an aspect has yet to be investigated by previous study is whether different activity levels prior to the measurement could affect the result. Activities can lead to certain level of change in the muscle capacity and property that contribute to the change in foot morphology. However, no study investigated if such transient change in foot morphology could affect the result of the measurement. If the transient change is sufficient to affect the result, we shall develop a scenario to control the timing and activity level prior to the foot arch measurement.

2.4. Shoe insole

2.4.1. Type and function of shoe insole

Shoe inserts is one of common treatment for individuals with symptomatic foot arch deformities such as flatfoot or pes cavus. Shoe inserts were classified into rigid, semi-rigid and soft. The studies reported a noticeable success in the mitigation of symptoms and reducing pain caused by flatfoot (Franco, 1987; Noll, 2001; Banwell et al., 2014). By the definition written in ISO 21064:2017— shoe inserts— uses, functions classification and description, are the device that covers the whole or the part of the foot intended to address the effect of neuromusculoskeletal impairment (International Organization of Standardization [ISO], 2017). Australian Inserts Prosthetic Association (AOPA) states that shoe inserts are effectively used for certain foot problems such as flatfoot (low-arched foot or flatfoot), pes cavus (high-arched foot), rheumatoid arthritis (an autoimmune disease brings in joint destruction, pain, deformity, and functional disability) and osteoarthritis (a degenerative condition of cartilage on joint surfaces and cause pain during joint movement) (“Clinical specialties in inserts and prosthetics”, 2020). According to the purpose of the users, there are two main types of shoe inserts: functional and accommodative. Different types of inserts are made of different materials and provides different levels of arch support to the user. Functional shoe inserts are used to adjust the subtalar joint that is to adjust the level of pronation and supination and used to change the foot biomechanics. Accommodative inserts minimize the changes to foot function while providing relief and protection to specific plantar areas to enable the user to walk and stand without pain (Lee et al., 2012; Chang et al., 2014; Baxi et al., 2019; Ratki et al., 2017). Both are prescribed to correct the foot position and reduce the pain or symptoms.

Accommodative shoe inserts aim to relieve the excessive plantar pressure from a painful or injured area (figure 2.27). Lee et al. (2012) used accommodative shoe inserts to improve plantar fasciitis. Chang et al. (2014) used accommodative shoe inserts to improve metatarsalgia by changing the plantar pressure distribution. Although the plantar pressure distribution can be changed by lower arch or flatfoot (Franco 1987; Chuckpaiwong et al., 2008), a literature search revealed no publication on the use of accommodative shoe inserts for flatfoot. Accommodative shoe inserts can be made of a wide range of material to create the pad and cushion for relieving the excessive plantar pressure. Less dense materials such as cork, foams, leather and rubber are the commonly used by accommodative shoe inserts to absorb shocks and adjust plantar pressure distribution to enable the users to stand and walk without pain. Compared to functional shoe inserts, accommodative shoe inserts are softer and more flexible. Accommodative shoe inserts can be easily made in the clinic by moulding directly from the user's feet or through a positive mould of the user's foot. It can be easily adjusted in shape to fit the user's foot and his footwear. However, accommodative shoe inserts are made of soft and mouldable material are not as durable as rigid functional insert because they can be compressed permanently (Janisse & Janisse et al., 2018). It may be beneficial for short-term usage, but it may need frequent adjustments or be repaired or replaced to function continuously (Baxi et al., 2019). Accommodative inserts are useful in the treatment of diabetic foot ulcerations (Ratki et al., 2017) and some of neuropathic and dysvascular feet (Baxi et al., 2019) by reducing the overall plantar pressure. However, accommodative insole may be less effective in changing the joint kinematic and supporting the fallen arch compared to functional insoles (Banwell et al., 2014; Murley et al., 2009c; Cunningham, 2008).

Figure. 2.27. Accommodative shoe inserts (Accuthotix, 2017)

Functional shoe inserts support foot position that is the position of subtalar bone and the motion of subtalar and ankle joint (i.e. the level of pronation and supination). They are used to correct the abnormal lower extremity function, prevent injury, relieve pain and symptoms and treat foot pathology such as foot instability, osteoarthritis, flatfoot (Slattery & Tinley, 2001; Esteves et al., 2019). Functional shoe inserts are commonly firmer and less flexible than accommodative shoe inserts and can be basically divided in two main types: rigid and semi-rigid, depending on their flexibility and support. Rigid functional inserts are made to maximally to adjust or correct the motion and position of the foot during gait. Chalmers et al. (2000) used rigid functional inserts to prevent the excessive pronation of flatfoot/flatfoot and decrease the loading on the forefoot; Woodburn et al. (2002) used it to relieve the pain on forefoot and rearfoot; and Budiman-Mak et al. (1995) applied it to reduce the risk of foot deformities such as hallux valgus. Rigid functional inserts are made with firmer material that has minimal flexibility. The rigidity can be adjusted by the thickness of the material and its intrinsic rigidity of the material, the size of the inserts according to the user's weight and the degree of instability of their foot (Prolab inserts, 2009). Rigid functional inserts enable feet to move properly during all phases of gait and prevent abnormal compensation and high injury risked or pathological positions (Banwell et al., 2014). Rigid functional shoe inserts are relatively thin and fit into most shoes compare to semi-rigid functional inserts and accommodative shoe inserts. Some rigid inserts are only two-third or half of the foot length because they are only to support the foot arch or the correct position and motion of the subtalar joint (Figure 2.28). The advantages of rigid functional shoe inserts are that they are comparatively durable than accommodative shoe inserts, so they don't need to be repaired or adjusted frequently, and since they are thinner than accommodative shoe inserts, they are more likely to fit into all the user's shoes. However, their advantages could be their disadvantages as they are relatively firm and less cushiony so the users might be difficult to adapt. Unlike rigid shoe inserts, accommodative once can be easier to adjust according to the feedback of users or the observation of the doctors. For example, accommodative shoe inserts could be adjusted by trimming the insole edges or attaching the additional materials or layers to absorb shocks.

Figure 2.28. Rigid functional shoe inserts (Prolab inserts, 2009)

Semi-rigid functional shoe inserts are used to partially control abnormal motion and position of the foot and leg during gait, such as excessive medial displacement of subtalar bone or excessive navicular drop in weight bearing (Eslami & Ferber, 2013) and foot excessive pronation in gait cycle caused by flatfoot (Banwell et al., 2014; Ibuki et al., 2010). The rigidity and flexibility of semi-rigid shoe inserts are between accommodative inserts and rigid functional inserts. Semi-rigid inserts are made from the materials that display moderate rigidity or flexibility in weight bearing condition. The rigidity and flexibility of the inserts can be controlled by material thickness, the inserts size, or the intrinsic rigidity of the material according to user's different bodyweight and the level of the foot instability (Prolab inserts, 2009). Semi-rigid inserts may share some similarity from accommodative shoe inserts and rigid functional shoe inserts (figure 2.29). They can be designed for user to accommodate the painful plantar area. The inserts could be mixed with different materials and to have a softer and more flexible pad to alleviate the impact at the heel or the metatarsophalangeal joints, where the peak plantar pressure normally occurs due to foot strike or toe-off in gait cycle (Hessert et al., 2005). Semi-rigid inserts can also have a firmer material to cover the medial longitudinal arch to correct the excessive foot pronation (Eslami & Ferber, 2013; Banwell et al., 2014; Ibuki et al., 2010).

In summary, accommodative insole is used to provide cushioning and shock absorption during gait, which is more effective in pain relief (Cunningham, 2008). Functional insole, on the other hand, is used to achieve weight bearing realignment of the lower extremity and to redistribute the load during gait (Banwell et al., 2014; Murley et al., 2009c). A more flexible deformity of a foot requires a more rigid inserts to support while a more rigid deformity of a foot requires a more flexible inserts to help it absorb or attenuate the impact or shock. Rigid shoe inserts are normally combined with ankle inserts to treat people with foot-ankle instability (Schmalz et al., 2006; Young & Jackson, 2019).

Figure. 2.29. Semi-rigid functional shoe inserts (Elite inserts, 2015)

2.4.2. Foot/ankle biomechanics on insole

Shoe inserts re-establish the skeletal alignment and improve the compromised force transmission and dissipation caused by fallen arch. A systematic review study reported a noticeable success for rigid and semi-rigid functional insole in improving physical function and energy cost during walking but low-level evidence in immediate pain relief (Banwell et al., 2014). However, few studies reported that arch-supporting insole is effective in mitigating symptoms and reducing pain by reducing the excessive plantar pressure induced by flatfoot (Franco, 1987; Noll, 2001). Arch-supported insole also prevents lateral column metatarsal stress fractures by reducing the peak pressure on the medial side of the foot (Chuckpaiwong et al., 2008).

Figure 2.30. Before and after the correction made by shoe inserts for flatfoot (lateral view)

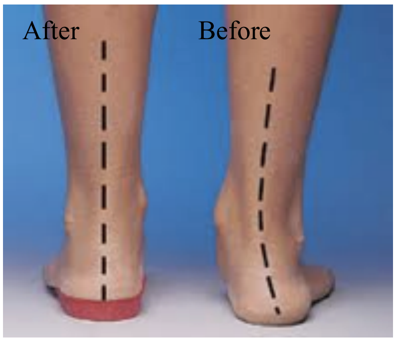

Figure 2.31. The correction by shoe inserts for flatfoot (posterior view)

Shoe inserts change the kinematic and kinetic in human's gait including joint's motion angle and moment (Urabe et al., 2014), centre of pressure (COP) excursion (Aboutorabi et al., 2015), plantar pressure distribution (Ledoux & Hillstrom, 2002), ground reaction force (Cornwall & McPoil 1992), muscle activity (Murley et al. 2010) and total energy expenditure (Karimi et al., 2013).

- **COP trajectory**

The studies demonstrate that people with flatfoot have a significantly medial deviation of COP during walking, and COP (i.e. displacement) is increased (Aboutorabi et al., 2015; Wong et al., 2008). In a review study, arch-supported insole decreased total COP mediolateral displacement for flatfoot indicating the decreased ROM of hindfoot eversion and inversion (Aboutorabi et al., 2015). Aboutorabi et al. (2014) reported COP mediolateral displacement has decreased from 6.55 ± 7.28mm to 5.87 ± 6.40mm by arch-supported insole for flatfoot. Compared to no insole, the insole increased the lateally directed COP as the indication of deceased hindfoot eversion.

- **Plantar pressure distribution**

Larger plantar pressure is present on the medial side of the foot, i.e. medial side of calcaneus, first and second metatarsal heads, hallux for flatfoot (Franco 1987; Ledoux and Hillstrom, 2002) because the foot arch is collapsed. Shoe inserts can direct the plantar pressure under first metatarsal head toward second to fifth metatarsal by elevating the fallen MLA (Albert and Rinoie, 1994). The excessive strain of plantar fascia can be absorbed by the shoe insert (Hodge et al., 1997).

- **EMG activation**

As flatfoot increased the EMG activation in tibialis anterior and tibialis posterior and decrease the activation in peroneus longus during stance phase, foot orthoses further increased the EMG activation of tibialis anterior and peroneus longus and may alter the muscle activity of lower back (Murley et al., 2009c). Furthermore, increase duration of tibialis anterior EMG activity was recorded following heel strike in shoe inserts condition (Tomaro and Burdett, 1993). This finding explained the muscle activity of flatfoot can be brought towards the pattern observed with normal-arched participants during the stance phase by shoe inserts.

- **Arch energy return and energy expenditure**

Kelly et al. (2015) reported the decrease of magnitude of arch recoil and the energy returned can be inevitably decreased when arch-supported insole applied. Stearne et al. (2015) also reported restricted arch compression when arch-supported insole applied (from 6.7± 4.1mm to 0.7± 4.8mm) followed by a decreasing in the elastic energy returned from the arch. Otman et al. (1988) reported that oximetry indicated that the use of insole for flatfoot decreased the energy consumption based on. Karimi et al. (2013) reported the similar result based on physiological cost index (PCI) based on heart rate monitoring [eq. 2.9]. As shown in Table 2.9.1, flatfoot increased the walking heart rate and decreased the walking speed leading to increased energy expenditure. Shoe insole facilitated increase in the walking speed and decrease the heart rate resulting in the significant reduction in energy expenditure.

$$PCI = {}^{THB}/_{walking\ speed} \qquad [2.9]$$

$$THB = Walking\ heart\ rate - resting\ heart\ rate$$

Table 2.9.1. Walking speed, PCI and THB for normal arch, flatfoot with and without insole.

	Walking speed (m/min)	PCI (beats/min)	THB (beats/min)
Normal arch	69.16 ± 11.85	0.36 ± 0.08	1.58 ± 0.27

Flatfoot without insole	67.44 ± 10.24	0.37 ± 0.07	1.60 ± 0.21
Flatfoot with insole	69.14 ± 11.43	0.32 ± 0.10	1.58 ± 0.23

Landorf and Keenan (2000) observed that most of the studies found an increase in oxygen consumption and energy expenditure when wearing insole for walking, running, and cycling because it brings the additional weight to the lower limbs. Rodrigo-Carranza et al. (2020) reported additional 100g per shoe increased the energy cost and compromised the running economy without changing the gait patterns and neuromuscular variables. Therefore, the insole for flatfoot is suggested as light as possible and not to exceed 100g per insole.

- **Joint kinematic in gait**

Insole with arch support function stabilizes the foot arch and the calcaneus by mitigating the excessive hindfoot eversion (Urabe et al., 2014). Studies showed that over-pronation and excessive rearfoot eversion can be reduced by foot orthoses for flatfoot in static position (Leung et al. 1998; Kido et al., 2014; Banwell et al., 2014). According to Han et al. (2019), peak rearfoot eversion/inversion and rearfoot ROM are significantly reduced by arch-supported insole compared to non-supported one for flatfoot. As the reduced the total eversion ROM was found in flatfoot during stance phase compared to the normal developed foot (Hösl et al., 2014). Arch-supported insole may further restrict the ROM of rearfoot eversion and the chain reaction kinematic (e.g. knee, hip, trunk, etc.). Less rearfoot eversion (reduced 2 degrees on average) was observed when foot orthoses are worn (Desmyttere et al., 2018) potentially resulting in less tibial internal rotation in stance phase (Telfer et al., 2013). McPoil & Cornwall (2000) reported both rigid and flexible orthoses has significantly reduced the magnitude of internal tibial rotation, which relatively increased the peak knee external rotation angle during mid stance. Nester et al. (2003) reported foot orthoses with medial wedges to significantly alter pelvis gait kinematics. Flatfoot with insole brought the pelvis in a more anterior tilted position and slightly decreased the ROM across the gait cycle when compared to no insole (Nester et al., 2003). Moreover, the hip internal rotation was increased along with the increased pelvis transverse plane motion during stance phase when the insole was applied (Nester et al., 2003). The reduced arch compression and recoil reported by Kelly et al. (2015) and Stearne et al. (2015) may be attributed to the decreasing rearfoot ROM due to arch-supported insole.

Table 2.9.2. Rearfoot average ROM in the comparison of normal foot, flatfoot, with non-supported insole, with arch-supported insole.

Average ROM	Hösl et al. (2014)		Han et al. (2019)	
	Normal foot	Flatfoot	Flatfoot with non-supported insole	Flatfoot with arch-supported insole
Rearfoot eversion (°)	8.1± 3.8	6.3± 2.6	5.40± 4.10	2.89± 3.10
Rearfoot inversion (°)	16.0± 4.1	14.4± 3.8	–6.00± 4.10	–4.70± 3.20

- **Joint kinetic in gait- ankle joint moment**

Insole with arch support has been reported to reduce the peak hindfoot eversion and evertor moment in during walking and running gait (Leung et al. 1998; Kido et al., 2014; Banwell et al., 2014). As Han et al. (2019) reported less rearfoot ROM for flatfoot with arch-supported insole compared to non-supported insole, significantly smaller peak evertor moment (arch support: 0.17±0.10Nm/kg; control: 0.25±0.10Nm/kg) and inverted moment (arch support: 0.05±0.10Nm/kg; control: 0.07±0.10Nm/kg) were also found in the same study. McPoil & Cornwall (2000) also reported the insole has significantly reduced the moment of knee internal rotation. However, no statistically significant difference was found between with and without insole by Desmyttere et al. (2018).

- **Joint kinetic in gait- GRF**

Han et al. (2019) reported significantly smaller GRF on the medial-lateral vector when arch-supported insole was applied to flatfoot in the stance phase. This finding corresponds to decreased ROM and moment of hindfoot and the decreased of COP mediolateral displacement when flatfoot with insole. Moreover, Han et al. (2019) also reported the timing of peak mediolateral GRF was different between flatfoot with and without insole. The results of the study of Miller et al. (1996) demonstrated significant vertical GRF reduction and reduced anteroposterior GRF in loading response and midstance phase.

2.4.3. Traditional insert manufacturing

Conventional approach to fabricate the personalize shoe inserts is to make the initial plastic cast of the person's feet (Weatherwax et al., 1981; Kennedy et al., 2004). After that, material sheet is placed on the plantar surface of the cast for the heating process to make the personalized shell of the insole. Normally some examinations including users' static posture, movement in gait, static or dynamic plantar pressure distribution, or joint's passive and active ROM, are needed to assess the arch motion and shape before the cast is made (Weatherwax et al., 1981; Kennedy et al., 2004). Different techniques for foot model casting have been used including neutral suspension casting (Carroll et al., 2011), plaster slipper casting (Weatherwax et al., 1981), synthetic sock casting, impression foam casting (Kennedy et al., 2004). Depending on the insert and the need of the patient, the foot shape can be obtained in user's non-weightbearing (i.e. supine or lying position), half-weightbearing (i.e. two legs standing) or full-weightbearing position (i.e. single leg standing position). Sometimes, users' current shoe inserts or footwear also need to be reviewed to make the shoe inserts fit the footwear. Sometimes the accommodative shoe inserts are bulky, so the footwear needs to be half size larger.

2.4.4. Traditional insert material

As there are three main types of shoe inserts: functional rigid, functional semi-rigid, accommodative according to the purpose of the users, the use of the materials is varied in the wide range of rigidity and flexibility (Franco, 1987; Noll, 2001; Banwell et al., 2014). The choice of material could be also determined by some user's considerations such as body weight, foot size or foot stability. The materials need to be biocompatible and do not cause any allergic reaction to user because the shoe inserts have the close contact to human's skin. They are also more likely to be wear for a long period of time, so whether the materials are comfortable or fabric breathable or perspiration and moisture resistant need to be considered. The materials used for shoe insert need to be compliant with the national or world-wide safety regulation such as International Organization for Standardization known as ISO. There are 11 ISO regulations (ISO 20535:2019, ISO 20866:2018, ISO 20867:2018, ISO 20868:2001, ISO 20869:2010, ISO 20876:2018, ISO/TR 20881:2007, ISO/CD TR 20881, ISO 22649:2016, ISO 22651:2002, ISO 22652:2002) regarding shoe insole under the regulations of footwear in ISO/TC 216 (International Organization for Standardization [ISO], 1998). ISO/TC 216 standardize the test methods, terminology and performance requirements for the components of footwear, and also the test methods and terminology for the whole shoe (ISO, 1998). However, it does not include footwear for professional use (under ISO/TC 94) and sizing system designation and marking for boots and shoes (under ISO/TC 137) (ISO, 1998). Moreover, there is only one ISO regulation regarding shoe inserts (ISO 21064:2017) covered by ISO/TC 168, prosthetics, and inserts. ISO/TC 168 established the standardization of prosthetics and inserts in the scope performance, safety, environmental factors, interchangeability, and other more aspects also include the procedures and devices in temporary and permanent use (ISO, 1977). ISO 21064:2017— shoe inserts— uses, functions classification and description, establishes a method of classifying and describing the devices that are used in the field of shoe inserts (ISO, 2017). However, the materials or manufacturing methods used for the fabrication of inserts are excluded from ISO 21064:2017.

There are two main categories of the material— nature and synthesis material, used for shoe inserts (Healy et al., 2010). Nature materials include cork, rubber and leather, which are used since the early years of shoe inserts. They could also be combined to each other to present the characteristic more suitable for insert. The combination of cork and rubber— ThermoCork, has been widely used in the past 30 years (Healy et al., 2010). The synthesis materials are thermoplastics, subortholen, acrylic, composite carbon fibre, cork, leather, ethyl-vinyl cetates (EVAs) (Healy et al., 2010). The material properties are described as following.

(A) Thermoplastics (TP)

Thermoplastics are the organic materials that have wide range of properties. It can be melted when heated and become harden after cooled. Thermoplastics are light weight with densities of 0.9 to 2 gm/cc. Some high temperature thermoplastic materials can withstand temperature extremes of up to 315°C (Mitra et al., 1987). There are several groups of thermoplastics which display different characteristics and properties such as strength, colour, elongation, temperature limits, etc. The common groups of thermoplastics are acrylonitrile butadiene styrene (ABS), polybutylene (PB), polyethylene (PE), polyethylene cross linked (PEX), polypropylene (PP), polyvinyl chloride (PVC), chlorinated polyvinyl chloride (CPVC), polyurethane (PU) and polyvinylidene fluoride (PVDF) (Engineering ToolBox, 2001).

- **ABS (acrylonitrile butadiene styrene)**

ABS is strong and rigid that is resistant to a variety of bases and acids. ABS may be damaged by some solvents and chlorinated hydrocarbons. Ciobanu (2012) has used computer aided design (CAD) and rapid fabrication technologies to manufacture shoe inserts in ABS.

- **PE (polyethylene)**

PE is a more flexible thermoplastic material, which is low in strength, hardness and rigidity. It has a high ductility, low friction and impact strength. It also has strong creep under persistent force Walther et al. (2013) produced foot PE inserts for improving plantar fasciitis, but they did not reduce the pain caused by plantar fasciitis as much as the other two that made in EVA and polyurethane (PU) (Walther et al., 2013).

Subortholen® is known for the high-molecular-weight, high-density, highly versatile polyethylene, which is highly suitable for inserts and protheses. Subortholen is a wax-like, lightweight, flexible and tough polymer that can provide high level of support and excellent stress crack resistance. Subortholen has a high melt strength that can be adjusted after heating and vacuum process. It is also easily cold-formed. Subortholen is ideally used for the frame of the semi-rigid shoe inserts because it can provide the strong support and also flexible enough to resist the stress without cracking. The heel cup (figure 2.32) of shoe inserts can be made from subortholen for people who experience instability of the subtalar joint in rearfoot eversion/inversion. Balsdon et al. (2019) reported that subortholen inserts has significantly reduced pain for participants with chronic ankle/subtalar joint pain in rheumatoid arthritis by improving the instability and functional limitation. Although we only find one literature used subortholen inserts for flatfoot (Balsdon et al., 2019), it is widely sold on marketplace as an intervention for flatfoot or rheumatoid arthritis due to foot instability.

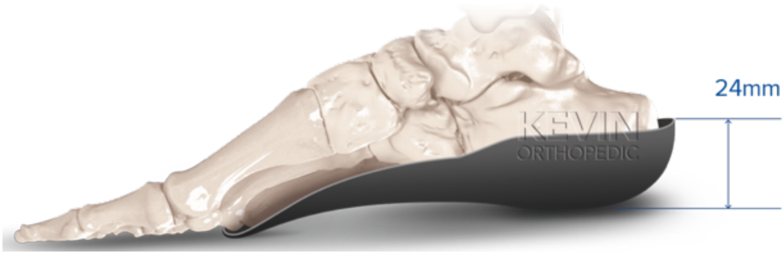

Figure 2.32. Heel cup that is made of subortholen for stabilizing subtalar joint (Kevin Orthopedic, n.d.).

- **PEX (polyethylene cross linked)**

PEX is a very broad category of materials including several patent products— Plastazote®, Pelite, Aliplast®, Dermaplast®, XPE, and Nickelplast™, put PEX as one of the materials in their inserts (Rogers et al., 2006; Leber and Evanski, 1986). PE foam is a common type of PEX category, it is a closed-cell foams that ideal for improving pain orin diabetic foot induced by excessive plantar pressure (Rogers et al., 2006; Leber and Evanski, 1986). Plastazote® is one of the well-known patent composites that has been widely used for orthotists to produce shoe inserts. Plastazote® is a closed cell construction (i.e. not able to absorb water) mainly made of PE foams. Plastazote® is claimed as the world's lightest cross-linked foam with a range of densities from 15 to 115kg/m3 (Zotefoams, 1981). Plastazote® has been widely used in packaging, automotive (thermoformed parts), aerospace, electronics, healthcare, construction, sport (protective padding), marine (where buoyancy is crucial), industrial (seals and gaskets) (Zotefoams, 1981). It is also widely used in the fabrication of shoe inserts to reduce plantar pressure at high pressure points (Leber and

Evanski, 1986). It does not only absorb the shocks or impact for foot but also able to reinforce the insole itself and provide the better protection of the foot in weight-bearing movement (Rogers et al., 2006).

Leber and Evanski (1986) compared thatsix materials— Latex foam (rubber), Plastazote®, Dynafoam® (polyvinyl chloride foam), Ortho felt (fabric composed of a blend of cotton and wool), PPT®, Spenco® (nitrogen-induced closed cells sponge product, covered with a multistretch nylon fabric on one side) and Molo® (combination of latex, leather, cork), in foot pain relieve due to excessive plantar pressure. It was established that Plastazote®, PPT®, and Spenco® are more effective than other materials for relieving foot pain due to excessive plantar pressure (Leber & Evanski, 1986). Moreover, Plastazote® is produced using pure nitrogen, unlike other composites using chemical blowing agents that may leave ammonia or urea on the inserts. The Code of Federal Regulations (Robert, 2003) has reported that Plastazote® which made up by PE foams, does not exceed the acceptable levels of the harmful chemicals. There are several types of Plastazote® based on their properties and densities – Plastazote® LD45 Pink (Density: 43kg/m^3), P-Cell (Density: 77kg/m^3), Plastacell-P (Density: 83kg/m^3), Plastazote® LD70 White (Density: 70kg/m^3) Evazote® VA65 White (Density: 64kg/m^3), Evazote® VA50 White (Density: 50kg/m^3) (Robert, 2003). P-Cell and Plastacell-P are denser than Plastazote® LD45 Pink, which perform the better compression set for shock absorption, but their volume is approximately twice than Plastazote® LD45 Pink (Robert, 2003). Therefore, Robert (2003) has claimed that Plastazote® LD45 Pink is still the safest and the appropriate choice of materials for orthotists to fabricate the top layer of shoe inserts.

- **PP (Polypropylene)**

PP is one of the world's widely produced synthetic plastic polymer (as well as polyethylene and polyvinyl chloride). It is lightweight, highly resistant to many acids, bases and solvents. Its usable temperature can be up to 82ºC and elongation is between 100 to 600. PP is used as the hard part of the shoe inserts (Bok et al., 2016). Because of the rigidity of PP, shoe inserts will not be compressed after prolonged use. Bok et al. (2016) made PP shoe inserts to investigate the effect of inverted angles to flatfoot. PP is a thin material that is not as bulky as EVA, PE and PEX. Shoe inserts has low profile if it is made by PP, which can be easily fit into the user’s current footwear. However, because of the rigidity of PP, it can take longer for users to adapt. Orthotist normally combines some other more flexible materials, such as EVA, PE or PEX with the PP based inserts. However, we only found few shoe insert patents that use PP (Mosher, 1980; Baum, 2000). PP are used more widely in ankle-foot patents.

According to Banwell et al. (2014), Australian podiatrists recommended the use of polypropylene as a shell material of shoe inserts for flatfoot. Its final rigidity could be adjusted based on users' perceived requirements and characteristics (Banwell et al., 2014).

- **PVC (Polyvinyl chloride)**

PVC is one of the world's most widely produced synthetic plastic polymer (as well as PE and PP), which is commonly used for water, gas, drainage systems. Like PP, PVC is also strong and rigid and is able to resistant to a variety of acids and bases.

Its usable temperature can be up to 60°C, which is slightly below than PP. Because of its rigidity, it is also commonly used by functional semi-rigid and rigid shoe inserts for applying force to certain plantar area in order to correct the abnormal foot position or joint motion. Kydex® is a PVC-based material that has been widely used for inserts and prosthetic devices. However, DeToro (2012) claimed that Kydex® contains certain level of carcinogens— the compound Dioxin,2 and DEHP di (2-ethylhexyl), which formed during the manufacturing of PVC and both of them show toxicity to human body that could irritate to the viscera of the eyes, nasal passages and lungs. Therefore, DeToro (2012) insisted that the long-term exposure to PVC-based inserts or prosthetics devices for manufacturers, users or health care professionals could expose them in a hazardous gaseous state. There are few more other studies investigated Health risks by using PVC-made medical devices (Tickner et al., 2001; Rossi & Schettler, 2000) while we cannot find any publication reports the health risk by using PVC shoe inserts and suggests PVC is an inappropriate material of shoe inserts. Dynafoam® is another PVC-based patent composite that is used for shoe inserts (Leber and Evanski, 1986). Dynafoam® is a PVC foam compound of closed cell construction, which is odourless and waterproof. It is mainly used for accommodative shoe inserts to relieve the pain area due to the excessive plantar pressure. Dynafoam® can be used for capturing the foot shape for foot mould design because it can be quickly formed a negative print by pressing foot into the foam.

- **EVA (Ethyl-vinyl cetates)**

EVA is a thermoplastic copolymer derived from petroleum, which is inexpensive and easy to handle and process (Dias et al., 2017 Normally EVA is used for accommodative shoe inserts, which is soft and easier to adjust and wear in compared to other firmer material such as, PE and PP shoe inserts. However, it could be easily compressed after prolonged use, so it needs to be replaced or repaired frequently EVA is also bulkier than firmer materials used for functional shoe inserts such as PP and PVC. EVA shoe inserts are widely used in the literatures for differnt researched such as the biomechanical effect on rheumatoid arthritis and plantar fasciitis, or the change of the lower extremities' kinematic and kinetic (MacSween et al., 1999; Baldassin et al., 2009; Mündermann et al., 2003).

The summary of the properties of thermoplastic materials is in Table 2.10

Table 2.10 Properties of the thermoplastics (Engineering ToolBox, 2001)

Thermoplastic	Specific Gravity - *SG* -	Tensile Yield Strength - σ_y - *(MPa)*	Tensile Modulus - *E* - *(GPa)*	Coefficient of Linear Expansion - *α* - *(10^{-6} in/in °F)*	Thermal Conductivity - *k* - *(Btu in /ft² h °F)*	Specific Heat - *c* - *(Btu/lb °F)*	Maximum Temperature Limit *(°F/°C)*
ABS	1.08	48.3	2.34	60	1.35	0.34	180/80
PVC	1.4	55.2	2.83	30	1.1	0.25	150/65
CPVC	1.54	55.2	2.9	35	1.0	0.20	210/100
PE	0.95	22.1	0.827	90	3.2	0.55	160/70
PEX	0.94	19.3	.	90	3.2	0.55	210/100
PB	0.92	29	0.379	72	1.5	0.45	210/100
PVDF	1.76	48.3	1.52	70	1.5	0.29	300/150

(B) Acrylic

Acrylic is the first synthetic material used for shoe inserts Séamus (2008). The disadvantage of acrylic is that due to its rigidity it is prone to stress cracking. Rohadur, Polydur, and Plexidur are some of the common trade names for acrylic. Rohadur has been used in the early years of shoe inserts in adjusting flatfoot, rheumatoid arthritis, or some rearfoot syndromes. (Budiman-Mak et al., 1995; Ferguson et al., 1991; Mckenzie, 1987). For recent years, Rohadur is not so common for the use of inserts as other thermoplastics. David & David (2005) has pointed out the danger of using polymers of methyl methacrylate. Cyanide fumes could be released if polymers methyl methacrylate is overheated during the processing. Cyanide is considered as a carcinogenic product that could cause some health issue and the fume also could be an issue for environment. Therefore, in recent years, Rohadur and Plexidur has been greatly withdrawn from manufacturer (David & David, 2005).

(C) Composite Carbon Fibres

Composite carbon fibres combine carbon fibres with acrylic plastic to create a sheet material, which also known as Carboplast™, Graphite™ and the TL-series in their trade names. Carboplast™ is a popular composite carbon fibre used in foot orthosis shells (Levitz & Sobel, 2002). Carboplast™ combines acrylic plastic with carbon fibres, which makes it as rigid as acrylic and polypropylene. Carboplast™ is only half in the thickness of acrylic and polypropylene (Levitz & Sobel, 2002), and this could benefit to the functional inserts which is normally bulky and hard to fit in the user's footwear. Carboplast™ is ideally for functional shoe inserts shells, which can be divided in the foot plate with normal toe's length or Morton's toe (i.e. first metatarsal is short in relation to the second metatarsal that makes the hallux is shorter than index toe) (figure 2.33) (Cascade, 2018). The TL-series start with a composite material, TL-61™, which has an acrylic core in the middle layer and two carbon graphite layers on the outer layer. An acrylic core in the middle layer is normally 1 mm in thickness, which makes the whole material sheet to have a thermoplastic property (Levitz & Sobel, 2002). Composite carbon fibres provide the similar property as thermoplastic to shoe inserts, but it is thinner. It improves a disadvantage of functional inserts which is bulky and sometimes hard to fit in user's footwear. However, composite carbon fibres are more difficult to work on it, which require a higher softening temperature to adjust the profile and contour of the insole, and faster and accuracy process during vacuuming since they cannot be reworked easily.

Figure 2.33. Functional shoe inserts shell made by Carboplast™ (Cascade, 2018)

(D) Cork

Cork is a natural material that is simple and cheap. ThermoCork is the material of the combination of cork and rubber binders that can be formed in heating process. Depends on its density, it can be varied in weights and thickness and its shore harness is normally around 60, which is firm enough to support/correct the foot abnormal joint's movement (e.g. excessive inversion/eversion, excessive pronation, etc.) Unlike thermoplastic, when it comes to the final product, cork inserts can be easily adjusted with a sanding wheel to cut the unwanted part. Because of its advantages, ThermoCork has been frequently applied on shoe inserts in the literatures in the past 30 years for studying in different foot issues or symptoms (Cornwall & McPoil, 1997; Kao & Perell, 2006; Wagner & Luna, 2018).

(E) Leather

Leather is the original material used for supporting medial longitudinal arch. Although it is less firm than thermoplastic, it can still provide the good support to the users that experience abnormal foot motion during in weight bearing condition. It could also benefit to those who needs arch support but cannot tolerate the firm plastic. However, compare to plastics, leather is bulky and heavier, which requires the extra space in footwear. A shoe inserts made by leather laminate has been reported by literatures to provide the good impact-absorbing and may further improve joint loading patterns and enhance joint stability (Esfandiari et al., 2013; Pollo, 1998).

Molo®, a combination of latex, leather and cork, is used for foot pain relieve due to excessive plantar pressure. However, it is reported less effective than other materials— Plastazote®, Spenco®, in reducing excessive plantar pressure in certain foot area (Leber and Evanski, 1986).

(F) Rubber

Rubber can be made in both natural and synthetic materials. Natural rubber is made from latex, a milky white liquid from certain plants. One of the versatile synthetic rubber is Neoprene, also known as polychloroprene. Neoprene displays a good chemical stability and flexibility in a wide range of temperature. Rubber is good for absorbing shock and reducing impact, which is ideal for making accommodative shoe inserts. Hodge et al. (1999) used rubber-made metatarsal pad to manage plantar pressure on forefoot and improve rheumatoid arthritis.

(G) Thermoplastic elastomer

Thermoplastic elastomer is a polymer that usually mixed by plastic and rubber, which has both thermoplastic and elastomeric property (Levensalor, 2016). Thermoplastic elastomer displays both the typical advantages from rubbery materials and plastic materials. It is able to be moderately stretched and return to its original shape as the external stress or tension is released, which acts like a spring. This ability that Thermoplastic elastomer could have greater longevity than other materials. Unlike rubber, thermoplastic elastomer materials can be recycled since it can be moulded at an elevated temperature. Addition to this, it can be extruded and reused. Its significant 'creep' property also makes it able to adopt to the external load (Wang et al., 2017). Based upon this advantage, thermoplastic elastomer has been widely used in manufacturing. In additive manufacturing (or so-called 3D printing), thermoplastic elastomer is one of the favourite flexible filaments. Thermoplastic elastomer has the outstanding stability that it only needs little or no compounding. There is no additional reinforce agent required to add for stabilizing or cure the thermoplastic elastomer 3D-printed product (Wang et al., 2017). In the production of thermoplastic elastomers, it consumes less energy that is very economically friendly. By taking the advantages of thermoplastic elastomer's material property, it has been used for footwear (Villwock et al., 2009), shoe insole and inserts (e.g. foot-ankle or shoe inserts) manufacturing.

(H) Thermoplastic polyurethane

Technically, thermoplastic polyurethane is a type of thermoplastic elastomer that consists of co-polymer with mixed hard and soft segments. Similar to thermoplastic elastomer, thermoplastic polyurethane has the property of both rubber and plastic. It has been reviewed as the material with excellent wear and tear resistant, high impact strength and stiffness (Kim et al., 2017). In addition, its considerably flexible property and the ability of resisting corrosion from many industrial chemicals makes it has been widely applied in industrial manufacturing in terms of additive manufacturing. Polyurethane also has a good biocompatibility that has been widely used in medical device such as pacemaker. It can be concluded that thermoplastic polyurethane is an endurable, flexible, light weight and biocompatibility material. It has been used in shoe inserts to prevent the excessive ankle eversion (Fong et al. 2008).

- **Material summary**

In summary, the material that used for shoe inserts should be compliant to the international regulations that listed in ISO, which should not bring anything that might be harmful to human body. Some materials that are compliant to ISO but have found out later that might be potentially harmful to human body should also be concerned. According to the Code of Federal Regulations (Robert, 2003), some composites may the residual chemicals such as ammonia or urea on the shoe inserts, which may exist a risk of irritation or allergic reaction to the user's foot. Plastazote® has been reported to address the allergic issue, which has no excess of the acceptable level of residual chemicals. Moreover, Plastazote® has been approved more effective to manage the plantar pressure to relieve pain in certain area of the foot (Leber and Evanski, 1986). Janisse & Janisse (2015) highly recommended A triple-layer orthosis to bring out the best outcome. A top two layers could be made of PE foam and urethane polymers for shock absorbing and bottom layer is made of dense and firm cork or EVA for the base support. Healy et al. (2010) claimed the research to date does not have a conclusive answer as to what are the most appropriate footwear orthosis materials. The material, density and thickness of shoe inserts could be very different depends on users' requirements. For shoe inserts treating flatfoot, Dars et al. (2018) suggested that PE, PP and rubber are three commonly used materials. Su et al. (2017) suggested the height of arch support is from 25mm to 33mm and the material hardness is ranged from 30 to 40 degrees.

2.5. Reverse engineering of shoe insole

Reverse engineering is to reproduce the existing product according to its construction and composition. It could be used for deconstructing the existing product for discovering or extracting the valuable knowledge from its original design and structure (Eilam, Eldad, 2005). It is a powerful technique to improve or/and analyse the existing product, which is commonly applied on mechanical, electronical, software, medical, chemical engineering for commercial, military or research and academic use (Chikofsky and Cross, 1990). Reverse engineering is the opposite process of forward engineering. Forward engineering is the traditional manufacturing process to fabricate products from requirement to design and then implementation (Figure 2.36) (Chikofsky and Cross, 1990). The design recovery changes the external structure, shape or material to improve the original design (figure 2.34). CAD software is a powerful tool that is feasible for reverse engineering to build a 3D model based on existing physical parts (Varady et al., 1997).

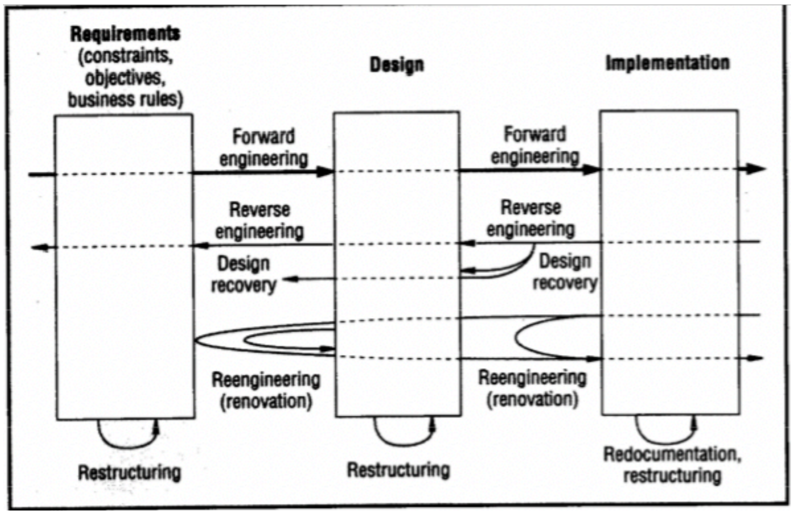

Figure 2.34. The schematic of reverse engineering (Chikofsky and Cross, 1990)

Reverse engineering has been applied to medical fields, such as dentistry (e.g. teeth brace), artificial hard and soft tissue (e.g. bone, joint), artificial heart, hearing aids, orthopaedic implant, prosthesis and insert (Wang, 2010). A Common method is to use 3D scanner or a laser scanner for external body part or Computed tomography (CT) scanner for internal segment. Then, the computer aided design (CAD) model of medical devices can be constructed according to the 3D image of human segments (Toshev et al., 2005). Prototyping of reverse engineering is often referred to as additive manufacturing or rapid manufacturing. This is to transfer the CAD model to 3D printer for prototyping but there are still some limitations regarding the accuracy, material selection and surface finishing (Wang, 2010). Several studies have layout the framework of customising shoe insert through reverse engineering as figure 2.35 (Lochner et al., 2012; Li et al., 2009; Huang et al., 2011). The framework consists of six parts— 3D data acquisition, foot image and digital insert modelling, foot biomechanics examination, material selection, analysis of insert and CAD of insert (figure 2.35).

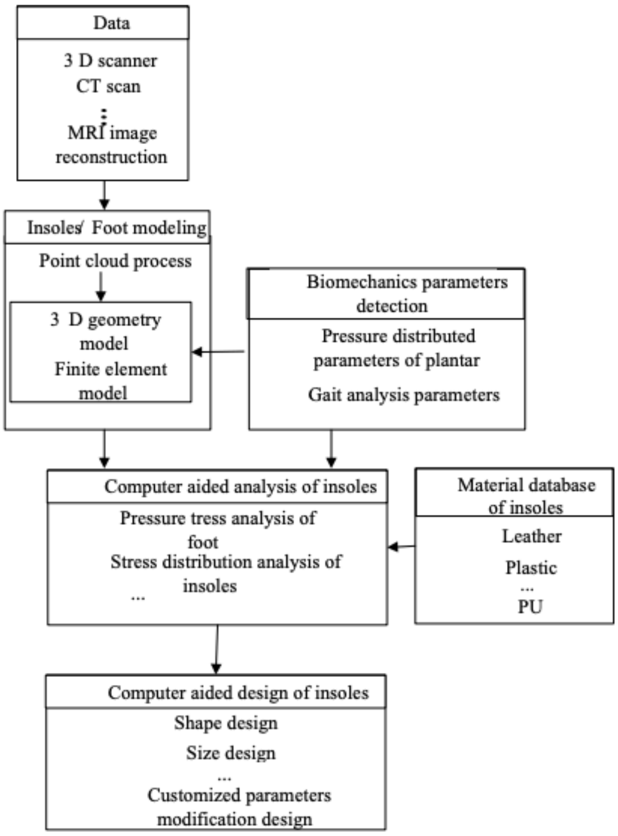

Figure 2.35. The framework of customizing shoe insert through reverse engineering (Li et al., 2009)

2.5.1. 3D foot scanning

1. **Digitizer for 3D foot image**

Foot contact digitizer captures the 3D foot image by placing the foot on the flat plate of digitizer and the probe can physically touch the foot to form the image (figure 2.38).

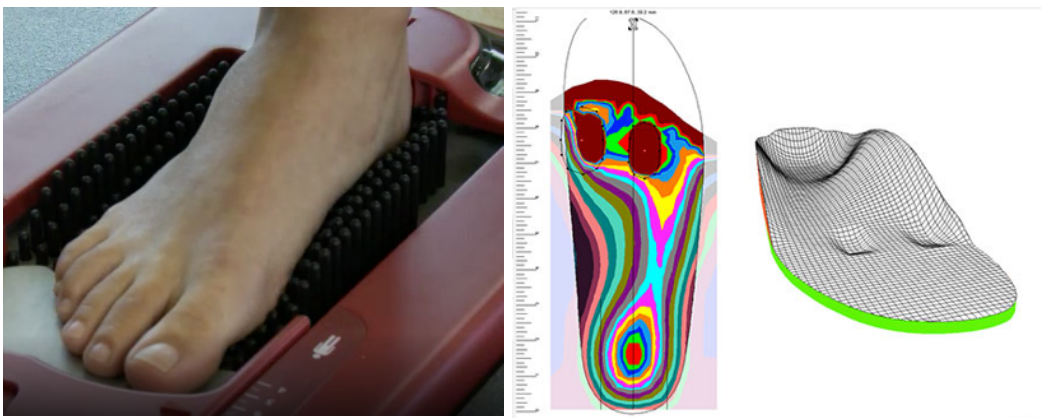

Figure 2.36. Amfit® foot contact digitizer (left); 3D foot image displayed in Amfit® correct and confirm software(right) (Bert Reld, 1977)

3D foot scans have been utilised to measure dimensions of foot (Telfer and Woodburn, 2010) and investigated for for validity and reliability compared to manual measure method (De Mits et al., 2010; Lee et al., 2014). 3D foot scans were found to be more reliable with higher intraclass correlation coefficients for linear values of radiography than manual measurements (De Mits et al., 2010; Lee et al., 2014). 3D foot scan processing can automatically derive the standard Euclidean distances between space points that can address the accuracy issues of manual approach. It has been widely used for designing the customized shoe inserts or footwear (Telfer et al., 2012). Compared to previous casting method, 3D foot scan duplicates a virtual foot model rather than create an entity (Figure 2.37). By using 3D foot scan, one step can be skipped since it directly obtains the foot model. Carroll et al. (2011) found that digital 3D foot scanning significantly reduced the variability of measurement in foot parameters (i.e. forefoot width, lateral arch height, medial arch height, rearfoot width, truncated foot length, the degree of forefoot to rearfoot alignment) compared to neutral suspension casting. De Mits et al. (2010) also reported high repeatability by evaluating the agreement between different trails. Recently, 3D foot scans were introduced to identify foot arch height and curve and have shown higher agreement with radiography than manual-measured tools (De Mits et al., 2010). Besides, the required time of measurement to index calculation is substantially decreased as 3D foot scan only takes approximately 10 seconds to acquire over 30 dimensions (De Mits et al., 2010). Williams and McClay (2000) found that experienced testers can produce variable results. 3D foot scan has performed highly repeatable and reproducible (Witana et al., 2006; De Mits et al., 2010) and is able to reduce the interference by tester’s experience.

Figure 2.37. Infoot® foot scan digitizer(left); Infoot® 3D foot image (right) (De Mits et al., 2010)

Telfer et al. (2012) reported the high reliability (i.e. intraclass correlation coefficients >0.75) between foot shape obtained from plaster casting, foam impression and 3D foot scans.

2. **Weightbearing condition while capturing foot image**

The plantar foot shape varies in different weightbearing conditions (Tsung et al., 2003). Tsung et al. (2003) divided the weightbearing conditions in three— non-weight bearing (i.e. sitting), semi-weightbearing (i.e. bilateral standing) and full-weightbearing (i.e. single leg standing) and found the contact area, foot length, foot width and rearfoot width increases and arch height and arch angle (represents height of medial longitudinal arch at midfoot) when weight increases on a healthy, normal-ached foot (Table 2.11).

Table 2.11. The change of foot parameters from non-weightbearing to semi- and full-weightbearing (Tsung et al., 2003)

	Semi- to Non-weightbearing	Full- to Non-weightbearing
Contact area	35.1% ± 21.6 %	60.4% ± 33.2%
Foot length	2.7% ± 1.2%	3.4% ± 1.3%
Foot width	2.9% ± 2.4%	6.0% ± 2.1%
Rearfoot width	5.9% ± 4.8%	8.7% ± 4.9%
Arch height	–15.4% ± 7.8%	–20.0% ± 9.2%
Arch angle	–21.7% ± 17.2%	–41.2% ± 16.2%

For people who acquired flexible flatfoot, arch angle (indicates arch height)— the angle between the horizontal plane and a line drawn from the inferior aspect of the medial cuneiform to the inferior aspect of the fifth metatarsal, in semi-weightbearing condition was decreased 52% compared to non-weightbearing (Ferri et al., 2008). Moreover, subtalar joint lateral subluxation (indicates calcaneus alignment)— the distance from the lateral margin of the calcaneal articular surface to the lateral margin of the talar articular surface (figure 2.38), occurred in 6.7% of flatfoot in non-weightbearing condition and in 26.7% in the semi-weightbearing condition (Ferri et al., 2008).

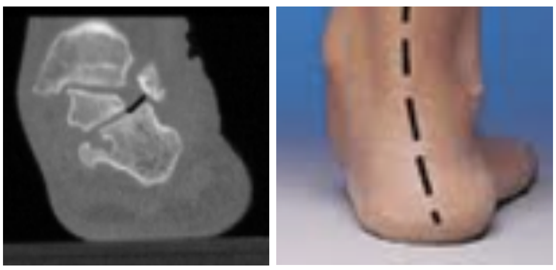

Figure 2.38. Subtalar joint lateral subluxation from foot posterior view through CT scans (left) and through rearfoot alignment of eye's observation (right) (Ferri et al., 2008)

The average plantar foot shape for a person occurs when he/she is in the semi-weightbearing condition (Tsung et al., 2003). This might explain why they capture 3D foot image in a bilateral standing position. As Ferri et al. (2008) pointed out arch height has dropped, and subtalar joint has deviated significantly in semi-weightbearing condition. If we capture flatfoot in semi-weightbearing condition, we may design a shoe insert that allows for deviation of subtalar joints to continuously occur. Therefore, we suggested 3D foot image need to be captured in non-weightbearing condition. Hence, participants were asked to sit on a chair next to foot scanner and their foot should be place on the glass of digitizer with slightly touch the glass. Handheld 3D scanner (Figure 2.39) may be applied in participants' supine or prone position to capture 3D foot image in a non-weightbearing position. However, the concerns of handheld 3D scanner could be its accuracy and reliability (Kersten et al., 2016). Normally the foot scanner takes only 10 seconds to capture image (De Mits et al., 2010), but handheld scanner requires tester to scan around the object that takes more time. This could affect the accuracy and efficiency when the tester is not familiar with the device or participant moves their foot.

Figure 2.39. Different kinds of handheld 3D scanner (Kersten et al., 2016)

2.5.2. Computer-aided design

1. **Optimized scanned data**

To create a shoe insert based on the scanned image, the first step is to optimize scanned result which is to clean up the foot image after we get the raw data of 3D scan. Three typical steps for this are object repair, background noise removal and spikes reduction. There are the software systems that can be accessed through RMIT University for image optimization—Artec®, Geomagic®, Meshmixer®, Meshkab®.

2. **Create insert model in CAD**

CAD nowadays is based on 3D data for the better accuracy and efficiency. CAD is a powerful tool used in reverse engineering to analyse a product (Macy, 2013; Eilam & Eldad, 2005). CAD design improves the accuracy and efficiency compare to the traditional manual techniques and also saves a lot of material spending on casting and moulding.

Lochner et al. (2012) used reverse engineering to reproduce functional shoe insert as follows.

- Obtain the primary anatomical landmarks required for insert design or foot alignment on the 3D image.]
- Layout the profile of insert using the series points on the contour of foot to form the outer perimeter (figure 2.40). Create arcs to connect the points on the contour of foot to the contact points between plantar and ground. The ball curve connects 1st and 5th metatarsal.

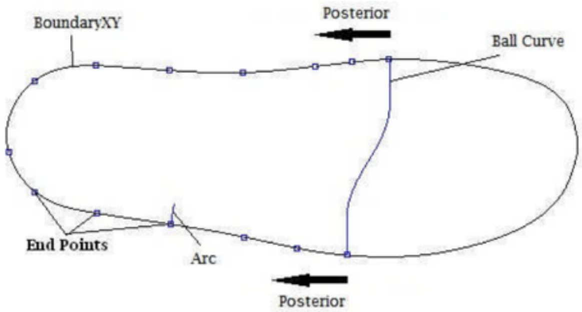

Figure 2.40. A series of points are created according to the foot contour. The ball curve connects 1st and 5th metatarsal, which sperate forefoot and midfoot/rearfoot. An arc is created for each point (Lochner et al., 2012)

- Connect the arcs that created in previous step to form the inner perimeter of the midfoot and rearfoot (Figure 2.41). Then, the primary arc is created from 1st metatarsal to hallux and duplicate this arc on 5th metatarsal (Figure 2.41) and the trimming curve is created to let the insert fit into footwear.

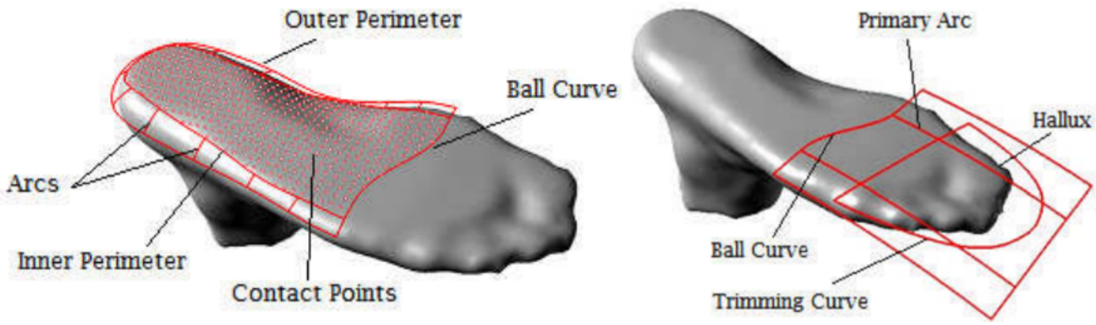

Figure 2.41. the CAD direct modelling method proposed by Lochner et al. (2012)

Numerous CAD software products can be usued incl. Catia® v5, v6 and 3D experience, Autodesk Fusion 360®, Gensole®. Among them Gensole® is a specialised software for designing shoe insert. Gensole® (figure 2.42) can be operated real-time in a web browser and create a shoe insert by following steps: input the parameters of insert profile suits the footwear, import foot scanned image and contour the insert to match the foot scan, adjust the hardness of the insert. It takes less time to create an insert in Gensole® than Catia® and Fusion 360®, but the flexibility is relatively low.

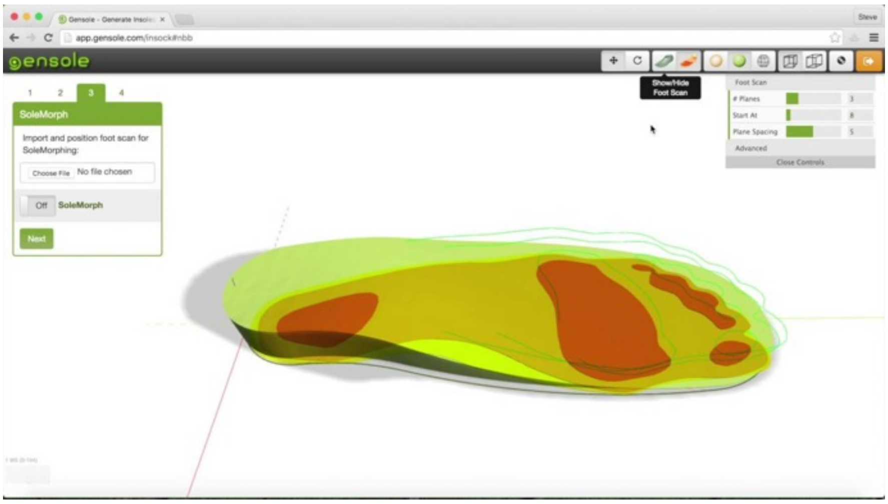

Figure 2.42. Gensole® interface view in web browser (Gyrobot, 2016)

Li & Tanaka (2018) reported the required time of CAD hand insert is up to 3 hours for a skilled operator. Although the required time of digital method is much less than traditional method, the substantial CAD tasks are still fairly challenging. Parametric insert modelling devises the geometry of shoe insert using input algorithms (Lochner et al., 2012). However, the current methodology still contains substantial volume of manual CAD tasks, which may not be feasible for those who are inexperience to CAD software to adopt in-house insert design.

2.5.3. Additive manufacturing & material selection

1. **Additive manufacturing**

Additive manufacturing (AM) has been gaining popularity as it offers advantages particularly in customization that requires unique geometrical structured customer-specific products. Several AM techniques that have been adopted to produce shoe insert— selective laser sintering (SLS), stereolithography (SLA), fused deposition modelling (FDM) (Noorani, 2006, Gibson et al., 2010). Yarwindran et al. (2017) reported the inserts made by fused deposition modelling (FDM) technique improving uneven plantar pressure distribution in dynamic and static conditions of the users. Davidson (2013) adopted the elastomer produced by SLS method to improve the performance of midsole in reducing injury risk and enhancing comfort of running.

The comparisons of three AM techniques are in detail as following.

- FDM technique

FDM is a solid-based printing system that is widely used in rapid prototyping technology. The raw materials are normally thermoplastic polymers. The greatest benefit of FDM is the lower cost. The solid, raw material

- SLS technique

SLS is a powder-based printing system that creates 3D objects by fusing polymer powder materials with carbon dioxide (CO_2) laser and turns powder material into solid objects (Gibson et al., 2010). The detailed process of creating 3D objects is shown in figure 2.43.

The strength of SLA is the high productively and low cost.

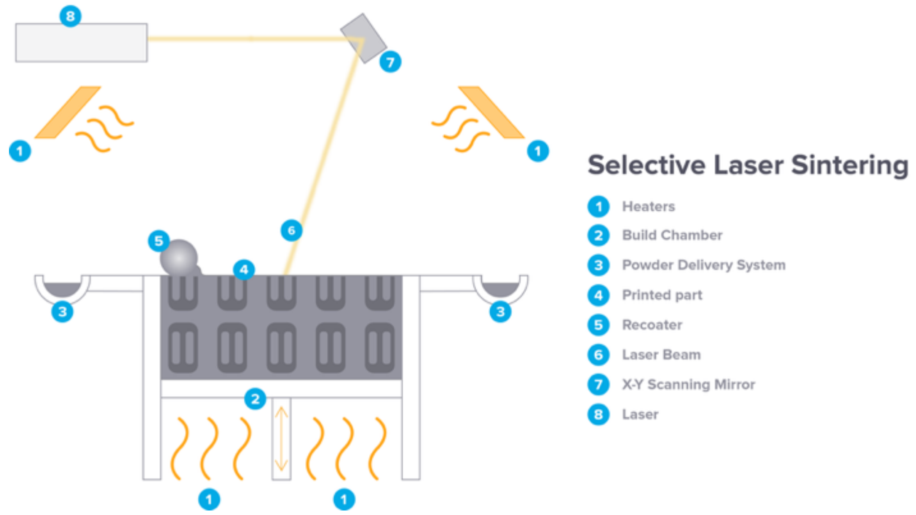

Figure 2.43. The system of selective laser sintering 3D printing (Source: https://formlabs.com/blog/what-is-selective-laser-sintering/)

- SLA technique

SLA is a liquid-based rapid manufacturing system that converts the polymer liquid materials layer by layer into solid object through Ultraviolet (UV) laser source, which is the process that so-called photopolymerization (Figure 2.44).

Compared to SLS, one of the advantages could be lower force and stress applied on the 3D object during the process. Since the object is under the liquid surface throughout the fabrication, it can further reduce the possibility of distortion may be caused by the external force or stress. Therefore, the accuracy then can be increased. However, the system of SLS require the higher initial investment and the material expense compared to SLS and FDM.

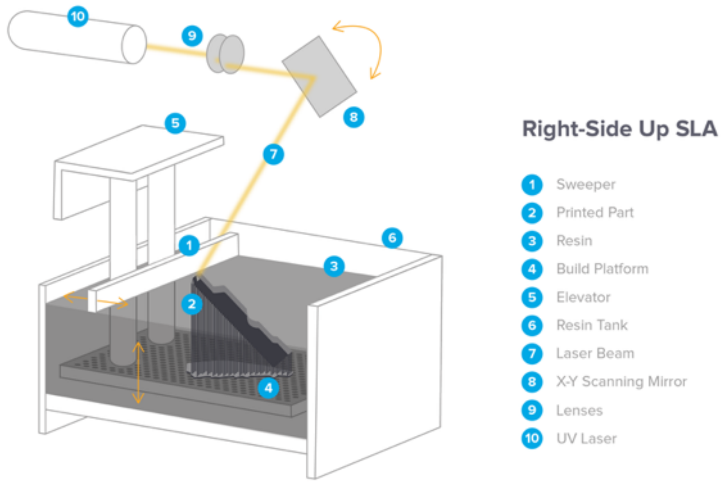

Figure 2.44. The system of right-side up stereolithography 3D printing (Source: https://formlabs.com/blog/ultimate-guide-to-stereolithography-sla-3d-printing/)

In order to address the issue mentioned above, the inverted or upside-down SLA is introduced (Figure 2.45). This invention inverts the processes of the previous SLA system. Inverted SLA does not require the whole building object in the resin tank until the final product is completed.

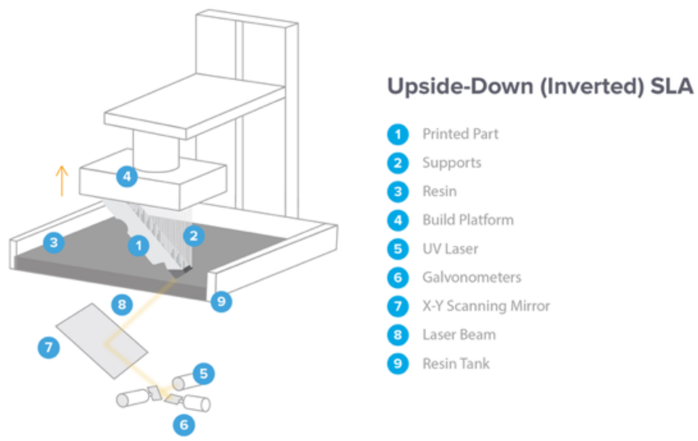

Figure 2.45. The system of upside-down stereolithography 3D printing (source: https://formlabs.com/blog/ultimate-guide-to-stereolithography-sla-3d-printing/)

Asummary. of rapid manufacturing techniques, the advantages and disadvantages of FDM, SLS and SLA are displayed in Table 2.12.

Table 2.12. The comparison between selective laser sintering (SLS), stereolithography (SLA), fused deposition modelling (FDM)

	Advantages	Disadvantages

FDM	• fast • lower cost in printer and raw material	• lower accuracy and resolution • design limitation
SLA	• higher accuracy, • smooth surface finish • wide range of material selection and application	• limited building object volume • large investment on printer and raw material • sensitive to long exposure to UV laser.
SLS	• not require the supported structure • very large design freedom	• expensive equipment and raw material • limited material options

2. Additive manufacturing material selection

In traditional manufacturing, thermoplastic elastomer (TPE), thermoplastic polyurethane (TPU), Acrylonitrile Butadiene Styrene (ABS), Polylactic acid (PLA), Polycarbonate (PC), Polyamide (PA), Polystyrene (PS), lignin, nylon and rubber are the materials for shoe insert. Literature shows the appropriate material properties of insert for low arch or flatfoot are required high hardness (shore hardness between 55 to 70), high strain and stress and low compression set and compression fatigue (Healy et al., 2010). To meet this requirement, the most suitable materials are polyurethane (PU) and ethylene vinyl acetate (EVA). According to BASF performance footwear standards, the material properties of PU at midsole are 330 to 380 kg/m^3 for density, 50 to 54 for shore A hardness, 3.6 to 4.5 N/mm^2 for tensile strength, and 200 to 230% Elongation at break (BASF, 2018).

In order to produce shoe inserts production appropriate AM materials need to be selected. The filaments of fused deposition modelling (FDM) have the similar properties as PLA, ABS, TPU or TPE can be used for inserts manufacturing (Dombroski et al., 2014). Filament has the similar properties as TPU is stiffer than other materials and it can be used to sustain the structure of insert (Davia-Aracil et al., 2018). This filament is reported to overcome some issues of traditional materials and improve the quality and functional of the insert (Davia-Aracil et al., 2018). Moreover, 3D printing filament with good abrasion resistance as TPE can also improve the function of flatshoe inserts (Yarwindran et al., 2016). AM material—Filaflex and NinjaFlex from Flashforge 3D printer, can produce products with similar properties as TPE that display good flexibility and rigidity (Yarwindran et al., 2016). In comparison, Filaflex has the best performance in of tensile strength and flexural strength with 70% of the infill (Yarwindran et al., 2016).

Elastomer could be the appropriate AM material in the use of insert. Elastomer preformed a low compression fatigue in the cyclic loading test, which indicates its capacity to absorb and return energy repeatedly during locomotion (Davidson, 2013). This ability allows elastomer to mimic the function of foot arch and facilitate the motion of foot arch in gait by elongate the arch when it is loaded and recoil the arch when it is unloaded. Other advantages of elastomers are the good thermal stability and low toxicity in production (Zheng et al., 2018). Moreover, the high conformity and contact stress and high permeability to oxygen make elastomer the appropriate material for inserts (Plott & Shih, 2017).

Agilus30 and TangoBlackPlus are the AM materials that are often used to produce elastomer by PolyJet technique (i.e. photopolymer jetting) from SLA technique (Das et al., 2018). PloyJet is the technology with a high accuracy and high efficiency additive manufacturing. The rubber-liked characteristic of Agilus30 and TangoBlackPlus is stiffer than the traditional material that could provide the support for fallen arch. Moreover, the elasticity of Agilus30 and TangoBlackPlus could be designed to mimic the function of foot arch that is to elongate when it is loaded and recoil when it is unloaded. Four different models of elastomer—Agilus30 (FLX2040) / Agilus30 Black (FLX9840), TANGOBLACKPLUS (FLX980) / TANGOPLUS FLX930 were found in the Stratasys materials data sheet. With VERO / VeroWhitePlus RGD835 as the secondary materials, Agilus30 (FLX2040) / Agilus30 Black (FLX9840), TANGOBLACKPLUS (FLX980) / TANGOPLUS FLX930 can be combined and provides twelves different ranges of mechanical properties ((Table 2.12.1 and 2). However, although there are twelve different material characters can be produced by the mixture of Agilus30 or TangoBlackPlus with Vero, the proportion of each material in such mixture is still unclear. The insufficient information regarding the material properties disclosed by material provider could be the challenges for insert manufacturer to optimize the material applications (Abayazid & Ghajari, 2020). Stratasys provides the tensile strength, elongation at break, tensile tear resistance and shore hardness (Table 2.12.1 and 2). However, Stratasys fails to disclose load rate and temperature as the important factors that the characteristics of elastomers dependent on. Therefore, there is an issue that the material properties listed by data sheet cannot address the correct response of material for our specific purpose— insert. Agilus30 and TangoBlackPlus are only introduced to the market in recent years and their material properties in responding insert use have not been fully investigated. Furthermore, there is no standard can be followed in additive manufacturing because the material properties could be different based on the printing speed, temperature, and orientation (Abayazid & Ghajari, 2020). As the material properties are tested by the specimen in the particular shape, there might be a discrepancy or inconsistence of the mechanical properties when the material in other geometries. Therefore, there might be a knowledge gap between the mechanical properties reported by Stratasys and insert use. In order to have the comprehensive information of material properties in insert use, the material testing is needed to be carried out in current study to optimize the material applications on insert.

Table 2.12.1. Mechanical property of required standards for material combination from Stratasys data sheet. Primary material: Agilus 30 (FLX2040) and Agilus Plus (FLX9840); secondary material: Vero

Property	ASTM	Unit	FLX9740	FLX9750	FLX9760	FLX9770	FLX9785	FLX9795
			FLX9840	FLX9850	FLX9860	FLX9870	FLX9885	FLX9895
Tensile Strength	D-412	MPa	3-4	3-4	3.5-4.5	4-6	6-10	10-14
Elongation at break	D-412	%	190-210	170-210	150-170	120-140	70-90	50-70
Shore hardness	D-2240	Scale A	40-50	50-55	55-60	60-70	80-85	85-90
Tensile tear resistance	D-624	Kg/cm	6.0-8.0	7.0-9.0	7.0-10.0	12.0-14.0	22.0-26.0	26.0-30.0

Table 2.12.2. Mechanical property of required standards for material combination from Stratasys data sheet. Primary material: TangoBlackPlus (FLX980) and TangoPlus (FLX930); secondary material: VeroWhitePlus RGD835

Property	ASTM	Unit	FLX9740-DM	FLX9750-DM	FLX9760-DM	FLX9770-DM	FLX9785-DM	FLX9795-DM
			FLX9840-DM	FLX9850-DM	FLX9860-DM	FLX9870-DM	FLX9885-DM	FLX9895-DM

Tensile Strength	D-412	MPa	1.3-1.8	1.9-3.0	2.5-4.0	3.5-5.0	5.0-7.0	8.5-10.0
Elongation at break	D-412	%	110-130	95-110	75-85	65-80	55-65	35-45
Shore hardness	D-2240	Scale A	35-40	45-50	57-63	68-72	80-85	92-95
Tensile tear resistance	D-624	Kg/cm	5.5-7.5	7.5-9.5	11-13	15.5-17.5	23-25	41-44

2.6. Limitations of current insole designs

- **Current shoe inserts restrict the compression and recoil of foot arch and reduce the movement efficiency**

The compression and recoil of the foot arch plays important role in kinetic chain of human locomotion as it stores and returns mechanical potential energy to improve the efficiency in gait (Kelly et al., 2015). It is synergetic with the restricted hindfoot motion and moment caused by arch-supported insole (Han et al., 2019) and it may further affect the kinematic and kinetic of knee, hip, and pelvis (Nester et al., 2003). The motion of foot arch absorbs the external force while landing as a protection of the joints and tissue (Ker et al. 1987). The multiple joints of the foot arch allow the body to balance on the uneven terrain (Ker et al. 1987). Flatfoot has little space between foot arch and ground and compromises foot arch compression and recoil. However, current shoe inserts use the rigid or semi-rigid support to lift up the fallen arch and restrict the motion of arch (i.e. compression and recoil) even more. Although inserts have been reported to correct some biomechanical parameters (e.g. dynamic foot pronation angle, center of pressure) (Urabe et al., 2014) close to the values of normal arch, it compromises the elastic mechanism of arch that may induce some other issues. Stearne et al. (2016) reported that arch compression and recoil are decreased, and total energy expenditure is increased when insert is applied. When the customised shoe inserts perfectly match the plantar shape in order to support the fallen foot arch it restricts movement during dynamic weightbearing condition. As the elastic function of the natural arch is lost, human's foot arch cannot temporarily store and release mechanical energy for saving the total energy cost during locomotion (Stearne et al. 2016). As the human body represents a single kinetic chain, any interference to the foot/ankle motion may affect to whole body motion (Waters &

Mulroy, 1999). The insole should be designed to ensure an effective utilization of the body's elastic function, that is to increase the energy return of foot arch. However, to date no flatfoot insole has increased or restored the arch displacement in gait. According to Rodrigo-Carranza et al. (2020), the additional weight of insole may increase the energy cost and compromise the movement economy. Therefore, the insole for flatfoot is suggested to be as light as possible and not to over 100g per insole.

- **Lack of the observation in long-term effect**

Literature shows that shoe insert can bring immediate change on foot kinematic such as joint's motion and moment. However, there is lack of acquired long-term evidence that shoe inserts can improve flatfoot individuals kinematically. Aboutorabi et al. (2015) suggested that the observation of CoP trajectory should be carried out in long-term because it could be the important indicator of arch height. Some works have reported the shoe insert long-term effects on overused injury such as knee syndrome (MacLean et al., 2008; Collins et al., 2008). However, the long-term change of foot biomechanics validated by kinematic data remains unclear.

- **Digital insert design and manual CAD task**

Computer aided design (CAD) system became a powerful tool for insert customization (Huang et al., 2011; Li et al., 2009). Huang et al. (2011) proposed a workflow includes acquiring plantar contact pattern, transforming it to mathematic models and using computer numerical control milling machines for manufacturing inserts. Li et al. (2009) proposed a framework includes MRI and CT foot image acquisition, plantar pressure measurement, CAD of insert, insert material selection, foot/insert FE modelling. Due to the complexity of morphology of human foot, direct modelling of CAD insert could be time-consuming because the design needs to be based on the actual contours. Hence, the required time of CAD hand insert is up to 3 hours for a skilled operator (Li & Tanaka, 2018). Parametric modelling was introduced to model the shoe insert geometry using input algorithms (Huang et al., 2011). However, the proposed methodology (Lochner et al., 2012) still required large portion of manual CAD design operations.

2.7. Data analysis

2.7.1. Motion analysis

Foot biomechanics can help us to have a better understanding of foot plantar external and internal feature (Li et al., 2009) Foot biomechanics can be analysed via i) in vivo experiment and ii) computer simulation.

1. **In vivo experiment**

- **Static/dynamic plantar pressure**

To design customized shoe inserts for patients with foot abnormality, it is important to understand dynamic plantar pressure distribution in gait. This can be complex because foot plantar pressure is variable during human's locomotion. The most commonly used method for monitoring the foot pressure distribution in gait is the application of capacitive sensors (Hessert et al., 2005). Hallemans et al. (2003) reported the dynamic plantar pressure distribution at different plantar areas during stance phase pointing that greatest plantar pressure normally occurs at heel and big toe. The first peak pressure is on heel after the foot strike and second at the metatarsal joint later in the stance phase before toe-off (Hallemans et al., 2003). Since the heel, hallux and metatarsal area are subjected to the highest pressure during static or dynamic weight bearing condition, in designing the shoe insole, the heel cup and arch support are two important components to improve the foot kinematic (Chen et al., 2014). The heel cup is designed to perfectly fit the heel in order to prevent the excessive pressure and improve the comfort of the user (Creaby, May and Bennell, 2011). The pressure concentration on the heel acts as impact dampener during the initial strike in gait. Additional medial arch support could reduce the depression of foot arch and prevent the over-pronation in gait. And the application of thicken pad at the metatarsal is commonly used for enhancing the absorption of the impact from foot contact to the ground. Li et al. (2009) analysed the dynamic plantar pressure of large number of people for improving CAD insert design (figure 2.47). Static and dynamic plantar pressure measurement can be also used after the fabrication of insert for assessing how the insert changes the kinematic of flatfoot (Zhai et al., 2016)

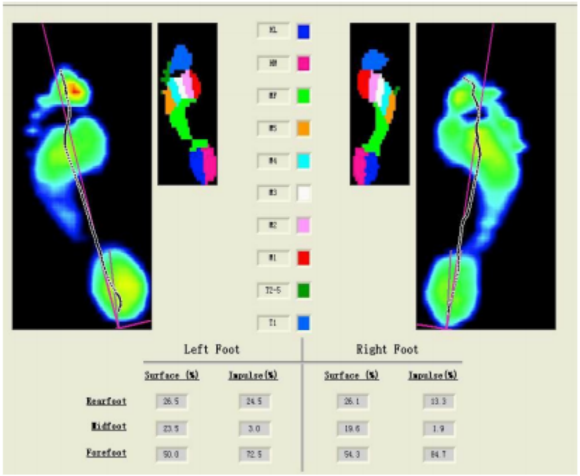

Figure 2.47. Measuring dynamic plantar pressure in nine areas of foot (Li et al., 2009)

2. Gait analysis through motion capture system

Human motion capture has been also applied for clinical purpose to study musculoskeletal biomechanics (Corazza et al., 2006). By tracking the trajectory of markers via high-speed cameras, a 3D multi-segment, kinematic model assesses dynamic motion of the participants (McCahill et al., 2018). Several studies compared the kinematics between different foot types (Levinger et al., 2010; Buldt et al., 2015), between with and without inserts (Stearne et al., 2016; Halstead et al., 2016) and between different type of inserts (Stearne et al., 2016). Milwaukee and Oxford foot model are the two most widely used multi-segment models for motion analysis in healthy and afflicted population (Saraswat et al., 2012; Leardini et al., 2019). The marker placement and description are in Table 2.13 (Canseco et al., 2008; McCahill et al., 2018). Both models have been widely used in different foot and ankle research. With the x-y-z axis triad on hallux, Milwaukee foot model is more suitable for study on forefoot or hallux deformity (e.g. hallux valgus, hallux rigidus) (Canseco et al., 2008). Oxford foot model, on the other hand, is more sensitive to the joint motion of rearfoot and midfoot. Since flatfoot normally related to a rearfoot excessive eversion and midfoot pronation (Stacoff et al. 2000a; Williams et al., 2001b),. McCahill et al. (2018) reported high repeatability of Oxford foot model on flatfoot subjects. However, a perceive shortcoming is a lack of marker on the navicular tuberosity as prominent displacements are on both talar and navicular bone of flatfoot (Younger et al., 2005; Franco, 1987; Cody et al., 2016). Oxford foot model has shown good intra-clinician repeatability and low inter-clinician variability (Leardini et al., 2019)

Table 2.13. The marker placement of Milwaukee and Oxford foot model (Canseco et al., 2008; McCahill et al., 2018)

Multi-segment model	Marker	Description
Milwaukee foot model 	MSAT	Medial superior anterior tibia
	MMAL	Medial malleolus
	LMAL	Lateral malleolus
	TCAL	Calcaneal tuberosity
	MCAL	Medial calcaneus
	LCAL	Lateral calcaneus
	T5ML	Tuberosity of 5th metatarsal laterally
	MH1M	Medial head of 1st metatarsal
	LH5M	Lateral head of 5th metatarsal
	XHAL	Hallux triad x-axis
	YHAL	Hallux triad y-axis
	ZHAL	Hallux triad z-axis
Oxford foot model 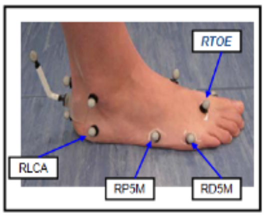	CPG	Posterior end of calcaneus
	HEE	Heel (on the bisecting line of calcaneus)
	PCA	Posterior calcaneus proximal
	STL	Sustentaculum tali
	P1M	1st metatarsal, proximal dorsal
	D1M	1st metatarsal, distal medial
	LCA	Lateral calcaneus
	P5M	5st metatarsal, proximal dorsal
	D5M	5st metatarsal, distal medial
	HLX	Hallux

However, a limitation of marker is the skin movement artefact, which occurs when the marker on skin moves without the actual bone movement (Corazza et al., 2006; Mündermann et al., 2006; Nester et al., 2007). Skin movement artefact could be exaggerated for foot and ankle analysis because the movement of foot and ankle could be relatively subtle compared to other body part such as limbs, hip and trunk. Nester et al. (2007) tried to address this limitation by attaching markers on rigid plate and bone anchor (i.e. the triad with three markers) rather than on skin directly (figure 2.48). However, the inconclusive results showed no advantages (Nester et al., 2007).

Figure 2.48 (Left) markers attached on the skin directly. (Middle) markers attached on the plates. (Right) markers attached on the bone anchor (i.e. triad) (Nester et al., 2007)

Furthermore, markers could also influence subject's movement, the process of marker placement is time-consuming, and tests need to be performed in specialised labs to acquire quality data (Corazza et al., 2006; Mündermann et al., 2006). The shod condition could potentially affect the quality of the data even more (Halstead et al., 2016). The model-based markerless approach was introduced to overcome these limitations and its good qualitative result demonstrates the effectiveness of this approach in clinical gait analysis (Corazza et al., 2006; Mündermann et al., 2006). According to Levinger et al. (2010) and Nester et al. (2007), foot and ankle motion includes five segmental (i.e. leg, calcaneus, navicular-cuboid, medial and lateral forefoot) relationship: (1) rearfoot to lower leg; (2) midfoot to rearfoot; (3) medial forefoot to midfoot (4) lateral forefoot to midfoot (5) hallux to medial forefoot. However, markerless approach from studies of Corazza et al. (2006) and Mündermann et al. (2006) can only analyse ankle (includes plantar/dorsi flexion and inversion/eversion) joints but did not include other foot motion such as abduction/adduction or pronation/supination. Therefore, despite markerless approach has been reported to enhance the drawbacks of markers, it cannot be applied to our study for now. As shown in figure 2.49, Levinger et al. (2010) used the marker placement of combination of plate and bone anchor demonstrated to analyse flatfoot.

Figure 2.49. Three different views of the leg and foot marker placement using plates and bone anchors (Levinger et al., 2010)

2.7.2. Finite element analysis (FEA)

One of powerful 3D computational models that has been used in many biomechanical investigations on foot and shoe insert is finite element (FE) model (Barani et al., 2005; Chen et al., 2003; Cheung & Zhang, 2005; Cheung & Zhang, 2006). FE model is able to simulate and predict the load or pressure distribution between foot and shoe inserts, which allows us to modify the digital insert design without fabricating the prototype for in vivo experiment (Cheung & Zhang, 2006).

Cheung & Zhang (2006) and Zhang et al. (2007) utilised magnetic resonance images (MRI) using SolidWork®, to process the raw data and form the models of each bony segments and foot surface and used FEA software— ABAQUS®, to create the FE mesh (figure 2.52.1). The insert model was designed by SolidWorks® and exported to ABAQUS® for the FE modelling as illustrated in Figure 2.50 below.

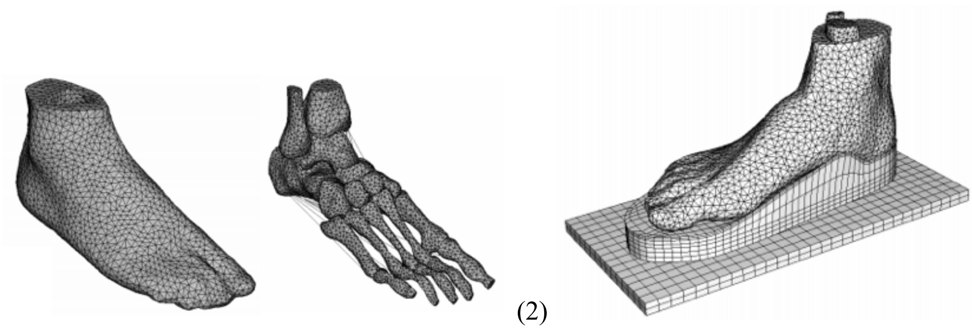

(1) (2)

Figure 2.50 (1) FE meshes of bone structure and foot surface (2) FE meshes for simulating the interaction between foot and insert and between bony segments (Cheung & Zhang, 2006; Zhang et al., 2007).

The FE models in figure 2.51.1 display the pressure distribution between bony segments. The peak pressure occurs at the third metatarsal where could be the highest point of the foot arch on barefoot standing. The FE models in figure 2.51.2 shows the plantar pressure distribution between with different uses and materials of shoe inserts. The peak pressure can be reduced by the use of shoe inserts.

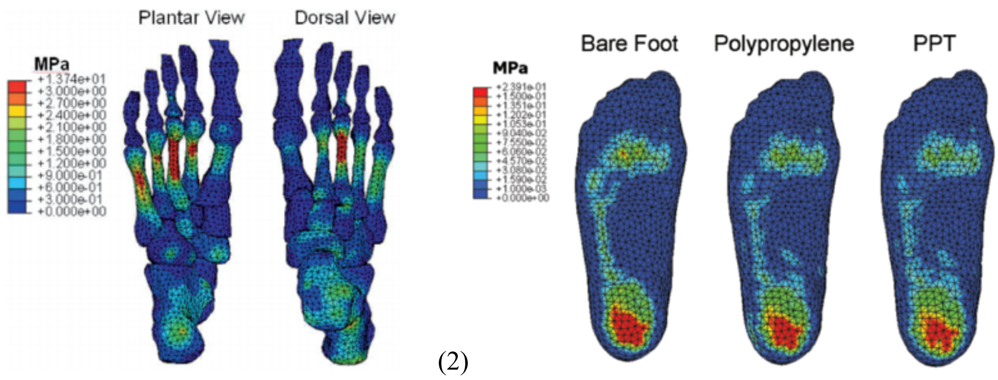

(1) (2)

Figure 2.51 (1) FE model display the pressure distribution on foot bones during barefoot bilateral standing. (2) FE model of prediction of plantar pressure distribution with different uses and material of shoe inserts (Cheung & Zhang, 2005; Zhang et al., 2007)

Savic et al. (2019) compared the FE models of flatfoot between with and without insert (Figure 2.51). We can clearly see the higher plantar pressure of flatfoot without insert is concentrate on the medial side of the foot since the collapse of medial longitudinal arch (figure 2.52.a). After the use of insert, the pressure distribution of flatfoot (figure 2.52.c) is similar to normal arch just as the FE model displayed in figure 2.52.2. (Cheung & Zhang, 2005; Zhang et al., 2007). As shown in figure 2.52.b and .c, higher pressure is in the metatarsal, heel and lateral region of the foot that could be altered by re-distributing the load distribution to bring it closer to normal arched person (figure 2.52.b and 2.52.e).

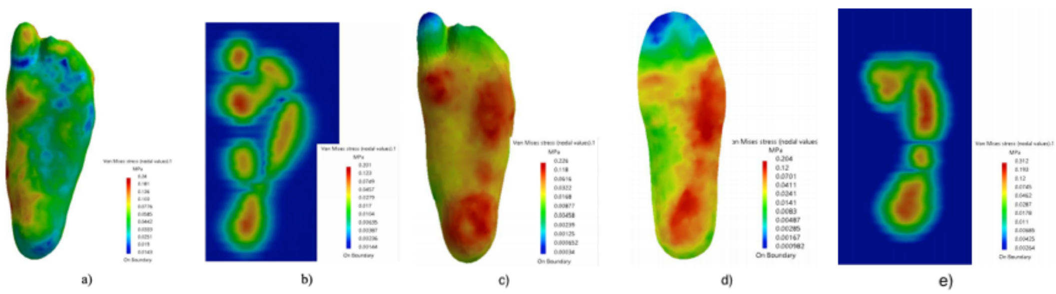

Figure 2.52. The distribution of von Mises stress for (a) flatfoot in barefoot, (b) on ground when flatfoot is barefooted, (c) flatfoot with insert, (d) shoe insert, (e) on ground when flatfoot wears insert, in bilateral standing position (Savic et al., 2019)

In summary, the application of FEA in flatfoot and shoe insert design allows us to predict insert performance before fabrication. It also allows us to detect potential flaws of the design and modify.

2.8. Knowledge gaps

In summary, the limitations of current foot arch assessment and shoe inserts are:

- Lack of standardized measurement for low arch/flatfoot identification
- Lack of protocol to control the preceding activities of measurement and reduce the interference
- Current insole designs do not improve arch's elastic recoil function or enhance the movement efficiency

2.9. Research questions

Five research questions are identified based on the existing knowledge gaps.

1. What are the thresholds for low arch/flatfoot identification that can minimize current type 1 and 2 errors in automated diagnostic process?
2. How different daily activity levels affect the arch measurement outcome?
3. How to use the foot geometry to design customized inserts?
4. What shoe inserts design could increase the magnitude of arch's compression and recoil in gait?
5. How could the entire process from diagnostics and monitoring through design, material selection and manufacturing be automated to allow health professionals deliver optimal help?

2.10. Study aims

In order to address the research questions listed above, the following study aims were formulated

- Propose a quantitative foot arch assessment to address the current inconsistency of low arch/flatfoot identification using a large population sample
- Assess the influence of different levels of daily activities on the human arch
- Develop a procedure for scanning the foot and parametrization of the resulting insert
- Design the shoe insert for low arch to improve the arch's elastic recoil function
- Identify and test appropriate materials and select appropriate manufacturing procedure.

Chapter 3. Overview

According to the aims, knowledge gaps and the research questions outlined in Chapter 2. The objectives of current study are to

1) propose a quantitative foot arch assessment using 3D subject specific imaging to establish classification thresholds for low arch and flatfoot for reducing the current inconsistency,
2) investigate the transient change of foot arch shape induced by preceding activities at different levels and establish a protocol encompassing activities prior to the measurement to reduce such interference,
3) reconstruct subject specific 3D foot model and implement 3D index for indicating the global curvature of foot arch in 3D perspective,
4) propose a parametric insert design by developing the algorithm connecting 3D foot scan and CAD software, and
5) design, manufacture and evaluate the novel inserts that can overcome the current limitations (i.e. inducing excessive joints and tissue stress and restricting the arch compression and recoil during locomotion) and correct the foot position for low arch and flatfoot.

In order to achieve the aims and the objectives listed above, the current study consists of seven main steps as following flow chart (Figure 3.1). From first to third steps is to focus on developing quantitative foot arch assessment. From fourth to seventh is to focus on develop novel shoe inserts.

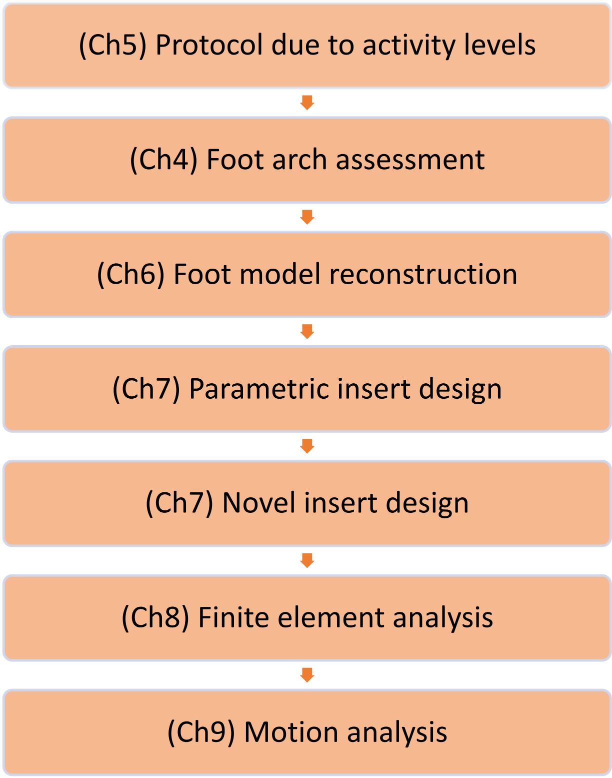

Figure 3.1. The flowchart from foot arch assessment to novel insert customization

Chapter 4— Quantitative foot arch assessment using subject specific 3D foot model. In this chapter, we identify most appropriate 2D indices to implement in 3D foot scanning to classify foot types, especially low arch and flatfoot. 3D foot scanner addressed the practical imprecision of manual measurement and help us to determine the important thresholds to identify flatfoot and low arch by statistical analysis. The content of Chapter 4, 5, 7 and 8 has been published on Journal of Medical Engineering and Physics, 2021 (via link: https://doi.org/10.1016/j.medengphy.2021.07.006), as the topic of 'Preventive strategy of flatfoot deformity using fully automated procedure'.

Chapter 5— Transient change of foot morphology due to activity levels. In this chapter, we investigate the transient change of foot morphology (i.e. foot arch height) due to activity levels

Chapter 6— Geometrical model for characterization of foot deformity using 3D imaging. The subject specific model is reconstructed by the generalized elliptical approximation proposed by Dabnichki and Zhivkov (2010). Dabnichki and Zhivkov (2010) proposed a 3D algorithm to reconstruct a pseudo-elliptical closed surface in space in order to approach the 3D objects. The content of Chapter 6 has been published on ELSEVIER, IFAC papers online, 2018 (via link: https://doi.org/10.1016/j.ifacol.2018.03.064), as the topic of 'Geometrical model for characterization of foot deformity using 3D imaging'.

Chapter 7— Parametric modelling and novel shoe insert design. In this chapter, the procedure of CAD inserts design is elaborated from 3D foot scans, 3D foot image processing, direct modelling of insert in CAD. Moreover, we introduce a parametric modelling of insert design by automatically transferring foot scanned data into parameters that can control the insert geometry through our new-developed algorithms. Three novel designs— Honeycomb, Bubble and Gyroid are proposed in current chapter.

Chapter 8— Finite element analysis (FEA) of novel inserts. FEA is used to simulate the character and performance of the insole to assist us to apply the most appropriate material and design before the production. The plantar pressure distribution and joint's internal stress were reported in four different conditions— no insole, solid insole, Honeycomb, Gyroid. Compared to no insole, solid insole has increased the peak plantar pressure and peak joint's internal stress, which potentially decreased the comfort level. Honeycomb and Gyroid have decreased the plantar pressure and joint's internal stress which may improve the comfort level of the users. Excessive peak plantar pressure and joint's internal stress may tend to cause further musculoskeletal symptoms.

Chapter 9— Motion analysis of novel shoe inserts. In the kinematic experiment, motion capture system was employed to record the trajectory of the joints motion in gait and evaluate whether the foot arch compression and recoil could be increased by the novel inserts. Multi-segment models of lower leg and foot were developed in Vicon® system. Three trials were taken to compare the differences between no insert, solid insert and novel insert in low arch subjects. The content of Chapter 9 has been submitted to Proceedings of the Institution of Mechanical Engineers, Part L: Journal of Materials: Design and Applications on 04/02/2022 and the revision was submitted on 12/05/2022 as the topic of 'A novel 3D printed personalised insole for improvement of flat foot arch compression and recoil— Preliminary study'

Chapter 4. Quantitative foot arch assessment using subject-specific 3D foot model

4.1. Introduction

Accurate flatfoot screening is crucial at early stage to develop and implement appropriate interventions to provide structural support, prevent injuries, and alleviate discomfort. As a common practice, medical clinicians use visual assessments to identify foot types (Dahle et al., 1991) based on their professional judgement. Such visual assessments (i.e. carried out by podiatrist, physiotherapist, osteopath, etc.) are deemed reliable for examination of foot morphology but are inevitably subjective. Visual assessment is also time-consuming as patient's feet must be evaluated from different aspects and postures. For non-medical professionals, there are specific quantitative measurements— radiography, footprint parameters and anthropometric values, to assess foot shape and more importantly to diagnose flatfeet by comparing the values to known population norms (Razeghi and Batt, 2002). However, image-based diagnostics is a complex as orthopaedists use a variety of measurements such as bones' size, shape and density, and joint configuration. As mentioned in Chapter 2, the limitations reported in literatures are:

- Substantial inconsistency (i.e. classification overlap) between foot types indicating type 1 and 2 errors
- Low agreement for the thresholds of foot type classification across the studies
- Low agreement between different quantitative measurements (i.e. footprint parameters and anthropometric indices)
- Outcome of manual measurement can be affected by tester's experience significantly

Overall, the outstanding limitation of current quantitative measurement is lack of a standardised assessment to establish the clear and reliable threshold to classify foot types (i.e. flatfoot, low arch, normal arch, high arch).

In Chapter 4, a foot arch assessment method using 3D imaging is developed to establish the reliable classification thresholds and reduce the type 1 and 2 errors. This is envisaged that the developed protocol will be used as a preliminary tool at early stage to identify foot deformity. Through the quantitative foot arch assessment method, the normal and low arch, flatfoot can be accurately identified.

The objectives of Chapter 4 are to:

- Evaluate foot arch indices in measure sensitivity in terms of gender differences, feet's differences in the same person.

- Establish the classification thresholds to reduce the type 1 and 2 errors in classification reported by previous study (Swedler et al., 2010)

4.2. Materials and methods

Participants

A cohort of 320 healthy participants (163 males, 157 females, age of 18 and above) were recruited for the study. Individuals with any injuries, surgeries or other medical conditions such as osteoarthritis in the foot or ankle within the last six months were not included. Individuals who participated in any moderate or vigorously intense physical activity, e.g. running, jogging, dancing, any sports activity, etc., prior to the test were also excluded. The participants were briefed about the purpose of the study and potential risks. They signed informed consent statements. Ethical approval for the study was obtained from the RMIT University Human Ethics Committee.

Instrumentation

Infoot® digitizer (USB High Type, Model: IFU-H-01, I-Ware Laboratory Co., Ltd.) was used to obtain foot dimensions and 3D digital images. Data collection methods adhered to the international protocols for 3D scanning and human body measurements.

Infoot® system can self-correct misplaced makers (i.e. green sticker). As five reference landmarks need to be manually placed on the foot prior to the scan, proper palpation is required. In order to test the self-correction of Infoot® scanner, we intentionally misplaced the stickers. The sphyrion fibulare sticker was moved to the most medial point of medial malleolus and navicular sticker was moved to somewhere below the correct point (Figure 4.1). Through the scanning process, the system gave us a warning to move the sticker to the correct spot. Moreover, if the stickers is not place at the right place, the dimension related to this landmark cannot be obtained after the scanning process. This function ensures that tester places the sticker correctly, which may help to reduce the error from the manual operation of the tester. Therefore, the self-correction of Infoot® scanner is able to address the issue of manual measurement (i.e. ruler, goniometer, and calliper) and the inconsistency induced by the experience of the tester mentioned by Williams and McClay (2000).

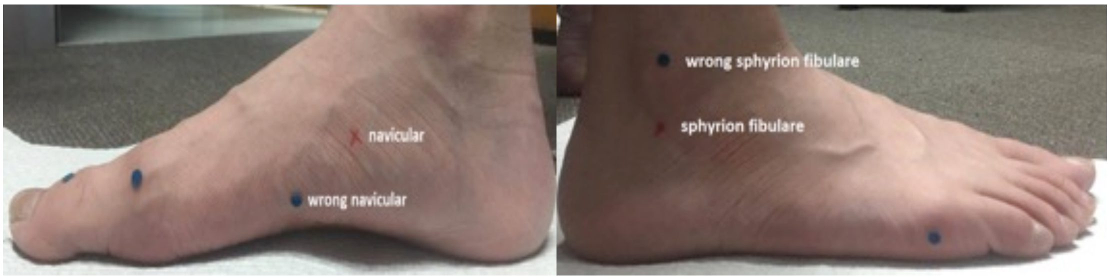

Figure 4.1 Red points: correct landmarks. Blue points: misplacing landmarks

Procedures

The procedure of foot scanning is identical as reported by De Mits et al. (2010). Infoot® scanner was calibrated every time prior to scanning participants. The calibration utilized a wooden foot model to ensure that every camera works properly and present the clear image. Participants stood barefooted in a symmetric bipedal position in shoulder width and the dust on their feet should be wiped out. The green velvet stickers (I-Ware Laboratory Co., Ltd.) with a diameter of 5 mm and a thickness of 2 mm were placed on five foot's prominent bone as the landmarks— metatarsale tibiale, great toe interphalangeal joint (toe #1 joint), navicular tuberosity, metatarsale fibulare, and sphyrion fibulare (Fig. 4.2). The glass plane of the scanner was wiped clean so that the 3D image is clearly detected by a laser beam. The participants were then asked to step on the glass plane with the right foot and the left foot was placed on a platform next to it at the same height. They were asked to maintain the torso upright and distribute their bodyweight symmetrically on both feet.

Since manual measurement is reported high affected by testers' experience, 3D foot scanning is used to improve such inconsistency. 3D foot scanning is used to measure foot arch height and display the arch curve, which has been shown higher agreement with radiography (current gold standard) than manual-measured tools (De Mits et al., 2010; Lee et al., 2014). 3D foot scanning automatically derives the standard Euclidean distances between space points that can address the accuracy issues of manual approach. Besides, the required time for measurement is substantially decreased as it only takes 10 to 15 seconds to obtain over 30 parameters for one foot (De Mits et al., 2010).

Figure 4.2. Five reference points for Infoot® scanner: (1) metatarsale tibiale (2) metatarsale fibulare (3) navicular tuberosity (4) first metatarsophalangeal joint (5) sphyrion fibulare. Two parameters obtained by Infoot® scanner: (a) navicular height: the vertical distance from the ground to the navicular tuberosity (b) Truncated foot length: the horizontal distance between first metatarsophalangeal joint and pternion.

Scanning was performed with a scan pitch of 1.0 mm using an optical laser scanning procedure. The scan process took around 10 seconds and the participants were not allowed to move during the scan (Fig. 4.3). The same procedure was followed for the left foot. The data were processed with the accompanying software— Measure (I-Ware Laboratory Co., Ltd), which provides: foot length, ball girth circumference, foot breadth, instep circumference, heel breadth, instep length, fibular instep length, height of top of ball girth, height of instep, toe 1 angle, toe 5 angle, height of toe 1 joint, height of toe 5 joint, height of navicular, height of sphyrion fibulare, height of sphyrion, height of the most lateral point of the lateral malleolus, height of the most medial point of the medial malleolus, heel girth circumference, the angle of the heel bone, and foot size (Fig. 4.4 and Table 4.1). It should be noted that there are two methods for foot length calculation in Infoot®. One is to measure the pternion (i.e. heel bone point) to the centre point of the foot breadth (i.e. the line pass through first and fifth MPJ). The other one is to measure the distance between the tips of the second toe to pternion. In the current study, we used the second method for foot length dimension.

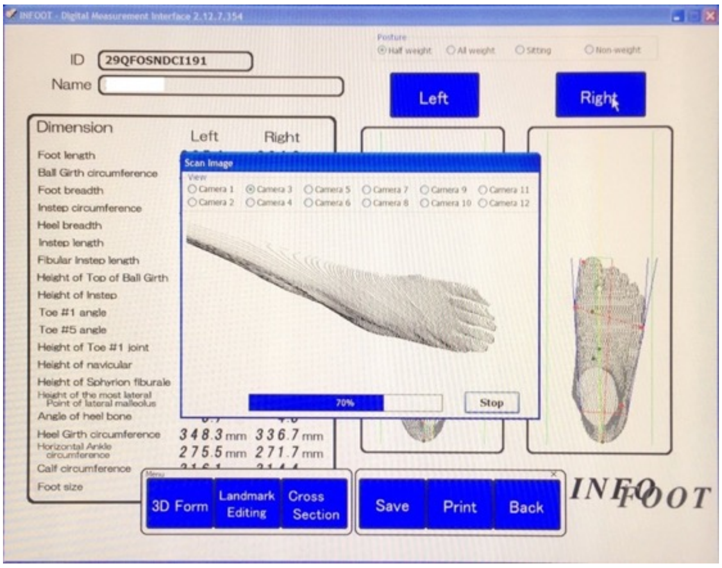

Figure 4.3. The interface of the software— Measure. The process of scanning takes up to 10 seconds.

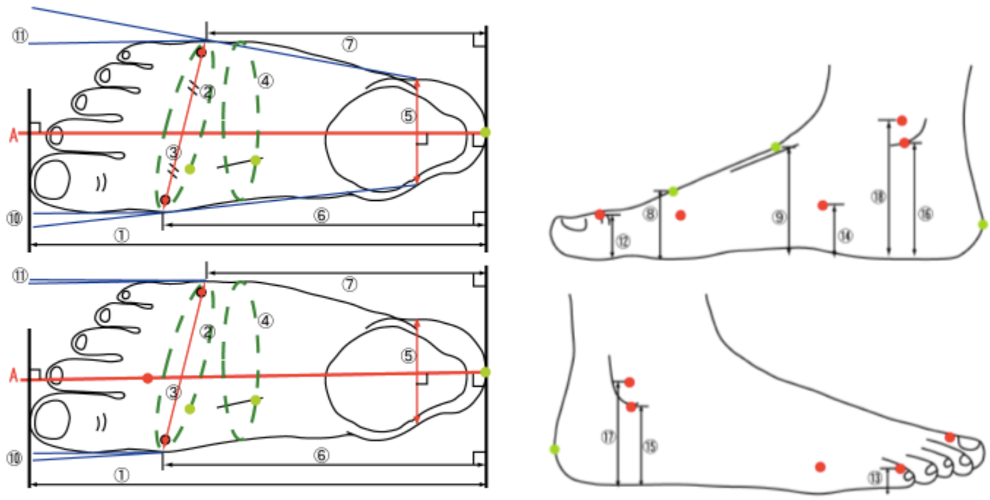

Figure 4.4. The foot dimensions that can be measured by Infoot® (see with Table 4.1)

Table 4.1. The foot dimensions that can be measured by Infoot® (see with Fig. 4.3)

1	Foot length	10	Toe #1 angle
2	Ball girth	11	Toe #5 angle
3	Foot breadth	12	Toe #1 height
4	Instep circumference	13	Toe #5 height
5	Heel breadth	14	Height of navicular
6	Instep length	15	Height of sphyrion fibulare
7	Fibulare instep length	16	Height of sphyrion
8	Height of ball girth	17	Height of the most lateral point of lateral malleolus
9	Height of instep	18	Height of the most lateral point of medial malleolus

Compare the most appropriate 2D indices— NH and NNHt

Four quantitative indices— Arch height index, Navicular height (NH), Normalized navicular height (NNH) and Normalized navicular height truncated (NNHt), can be directly obtained from Infoot® foot scans. All of them have been widely used in the traditional manual approach. In the measurement of arch height or arch curvature, navicular bone serves as the most significant bone of the medial longitudinal arch. Therefore, arch height index is considered less representative of the curvature of foot arch because it measures dorsal height rather than the height of navicular (Robert et al., 2008). NH displays the vertical distance from the ground to navicular tuberosity and is strongly related to the foot curvature (Puszczalowska-Lizis et al., 2017; Swedler et al., 2010). Besides the height of navicular, foot curvature is also strongly related to foot size, which is neglected by NH. People with same NH but different foot length can result in different foot curvature. However, they may be classified in the same foot type by using NH. Therefore, NNH, was suggested to address the outstanding issue of NH by dividing NH by foot length, (Menz et al., 2005). However, it has been found that the value of NNH can be easily affected by toe length or toe deformity (McPoil et al., 2008). NNHt, by dividing NH by truncated foot length (i.e. foot length excluding toes), addresses the issue of NNH, which seems the most appropriate index of these four indices. Despite the issue of NH, it is still the most widely used index for foot arch assessment throughout the studies. Therefore, NH and NNHt were selected in current study for statistical analysis in order to find out the most appropriate index for foot type classification using 3D scanning. We established the classifications for right and left feet separately as the conceptual and statistical issues of using pooling data of the human body is reported (Menz, 2004). The use of pooling data (i.e. mix right and left foot) may double the sample size and increase the statistical power. However, Menz (2004) suggested that the data of right and left foot should not be pooled to preserve the assumptions of independence for statistical analysis.

Definitioneition of thresholds for foot type classification

Three **s**tatistical approaches were commonly used in the literature—the mean and standard deviation (SD), quartiles and quintiles. The mean and standard deviation is more appropriate and reliable to establish the classification thresholds because the data distribution based on population norm is considered. The mean and SD provide conjunction and summarize continuous variables for presenting more accurately the data distribution, hence can provide the more reliable cut-off threshold for identify foot types. We used the same criteria as the study of Murley et al. (2009); Jonson and Gross (1997); Nilsson et al. (2012) to define flatfoot (i.e. < mean – 2SD), low arch (i.e. < mean – SD), normal arch (i.e. between mean ± SD) and high arch (i.e. > mean + SD). The threshold values were adjusted to minimise the overlap between the two classifications.

Normality test

As we used the mean and SD to establish the classification threshold, the normality of set of sample data should be assessed beforehand. The normality test displays the normality of the population distribution of a random characteristic. As we mentioned earlier, mean and standard deviation is more tractable in forecasting of natural phenomena, which is more suitable for foot type classification. A normal distribution presents more symmetric in plot (i.e. the bell shape) that develops into a standard of reference for many probability problems. It can be used to approximate natural phenomena in a variety of distributions in large samples, which makes an appealing choice for several analytical models. Shapiro-Wilk test, Kolmogorov-Smirnov test, eyeball test (i.e. Normal Q-Q plot) are the normality tests that has been widely used. Shapiro-Wilk test would be the most popular one, which assesses the null hypothesis from a normally distribution sample data. The formula of Shapiro-Wilk test is as following eq. [1].

$$W = \left(\sum_{i=1}^{n} a_i x_{(i)}\right)^2 \Big/ \sum_{i=1}^{n}(x_i - \bar{x})^2 \qquad [4.1]$$

Where x_i are the values of random sample, a_i are constants that generated from the covariance, variances and means of the sample from a normally distributed sample. The smaller value indicates the sample data is less normally distributed. If significance level of W value is greater than 0.05, the sample data is normally distributed. If the significance level is less than 0.05, the sample data deviates from normally distributed. Kolmogorov-Smirnov test is a nonparametric method to compare two samples, which quantifies the distance between empirical distribution function and accumulation distribution function. When it used for testing normality, it compares the sample to the standard normal distribution and calculate the distance between them. A large deviation of sample data has a *low* p-value of Kolmogorov-Smirnov test. When the p-value less than 0.05, it rejects the null hypothesis that the sample is deviated from normal distribution. The degree of normality of Normal Q-Q plot is tested graphically. The more the data points close to the diagonal line, the sample data is closer to the normal distribution. The more the data points scatter, the more the sample data deviated from normal distribution. Kim (2012) pointed out the issue that the Normal Q-Q plot, Shapiro-Wilk test and Kolmogorov-Smirnov test can conflict to each other when test the normality on large sample size (i.e. sample data large than 300). Kim (2012) tested the normality for a sample data of 500 subjects and found the sample data is closed to diagonal line in Normal Q-Q plot (approximately normal distribution) but have the p-value less than 0.05 in Shapiro-Wilk test (p=0.02) and Kolmogorov-Smirnov test (p=0.02) (deviated from normal distribution) indicating the inconsistency of the testing result. Kim (2013) then suggested Normal Q-Q plot to be used when samples size is less than 50 and Shapiro-Wilk test and Kolmogorov-Smirnov test can be used when sample size of less than 300. For than 300, Kim (2013) assessed normality test by using skewness and kurtosis. A z-test is applied for the normality test and the z-value is obtained as the equation [4.2] and [4.3].

$$Z_{skewness} = \frac{skewness}{SE_{skewness}} \qquad [4.2]$$

$$Z_{kurtosis} = \frac{kurtosis}{SE_{kurtosis}} \qquad [4.3]$$

where SE is the standard error.

Skewness and kurtosis are the measure of the asymmetry and peakedness of the distribution respectively (Kim, 2013). An absolute z-value of skewness or kurtosis less 2 indicating the sample was normally distributed (Kim, 2013).

For univariate data $X_1, X_2, \ldots, X_N$, the formula for skewness [4.4] and kurtosis [4.5] are:

$$Z_{skewness} = \frac{\sum_{i=1}^{N}(X_i - m)^3/N}{s^3} \qquad [4.4]$$

$$Z_{kurtosis} = \frac{\sum_{i=1}^{N}(X_i - m)^4/N}{s^4} \qquad [4.5]$$

where *m* is the mean, *s* is SD and N is the number of the data.

As the standard error is smaller when the sample size is increased, the z-value could be affected. Therefore, Kim (2013) suggested small, medium, and large size of sample data should have different criteria for normality test. For small sample (i.e. $n < 50$), the absolute z-values for either skewness or kurtosis is larger than 1.96 can conclude the distribution of the sample data is non-normal. For medium sample (i.e. $50 < n < 300$), the absolute z-values for either skewness or kurtosis is over 3.29 can conclude the distribution of the sample data is non-normal. For large sample (i.e. $n > 300$), either the absolute z-values of skewness is over 2 or absolute z-values of kurtosis is over 7 can conclude the distribution of the sample data is non-normal. As our sample size is over 300 (n=320), Normal Q-Q plot, Shapiro-Wilk test or Kolmogorov-Smirnov test may not be appropriate. Therefore, we used z-values of skewness and kurtosis to test the normality of our data set.

Overlap between two classifications

Swedler et al. (2010) used the overlap area between two classifications indicating the inconsistency by the established thresholds. In our study, we identified the overlap area between 95% confidence interval (CI) of two distributions. The overlap area was used to identify the inconsistency in foot type classification according to the thresholds proposed by the current study and Swedler et al. (2010). Moreover, 95% CI overlap was also used to access the arch height differences between genders. The overlap area between 95% CI of two distributions was obtained based on the intersection (x) calculated from eq. [4.6]:

$$\frac{(x-m_2)^2}{2s_2^2}+\frac{(x-m_1)^2}{2s_1^2}=log\frac{s_1}{s_2} \qquad [4.6]$$

where m_1 and m_2 are the mean of two variables; s_1 *and* s_2 are the standard deviation (SD). For assessing the consistency between foot type classifications, the smaller overlap area indicates the smaller type 1 and type 2 errors. It also shows the established thresholds have the better performance in distinguishing foot types or foot deformities.

Differences between gender

In the gender differences test, the overlap area between 95% confidence interval (CI) was assessed. The large overlap indicates the greater agreement between male and female. Index with greater overlap area is more applicable in cross-gender foot type classification. However, the smaller overlap indicates two distributions (i.e. male and female) are more independent, which is not suggested to apply to cross-gender foot type classification.

Differences between a person's feet— paired samples *t*-test

The effect size (Cohen's d) in a paired samples *t*-test (also known as dependent t-test) was used to assess the differences between left and right foot. The explanation and the application of P-value and T-value are displayed as following.

- **P-value**

For the hypothesis testing, p-value is to display the probability of observed results when the null hypothesis (H_0) is true. A lower *p*-value shows the lower probability to support the null hypothesis is true and the higher p-value shows the higher probability to support the null hypothesis is true (Field, 2009). In the current study, null hypothesis (H_0) means that there is no statistically significant difference between two variables and alternative hypothesis (H_A) - there is a statically significant difference between two variables. The level of significant (α) refers to a pre-chosen probability, which 0.05 the threshold of current analysis. When the p-value is less than 0.05, it is to reject the null hypothesis is true showing the statistically significant difference between two variables. When p-value is greater than 0.05, the variables fail to reject null hypothesis, which means there is no statistically significant difference between variables.

- **T-value**

The t-value calculates the difference relative to the variations in the set of data. Namely, t-value measures the difference in unit of standard error. A higher absolute t-value indicates the greater difference between the sample data meaning the greater evidence that there is a statistically significant difference. This also means the sample data has the greater evidence against the null hypothesis. In contrast, a lower absolute t-value indicates a smaller difference between the sample data showing the greater evidence that there is no statistically significant difference. In other word, lower t-value shows the sample data has greater evidence to support the null hypothesis. The formula of the t-value is as following eq. [4.7].

$$t = \frac{m_1 - m_2}{\sqrt{\frac{s^2}{n_1} + \frac{s^2}{n_2}}} \qquad [4.7]$$

where m_1 and m_2 are the mean of two variables; s is the standard deviation (SD); n_1 and n_2 are the sample size of two variables.

Degree of freedom (df) is the minimum number of independent values that are free to vary and specify their position of the system without violating any constraints [4.8].

$$df = n - 1 \qquad [4.8]$$

n is the total sample size.

For compare the NNHt and NH in the detection of feet's difference, we calculated 'Cohen's d' in the paired sample t-test. Cohen's *d* is an effect size used to indicate the standardised difference between two means. The larger effect size presents the greater differences between two variables and the smaller effect size presents the less different. For the value of Cohen's *d,* 0.2 indicates a small effect size, 0.5 - medium and 0.8 large effect size. Cohen's *d* is used to accompany reporting of *t*-test and ANOVA results. In our case, the larger effect size indicates such index can be more sensitive to detect the feet's difference than the other. The Cohen's d can be calculated as eq. [4.9].

$$d = {|m|}/{SD_{joint}} = {t}/{\sqrt{N}} \qquad [4.9]$$

where m is the mean difference between two means, SD_{joint} is joint standard deviation between two means, t is t value, N is the total subject number. All the values in the equation should be generated in a paired sample t-test.

The receiver operating characteristic (ROC)

A receiver operating characteristic (ROC) curve analysis was used to evaluate the classification thresholds established by the current study and that of Swedler et al. (2010). The ROC was tested in eight categories— NH(R_L), NH(R_H), NNHt(R_L), NNHt(R_H), NH(L_L), NH(L_H), NNHt(L_L), NNHt(L_H).

- (R_L): right foot for the classification of low and normal arch
- (R_H): right foot for the classification of normal and high arch
- (L_L): left foot for the classification of low and normal arch
- (L_H): left foot for the classification of normal and high arch.

The interpretation of positive and negative of ROC curves were compared as:

- Positive: the foot was classified into the same foot type by our and Swedler et al.'s (2010) thresholds
- Negative: the foot was classified into the different foot types by our and Swedler et al.'s (2010) thresholds

Figure 4.4 shows the ROC curves of different classifiers that plots the true positive rate (i.e. the sensitivity depicts on the y-axis) against the false positive rate (1 minus specificity depicts on the x-axis). The interpretation of sensitivity and specificity is determined as the following:

- Sensitivity (i.e. true positive): The fraction of subject that was correctly identified as positive.
- Specificity (i.e. true negative): The fraction of subject that was correctly identified as negative.

4.3. Results

Table 4.2 shows the descriptive statistics for NH and NNHt. All data were normally distributed as the absolute z-value of skewness or kurtosis was less than 2. The classification thresholds of flatfoot, low arch, normal arch, and high arch were established for NH and NNHt in both feet in Table 4.2. Table 4.3 displays the ranges of NH and NNHt for the genders and foot types. In Table 4.4, 95% CI overlap between classifications is reported and NNHt shows the greater 95% CI overlap than NH between genders. Table 4.4 also shows the classification thresholds established in the current study reduced the 95% CI overlap from above 55.0% as reported by Swedler et al. (2010) to below 10.7%. Table 4.5 displays the paired sample t-test between left and right foot showing NNHt has the greater effect size than NH. In Table 4.6, the area under curve of ROC curve is presented in the interval from 0.770

to 0.841. AUC indicates the diagnostic ability of the classification thresholds, in which the higher AUC represents a higher ability in distinguishing foot deformity from the normal arch. As shown in Figure 4.5, ROC tests were demonstrated in eight categories by plotting the sensitivity against the specificity.

Table 4.2. Descriptive Statistics and classification thresholds (i.e. flatfoot, low, normal and high arch) of NH and NNHt.

	Mean (SE)	SD	Skewness (SE)	$\mathbf{Z}_{\mathbf{skewness}}$	Kurtosis (SE)	$\mathbf{Z}_{\mathbf{kurtosis}}$	Classification threshold			
							flatfoot	low	normal	high
NH(R)	39.3(.479)	8.6	.038(.136)	.279*	-.592(.272)	-2.176	<22.1	<30.7	30.7~47.9	>47.9
NH(L)	39.2(.488)	8.7	.019(.136)	.140*	-.238(.272)	-.875*	<21.8	<.30.5	30.5~47.9	>47.9
NNHt(R)	.216(.003)	.047	-.021(.136)	-.154*	-.382(.272)	-1.404*	<.122	<.177	.177~.263	>.263
NNHt(L)	.214(.003)	.047	-.172(.136)	-1.263*	-.167(.272)	-.614*	<.120	<.175	.175~.261	>.261

* |**Z**| < 2 indicates the sample is normally distributed

(R): right foot; (L): left foot

The units for NH classification threshold are millimetre (mm)

Table 4.3. Comparison of NH and NNHt level in three foot types between the current study and the study of Swedler et al.'s (2010) in term of visual assessment and quantitative measurement using the mean and SD

		(1) Gender		(2) Foot type classification		
		Male	Female	Low arch	Normal arch	High arch
Swedler et al. (2010)	NH(R)	-	-	33.4±6.7	40.4±7.2	43.1±7.3
	95% CI	-	-	(20.0, 46.8)	(25.8, 54.8)	(28.5, 57.7)
	NNHt(R)	-	-	0.17±0.03	0.21±0.04	0.23±0.04
	95% CI	-	-	(0.110, 0.230)	(0.130, 0.290)	(0.150, 0.310)
	NH(R)	40.9±9.1	37.5±7.7	26.6±2.7	39.3±4.6	52.1±3.0

Current study	95% CI	(22.7, 59.1)	(22.1, 52.9)	(21.2, 32.0)	(30.1, 48.5)	(46.1, 58.1)
	NNHt(R)	0.216± 0.050	0.216± 0.043	0.144± 0.016	0.218± 0.025	0.287± 0.018
	95% CI	(0.106, 0.326)	(0.130, 0.302)	(0.112, 0.176)	(0.168, 0.268)	(0.251, 0.323)

(R): right foot

Table 4.4. The 95% CI overlap area between genders, low and normal arch, and normal and high arch

	Index	95% CI overlap		
		(1) Gender	(2) Foot types	
		Male/Female	Low arch identification[1]	High arch identification[2]
Swedler et al. (2010)	NH(R)	-	61.1%	80.7%
	NNHt(R)	-	55.0%	79.7%
Current study	NH(R)	80.6%	7.9%	9.0%
	NNHt(R)	89.4%	6.9%	10.7%

[1]the 95% CI overlap between low and normal arch.

[2]the 95% CI overlap between normal anf high arch.

(R): right foot

Table 4.5. Effect size in a paired sample t-test in the comparison of right to left foot

	Mean	SD	95% CI	t	df	P	Effect size (d)
NH(R)-(L)	.085	7.086	(-.694, .864)	.215	319	.830	0.012
NNHt(R)-(L)	.001	.041	(-.003, .006)	.653	319	.515	0.024

Table 4.6. ROC curve analysis. The level of agreement of the classification thresholds established by this study and the ones of Swedler et al. (2010)
(R_L): classification of low and normal arch in right foot; (R_H): classification of low and normal arch in right foot; (L_L): classification of low and normal arch in left foot; (L_H): classification of low and normal arch in left foot.

Classifier	N[1]	Positive[2]/ Negative[3]	Area Under Curve	SE	Significance level (*Area=0.5*)	95% Confidence Interval	
						Lower Bound	Upper Bound
NH (R_L)	261	244/17	.770	.027	.000*	.718	.823
NH (R_H)	247	243/4	.774	.027	.061	.721	.826
NNHt (R_L)	244	242/2	.773	.027	.184	.720	.826
NNHt (R_H)	263	236/27	.792	.026	.000*	.741	.844
NH (L_L)	257	256/1	.809	.025	.287	.760	.857
NH (L_H)	270	257/13	.805	.025	.000*	.757	.854
NNHt (L_L)	241	227/14	.841	.024	.000*	.794	.889
NNHt (L_H)	270	243/27	.786	.026	.000*	.734	.838

[1]Total subject number across two foot types (i.e. low and normal arch or normal and high arch).

[2]Positive: the foot was classified into the same foot type by our and Swedler et al.'s thresholds

[3]Negative: the foot was classified into the different foot types by our and Swedler et al.'s thresholds

*$p < 0.05$ indicates the least false positive rate

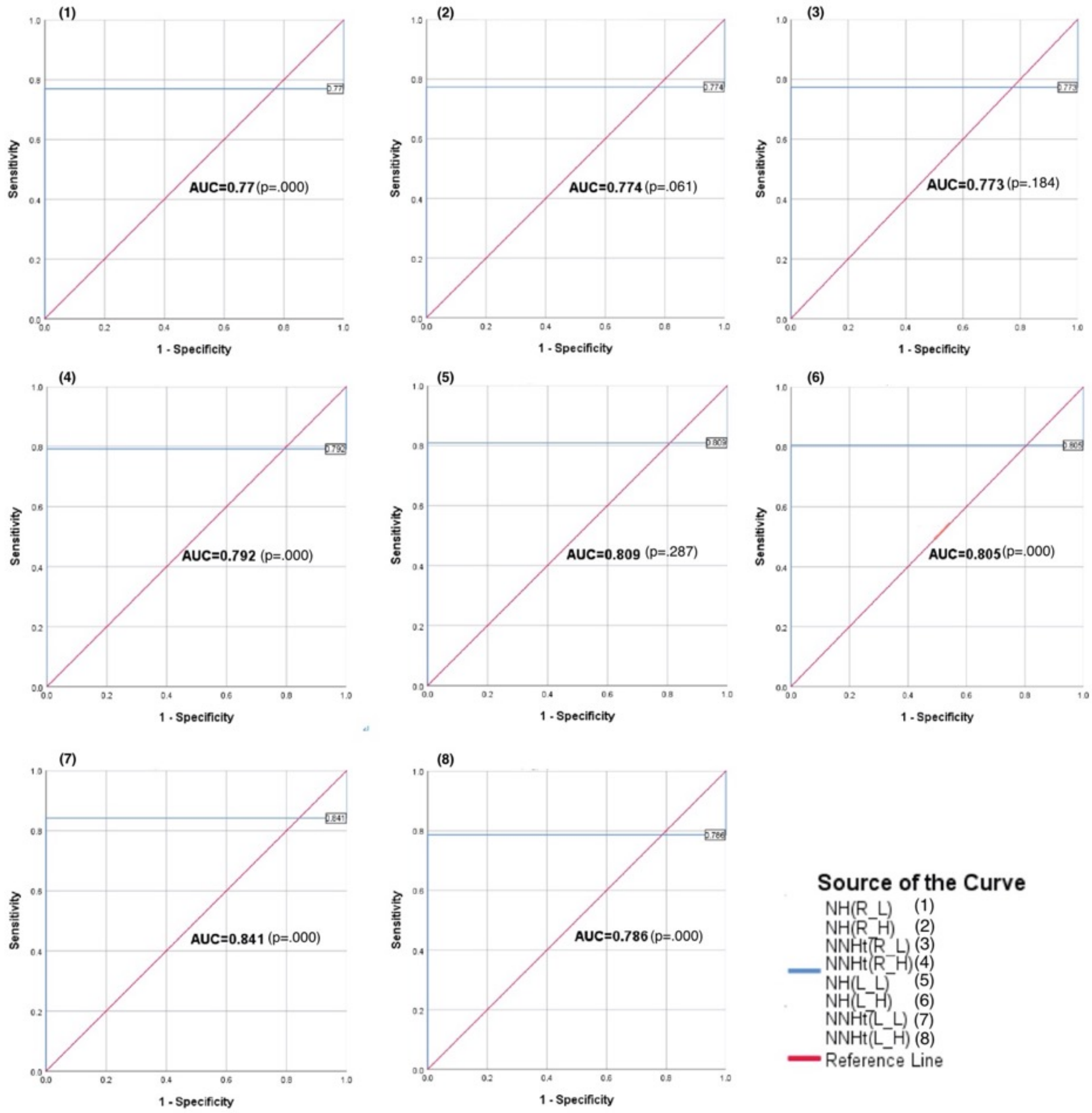

Figure 4.5. ROC curve of the classifiers— the true positive rate (i.e. the sensitivity depicts on the y-axis) against the false positive rate (1 minus specificity depicts on the x-axis). The larger area under curve (AUC) indicates the better diagnostic ability. P<.05 indicates the more reliable AUC to distinguish foot types. (R_L): right foot for the classification of low and normal arch; (R_H): right foot for the classification of low and normal arch; (L_L): left foot for the classification of low and normal arch; (L_H): left foot for the classification of low and normal arch. (1) NH(R_L) ROC curve; (2) NH(R_H) ROC curve; (3) NNHt(R_L) ROC curve; (4) NNHt(R_H) ROC curve; (5) NH(L_L) ROC curve; (6) NH(L_H) ROC curve; (7) NNHt(L_L) ROC curve; (8) NNHt(L_H) ROC curve.

4.4. Discussion

Threshold for foot classifications

The proposed protocol extracted NH and NNHt from the 3D foot image and established the thresholds for foot type classification. For the normality test, the z-value of skewness and kurtosis was used as proposed by Kim (2013) because it is more accurate when the sample size is over 300 compared to the traditional method— Shapiro-Wilk test and Kolmogorov-Smirnov test. As shown in Table 4.2, the absolute z-value of skewness is less than 2 or kurtosis is less than 7 showing the sample data is normally distributed. For foot type classification, the same method as proposed by Murley et al. (2009) was used to identify a normal arch when the value was between the mean ± SD, a low arch when the value is less than the mean – SD, a high arch when the value is large than the mean + SD, a flatfoot when the value is less than mean – 2SD. Therefore, the flatfoot was identified when NH was less than 22.1 mm on the right foot and 21.8 mm on the left foot, or when NNHt was less than 0.122 on the right foot or 0.120 on the left foot. Several studies (Murley et al., 2009; Nilsson et al., 2012) have presented on the existence of differences between a person's feet, which indicates a foot screening protocol should establish the classification thresholds for right and left foot separately.

The 'low arch classification' shown in Table 4.3, the mean NH and NNHt of our data are less than Swedler et al.'s (2010). Swedler et al. (2010) examined military trainees and the person with low arch or flatfoot may not meet the physical requirements to serve in the military. The recruited participants from Swedler et al. (2010) excluded the low-arch because such people are not deemed fit to serve in the army. Therefore, we might explain why the average height of arch is higher in Swedler et al.'s (2010) as they have a potential bias to unwittingly shifted the classification criteria upwards. The other factor may affect the classification threshold is participant's gender. As male are averagely higher in NH than female as previously reported (Hill et al., 2017, Saghazadeh et al., 2015), more males involved might lead to higher NH mean while no study has found average NNHt value is affected by gender. The male participants were twice the number of females (Swedler et al., 2010) while the current sample is more gender balanced (male and female are 163 and 157).

Overlap between foot types

Due to the overlap between low and normal arch, an increase in the upper limit of low arch threshold is proposed to reduce type 1 errors. In this way, type 2 errors may increase and wrongly identify normal arch as low arch. However, as we intended to prevent any omission of low arch, we would rather increase false positives. We have examined different thresholds and finalized 5% increase of $\bar{X} - SD$ as the upper limits of low arch threshold. As shown in Table 4.3, the upper bound of 95% CI of low arch is 0.176 for right foot. The low arch threshold of right foot, 0.177, is just above 0.176, which ensures the unnecessary type 2 errors were not excessively increased. The lower limits of low arch threshold, 0.122 and 0.120 for right and left foot respectively, remained unchanged (Table 4.2). As there were only four right feet and eight left feet classified into flatfoot, such subject number does not provide statistical significance for investigating the misclassification issue.

The diagnostic thresholds of foot type classification were assessed by the overlap area between two distributions for indicating type 1 and 2 errors. Before we calculated the overlap area between two classification, the substantial overlap may be observed from 95% CI in Table 4.3. As shown in Table 4.3, the substantial overlap is found in Swedler et al.'s (2010) data as the upper bond of 95% CI in low arch is higher than the mean value of normal arch and the lower bond of 95% CI in normal arch is lower than the mean value of low arch. Moreover, the lower bond of 95% CI in high arch is lower than the mean of the low arch and the upper bond of 95% CI in normal arch is almost equal to the upper bond of 95% CI in high arch. The overlap of our data can be also recognised from the upper and lower bonds of 95% CI, but it is not substantial as the data of Swedler et al. (2010). In the study of Swedler et al. (2010), the plantar surface of the foot was visually assessed on the basis of predetermined footprint templates. The assessors visually classified the subjects as low, normal and high arch. The absence of cut-off value in visual assessment may be the critical cause of this substantial overlap. In our data, the classification thresholds were established by using the mean and SD, and we assume that the overlap cause by visual assessment could be greatly reduced by the mean and SD. As shown in Table 4.4, the classification thresholds proposed in the current study reduced the 95% CI overlap from 61.1% and 55.0% to 7.9% and 6.9% in NH and NNHt respectively for low arch identification, and from 80.7% and 79.7% to 9.0% and 10.7% in NH and NNHt respectively for high arch identification. The 95% CI overlap indicates type 1 (wrongly identifying low arch as normal arch) and type 2 errors (wrongly identifying normal arch as low arch). The lower 95% CI overlap shows the better performance in foot type classification. In Table 4.4., NNHt has smaller 95% CI overlap than NH in low arch but larger 95% CI overlap in high arch, which may indicate NNHt performed better in identifying low arch and NH performed better in identifying high arch.

Swedler et al. (2010) employed the simple and practical foot arch index, NNHt, to classify large number of subjects into three different foot types. However, the significant overlap between classification indicating 55% misclassification rate was reported. This limitation can be improved by the thresholds and 3D foot scan technique proposed in the current study.

Arch height differences in gender

As shown in Table 4.8, several studies have found foot arch is higher in male than female (Swedler et al., 2012; Saghazadeh et al., 2015; Zifchock et al., 2006) when measured by NH. NH values reported by previous studies were similar to our finding, which NH is 40.9 ± 9.1mm for male and 37.5 ± 7.7mm for female (Table 4.3). Such differences in NH may be adverse for establishing thresholds in mixed-gender classification because the mean NH could shift upwards when more male subjects were recruited and shift downward when more female subjects were recruited. As shown in Table 4.4, NNHt (89.4%) has larger overlap than NH (80.6%) between male and female indicates NNHt are more gender neutral. Saghazadeh et al. (2015) reported statistically significant difference between genders in NH and gender differences in NNHt is not statistically significant. Therefore, NNHt is considered more applicable than NH in mixed-gender foot type classification. As NNHt is less affected by gender, the value of population norm is more stable regardless the proportion of the male and female in a sample data.

Table 4.8. The differences between male and female in arch height using different index

	Study	Male	Female
Mean NH (mm)	Hill et al. (2017)	45.14	40.27
	Saghazadeh et al. (2015)	41.77	35.76
	Swedler et al. (2010)	41.2	37.6
	Our data	40.9	37.5
Mean NNHt	Saghazadeh et al. (2015)	0.229	0.212
	Swedler et al. (2010)	0.211	0.210
	Our data	0.216	0.216

Arch height difference between left and right foot

Murley et al. (2009) reported that people tend to have a flatfoot in one foot and normal arch in the other. The asymmetric arch height in flatfooted people indicates differences between a person's right and left foot. Zifchock et al. (2006) reported the greater arch height in the dominant foot, which emphasizes the differences between a person's feet. The study of Swedler et al. (2010), as the current largest sample size investigating subject's NH and NNHt, also reported 40.0 ± 7.6 (mm), 38.4 ± 7.4 (mm), 0.211 ± 0.042, and 0.202 ± 0.043 for NH(R), NH(L), NNHt(R), and NNHt(L) respectively showing the substantial difference in left and right foot. As shown in Table 4.5, NNHt demonstrates the greater effect size than NH, which is more sensitive to detect the difference between a person's feet. In Table 4.5, NH is 0.085 cm and NNHt is 0.001 higher in the right than the left foot, which could infer that most subjects in our study have the higher arch in their right foot. Similarly, in Table 4.7, the right foot is higher than left foot in both NH and NNHt. Zifchock et al. (2006) has reported that people have the greater arch height in the dominant foot but in current study we cannot such conclusion without conducting specific tests to assess dominance. We cannot either rely on self-reported foot dominance as people assume wrongly it is the same as hand dominiance (Taylor et al., 2006). Our finding supports that NNHt is more sensitive to detect the arch differences in a person's feet. As NNHt normalizes NH by truncated foot length, NNHt is expected to be better related to the arch curvature than NH (Williams and McClay, 2000).

ROC curve

The ROC curve is used to assess the performance of classification at different thresholds and the value of AUC indicates the diagnostic ability of the classification thresholds. The higher AUC represents the higher ability in distinguishing foot deformity (i.e. flatfoot) from normal arch. The AUC values provide the probability of randomly selected a true positive, which ranges from 0.5 (no diagnostic ability) to 1.0 (perfect diagnostic ability) (Berrar & Flach, 2011). In Table 4.6, all NNHt has greater AUC than NH except for NNHt (L_H), which corresponds to the result in Table 4.4 that NNHt from our study present better performance than NH in identifying low arch. In Table 4.6, NNHt (R_H) has greater AUC than NH (R_H) for high arch classification contradicts the results shown in Table 4.4 where NNHt showed greater 95% CI overlap area suggesting poorer performance than NH. This disagreement demonstrates an inconclusive result in determining which index has better performance in high arch identification. In addition, the significance level (i.e. p-value) of AUC shows the probability to make a false positive decision. The higher p-value, the higher probability of type 1 error (Berrar & Flach, 2011), NH(R_L), NNHt(R_H), NH(L_H), NNHt(L_L) and NNHt(L_H) display $p < 0.05$ indicating the least false positive rate (Table 4.6).

Weightbearing condition for scans

Foot posture and shape in terms of the foot dimension can be varied when the subjects are scanned in the different weightbearing conditions, as it is responding to the weight or loading on the foot (Tsung et al., 2003). Tsung et al. (2003) found increased plantar contact area, foot length, foot breath and rearfoot width and decreased arch height and arch angle (a parameter indicates arch height) in full body weight measurement compared to half or non-bodyweight measurement. The arch height differences between weightbearing conditions can be even greater for a flexible foot arch (i.e. low arch or flatfoot) because the foot posture is harder to maintain when loading. Foot arch decreased 52% in height from non-weightbearing (i.e. sitting) to semi-weightbearing (i.e. bilateral standing) (Ferri et al., 2008). In our foot scanning for foot assessment, the participants were scanned in bilateral standing (i.e. semi-weightbearing) position in order to differentiate foot types especially normal and low arch under load. If a participant was classified as low arch by defined NNHt, the feet were scanned again in the non-weightbearing condition to acquire the parameter and 3D image for customized insert design as detailed in Chapter 7.

Self-reported low arch population

According to our diagnostic threshold, low arch/flatfoot can be identified when the right foot NNHt < 0.177. Based upon the threshold, 55 out of 320 participants were classified as low arch. However, only six participants aware they have low arch before the measurement. This may explain the importance of mass screening, as in this case only 11% of population were aware of their low arch. Although none of the subjects reported any related injuries or muscular syndromes, it is likely to occur later due to aging (Puszczalowska-Lizis et al., 2017), sport (Michelson et al., 2002) or physical training (Swedler et al., 2010). Through statistical analysis, the current study provides a preliminary screening protocol to identify foot deformity at early stage (i.e. low arch) in order to adopt appropriate corrective strategies (i.e. shoe insert). The classified flatfoot individuals (i.e. NNHt<0.122 at right foot; <0.120 at left foot) is proposed to refer to medical professional for further investigation.

Establishment of new classification thresholds for insert design

From our result, NNHt is more appropriate than NH to combine 3D imaging for low arch and flatfoot identification. Moreover, current low arch threshold of NNHt has brought down the inconsistency reported by previous study from 55% to 6.9%. However, 6.9% of overlap between normal and low arch still represent the potential type 1 and 2 errors. As we intended to select all the low arch for customized insert design in the later chapter, we increased the threshold to minimize type 1 error (i.e. wrongly identify low arch as normal arch). This may inevitably increase type 2 error (i.e. wrongly identify normal arch as low arch) but there is no evidence that the insert brings the negative effect to normal arch people. Therefore, we increase 5% of the upper limit of the low arch threshold of NNHt which is 0.177 and 0.175 for right and left foot respectively. The new threshold is only 0.001 greater than the upper limit of 95% CI threshold that may not increase the unnecessary type 2 errors.

4.5. Conclusion

The proposed foot arch assessment established clear classification thresholds to identify flatfoot, low arch and normal or high arch. The retrospective application of the thresholds established by our protocol substantially reduced the overlap among classification outlined by Swedler et al. (2010) from above 55% to below 11%, which indicates that uncertainty in classification can be greatly reduced. The foot arch assessment we developed can be used not only for screening but also as a diagnostic aid. In the choice of foot arch index, NNHt is more appropriate than NH because it is not gender-biased and more sensitive to detecting the difference between a person's right and left foot. The proposed procedure using a 3D foot scanning addressed the practical imprecision of manual measurement and provided a faster and simpler method. The established thresholds classify foot in three types— flatfoot, low arch and normal/high arch. Flatfoot is normally considered as pathologic and should be referred to a medical professional for diagnosis. Normal and high arch were excluded from insert design in later chapters as they outside the scope of this work. Only low arch participants with NNHt between 0.122 and 0.177 in right foot or between 0.120 and 0.175 in left foot were referred for insert design and kinematic assessment. This study is the first step in the selection of enhanced 3D characteristics to classify unique borderline cases. In the future we consider utilizing 3D index (e.g. foot volume) for more detailed and accurate foot arch characterization. The geometrical model of the plantar and dorsal surfaces has been developed by Hu et al. (2018) using a method similar to the one proposed but supplemented by some of the invariances used by Dabnichki and Zhivkov (2010; 2005). The first research question— what are the thresholds for low arch/flatfoot identification that can minimize current type 1 and 2 errors, were addressed in Chapter 4.

Chapter 5. Transient change of foot arch due to activity levels

5.1. Introduction

Foot arch is passively supported by bone and ligament, and actively supported by muscle and tendon. Physical activity may induce muscle fatigue that attenuate muscle's capacity of resisting load and temporary alters the muscle-bone interaction (Avin et al., 2015). As shown in Table 5.1, other studies showed fatigue-induced activities can change the form of medial longitudinal arch (MLA) in standing (Headlee et al., 2008; Cowley and Marsden, 2013; Okamura et al. 2017).

Table 5.1. The change of Navicular height after fatigue-induced activities

Studies	Activity	Measurement	Result (mean)
Headlee et al., 2008	Toe curl exercise	Standing Navicular Height	Reduce 1.8mm
Cowley and Marsden, 2013	Half marathon		Reduce 5mm
Okamura et al. 2017	Toe curl exercise		Increase 1mm

Headlee et al. (2008) found the significant reduction in height of MLA after isolated fatiguing protocols of foot intrinsic muscle. Cowley and Marsden (2013) observed a significant reduction in MLA after subjects participated in a half marathon race. However, Okamura et al. (2017) found a conflicting result, which the height of MLA increased after the isolated fatiguing protocols of foot intrinsic muscle. This conflicting result may be explained by the foot core system paradigm presented by McKeon et al. (2014), which the fatigue foot intrinsic muscle might be induced by the surrounded muscle to provide compensatory support for MLA and cause the increment of arch height. Based upon these finding, any moderate or vigorous-intensity physical activities (e.g. running, jogging, dancing) (Lee and Paffenbarger, 2000) that is more likely to cause foot muscle fatigue shall be avoided prior to the MLA measurements since it is more likely to affect the measure results. These studies investigated extreme circumstances where measurements were taken directly after muscle-fatiguing protocols. However, it is unclear whether the physical activities of daily living (e.g. sitting, standing, and walking) could cause the change in MLA and affect the measure results. MLA is changed when the foot is at the fatigue stage, which seems the higher activity levels is more likely to lead to the change in MLA. Furthermore, significant foot swelling (5.7% increase in foot volume) was found in sedentary individuals after 8 hours of sitting (Noddeland & Winkel, 1988). It shows that foot morphology can be also changed more in less-active individuals. Muscle temperature surrounding foot and leg decreased for individuals who experienced two to four hours of prolonged sitting (Morishima et al., 2016; Noddeland & Winkel, 1988). A drop of muscle temperature can increase foot volume and change the nervous conduction and force production of foot muscle, and that may affect arch maintenance (Bishop, 2003; Fiolkowski et al., 2003). It seems that the curvature of the foot might be temporarily changed by different activity levels, and this could potentially affect the measurement results. However, none of the study provides the insight into whether the physical activities of daily living affect the foot arch measurements of.

Therefore, the aim of current chapter is to investigate how different activities of daily living affect the foot type classification. The change of MLA in active and sedentary population was accessed using the method proposed in Chapter 4. According to the test result, the control protocol of the measurement should be proposed to reduce the interferences induced by the activities.

5.2. Materials and methods

Participants

A cohort of 60 healthy adult volunteers (39 males, 21 females, mean age: 31.8± 10.03 years) were randomly selected from a cohort of 320 healthy participants (163 males, 157 females, age 18 and above). Individuals with any injuries, surgery, or other medical condition such as osteoarthritis in foot or ankle within the last six months were not accepted. Individuals who regularly used therapeutic foot orthoses were also excluded. All participants were informed about the purpose of the study and potential risks and then signed the informed consent statement. The ethical approval was obtained from the University Human Ethics Committee.

Instrumentation

Infoot® digitizer (I-Ware Laboratory Co. Ltd.) was used to obtain the foot dimensions. Data collection methods adhered to the international protocols for 3D scanning and human body measurements (Bonita et al., 2006). An Omron® pedometer (Omron Healthcare Inc.) was used to record the step count of participant between two measurements for classifying the activity levels.

Procedure

The procedure to measure foot dimensions of participants using Infoot® scanner is available in Chapter 4. For the reliability test of ICC and MDC, the participants had scanned right and then left foot which was repeated for three times. Therefore, ICC and MDC can be calculated by three groups of data sets. For the within-day transient change of foot arch, two anthropometric values— 'height of navicular', 'instep length (i.e. truncated foot length)' were obtained by foot scan, and two anthropometric indices—navicular height (NH) and normalized navicular height truncated (NNHt) were calculated as eq. [5.1] and [5.2] respectively.

$$NH = height\ of\ navicular \qquad [5.1]$$

$$NNHt = {}^{height\ of\ navicular}/_{instep\ length} \qquad [5.2]$$

The initial measurement was taken between 9 to 12am. The participants were asked to return for the follow-up measurement 4 to 6 hours after the initial measurement. This is because a significant increase in foot volume was reported in the first 4 hours for sedentary people (Winkel and Jørgensen, 1986). Each participant was given an Omron® pedometer (Omron Healthcare Inc.) to record their step count between two measurements. In addition, they were asked to record the sedentary time and the physical activities between two measurements. Moreover, for mitigating the unwanted variations to the measures, all participants should adhere to the following between two measurements.

1) Footwear control

Participants were required to wear closed-toe shoes with heel elevation less than 3cm between two measurements. The change of skin temperatures alters muscle activation (Winkel & Jørgensen, 1991) and increased heel elevation (Yung-Hui and Wei-Hsien, 2005) affect the plantar pressure and impact force that could possibly affect the validity of the measurement.

2) Physical activity control

Participants were required to avoid any moderate and/or vigorous intensity physical activity (e.g. running, jogging, dancing, basketball, mountain climbing, etc.) (Lee and Paffenbarger, 2000) that are more likely to induce foot muscle fatigue and affect the result of the measurement.

Activity level classification

Participants were classified into 'active' or 'sedentary' group based on the step count and self-reported sedentary time between two measurements. Participants selected in active group required to meet at least one of following criteria. Participants failed to meet any criterion below were classified into sedentary group.

1) Average step count above 588 steps per hour

The threshold, 588 steps per hour, is obtained by the ratio of active individual's daily average steps to daily average waking hours. Active individual is identified when the daily step count more than 10000 steps (Tudor-Locke and Bassett, 2004). Australian average waking hours is 17 hours per day (Adams et al., 2017). Thus, 588 steps per hour is obtained by 10000 steps divided by 17 hours.

2) Self-reported sedentary time was greater than 40%

For prolonged standing individuals, they may not reach the step count threshold, but their foot was still in a prolonged weight-bearing condition. Therefore, individuals who reported sedentary time greater than 40% of the total time between two measurements were classified as active.

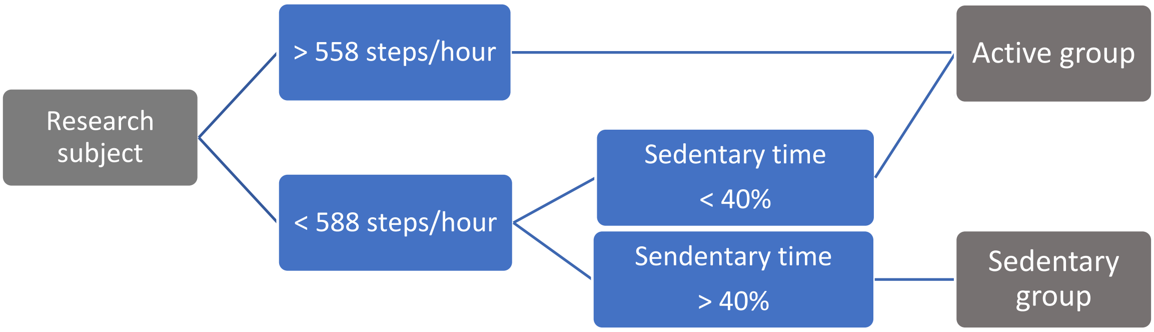

Figure 5.1. The flow chart of classification of activity levels

Statistical analysis

- **Reliability**

A reliability test was carried out before the experiment began for ensuring we measure the real change of the foot arch height instead of the error. The reliability test can be assessed by intraclass correlation coefficient (ICC) and minimal detectable change (MDC).

1. Intraclass correlation coefficient

Analysis of the reliability refers to the consistency of the measurement protocol, which assesses the homogeneity or consensus between different measures. A measurement is considered more reliable if the variance between the results could be reduced. Two reliability tests— inter-rater and intra-rater reliability has been done in current study. Inter-rater reliability is to assess the agreement between the results measured by more than two raters. Inter-rater reliability is to assess the agreement between the two or more trails measured by the same rater. Intraclass correlation coefficients (ICCs) can be used as the indicator of reliability, which expresses a ratio of variance of between-subjects variability to that of within-subjects as following equation (Shrout and Fleiss, 1979)

$$ICC = {S^2(b)}\Big/{(S^2(b) + S^2(w))} \qquad [5.3]$$

Where $S^2(b)$ is the variance of the feature between subjects and $S^2(w)$ is the pooled variance within subjects. $S^2(b)+ S^2(w)$ is the variance for all rating regardless of whether the subjects are repeated or not.

There is other statistical indicator such as Cohen's Kappa and Fleiss Kappa that can assess the reliability, but ICCs is the one that can be used for the continuous variables. The value of ICCs is between 0 to 1 and the higher reliability is closer to 1. For the interpretation of ICCs, value above 0.9 indicates excellent reliability, value between 0.75 and 0.9 - good reliability, value between 0.5 and 0.75 - moderate reliability, and values less than 0.5 are indicative of poor reliability (Koo and Li, 2016). The measurement for clinical use requires ICCs above 0.9. There are three models for ICCs— one-way random, two-way random, and two-way mixed. One-way random means the random effects can only come from either the raters or the subjects and this is used rarely since it is difficult to distinguish random subjects. Two-way random chooses the rater and subjects randomly so that the random effect can come from two resources and this model is more commonly to use. Two-way mixed fixes the rater to assess the random subjects. And there are two types of analysis for ICCs— consistency and absolute agreement. Consistency is to establish the correlation between two variations that is very similar to Pearson's correlation. This can evaluate whether two variables are linear related to each other but cannot detect how the variables are consistent between different measurements in term of the agreement in the measurement. For instance, the variables can be linear related to each other but not necessarily consistent in the measurement. Absolute agreement assesses the agreement between raters in the single item that is to confirm the raters are agreed absolutely the measure they get it. Different models and types of ICCs are also presented by Shrout and Fleiss (1979) as two numbers in parentheses— ICC(1,1), ICC(2,1), ICC(3,1), ICC(1,k), ICC(2,k) and ICC(3,k), as following.

- ICC(1,1): each subjects is assessed by a different set of randomly selected raters and the reliability is calculated from a single measurement. It is not commonly used for reliability test in clinical studies. (i.e. one-way random effects, absolute agreement, single rater/measurement).
- ICC(2,1): each subject is measured by each raters and the raters have been randomly selected. The raters are considered representative of a larger population of similar raters. Reliability calculated from a single measurement (i.e. two-way random effects, absolute agreement, single rater/measurement).

- ICC(3,1): each subjects is measured by each raters and the raters are only raters of interest. Reliability calculated from a single measurement (i.e. two-way mixed effects, consistency, single rater/measurement).
- ICC(1,k): each subjects is assessed by a different set of randomly selected raters and the reliability is calculated by taking the average of the raters' measurement (i.e. one-way random effects, absolute agreement, multiple raters/measurements).
- ICC(2,k): each subjects is measured by each raters and the raters are considered representative of a larger population of similar raters. The reliability is calculated by taking the average of the raters' measurement (i.e. two-way random effects, absolute agreement, multiple raters/measurements).
- ICC(3,k): each subjects is measured by each raters and the raters are only raters of interest. The reliability is calculated by taking the average of the raters' measurement (i.e. two-way mixed effects, consistency, multiple raters/measurements).

SPSS software, Version 25 (IBM SPSS Inc.) was employed to operate the calculation of ICCs as following procedures (Landers, 2015).

1) Determine the appropriate ICC model

As there are generally six ICC model as we mentioned above, first we have to select the appropriate model from one-way random, two-way random, two-way mixed that can be used in current case. As we had three raters to review the subjects, we crossed off 'one-way random', which might use the random raters. We selected subject randomly to be assessed. We determine that we a population of raters and our raters were chosen to represent the population of the raters. Throughout the measurement, the raters were fixed. Therefore, we crossed off 'two-way random' in SPSS, which is used when the rater is randomly selected (Fig. 5.1).

2) Determine the appropriate ICC type

We used 'two-way mixed' as we have the same population of raters to review the subject that has randomly selected. Determine the value that is used for assessing— single or average measures. As we used a single individual as our ratee, we used 'single measure' rather than 'average measure', which is calculated by the mean of the measurement. Determine which set of values we ultimately want the reliability for— consistency or absolute agreement. In both consistency assessment of ICCs, we want to not only have the insight whether the variables is linear related to each other, but also to assess the consistency of the variables in each items. Therefore, we selected 'absolute agreement' rather than 'consistency', which only present how each variable is linearly related. The procedure in SPSS: Analyse > Scale > Reliability analysis > Select 'Statistics' > Check 'Intraclass correlation coefficient' > Select the 'Model' and 'Type' as we determined above > Click 'Continue' > Click 'OK' (Fig. 5.2).

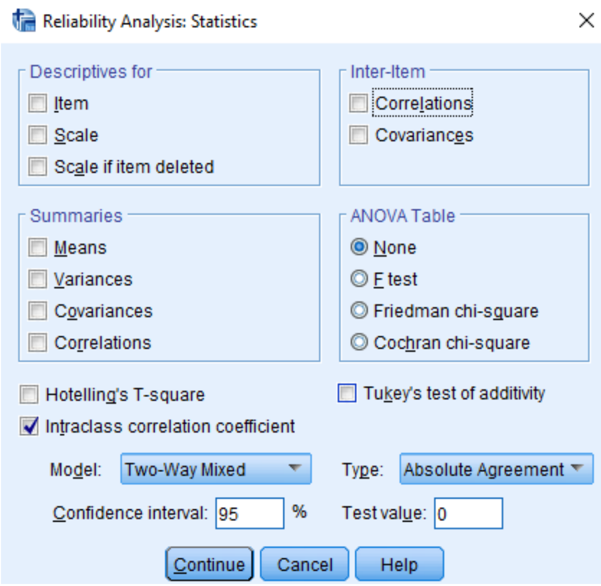

Figure 5.2. The interface of SPSS— select the model and type of ICC

2. Minimal detectable change

The minimal detectable change (MDC) is defined as the minimal change can be detected by the instrument or tool beyond the random measurement error with a 95% confidence interval (Lee et al., 2013). As we measured the real change in the height of foot arch rather than the error of measurement, MDC provided the statistical threshold that estimates the smallest magnitude of change that is likely to be real. In the current study, we used MDC as an indicator for the responsiveness of the Infoot scanner and the sensitivity of the test procedure and statistical method. MDC is calculated based on the result of SEM as eq. [5.4].

$$MDC = \sqrt{2} \times 1.96 \times SEM \qquad [5.4]$$

The root square of 2 is used to account for the underlying extra uncertainty during two different measurements. The value 1.96 is the z-value correlated to 95% confidence interval. SEM is 'standard error of measurement' expressing variability in the same unit as the original measure (Weir, 2005). The formula of SEM is as eq. [4] that observed test scores for a given true score using the standard deviation.

$$SEM = SD \times \sqrt{1 - ICCs} \qquad [5.5]$$

Where SD is standard deviation of the scale's score (i.e. the all test's score).

SEM and MDC can be transferred into SEM% and MDC% respectively as eq. [5.6] and [5.7], which is the relative amount of random measurement error for comparing the different variables.

$$SEM\% = \left({SEM}/{m}\right) \times 100\% \quad [5.6]$$

$$MDC\% = \left({MDC}/{m}\right) \times 100\% \quad [5.7]$$

Where m is the mean of the scale's score (i.e. the mean score of all tests). When MDC% is less than <30%, it means the responsiveness of measurement and the sensitivity of the statistical method is considered as acceptable and less than 10% is excellent.

The data were analysed in SPSS software, Version 25 (IBM SPSS Inc.). Shapiro-Wilks test was used to evaluate the normality of the sample data of initial measurement as eq. [5.8].

$$W = {\left(\sum_{i=1}^{n} a_i x_{(i)}\right)^2}\Big/{\sum_{i=1}^{n}(x_i - \bar{x})^2} \quad [5.8]$$

Where xi are the values of random sample, a_i are constants generated from the covariance, variances and means of the sample from a normally distributed sample. Smaller value indicates that sample data deviates from normal distribution. If significance level of W value is greater than 0.05, the sample data is normally distributed. As the statistical issue for normality test that Kim (2012) pointed out is more like to occur when the sample size is over than 300, we used Shapiro-Wilks test rather than the z-value of skewness and kurtosis for assessing the normality because the current sample size is only 60.

In order to assess whether the active and sedentary group start at a similar baseline, we compared the initial measurements. Therefore, we used independent samples t-test and the 95% overlapping confidence interval to assess whether there is statistically significant difference between sedentary and active group in the initial measurement. We hypothesize that more changes would be found in active individuals than sedentary individuals in the second foot scanning.

- **The effect size of t-test**

For indicating the changes before and after the physical activity of daily living, we used both parametric and non-parametric test. By the parametric test (i.e. paired sample t-tests), we measure the actual value of the arch height changed and identify whether the change is statistically significant. The effect size (Cohen's d) in the pair sample t-tests was used to compare the change of follow-up measurement to the initial measurement. The effect size is obtained by eq. [5.9]:

$$d = {mean}/{SD} = {t}/{\sqrt{n}} \quad [5.9]$$

n is the total sample size, and t is the t-value that can be calculated as eq. [5.10]:

$$t = \frac{m_1 - m_2}{\sqrt{\frac{s_1^2}{n_1} + \frac{s_2^2}{n_2}}} \qquad [5.10]$$

Where m_1 and m_2 are the mean of two variables; s_1 and s_2 is the standard deviation (SD) of two variables; the n_1 and n_2 are the sample size of two variables.

The larger effect size presents the greater differences between two variables and the smaller effect size presents the less different. For the value of Cohen's d, 0.2 indicates small effect size, 0.5 medium and 0.8 large.

- **The Wilcoxon signed-rank test**

The non-parametric test (Wilcoxon signed ranks test) is to assess whether the foot type classification could be changed in the follow-up measurement. In this test, we only compare the differences on NNHt in the right foot. The participants were classified into three groups according to the classification thresholds established in chapter 4: low arch (<0.169), normal arch (from 0.169 to 0.261), high arch (> 0.261) in the two measurements. The rank for low, normal, and high arch were 1, 2 and 3, respectively. We used the rank of follow-up measurement to minus the initial measurement so that the Z-value is obtained as eq. [5.11] indicating the change of the classification.

$$z = {W - m_w \pm 0.5}/{\sigma_w} \qquad [5.11]$$

where W is the sum of the ranks. For large samples with n>10 the W-statistics approximates normal distribution. In our Wilcoxon signed rank test, the null hypothesis is that there is on average no difference between the two measurements. Therefore, we assume that m_w is 0. The standard deviation (σ_w) is calculated as eq. [5.12].

$$\sigma_w = \sqrt{{n(n+1)(2n+1)}/{6}} \qquad [5.12]$$

5.3. Results

Table 5.1 show ICCs of NH and NNHt are 0.987 and 0.959 respectively. Both of their lower bound of 95% confidence interval are still very high representing excellent reliability. The significant level was both less than .0005 (display as .000 by the system) representing the result was statistically significant. The Standard error measurement (SEM) is 1.222mm for NH and 0.008 for NNHt. And based on the SEM value, minimal detectable change (MDC) is 3.388mm for NH and 0.002 NNHt. In other word, the value difference between follow-up and initial measurement should be beyond MDC to represent the real change instead of the error.

Both the MDC% of NH (2.87%) and NNHt (3.68%) are less than 10%, which is excellent in reliability.

Table 5.1. The Interclass correlation, standard error measurement and minimal detectable change of NH and NNHt

	Intraclass Correlation	95% Confidence Interval		F Test with True Value 0		Mean	SD	SEM (%)	MDC (%)
		Lower Bound	Upper Bound	Value	Sig.				
NH (mm)	.987	.948	.998	70.38	.000	117.97	9.11	1.222 (1.04%)	3.388 (2.87%)
NNHt	.959	.834	.994	21.98	.000	.663	.047	0.008 (1.33%)	0.002 (3.68%)

Table 5.2 shows the demographics of the participants in active and sedentary group. Table 5.3 displays statistics description and the result of Shapiro-Wilks test for the initial measurement. The sample data of initial measurement is normally distributed when the p-value of Shapiro-Wilks test is greater or equal than 0.05 (Field, 2009). All indices were found to be normally distributed. Table 5.4 shows the independent samples t-test that compare the values of sedentary to active group in the initial measurement, and the overlapping confidence interval between sedentary and active group in each anthropometric index. The height of arch is greater in sedentary than active group for NH and NNHt. However, their p-values are all greater than the significance level (α=0.05) indicating such difference is not statistically significant. The overlapping 95% confidence interval (CI) between sedentary and active group are between 0.902 for NNHt(R) and 0.916 for NH(R), which shows the high consistency between two groups in the initial measurement. Table 5.5 demonstrates the effect size in the paired samples t-test compare the follow-up measurements to initial measurement for active and sedentary group. From the paired t-test, all the mean is positive value showing the height of foot arch is greater in follow-up measurement than initial measurement. The effect size of the sedentary group is much greater than that of the active group except for NH (L), indicating the greater change in foot arch height is found in less active individuals. Our finding contradicts our hypothesis that more change in anthropometric values would be found in active individuals than less-active individuals. In table 5.6, 10 people shifted to the higher classification in the follow-up measurement and only 2 people shifted to the lower

classification. The z-values based on the positive rank are positive in both sedentary and active groups because more participants had moved to the higher classification than the lower on the follow-up measurement. The higher absolute z-value was found in sedentary group indicating they have greater chance to influence the outcome of measurements than active group.

Table 5.2. Test subject demographics in active and sedentary group (Mean ± SD)

	Active group	Sedentary group
N	21	39
Gender	14 males; 7 females	25 males; 14 females
Age (years)	33.1 ± 14.8	31.1 ± 6.3
Height (cm)	173.2 ± 9.7	170.2 ± 9.4
Body mass (kg)	67.1 ± 17.1	67.2 ± 10.8
Body mass index	22.1 ± 3.8	23.1 ± 2.6

Table 5.3. The statistics description of initial and follow-up measurement and the normality test of initial measurement

Activity group	Index	Foot	Statistics description (mean ± SD)		Shapiro-Wilk of initial measurement		
			Initial	Follow-up	Statistic	df	p
Active group	NH (mm)	R	43.1±9.3	43.7±8.5	.965	21	.613*
		L	42.2±7.1	44.8±7.7	.973	21	.798*
	NNHt	R	.231±.049	.236±.044	.977	21	.875*
		L	.228±.037	.243±.040	.976	21	.857*
Sedentary group	NH (mm)	R	42.5±8.5	44.1±8.2	.979	39	.669*
		L	41.4±8.0	43.9±7.2	.983	39	.809*
	NNHt	R	.232±.043	.242±.040	.985	39	.870*

	L	.228±.043	.242±.038	.983	39	.818*

* $p > .05$ indicates the sample is normally distributed

(R): right foot; (L): left foot

Table 5.4. Independent samples t-test compare sedentary to active group for the initial measurement and the overlapping confidence interval between sedentary and active group

Activity group	Index	foot	Mean	*t*	*Df*	*P*	*Overlapping 95% CI*
Active	NH	R	-11.6	-.527	58	.600	.916
vs.		L	-9.0	-.439	58	.662	.900
sedentary group	NNHt	R	-.003	-.292	58	.772	.902
		L	-.003	-.269	58	.789	.895

Table 5.5. Effect size in the paired samples t-test compare the follow-up measurement to the initial measurement for active and sedentary group

Activity group	Index	foot	Mean	SD	95% CI	*t*	*Df*	*p*	*Effect size (d)*
Active group	NH	R	5.8	49.4	(-16.7, 28.2)	.534	20	.599	.12
		L	25.8	47.3	(4.2, 47.3)	2.494	20	.022	.54
	NNHt	R	.004	.024	(-.007, .015)	.821	20	.421	.18
		L	.015	.027	(.002, .027)	2.463	20	.023	.54
Sedentary group	NH	R	27.2	58.0	(8.4, 46.0)	2.929	38	.006	.46
		L	26.9	49.4	(10.8, 42.9)	3.393	38	.002	.54
	NNHt	R	.016	.033	(.006, .027)	3.073	38	.004	.49

	L	.016	.026	(.008,.024)	3.849	38	.000	.61

(R): right foot; (L): left foot

The unit of mean of NH is millimeter (mm)

Table 5.6. Wilcoxon signed ranks test. Compare the follow-up to the initial measurement for active and sedentary group using NNHt (R).

		Sedentary	Active
Follow-up - initial measurement	Positive Ranks [a]	7	3
	Negative Ranks [b]	1	1
	Ties [c]	31	17
	Total	39	21
	Z[d]	2.126	1.000
	Sig. (p-value)	.033	.317

a. Initial < Follow-up
b. Initial > Follow-up
c. Initial = Follow-up
d. Based on the positive rank

5.4. Discussion

Transient change of foot arch

For the parametric analysis on transient change of the foot arch, as shown in Table 5.5, all data in sedentary group have greater effect size than active group except for NH (L), which has the same effect size for both sedentary and active groups. This result shows people who are less active has the greater change in height of arch compared to more active individuals. Compared to the initial measurement, the height of arch is found to be increased in the follow-up measurement. In Table 5.5, all p-values in sedentary group are less than 0.05 showing the over 95% probability that such differences could be true. Therefore, the differences in sedentary group are statistically significant. In active group, not all the differences between two measurements are statistically significant because not all p-values are less than 0.05. The NH(R) and NNHt(R) show the lower probability that the differences are only 40.1% and 57.9% could be true. We are not able to explain why the right and left foot were different in arch change in active group. It might be contributed by the different nature of left and right foot (e.g. different mechanism or foot arch height between dominant and non-dominant foot) as Zifchock et al. (2006) reported that people tend to have greater arch height in the dominant foot. As shown in Table 5.6, the non-parametric test— Wilcoxon signed ranks test, found both groups tend to shift to a higher classification at the follow-up measurement. Moreover, the higher absolute z-value in the sedentary group ($z = 2.126$) was found, which indicates sedentary individuals are more likely to change classification than active individuals ($z = 1.000$). Based upon the results above, it can be concluded that the height of foot arch in sedentary group is more likely to have statistically significant change in the follow-up measurement than active group. Moreover, the sedentary individuals are more likely to change their foot type classification in the follow-up measurement than active individuals. Therefore, prolonged sedentary activity may bring interference and affect the measurement outcome. However, our finding contradicts the finding of several studies (Cowley & Marsden, 2013; Headlee et al., 2008; Okamura et al., 2017) showing individuals who are active have more changes in arch height. Unlike Cowley & Marsden (2013), Headlee et al. (2008) and Okamura et al. (2017) studied the extreme cases of foot muscle fatigue, the current study focuses on daily activity that may not induce fatigue in foot muscle. This may explain the active participants did not result in greater change in arch height. It should be noted that both active and sedentary group have the greater arch height in the follow-up measurement than the initial measurement. In Table 5.6, 8 out of 10 participants shift to the higher foot type classification in the follow-up measurement showing the increase in foot arch height after a four to six hours of daily activity. Okamura et al. (2017) has reported the similar results that the foot arch height was increased when intrinsic foot muscle is fatigue because of the compensation of surrounded muscle.

Constant load on connective tissue

The bones of the foot are passively supported by a series of fibrous collagenous tissue (e.g. tendon and ligament) that possesses the viscoelastic property. One of the viscoelastic behaviours of these tissue is ‘creep response’, which is the phenomenon that the constant load can cause the temporary deformation of the tissue (Whiting and Zernicke, 2008). Creep response is reversible that the original shape of the tissue can be gradually recovered after the load is removed (Whiting and Zernicke, 2008). The muscle who are less active are more likely to be affected by creep response and change the neuromuscular mechanism. Foot and legs muscle may be less active in prolonged standing and sitting participants and the creep response may bring change on the foot arch.

Temperature-related effect

Further difference between the active and sedentary group can be the skin temperature of the foot and lower limbs (Noddeland & Winkel, 1988). The reduction of skin temperature (2 to 3˚C) has been found in the less-active people compare to the active people (Noddeland & Winkel, 1988). The change of skin temperature can alter some mechanisms including neuromuscular conduction rate and neuromuscular force production (Bishop, 2003).

1. Neuromuscular conduction rate

Foot arch is actively supported by muscle and tendon tissue that controlled by central nervous system. The anaesthetically inhibiting nerve signals to the intrinsic foot muscles was found to significantly affect the height of MLA (Fiolkowski et al. 2003). This finding shows that neural control plays an important role for maintaining foot posture in weight-bearing condition. The increased muscle temperature is reported to improve central nervous system function that can facilitate the transmission speed of nervous impulses (Karvonen, 1992). In the contrast, a reduction of muscle temperature decreases the nervous transmission speed by increasing the duration of action potential propagating along the muscle fibres (Noddeland & Winkel, 1988). As the lower muscle temperature of lower extremities caused by sedentary activity may affect the nerve conduction, which affect the arch height accordingly. This may explain our finding that the drop temperature of sedentary group is less likely to maintain the same MLA height than active group. Active individuals, on the other hand, have the better MLA maintenance because the activity maintain the muscle temperature.

2. Neuromuscular force production

Another important temperature-related mechanism to neuromuscular system is force production. The increased isometric and dynamic force production have been found after the warm-up routines prior to exercises as the muscle temperature is raised (Bishop, 2003). The reduced muscle temperature has been reported to decrease the capacity of muscle fibre in neuromuscular force production (Rome et al. 1984). MLA has been reported to change significantly when intrinsic foot muscle is fatigue because and the force production is attenuated accordingly (Headlee et al., 2008; Okamura et al., 2017). Despite the force production of foot muscle is decreased when it is fatigue, it is still unclear whether MLA is increased or decreased at this stage. Headlee et al. (2008) found a decreased MLA height while Okamura et al. (2017) reported an increased MLA when foot muscle is fatigued. The finding of Headlee et al. (2008) explained the reduced force production can result in a loss of structural support in MLA. However, Okamura et al. (2017) argued a reduced force output of foot muscle can be compensated for by other muscles to maintain MLA in weight-bearing condition. In addition, Pohl et al. (2010) also reported other muscles can compensate for the lack of force production of foot muscles to maintain foot kinematic during walking. As shown in Table 5.6, sedentary group has increased in MLA height showing our result as agree with Okamura et al. (2017) and Pohl et al. (2010). Although muscle temperature and force production were not measured in the current study, it could be speculated that the sedentary individuals might have greater change in muscle temperature and neuromuscular activity due to a greater change in arch height.

From the finding above, it can be summarized that the change of temperature-related mechanisms due to activity levels affect the MLA maintenance in terms of the anthropometric values (i.e. NH and NNHt). Temperature-related mechanisms (i.e. neuromuscular conduction rate and force production) might explain our finding, which the sedentary group displayed greater difference in follow-up measurements. Furthermore, people with prolonged sitting are more likely to affect the outcome of foot type classification especially for those whose measure outcome is close to the classification thresholds.

Other factors might affect the results

Besides the activity levels of daily living, three other factors that are considered to affect the result of foot arch assessment, which are the bodyweight of participants (i.e. BMI), t-test control, and the between-group MLA differences in the initial measurement.

1. BMI

Obesity (i.e. BMI > 30) is one of the factors for changing the form of MLA and the lower extremities kinematic (Villarroya et al., 2009; Lai et al., 2008; Birtane and Tuna, 2004) Obesity population was reported to have the relatively lower MLA than the ones within normal-weight range (Villarroya et al., 2009). Furthermore, obesity participants were found to have remarkable differences in lower extremities kinematic during gait (Lai et al., 2008) and plantar pressure distribution in the static and dynamic condition (Birtane and Tuna, 2004) compared to normal-weight participants. Therefore, people with obesity is more likely to affect the measure result. In our experiment, there was only one participant whose BMI was greater than 30. As shown in Table 5.2, the mean body mass index (BMI) of active and sedentary group are similar and both within the same categories— normal-weight (i.e. BMI is between 18.5 and 24.9) (Villarroya et al., 2009). Therefore, we can confidently state that the measure result is less likely to be affected by participants' bodyweight in current study.

2. T-test control

In order to ensure the quality of the t-test, we also assessed our data by following parametric procedures (Field, 2009; Mittlböck, 2008).

- The data is continuous and normally distributed
- The observations are independent of one another that the data collection process was random without replacement.
- No outlier that is far away from the majority of the data

All our data met the requirements above, which is able to deliver high-quality t-test result (Table 5.3).

3. Between-group MLA differences in initial measurement

The lower extremity kinematics (e.g. joint's range of motion, plantar pressure, etc.) can be significantly different for foot types (i.e. normal, low or high arch) (Buldt et al., 2015; Chang et al., 2012). Because of the different kinematics of lower extremity and foot, it may bring about different results in changing arch height. Thus, it is crucial to understand the foot types of the participant in order to reduce the interference of foot type differences. We assessed the MLA difference between active and sedentary group in initial measurement in order to examine whether two groups started from a similar baseline. As shown in Table 5.3, NH and NNHt in sedentary group in greater than active group at the initial measurement. However, foot arch differences are not statistically significant between active and sedentary group since the p-value is greater than significance level, 0.05. Moreover, according to the SEM and MDC reported in Table 5.1, the arch difference between sedentary and active group in the initial measurement is statistically insignificant. Based upon this result, we can claim that the active and sedentary groups are stared with on the same baseline with no noticeable arch differences. This finding helps us to ensure the change of the foot arch is contributed by the activity levels rather than the predetermined arch height difference between activity groups.

Control protocol for foot arch assessment

Results show that sedentary group exhibited a greater change than the active group, and both groups have a tendency to shift to a higher classification after 4 to 6 hours of activities. Therefore, a control protocol is required to reduce interferences of preceding activities/lifestyle on foot arch measurement. As the minimum 4 hours interval and the 40% sitting time cut-off between two measurements was proposed as the minimal cut-off of sedentary group was 96 minutes. Hence, a control protocol was established stipulating that measurement is not taken if there is 100 minutes continuous sitting prior to it. For the eligible participant who may be seated before measurement but less than 100 minutes, a warm-up exercise needs to be carried out. The implemented warm-up exercise suggested by Bishop (2003) can increase the core and muscle temperature and facilitate the muscle support foot arch. Therefore, the eligible participants were asked to walk in a normal pace on a spot for one minute. We did not further investigate whether two minutes is more appropriate than one minute or whether walking is better than spot walking. We qualitatively observed one minute spot walking is sufficient to facilitate foot and lower leg's circulation and activate the neuromuscular system for a participant who was sitting prior to the measurement, and it was practical our scanning room with limited space.

5.5. Conclusion

As we developed the foot arch assessment using 3D imaging in Chapter 4 to provide the clear cut-off threshold for identifying foot types in order to identify the foot abnormalities, it may raise a question as 'is there any other variation need to be controlled for reducing the bias in the results?' Interclass correlation, standard error measurement and minimal detectable change of NH and NNHt have shown the high reliability of the current measurement. Literatures have also reported 3D foot scans is superior to other manual measure techniques according to its relatively higher agreement with radiography (Williams and McClay, 2000; De Mits et al., 2010; Butler et al., 2008). The reliability test focuses on the consistency of the measuring tool or the tester. However, an aspect has yet to be investigated by previous study is whether the height of foot arch can be dynamically changed within a day due to the level of daily activities (i.e. walking, standing or sitting) and affect the results. According to the findings of the current study, we can conclude that prolonged sedentary activities affect foot arch measurement and influence the identification of a foot deformity. In the current chapter, sedentary group displayed statistically significant differences in foot arch height between two measurements. Moreover, more foot morphology changes were found among sedentary people than active people. Sedentary group tends to change the foot type classification than active group after four to six hours daily activity, which may bring the inaccuracy of foot arch measurement. This finding helps us to answer the second research question: "How different daily activity levels affect foot arch measurement outcome?". Based on our finding, we established a control protocol to reduce the interference of participant's daily activity— foot arch measurement is not taken if there is a continuous sitting prior to it. Additionally, a one-minute on spot walking need to be carried out as warm-up for the participant has any sitting within 30 minutes before foot arch measurement. The cause of the changing of arch height or foot morphology might be temperature-related mechanism including neuromuscular conduction rate and neuromuscular force production. However, without further measuring the foot muscle temperature, nerves conduction or force production, it is difficult to draw a conclusion that these are the exact mechanisms that made the sedentary group have more change on arch height than the active group. Lastly, we considered there are three other factors that might affect the outcome— bodyweight, foot types, and T-test control factors. Therefore, we suggested these factors need to be controlled for the future study that related to foot arch and human activity. The outlier is required to be excluded that the obesity is suggested to be excluded and foot type differences need to be analysed and exclude the outlier.

For the future work, it is also important to investigate whether the physical activity of daily living affect the result of foot kinematic. Addition to static anthropometric values of MLA, foot kinematic in gait has been widely used to assess the foot abnormalities. Therefore, it is crucial to study the relationship between foot kinematic and participants daily activity. For investigating whether the physical activity of daily living affect MLA maintenance in dynamic, the novel wearable technologies with integrated acceleration sensors could be used to monitor individual's physical activity and quantify their activity level more precisely (Arif & Kattan, 2015).

Chapter 6. Foot model geometrical reconstruction in 3D image

6.1. Introduction

Current foot arch assessment is based on utilized 2D plane projected image (e.g. footprint or anthropometric parameters) for foot type classification and foot deformity identification. It was used to speed up the process but in turn compromised the accuracy (Swedler et al. 2010; Tenenbaum et al. 2013). Literatures reported a big variation in the incidence of flatfoot people from 0.7% to 14% identified by foot arch assessment using 2D parameters (Çilli et al. 2009; Tenenbaum et al. 2013). One of the perceived reasons for this is that the objective indices are applied to plane projections, i.e. three-dimensional (3D) characteristics are inferred from partial two-dimensional (2D) information, which is insufficient to reflect the complexity of the foot arch shape. Therefore, an algorithm for assessing foot arch characteristics in 3D is necessary to produce a more accurate and reliable results.

Liu, Kim and Drerup (2004) tried to utilize the Gaussian curvature of both the dorsal and plantar surfaces to quantitatively assess the morphology of the foot arch in 3D. However, due to the complex limb shape and the uneven skin surface, the Gaussian curvature varied widely across the foot and did not provide a unique identifier. Therefore, unless the foot arch is approximated by a simpler shape 3D index, it may not be practically utilized for foot assessment or insert design. Meneses et al. (2002) compared the arch volume (i.e. space between arch and ground) between non-weightbearing and weightbearing positions to identify normal and low arch. However, the absolute arch volume may be greatly affected foot volume and dynamic foot posture, which fail to deliver a repeatable indicator for foot types. Moreover, foot volume may not be useful for designing the shape of insert. Therefore, a research question as to whether there is a geometrical invariant that could be used reliably and objectively for the diagnosis/classification of the foot arch and insert personalization.

Dabnichki and Zhivkov (2010) proposed a 3D algorithm to reconstruct a pseudo-elliptical closed surface in space in order to approach 3D objects by (Fig. 6.1). This algorithm was applied to biological cells and the same algorithm might be used to apply on the foot arch for foot reconstruction.

In current study, we proposed a mathematical model for the objective assessment of foot arch geometrical characteristics by using 3D imaging. It is aiming to geometrically reconstruct 3D foot model in order to apply to foot arch assessment and insert design. Through different image processing procedures and geometrical approximation, the foot model is well prepared for flatfoot identification and insert personalization.

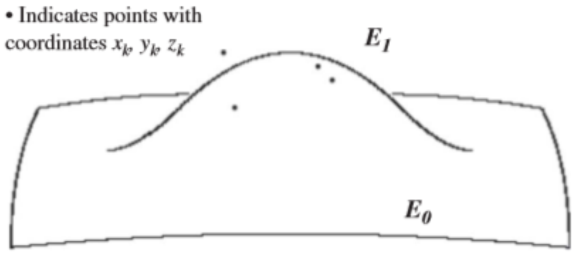

Figure 6.1. the pseudo-elliptical closed surface in space to approach 3D objects (Dabnichki and Zhivkov (2010)

6.2. Materials and methods

Approach 1— normalized arch volume

Meneses et al. (2002) used the arch volume— space between arch and ground to classify foot types. Bias may be found according to the foot size, i.e. bigger foot might have larger arch volume and smaller foot might have smaller arch volume. Therefore, we normalized the arch volume (i.e. arch cavity) by sectional foot volume to improve the bias induced by foot size. By setting a plane parallel to the ground and through medial malleolus, foot volume can be obtained below this plane (Fig. 6.2). Medial malleolus could be the best point for calculate the foot volume since it is the joint between foot and lower leg from anatomical aspect. More importantly, foot volume below Medial malleolus may not be sensitive to different standing postures or the weight-bearing conditions. The arch cavity is to encloses the space between plantar and the surface (i.e. the ground). The larger normalized arch volume indicates the higher foot arch and the smaller volume indicates the lower arch.

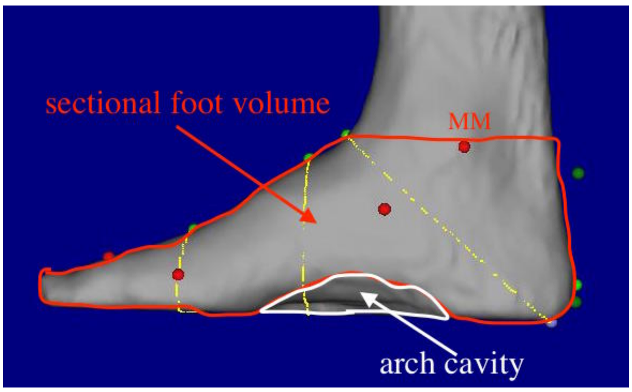

Figure 6.2. MM: medial malleolus. Red contour is the sectional foot volume and the white contour is the arch cavity

3D image was obtained by the Infoot® scanner as the procedure we mentioned in Chapter 4. Geomagic Studio® (version 12) was employed to process the image and calculate the volume.

The procedure of image processing is as following.

1) Import 3D foot image:

- Starts Geomagic Qualify 12 and import the *.stl file from Infoot® scanner to Geomagic®

2) Repair the foot image

- Repair a polygon object by cleaning unwanted or unnecessary points
- Remove spikes by adjusting the 'Smoothness Level' from 50 to 35 to obtain a smoother foot surface. A less aggressive 'Smoothing Level' helps to preserve edges and rounds of the image.
- Reduce noise by reducing the 'Smoothness Level' to 3 in 'Prismatic shapes (aggressive)' function. Adjusting the 'Deviation Limit' in the 'Parameters group' to '0.3 mm'.
- By using Mesh Doctor in Geomagic®, we can analysis the defects in our mesh and repair it automatically.

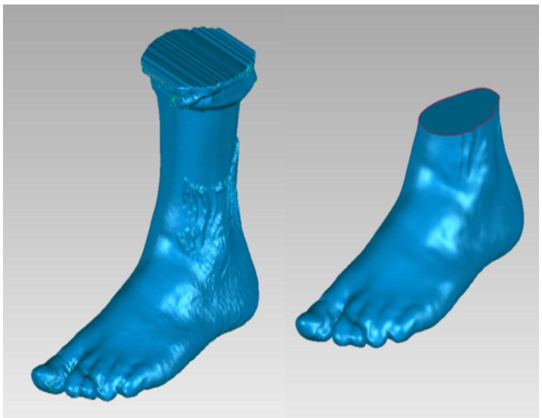

Figure 6.3. Before (left) and after (right) of the imaging repair

The procedures of foot and arch volume calculation is as following.

1) Set 'The ground plane':

Select 'Feature' > 'Plane' > '3 points': select 3 random surface points on the foot contact area to the floor and click 'Apply' to set 'Plane 1' that tangential to foot contact area. Click 'OK' to exit the dialog.

2) Set 'Plane' through medial malleolus:

Select 'Feature' > 'Plane' > 'Parallel through point'. Select 'Plane 1' and select a surface point on the foot image at "the most medial point of medial malleolus (refer to the INFOOT landmark)" and click 'Apply' to set 'Plane 2'

3) Trim the foot image by Plane 2

Select 'Polygons' > 'Trim with plane'. Select Plane 2 and click 'Intersect Plane' > 'Delete Intersection', to delete the unneeded image. Select 'Fill Single' > 'Flat' > 'Complete', to fill the hole that occurred from the trim. Click 'OK' to exit the dialog. Then, the volume of the foot image at this stage is the sectional foot volume.

4) Create 'Plane' on the plantar surface

Select three points on the surface of foot plantar— centre of the midfoot, the first metatarsal head and the medial point on the half of the heel, according to the Infoot landmarks. click 'Apply' to set 'Plane 3' as the surface underneath the foot. Click 'OK' to exit the dialog.

5) Enclose the space between foot arch and the ground

Use the contour of 'Plane 3' projects to 'plane 1'. Enclose the space between 'Plane 3' and 'Plane 1' as the 'arch cavity'.

6) Calculate the volume

Select 'Tools' > 'Compute Volume' to obtain the volume of the sectional foot and arch cavity (Fig. 6.3).

Therefore, normalize arch volume is calculated as eq. [6.1]

$$normalized\ arch\ volume\ = \frac{arch\ cavity}{sectional\ foot\ volume} \qquad [6.1]$$

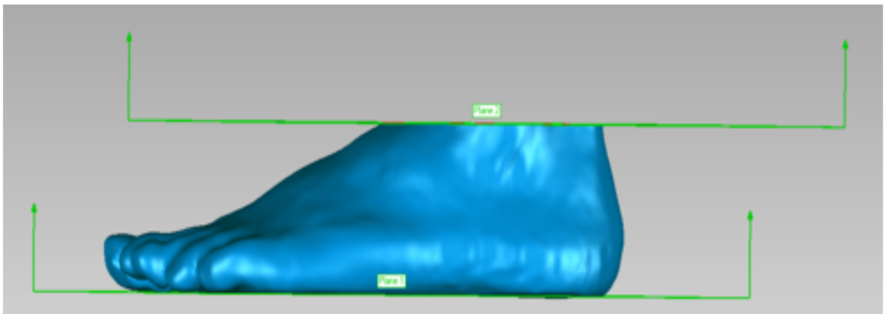

Figure 6.4. Calculate the arch volume between two planes

Approach 2— Arch curvature by generalized ellipsoids for approximation

The 'direct 3D reconstruction' method introduced by Dabnichki and Zhivkov (2010) is utilized for the uneven surface of the dorsal and plantar of the foot. The analytical shapes applied on both dorsal and plantar curvature is used the method called generalized ellipsoids for approximation. The ellipsoids were created by the cluster of points extracted from the scan to approach the contour of plantar surface and dorsum. The initial ellipsoid was generated by the first group of scanned points by eq [6.2]. The foot landmarks were put in the existing indices for defining the zero approximation.

$$E_0: A_1x^2 + A_2y^2 + A_3z^2 + A_4xy + A_5xz + A_6yz + A_7x + A_8y + A_9z - A_0 = 0 \qquad [6.2]$$

where $E_0 \therefore min \sum_{i=1}^{N}[dist(i, E_0)]^2$ as i indicates the i-th point of the cluster.

A simple distance-based criterion for 'permissible deviation' is assumed by eq [6.3] in order to assess the accuracy of the approximation:

$$m \cdot res \leq dist(i, E_0) \leq n \cdot res \qquad [6.3]$$

Where *res* indicates the system's resolution in real-life scale and *m, n (m < n)* indicates integers that are chosen as to ignore the noise caused by pixel grade – m (smoothing factor) and *n* reflects the biological resolution – that is based on morphological characteristics such as including bony prominences but ignoring skin folds. It should be pointed out that the coordinates need not be real-life coordinates but could be alternative values such as pixel data. The smoothing factor plays a very minor role in our case as a high-quality scanner was used. However, when lower grade equipment is used, the smoothing factor will need to be envisaged. The degree of approximation is assessed based on preliminary-defined criteria, which are normally related to the accuracy of the image system. In current case, the resolution greatly exceeds the significant figures showing great accuracy of the respective volumes. Next step is to identify points clusters that are sufficiently far from the initial ellipsoid and on the plantar surface or dorsum for the potential cluster formation; cluster is defined as a number of points were compliant to eq [6.4]

$$m \cdot res \leq dist(i, j) \leq sf g_1 \qquad [6.4]$$

where *sf* denotes a shape factor that related to the morphology of the pseudo-elliptical shape and g_1 is the smallest semi-axis of E_0. The following condition also holds:

$$sf g_1 \leq n \cdot res \qquad [6.5]$$

This condition reflects two important points:

I. The algorithm is devised to ignore small undulations on the surface normally caused by the resolution of the system and,
II. The condition of pseudo-ellipsoid is further re-enforced by capping the deviation from the initial approximation.

Once a point with coordinates (x_k ,y_k, z_k) is identified, then the shape of the zero-step approximation (analytical ellipsoid) is 'disturbed' as eq [6.6] to form the new geometries:

$$E_1 : E_0 + \varepsilon_1 exp\{-\sum_{k=1}^{N_1} \delta_k \cdot [(x - x_k)^2 + (y - y_k)^2 + +(z - z_k)^2]\} \qquad [6.6]$$

Where E_1 is positive when the cluster is convex, that is, all points are outside the existing ellipsoid, this geometrically represents a bump on the ellipsoid and we avoided to generate the concave of new geometries. The deformed ellipsoids need to include all the selected points on the foot surface(s). This step is repeated until the most representative geometries were made for plantar surface and dorsum.

$\delta_k > 0$ is a shape coefficient related to the curvature of the ellipsoid;

$(x_k, y_k, z_k)k = 1, 2, 3$ are the experimentally measured coordinates of the k-th point; $\varepsilon_1$and δ_k, $k= 1,...,N_1$ are obtained through the least squares method so the quadratic deviation of all the points of the cluster is obtained. The process is repeated until a satisfactory approximation is reached, i.e.

$$E_{\text{acc}}: E_0 + \sum_{k=1}^{N_1} E_k \quad [6.7]$$

The number of steps is decided objectively by checking the addition of volume they bring.

The detailed plantar approximation procedure is as following.

1) The plantar contour (red line) on the projected mediolateral view of foot scan is used. Locating d and e at the ends of the plantar contour (red line), which are the conjunct points between contact and non-contact area in the forefoot and rearfoot respectively.

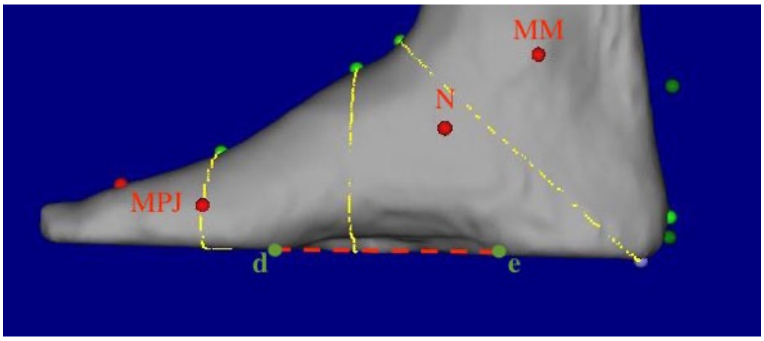

Figure 6.5. define the points from foot image for E_0

2) Sketch the plantar contour as the pink line. Then, we define the initial ellipsoid (E_0) by approximating the plantar surface (pink line) with additional cluster from the scan.

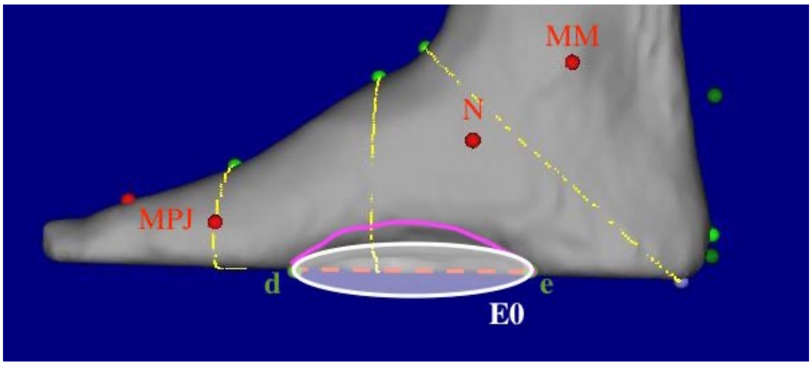

Figure 6.6. Once E_0 is created the plantar surface is defined as pink line.

3) Define point g as the projected point on the plantar contour in the middle of point d and e

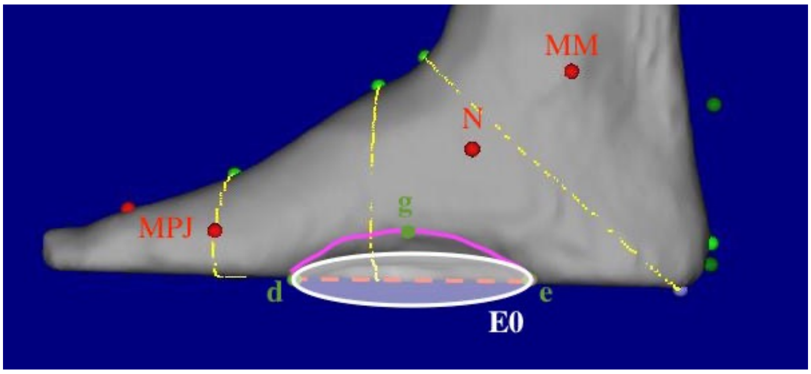

Figure 6.7. Point g is defined as the potential landmark for E_1

4) Define the undulation, E_1 (yellow line) convex the initial ellipsoid (E_0) to encompass point N and DH to approximate the shape at the higher dorsal surface.

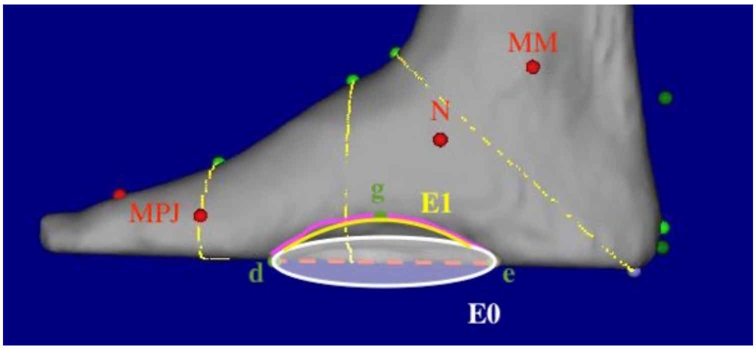

Figure 6.8. E_1 is formed based on E_0 on point g, d and e.

The detailed dorsal approximation procedure is as following.

1) The dorsal contour is outlined on the projected mediolateral view of the foot scan image to define f through a line perpendicular to the ground and through point MM and draw another line parallel to the ground and through point MPJ. Point f is obtained as the intersection of these two lines.

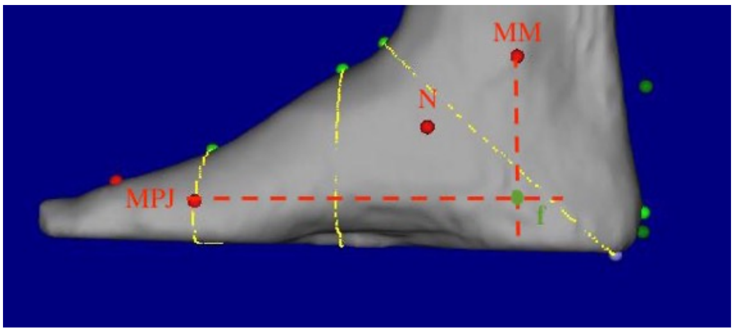

Figure 6.9. define point f by the vertical and horizontal lines through MM and MPJ.

2) Define the dorsal contour as the pink line and to draw the initial ellipsoid, E_0 (white area). Point MPJ and f are the two anchor points. Then, we define the initial ellipsoid (E_0) also

encompass point N approaching the dorsal contour.

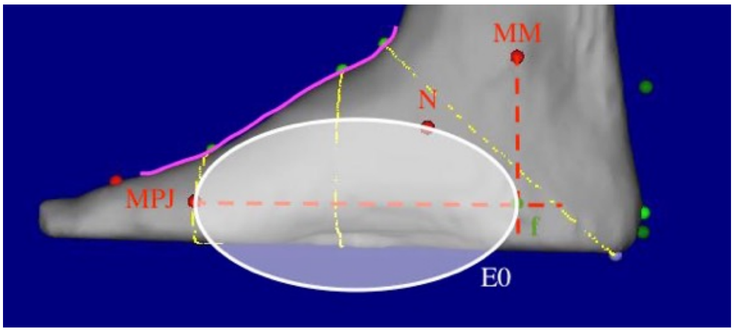

Figure 6.10. E_0 is created on point f, MPJ and N; and pink line is used to define dorsum

3) Define the landmark from the scanned data on the dorsal— Point DH is the dorsal height at 50% of foot length. Point BT is the ball girth top. These are the landmarks used for the 'disturbed' ellipsoid.

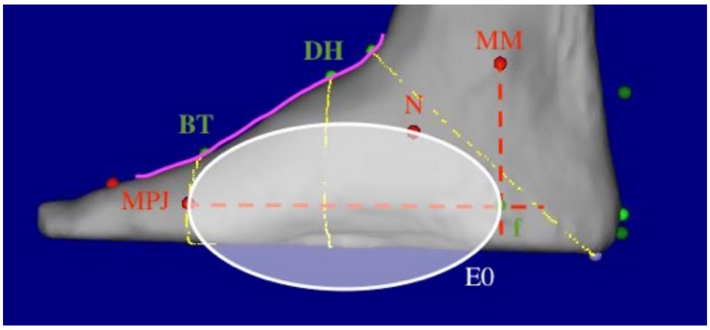

Figure 6.11. point BT and DH is defined on dorsum as the potential cluster formation. Point DH is the dorsal height at 50% of foot length. Point BT is the ball girth top.

4) Define the undulation, E_1 (purple line) convex the initial ellipsoid (E_0) to encompass point N and DH to approximate the shape to the higher dorsal surface.
5) Define the illustrated E_2 (yellow line) convex the E_0 and E_1 to encompass points BT. The process can be repeated to enlarge the ellipsoid until accuracy is achieved.

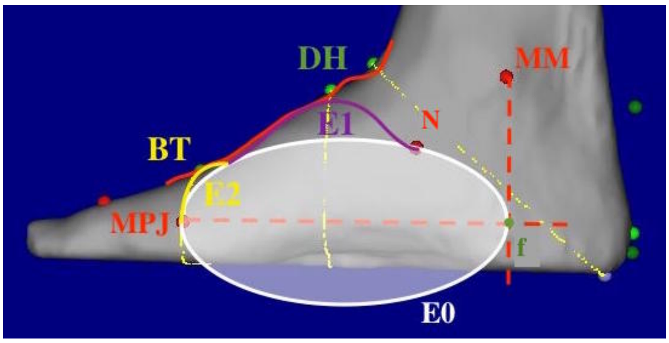

Figure 6.12. E_1 and E_2 are made based on the initial ellipsoid (E_0) as the dorsum ellipsoid approximation.

In summary, the foot reconstruction requires 3 steps:

1. Identifying the surface to be approximated by using anatomical landmarks as the explanation above. Since the arch is dynamic in real life, foot structure may be deformed in different weight bearing conditions. Therefore, a small number of key points to render a sensible and realistic for initial approximation were identified according to our procedure. The established landmarks ensure the good repeatability and accuracy of this approach.
2. The initial geometric shape was based on the ordinary ellipsoid (i.e. E_1) and generalized ellipsoids (i.e. E_1, E_2, …) and the ellipsoids generation is based on selected points.
3. Definition of a stop factor— in our case is the change in volume (the algorithm is devised to always add volume). The stop criterion is when the added volume is ≤ 0.1% of the pre-existing volume. Theoretically the algorithm could stop at the E_0 stage if there is no gain in the ellipsoid "deformation".

In short, we select initial ellipsoid and then deform it to encompass the further away points until an accuracy of 0.1% is achieved. In practice, only a handful of additions are required. With the current scan facilities, we need 3-5 steps. This will change with a less reliable equipment or relaxation of the strict measuring protocol we have been applying. It is likely that in practical situation the convergence criteria need to be relaxed as shape would become unnecessarily complicated and this would compromise the benefits of this approach.

6.3. Discussion

Normalized arch volume, the first approach we introduced, using the important 3D characteristic, i.e. the relative volume of the foot arch cavity with respect to an appropriately chosen foot section. This approach might address the bias of arch volume that induced by foot sizes. Compared to 2D indices, the foot arch volume assesses the natural foot morphology in 3D perspective. However, the complex biological foot shapes and foot surface undulations, the accuracy and reliability could be affected. Moreover, the foot volume measurement is not applicable to insert personalization as the ultimate goal of current study. Therefore, a simpler geometry using analytical shapes needs to be applied in order to describe foot morphology. The generalized ellipsoids approximation was used to address the drawbacks mentioned in our first approach. The foot reconstruction reflects the 3D characteristic of both dorsal and plantar curvature with highly repeatable procedure. The consistent landmarks were selected from foot image to reproduce the ellipsoid for foot reconstruction. However, it should be pointed out that current practices used general perception term but have not yet defined the foot arch mathematically. Furthermore, the 3D shape of the formed cavity is still an open question. The initial ellipsoid should be obtained (as we already experimented) by the landmark points rather than calculating the whole foot volume and space. This process needs to further refine before a large sample measurement is conducted. The utmost challenge may be landmark selection that provides best characterization of the internal bone configuration. The landmark selection requires the opinions from both medical professionals and engineers in order to create a mathematical and biomedical model. Ellipsoid approximation cannot be utilized until the agreement is made between with medical professionals and engineers. However, how the opinion of medical professionals is formed is a complex process that is currently not formalized and is open for interpretation. Once the agreement is made, the actual algorithm can be finalized, and the generalized ellipsoid approximation can be applied to foot arch mathematically in a very fast and simple manner.

6.4. Conclusion

The current study developed the experimental procedure for 3D foot model reconstruction to assess foot arch in its 3D characteristic Moreover, the proposed algorithm is also envisaged to be used for the development of shoe inserts that could be used for arch correction. By using the algorithm of built-in ellipsoid deformation that has been tested in other applications (Dabnichki, 2005), the insert can be personalized to support different levels of arch collapse. The above development can be a first step in an artificial intelligence approach that is based on feature observation and mathematical logic formalization. Potentially we consider adding formal version of some of the current clinical assessment features such as foot imprint in the transversal plane and dorsal and plantar arch projections in the sagittal plane. Then the proposed approach can become a simple and repeatable method used by medical or health professionals in foot arch assessment and insert design. In the future, the artificial intelligence type multi-criteria decision making is to utilize the Gaussian curve at a global shape level using ellipsoids for shape characterization. The work on this is still in progress as key characteristics for image reconstruction need to be finalized as well as the degree of complexity of the shape approximation.

Chapter 7. Customized 3D printed novel shoe insole for flatfoot individuals

7.1. Introduction

In Chapter 5, the foot arch assessment system was developed to more effectively and accurately select to eligible participant by accurately classifying the foot types. In Chapter 6, 3D foot reconstruction method was developed for further analysis of the selected participants. In current chapter, the novel shoe insoles were designed according to the foot image of selected participants to improve the flatfoot and address the limitation of traditional solid insoles. The procedure of customized insole development is shown in Figure 7.1. The first to fourth steps (3D foot scans, image processing, computer aided insole design, insole material test) were included in current chapter and the other steps were elaborated in Chapter 8 and 9. The first step is to produce a 3D scan of subject's feet for the foot arch assessment and inserts customization. Only the 3D image of low arch is proceeded to image processing to optimize the quality of the 3D foot image, which includes image damage repair, reduction of noise and spike. Image processing is an important procedure that makes the foot image clearer and easier for insert design. Next, computer aided design (CAD) is employed to construct the shoe insole based on foot shape and arch height. According to previous research (Huang et al., 2011; Cheung &Zhang, 2008) and our own experience, CAD insert made by direct modelling is time consuming requiring at least 3 hours for one customized design. Therefore, an algorithm was developed to automatically transfer the scanned data to the parameters to control the geometry of the insert. Our newly developed parametric modelling dramatically decreased the design time to less than three minutes. Moreover, parametric modelling may be more feasible to podiatrists who may not have any background knowledge of CAD to customize insert digitally. The new developed algorithm aims to help podiatrists to adopt in-house digital insert design. For novel design, three customized 3D printed insoles—Honeycomb, Bubble and Gyroid, were developed based on the proposed framework. In addition, the additive manufacture (AM) materials that used for novel insole were tested.

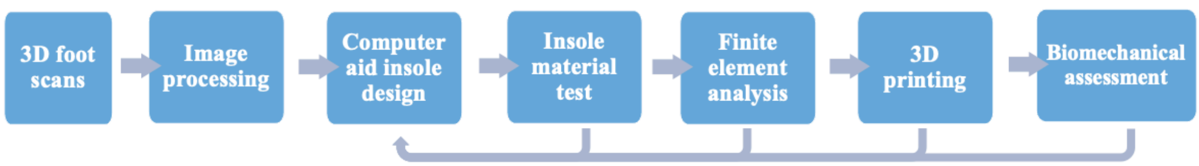

Figure 7.1. The flowchart of the design and production of shoe insole

7.2. 3D subject-specific foot model

7.2.1. Participant

Two male low arch participants were recruited from university of Vienna. Participant 1 is 28 years of age, 200 cm in height and 115kg in body mass; participant 2 is aged 26, 188cm in height and 88kg in body mass. Both participants have no leg injuries, operations, or other medical conditions such as osteoarthritis within the last six months. Participants were asked to not perform any moderate or vigorously intense physical activity, e.g. running, jogging, dancing, any sports activity, etc., prior to the test. No prolonged sitting (i.e. over 100 minutes) was allowed prior to the assessment according to the control protocol established earlier (Chapter 5). Participants were briefed on the purpose of the study and potential risks. They were informed and signed the consent statements. Following by the threshold purposed established in Chapter 4, Normalized Navicular Height truncated (NNHt) of both participants are < 0.169 for right foot and < 0.167 for left foot.

7.2.2. Foot image capture

3D foot image that used for insole customization needs to be acquired in non-weightbearing condition. The common way to scan the non-weightbearing foot shape is using the mobile foot scanner when the participant is lying in prone or supine position. When compared to the mobile foot scanner, Infoot® scanner provide better resolution and less background noise. As a result, Infoot® digitizer is the best option for foot shape capturing. Unlike the 3D scans for foot arch assessment scanning foot in a bilateral standing weightbearing condition, the participant was asked to be scanned in a seated non-weightbearing position (Fig. 7.5) for insole design. Five stickers for the reference points including sphyrion fibulare, metatarsale fibulare, toe#1 joint, navicular, sphyrion were placed on the participant's feet before scanning when participant was seated. The participant was seated but not standing when the stickers were placed to minimize the inconsistency or errors caused by the skin movement induced by changing position. As the shoe insole is normally designed for closed-toe shoes, it needs to not only fit the users' feet but also their footwear. The design of the closed-toe shoe normally makes the toes slightly touch together. As Fig. 7.6. shown, our first design failed to fit into user's shoes because we captured the subject's feet without binding the toes, which made the design has wider forefoot area than user's current insert. As the participant was normally scanned in barefoot, the toes are slightly apart from each other. Therefore, the participants' toes were slightly bound together by scotch tape while scanning to address this issue. It must be aware that the tape does not squeeze the toe and affect the shape of the foot especially the plantar surface. Once the foot image is obtained, the image document was saved, and the format converter was used to convert it to *stl. file. As shown in Fig. 7.7, the full procedure of 3D foot scanning for insert design, which is slightly different from the procedure for foot arch assessment mentioned in Chapter 4.

Figure 7.5. 3D foot image for insert desgin is scanned in non-weightbearing condition to keep the natural curve of the foot arch

Figure 7.6. Our first customized insert (left) has the wider forefoot area than the user's current insert from the marketplace (right)

Figure 7.7. Procedure of foot image capturing for insert design

7.2.3. Foot image processing

Image processing includes the following six steps as shown in. Fig 7.8 below.

Figure 7.8. Procedure of foot image processing

- **Image repair**

Geomagic® is employed for 3D image optimization and modification. As a first step we restored the missing data and reduced the noise and the spikes to smooth the surface of the foot especially plantar surface. After the 3D foot image was imported as stl. format to Geomagic®, "Mesh Doctor" was used to automatically detect mesh issues. By applying "Mesh Doctor" (Figure 7.9), the system addresses the most mesh issue presented by the image. It is still required the following steps to manually repair the rest of the image defects.

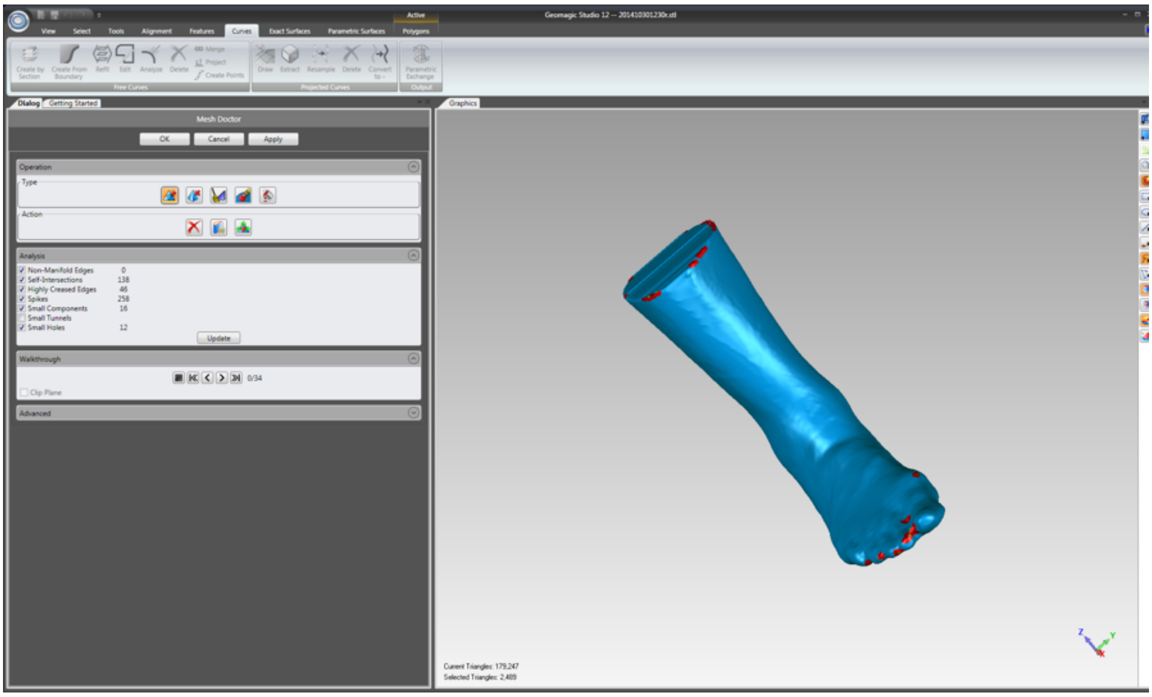

Figure 7.9. Mesh doctor automatically detect the issues of the image once we imported it.

The noise reduction was performed at *smoothness level* 35 and *deviation limit* in the *parameters group* of 0.3 mm. Click on *Polygons* > *Smooth* > *Remove Spikes* for reducing the spikes. We adjusted the *smoothness level* from 50 to 35 as mentioned by user manual. It should be noticed that the edges or rounds of the foot need to be preserved to remain the intact image as it is the most important part for insert design.

- **Positioning foot image**

The coordinate system in Infoot® scanning is different from Geomagic® and the CAD software (3D experience®, Fusion 360®) we used. Therefore, coordinate system is needed to redefine, or the foot model needs to be repositioned because each foot is needed to be in the identical direction for our operation conveniency. The foot axis (i.e. foot direction) in Infoot® system is from the tip of heel to the tips of second toe. Meshmixer® was used to adjust the position of foot image in 3D space. By using the function of vertical and horizontal displacement and rotation, we positioned the foot plantar on xy-plane (i.e. horizontal plane) and heel tip on the origin of the coordinate system and X-axis is aligned with the heel tip and tip of the second toe. *Soft transform* is a powerful function in Meshmixer® for adjusting foot posture in 3D image. "Soft transform" was used to adjust the subtalar position when the original arch shape changed by the non-neutral foot posture. The subtalar joint can be everted or inverted by "Soft transform" as we selected the rearfoot area for adjusting following the procedure below:

(A) Open 'Meshmixer' and click 'import'. Select the foot scan which was done by INFOOT digitizer. Click 'View' and then select 'Show objects browser'.
(B) Duplicate the foot scan in order to compare with the original one. Hide the original foot scan, then click 'Select' and hold the left click of the mouse to select the area intended to be adjusted until they become shaded.
(C) Expand the tab 'deform' and find 'soft transform'. Adjust the foot position by changing the arrow up and down. After we adjusted the motion of eversion and inversion, the foot plantar could be slightly off the ground (i.e. xy-plane).
(D) Repeat the same procedure to adjust the forefoot to meet the subtalar joint neutral. Click 'select' and hold the left button of the mouse to circle the forefoot area until it became shaded and repeated the procedure to adjust (Fig. 7.10). By adjusting the arrow, we positioned foot plantar on the ground.
(E) Since the tip of the heel and the second toe could be deviated from the origin and x-axis, it needs to position the entire foot again by horizontal and vertical displacement and rotate to the predetermine position— foot plantar on xy-plane, heel tip on origin, and tip of second toe is on x-axis.

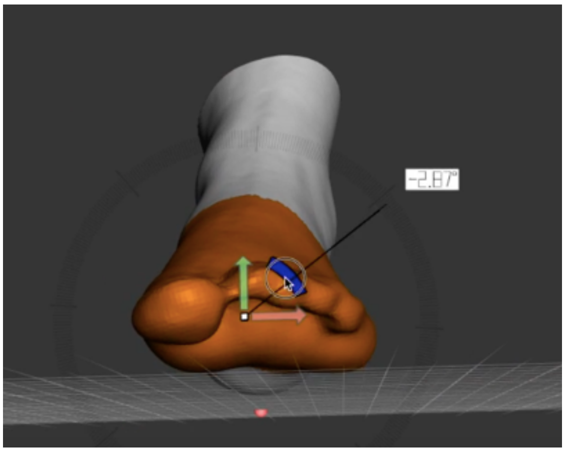

Figure 7.10. Adjust the forefoot position to meet subtalar joint neutral using Meshmixer®

- **Unnecessary foot image features removal**

In order to process the image more effectively, the unnecessary part of the foot is required to remove as to reduce the document size. The image file could be quite large and slow down the process of the CAD software significantly. Therefore, the image above the subtalar joint was removed by Meshmixer® as it is the unnecessary part for insert design. The remained foot image is sufficient to design the insert as the whole plantar surface is retained. The edge of the foot is also retained for designing the cup of the insert for stabilizing the motion of foot. The procedure of remove the parts is as following:

(A) Go to ‘Edit’, and select plane cut for removing image above the ankle.
(B) Click ‘invert selection’ and adjust a proper angle to cut.
(C) After deciding the cutting plane, press ‘accept’ to end this operation.
(D) Go to object browser on the right corner at the bottom, which display the original foot scan to compare with the modified file.

- **Object simplification & Export *stl file**

Meshlab® was employed to further simplify the object and reduce the file size. Fusion 360® can only accept the object with the “face number” no more than 10000. However, it is important to simplify the object without compromising its authenticity. The procedure of object simplification and Export *stl file is as following:

(A) Open ‘Meshlab’ and then click on ‘Import Mesh’ to import the saved foot scan file from ‘Meshmixer’.
(B) Find ‘Filters’ in the tab on the top. Then, expand ‘Remeshing, Simplification and Reconstruction’ for select ‘Simplification Quadric Edge Collapse Decimation’.
(C) Set 10000 as the target number of faces because Fusion 360 Autodesk can only accept the image lower than 10000 faces.

(D) Click ‘Apply’ to process the simplification. Click on ‘Export Mesh as’ when the simplification process was completed.

(E) Expand ‘File’ to select export the foot image as *stl file (because the software we used for the next step can only accept *stl file). Figure 7.11 shows the foot model that have been gone through all the steps of image processing and it is ready for insert design.

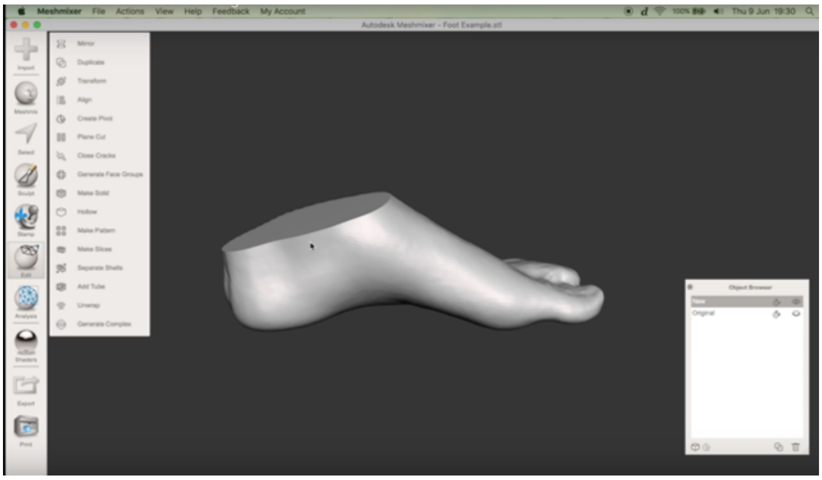

Figure 7.11. The foot image has completed image processing and ready for insert design

7.3. CAD insert modelling

7.3.1. Direct modelling

Once the optimized foot image is ready in *stl file, the Catia v5 was used for CAD insert design. Compared to Catia v6, Catia v5 is simpler when uneven surface on mechanical drawing needed to be created. According to the direct modelling CAD insert design mentioned by Lochner et al. (2012), the series of points were connected to form contour of the insert (Figure 7.12.1). We created the two sketches to construct different layers on planes parallel to x-y plane to make the insert. As shown in Figure 7.12.2, the first sketch (i.e. the bottom layer) was formed by a number of contact points between plantar and ground (i.e. xy-plane). The second sketch (i.e. the top layer) was created on a plane 3mm above the ground and it was formed by the intersecting points between foot and the plane 3mm above the ground. We connected two sketches and created the insert as Figure 7.12.2. However, in this case, the points of the contour were only defined in a random manner, which low in repeatability and reproductivity.

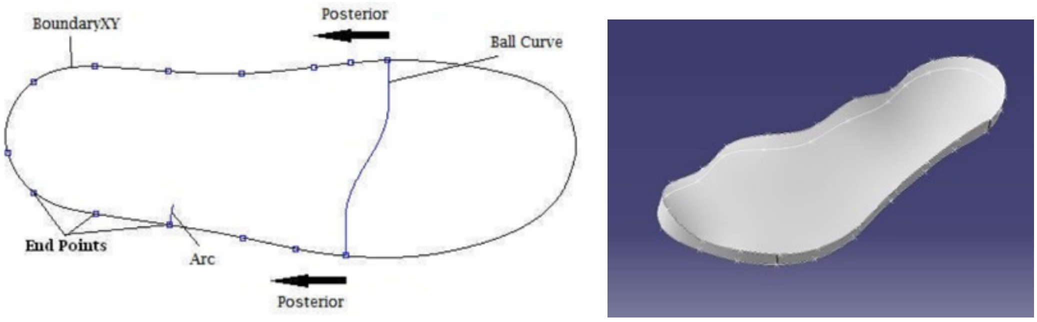

Figure 7.12. (1) A method that mentioned in Lochner et al. (2012), which connects series of points using foot contour. (2) shoe insole design using splint connected with points in Catia v5

Therefore, the intersecting points between different planes and the foot image were used to construct the insert in Autodesk Fusion 360®. The plantar surface of the foot image was positioned on xy-plane and the foot axis (i.e. from heel tip to second toe tip) was along with x-axis and on xz-plane, and heel tip was adjusted on yz-plane. First, we set yz-plane as the reference plane and created an offset plane paralleled to yz-plane to intersect with second toe tip, which is named as yz-plane-1. The offset distance was the distance between heel tip and second toe tip. The other twelve offset planes were created between yz-plane and yz-plane-1 with the same distance in between and paralleled to each other. Figure 7.13.1 illustrates the offset planes that were paralleled to yz-plane. The contact points of the planes and the foot were found as the purple points in Figure 7.13.2. The same strategy was used to set xz-plane as a reference plane. Two parallel offset planes of xz-plane were set and to intersect with the most lateral and medial points of the foot, which named as xz-plane-1 and xz-plane-2 respectively. Five other offset planes were created between xz-plane-1 and 2, paralleled to each other with same offset distance. The contact points of the planes and the foot were defined to create the contour of the insert. Finally, all the intersected points were connected to each other to create the personalized insert. In Figure 7.13 and 7.14, we only created the insert covers the midfoot and rearfoot. By using the intersected points to construct the insert can be more repeatable and reproducible than the previous method, which selected random points of foot image to construct the insert. However, the later method could be more time-consuming compared to the previous one. Generally, CAD design in direct modelling requires at least three hours for one insert and it takes much longer time for people unfamiliar with CAD software.

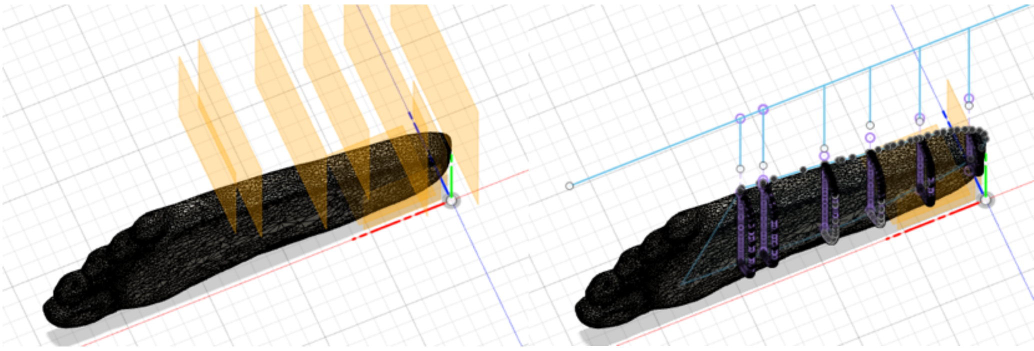

Figure 7.13. (1) Create the offset planes according to the reference planes (2) Find out the intersecting points of planes and foot to construct the insert

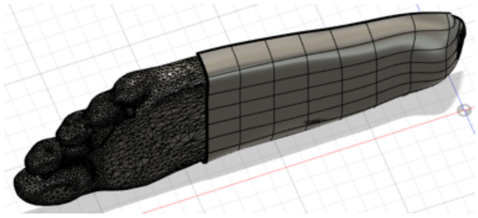

Figure 7.14. Insert created by the intersecting points in Fusion 360®

7.3.2. Parametric modelling

The direct modelling can be time consuming and can be an obstacle for podiatrists to adopt the in-house CAD insert design. Parametric modelling uses the parameters to control the geometry of the insert may address the issue of direct modelling and simplify the CAD process. The algorithm was developed in current study to automatically translate the foot scan data to insert parameters, which drastically reduce the design time from three hours to three minutes. Our new developed algorithm not only decrease the required time of design but also allow people who are not familiar with CAD software to adopt in-house digital insert design in a simpler and faster manner. The procedure to parametrically create the insert model is as following (Figure 7.15):

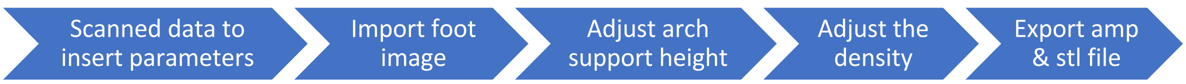

Figure 7.15. Insert created by the intersecting points in Fusion 360®

- **Translate foot scan data to insert parameters**

Gensole®, an open-source software, was used for parametric design of customized inserts. The geometry of insert can be controlled by the major twelve parameters: toe radius, outside width, inside width, instep offset, outside offset, total length, inside length, outside length, heel radius, heel thickness, toe thickness, draft angle, and arch height (Figure 7.16).

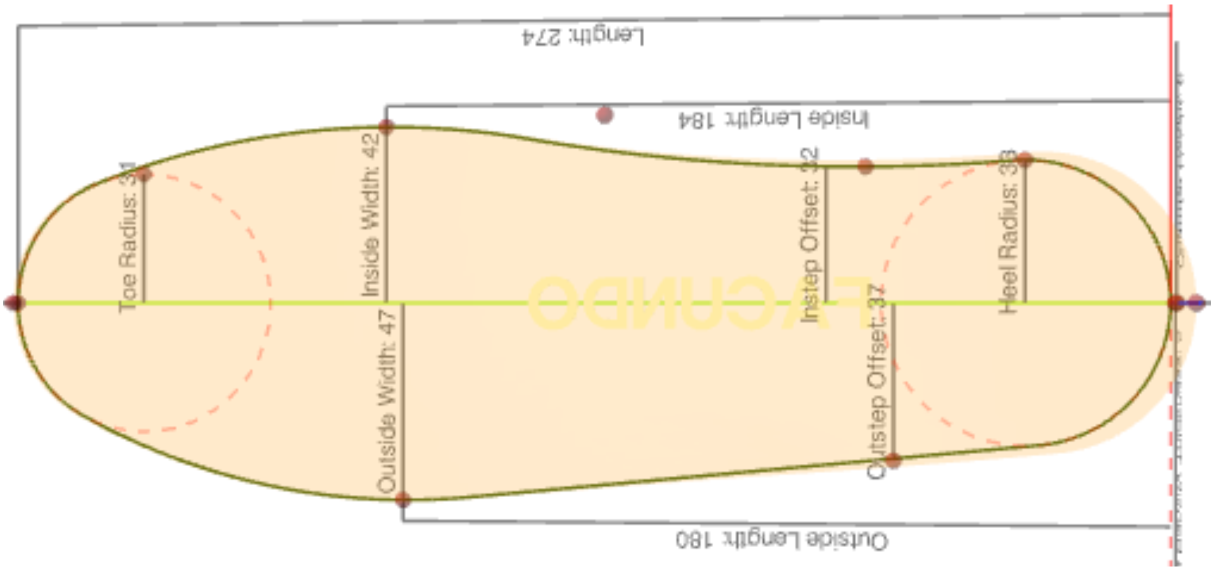

Figure 7.16. Major parameters control the geometry of the insert in Gensole®

We selected the five scanned data from Infoot®— foot length, Fibulare instep length, instep length, foot breath, heel breath, for insert design. The algorithms listed below translated the individual's foot scanned data to the insert parameters and input to Gensole® (Figure 7.17). On the left side of the equal sign are the Gensole® parameters and on the right side of the equal sign are the scanned data from Infoot®.

1) Total length= *Foot length*
2) Outside length= *Fibulare Instep length*
3) Inside length= *Instep length*

These three parameters are directly obtained from the scanned data without proceeding through algorithm. Total length is equal to *Foot length* from pternion to tip of second toe. Outside length is equal to *Fibulare instep length* from pternion to 5th MPJ. Inside length is equal to *Instep length* from pternion to 1st MPJ.

4) $\text{Toe radius} = 1/2 \times (\text{foot length} - \text{instep length})$

As Figure 7.17, the circle diameter at toe area is from the tip of second toe to 2nd MPJ. 2nd MPJ is about the same distance as 1st MPJ from the pternion, so *Foot length* minus *Instep length* and divided by 2 is Toe radius.

5) $\text{Outside width} = 3/5 \times$

$$\sqrt[2]{(foot\ breath)^2 - (Instep\ length - Fibulare\ Instep\ length)^2}$$

6) $\text{Inside width} = 2/5 \times$

$$\sqrt[2]{(Foot\ breath)^2 - (Instep\ length - \ Fibulare\ instep\ length)^2}$$

Foot breath is the distance between 1st and 5th MPJ from scans. The horizontal distance of 1st and 5th MPJ is *Instep length* minus *Fibulare instep length*. Therefore, the insert width, the vertical distance between 1st and 5th MPJ, is obtained by right angled triangle formula as following.

$$\sqrt[2]{(Foot\ breath)^2 - (Instep\ length— \ Fibulare\ instep\ length)^2}$$

Outside and inside width are the vertical distance from foot axis to 1st MPJ and to 5th MPJ respectively. Foot axis passes through pternion and 2nd MPJ divides a foot into two-fifths on medial side and three-fifths on lateral side. Therefore, outside and inside width is three-fifths and two-fifths of the insert width respectively.

7) $\text{Heel radius} = 1/2 \times Heel\ breadth$

Heel breadth is the distance between two prominent tuberosities on the lateral sides of calcaneus, which is also the diameter of heel. Therefore, the heel radius is a half of *Heel breadth*.

8) $\text{Outside offset} = 3/5 \times Heel\ breadth$

9) $\text{Instep offset} = 2/5 \times Heel\ breadth$

The sum of outside and inside offset approximate to *Heel breadth*. As the foot axis divides a foot into three-fifths on lateral side and two-fifths on medial side, outside offset is three-fifths of *Heel breadth* and inside offset is two-fifths of *Heel breadth*.

10) $\text{Toe thickness} = 0.13 \times Big\ toe\ height$

11) $\text{Heel thickness} = 0.13 \times Big\ toe\ height$

The thickness of toe and heel are the same because they both represent thickness of the shell. According to Menz et al. (2017), the thickness of the shell of insert ranged from 1 to 6 mm, with 3 mm as the most commonly prescribed thickness. From our scanned data, big toe height ranged from 9 to 32mm, with an average 23mm. We used our average big toe height 23mm to divide the most commonly prescribed thickness 3 mm and obtained 0.13. Therefore, the thickness of our custom-made insert was ranged from 1.2 to 4.2mm, with an average 3mm.

12) $\text{Arch height} = 1/2 \times Navicular\ height$

Navicular height is the vertical distance between top of the foot arch and the ground. Ideally, arch height of an insert should approximate to Navicular height for correcting excessive pronation of low arch. However, it might compress the soft tissue under navicular bone that potentially affect blood circulation or nerve conduction. Thus, we used a half of *Navicular* *height* as arch height of insert. Arch height may be adjusted according to the actual curve of the arch, which is detailed in Step 3.

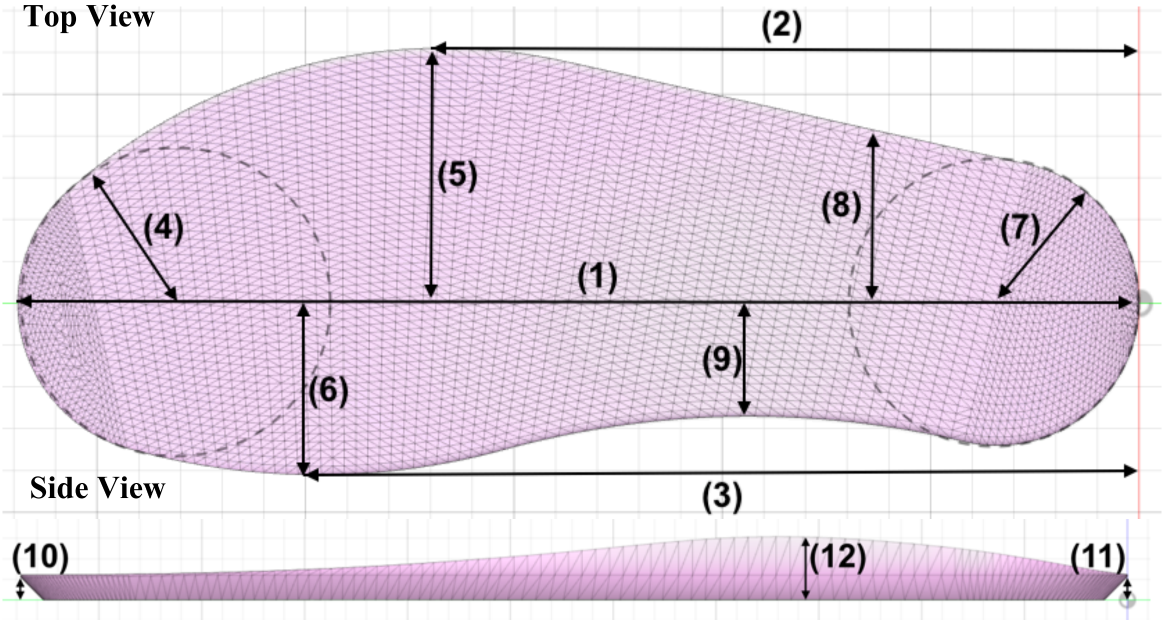

Figure 7.17. Parametric design of customized insert (1) Total length (2) Outside length (3) Inside length (4) Toe radius (5) Outside width (6) Inside width (7) Heel radius (8) Outside offset (9) Instep offset (10) Toe thickness (11) Heel thickness (12) Arch height

- **Import and position the foot image**

After the initial insert model is constructed by parameters listed above, the foot scan image was imported to fit the insert model. It should be noted the insert needs to be designed to fit the user's foot as well as their footwear. The contour of the insole shall be a bit larger than user's foot and smaller than their footwear. Normally, the user should wear half US size bigger than the size they used to wear if the insert is applied. As *stl format has two representations—ASCII and binary and Gensole® can only accept ASCII format. Therefore, Meshlab® was used to convert the image from binary *.stl to ASCII *.stl file. As Gensole® cannot change the direction of foot image once it has been successfully imported, the foot direction is required to be adjusted by Meshlab® to align with the insert. Once the foot direction is set, the foot image can be translated along with the x or y or z axis to fit into the insert in Gensole® (figure 7.18).

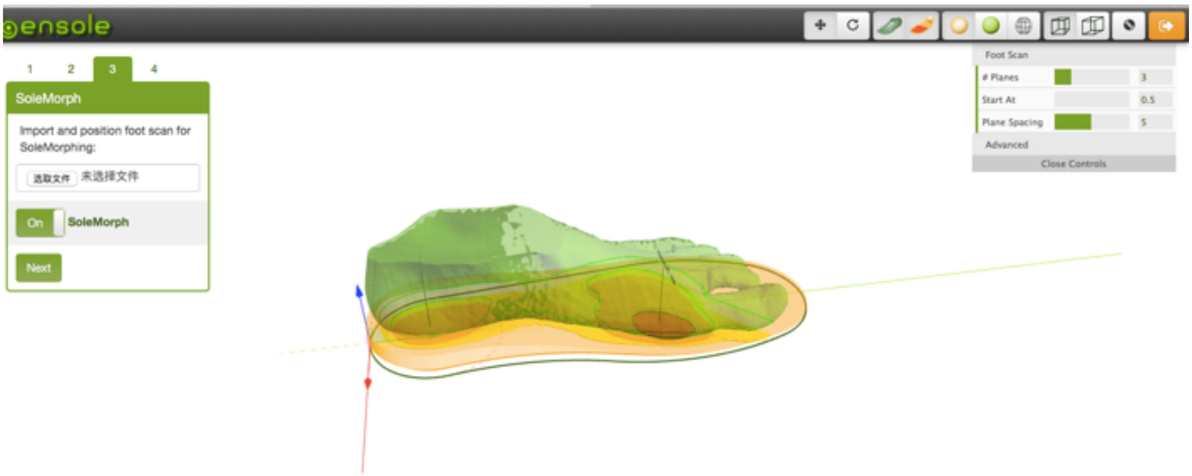

Figure 7.18. Moving the foot image on X-Y-Z axis to fit the insert in Gensole®

- **Adjust the height of arch support**

Although the height of arch support of insert is determined by the navicular height, the actual the arch support may need to slight adjusted according to the foot image. The red dot on the arch support can be dragged to adjust the height in Gensole®. Wherever we put the red dot, the system will automatically generate the curve of arch support. Therefore, we dragged the red dot to the highest point of the plantar foot arch and the system will automatically generate the curve of arch support. As the height of arch support cannot be measured in Gensole, the insert was imported to Fusion 360® to measure the actual height of arch support. The height of arch support needs to be accessed according to the actual height of foot arch to see if the value falls between 0.5 to 0.8 times of navicular height. The range of value may provide the sufficient support to the foot arch as arch support should be lower than navicular, which allows room for the soft tissue under the bone for blood circulation. The arch support can be adjusted lower if the user feels pain or discomfort when we apply 0.8 times of navicular height. 0.5 times of navicular height can be applied to the arch support and to gradually increase the arch height once user adapt the external support for the fallen arch.

- **The density of the insole**

The pressure distribution of the foot can be uneven and changed dynamically in gait so the density can be adjusted according to such difference. The multiple density zones may be adjusted according to the static foot pressure distribution (bilateral standing position). Theoretically, the area with higher foot pressure such as heel and metatarsal joints required less density to absorb the impact. The area that needs more support such as midfoot and toes was given the higher density. The density can be adjusted from level 10 to 30 and the darker colour represents the higher density. As the foot pressure was simulated by finite element analysis in Chapter 8, the density may be adjusted according to simulation results. The protocol is required to control the repeatability and consistency of the density distribution.

- **Save the parameters and applied to the other foot**

The insert 3D image was saved as zip format once it is done. All the parameters of the insert were saved for the other foot as the same parameters were applied to both feet except for the height of arch support. In this way, the inserts on both feet may fit into the same pair of footwear. 3D image of the insert was saved in *.amf file and *.stl files for 3D printing.
We open a new document in Gensole® for the other foot and imported the parameters we just saved. We followed the same procedure— input 13 parameters, convert the format of the *.stl file from binary to ASCII, adjust the direction of the foot in Meshlab®, adjust the height of the arch support and insert density. Finally, the parameters of the insert were saved and 3D image was exported in *.amf and *.stl format for 3D printing. As shown in Fig. 7.19, the insert design was completed by Gensole®.

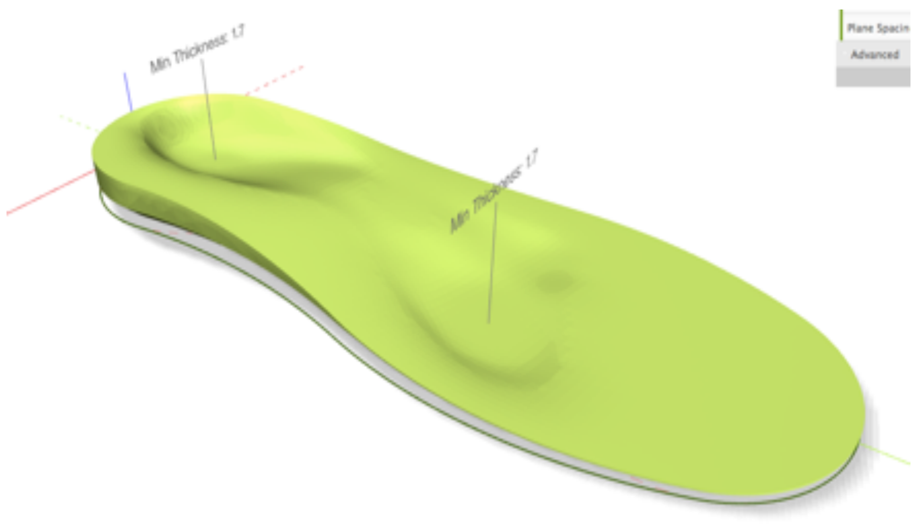

Figure 7.19. The 3D image of shoe insole created in Gensole®

7.4. Novel insole design

The significant issue of low arch or flatfoot is the excessive foot pronation induced by collapse foot arch. Current shoe insoles are to support the medial arch area in order to reduce the excessive pronation and neutralized the foot position. However, the limitation of current shoe insole is to limit the movement of midfoot so it can compromise the compression and recoil of the foot arch. Foot arch is like the sling or spring that can absorb the mechanical energy when it is loaded and return the partial energy when the load is released. This elastic recoil mechanism helps human propel in a more effective and energy-saving manner. Therefore, in the novel design, we were looking for a material or structure that can correct the excessive pronation issue as well as enhance the elastic function of the arch. As shown in Fig 7.20, an elastic mesh pad was created in the middle foot area where the arch collapses to mimic the function of foot arch. Compared to current shoe insole, the novel design removed the midfoot support and replaced by the elastic mesh pad. The elastic mesh can pull the two ends of the insert when loads apply top down. The elastic mesh pad can absorb the load and return the mechanical energy when the load releases. The elastic mesh pad can be loaded when the foot pronates due to external force (e.g. foot landing) and return the mechanical energy to enhance the explosive power of the foot and it is to mimic the function of a foot arch. The elastic mesh pad can support the fallen medial longitudinal arch but not fully restrict midfoot motion.

Figure 7.20. Compare the current shoe insole (left) to our novel design (right). The grey arrows represent the direction of the external force and reaction force

7.4.1. Design 1— Honeycomb

Honeycomb is the first design to achieve the idea that elaborated above. We created a number of triangular cavities in the middle area of the insert based on the traditional insert (Figure 7.21).

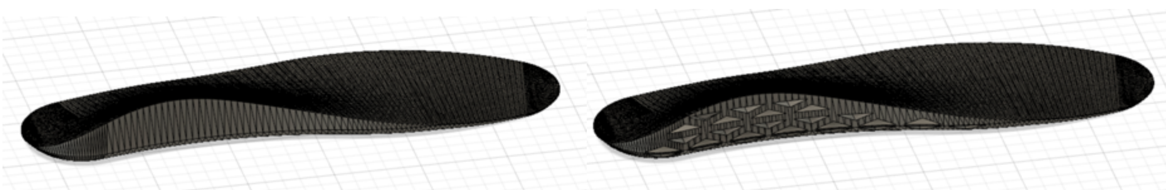

Figure 7.21 (Left) traditional insert (Right) novel insert— Honeycomb

We imported the insert image that created in Section 7.3 by Gensole® to Fusion 360® for creating the triangular prisms. Two layers in the insert were generated by Gensole®, which the bottom layer is fixed in 8.5mm for thickness (figure 7.22). Twenty-six isosceles triangular slices with the same dimension— 20mm of the base and 4mm of the height, were created in the medial side of the insert to facilitate the compression and recoil of MLA in gait (Figure 7.22). There is one line of triangles on the bottom layer and four lines of triangles on the top layer. As shown in Figure 7.23, the apex of the triangle is 3.5mm away from the bottom of the lower layer and the base of the triangle is 1mm away from the top of the lower layer. Each triangle is 4mm away from each other (Figure 7.23). Unlike the bottom layer, the thickness of the top layer is changed by the height of arch or length of foot. The height of insert is from 26.6-27.8mm for our current participants. We sketched the same triangles as the lower layer and arranged them into four lines as shown in figure 7.23. The first line (i.e. lowest line) of the triangles are 4mm away from each other and 1mm away from the bottom of the top layer. And the legs of the second lines of triangles are 4mm away from the first line triangles. And the base of the third line of triangles is 4mm away from the second line of triangles. And the fourth line is the same as second line. Based on the sketch of the triangles, we then applied 'extrude' in Fusion 360 and let the triangles became triangular prism to intersect with the insert. And we removed the inserts from the intersections but not remove any area that is within 3mm from the edges. The structure could easily collapse if the cavities are too close to the edges of insert.

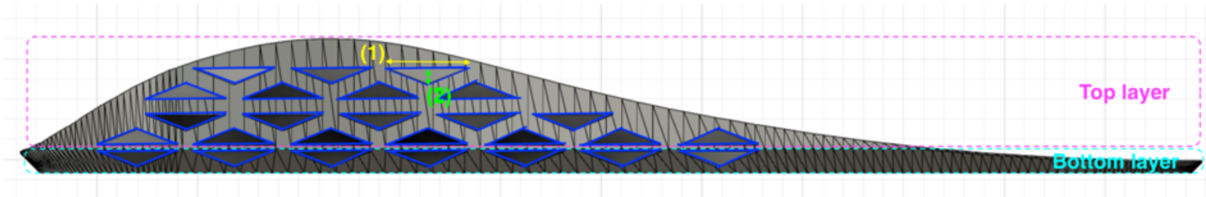

Figure 7.22. Medial view of left shoe insole. Twenty-six isosceles triangular slices (blue line) with the same dimension— (1) 20mm of the base and (2) 4mm of the height. Top and bottom layer of the insert consist of one and four rows of isosceles triangular slices respectively.

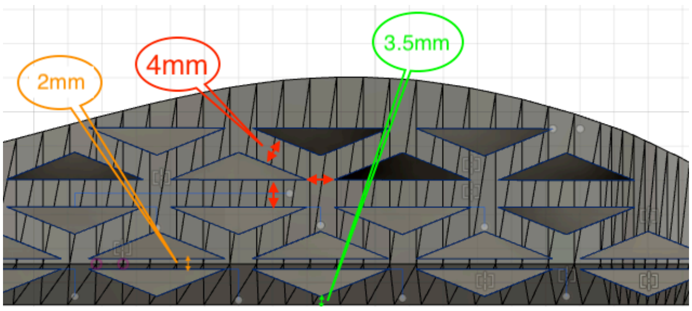

Figure 7.23. The arrangement of the triangular cavities. Each triangle is 20mm of the base and 10.77mm of the legs (i.e. 4mm of the height)

Both inserts were imported in the same drawing and applied the triangular prism at the same time for consistency in design. Both inserts were set at the same direction, which the plantar is on xy-plane and the axis of the insert (same as foot axis) is along with +x direction from the heel tip towards the tip of the second toes. A plane passes through insert axis and perpendicular to xy-plane was created for each insert and another plane in the middle of these two planes was created (i.e. the green line shown in Figure 7.24). The sketches of the triangles were created on the green plane to ensure the same cavities were applied to both inserts after we extrude the triangle cavities. We used the same size and same pattern of triangular cavities to both participants and make sure there is no cavities within 3mm from the edge. The height of the arch support of individual inserts could be different and require different size of the triangular cavities. Our two participants are in US 11.5 and 13 size shoe which their foot length is 283mm and 295mm respectively. In the future, we may change the size of the triangular cavities according to the size of participant's feet once the consistency and repeatability can be controlled.

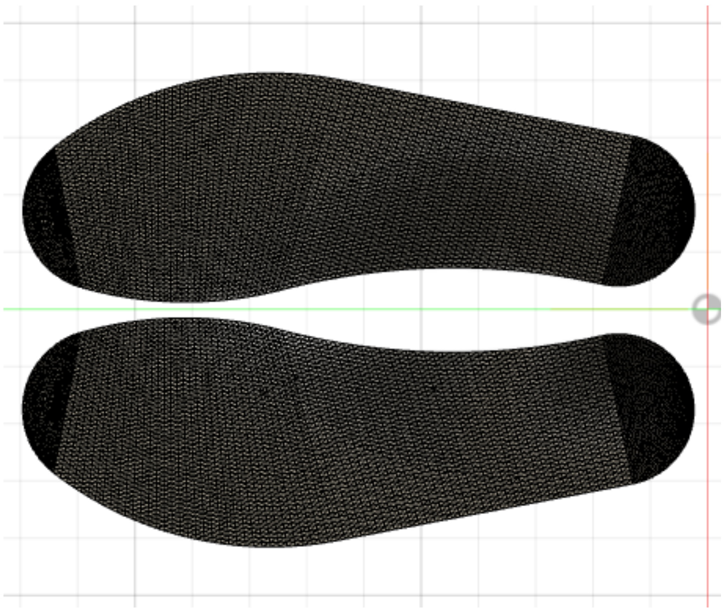

Figure 7.24. The inserts for the same participant were designed at the same time to increase the repeatability and consistency for the triangular prism cavity. The green line is the middle plane used for the sketch of triangles.

7.4.2. Design 2— Bubble

The potential drawback of Honeycomb could be the pressure is concentrated on the edges of the triangle when load applies, and it could be an issue regarding durability and force transmission. Therefore, we replaced the triangular cavities to sphere cavities and created the second design called Bubble. The pressure distribution of bubble may be more even around the cavities since the edges were replaced by the round surface. Three different designs with different sphere size and densities were created as figure 7.25 and 7.26. As shown in Figure 7.25, the initial design was created with the sphere cavity 5mm in diameter. However, the issue may be revealed as the density of the cavity is too high so the structure may not be durable and easily to collapse. The high density of cavity may not provide the sufficient support to the fallen arch and prevent the excessive pronation for low arch or flatfoot.

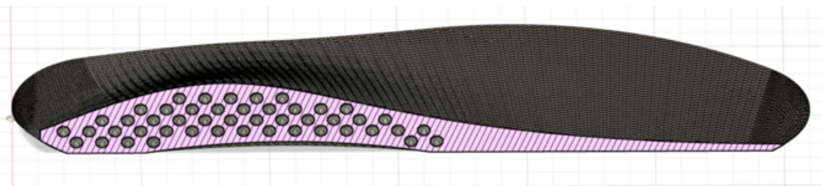

Figure 7.25. The initial design of Bubble with high density of sphere cavities

Therefore, the other two Bubble designs were created as shown in figure 7.26 with lower density and different sizes of sphere cavities. The second design is with the small sphere (2.5mm in diameter) with the greater density and the third design is with larger sphere (5mm in diameter) with the lower density. In the second design, the distance between the centre of each sphere is 7.5mm. In the third design, the distance between the centre of each sphere is 15mm. All the cavities should have at least 3mm from the edge of insert. The distance between the cavities and the edge of the insert has greatly increased to avoid the potential issue of the initial Bubble. Four sectional planes were created to create the sphere cavities. The most lateral planes shown in Figure 7.26 are the plane closest to the insert axis and they contain the greatest number of the sphere cavities because the largest sectional area. In greatest section area, the second design has three line of sphere cavities, and the third design has two (Figure 7.26). The number of lines of sphere may decrease as the area of section plane decreases. The sectional planes next to the most lateral plane has three lines in second Bubble and two lines of third Bubble. The other two planes only have two lines in second Bubble, and one lines in third Bubble. The procedure of creating sectional planes is to firstly create the reference plane paralleled to the insert axis (i.e. foot axis), perpendicular to xy-plane, and tangent to the most medial point of the insert was created. The other four planes paralleled to the reference plane were created with 10mm interval and the number of sphere cavities were different on each plane. The potential drawback may be found in 3D printing process. In 3D printing process, some structures are required to build in sphere cavities to support the whole structure. Therefore, some material may remain in the sphere cavity and cannot be removed. However, it is unclear how the remaining material affect the performance in terms of the force distribution and force transmission of the insert.

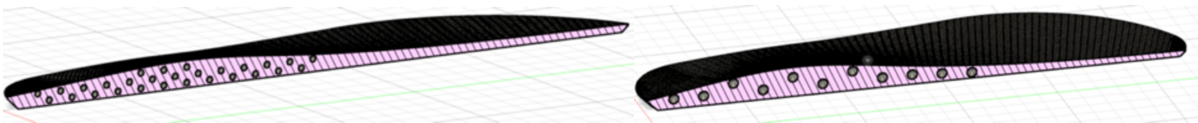

Figure 7.26. The smaller sphere with higher density (left) and the larger sphere with lower density (right)

7.4.3. Design 3— Gyroid

Gyroid (Schwarz G) is the unique non-trivial embedded member of the Schwarz P and D surfaces with angle of association approximately 38.01° (figure 7.27), which first discovered by NASA scientist, Alan Schoen (Schoen, 1970).

The formula of Schwarz (Rossi & Buratti, 2017) are

$$P: cos(x) + cos(y) + cos(z) = 0 \tag{7.1}$$

and

$$D: sin(x)sin(y)sin(z) + sin(x)cos(y)cos(z) + cos(x)sin(y)cos(z) + cos(x)cos(y)sin(z) = 0 \tag{7.2}$$

The formula of Gyroid (Rossi & Buratti, 2017) is

$$G: cos(x) * sin(y) + cos(y) * sin(z) + cos(z) * sin(x) \tag{7.3}$$

and the top, side, and section view of Gyroid are shown in 7.28. Gyroid is designed for lightweight high-strength materials such as titanium and it has been evolved over time, which is applied to implant for bone defect through addictive manufacturing in recent years (Yánez et al., 2018; Ataee et al., 2018). The reason we used Gyroid to apply on our insert is because it conducts the geometric and rotational symmetry properties. As shown in figure 7.29, the Gyroid shows high consistency in structures and patterns in different section views. The stiffness, strength and elastic response of the gyroid lattice has been investigated in different studies through computational simulation (e.g. FEA) or onsite test (e.g. compression test)

(Khaderi et al., 2014; Yánez et al., 2016) and its characteristic can be applied to insert design. Yánez et al. (2016) also found the specific properties of the gyroid structures can be similar to hard tissue of human (e.g. skeleton).

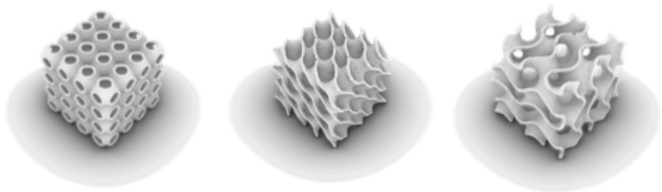

Figure 7.27. Schwarz P (left); Schwarz D (middle); Schwarz G (i.e. Gyroid) (right) (Rossi & Buratti, 2017)

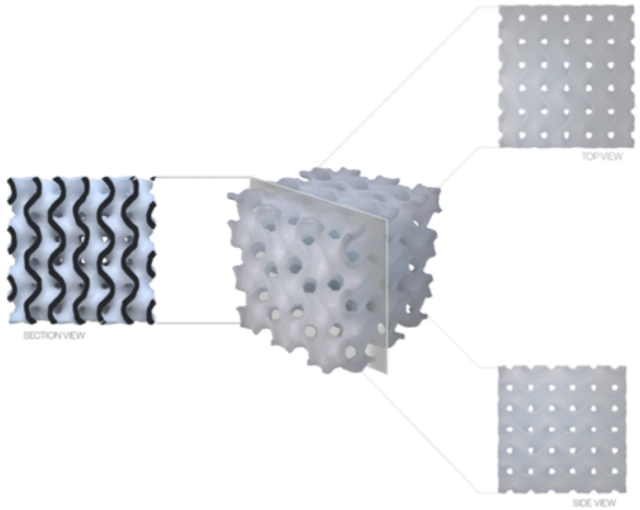

Figure 7.28 The top view, side view and section view of Gyroid.

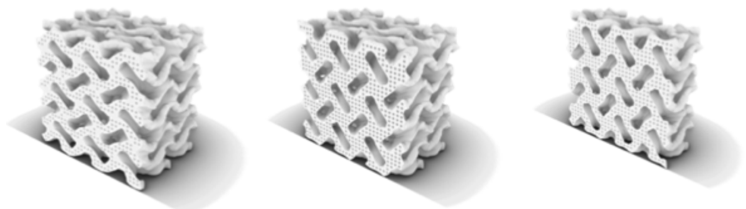

Figure 7.29. Gyroid has geometric and rotational symmetry properties. The pattern of different section views is highly consistent.

The process for generating minimal surface Gyroid geometry and Gyroid insert are as following (Figure 7.30.1):

(A) Define a region (10*10*10mm) to generate the geometry of a unit of Gyroid

(B) Generate points regarding to the resolution or density we want. We can also add more points later in the process to increase the resolution if it is required for the mesh.

(C) Using the x-y-z coordinates of each point to solve the minimum spanning surface formula value. The formula of Gyroid is cos(x)*sin(y)+cos(y)*sin(z)+cos(z)*sin(x)

(D) Generate an isosurface within the region using the points and their corresponding values. The values of each point are still represented by the relative size of each point in the left image.

(E) Parametrically alter the repetition of the Gyroid structure and density within the region defined in step 1

(F) Parametrically alter the wall thickness of the structure

(G) The final step is to apply the shape of insert we designed earlier to shaping the Gyroid insert from the large Gyroid block

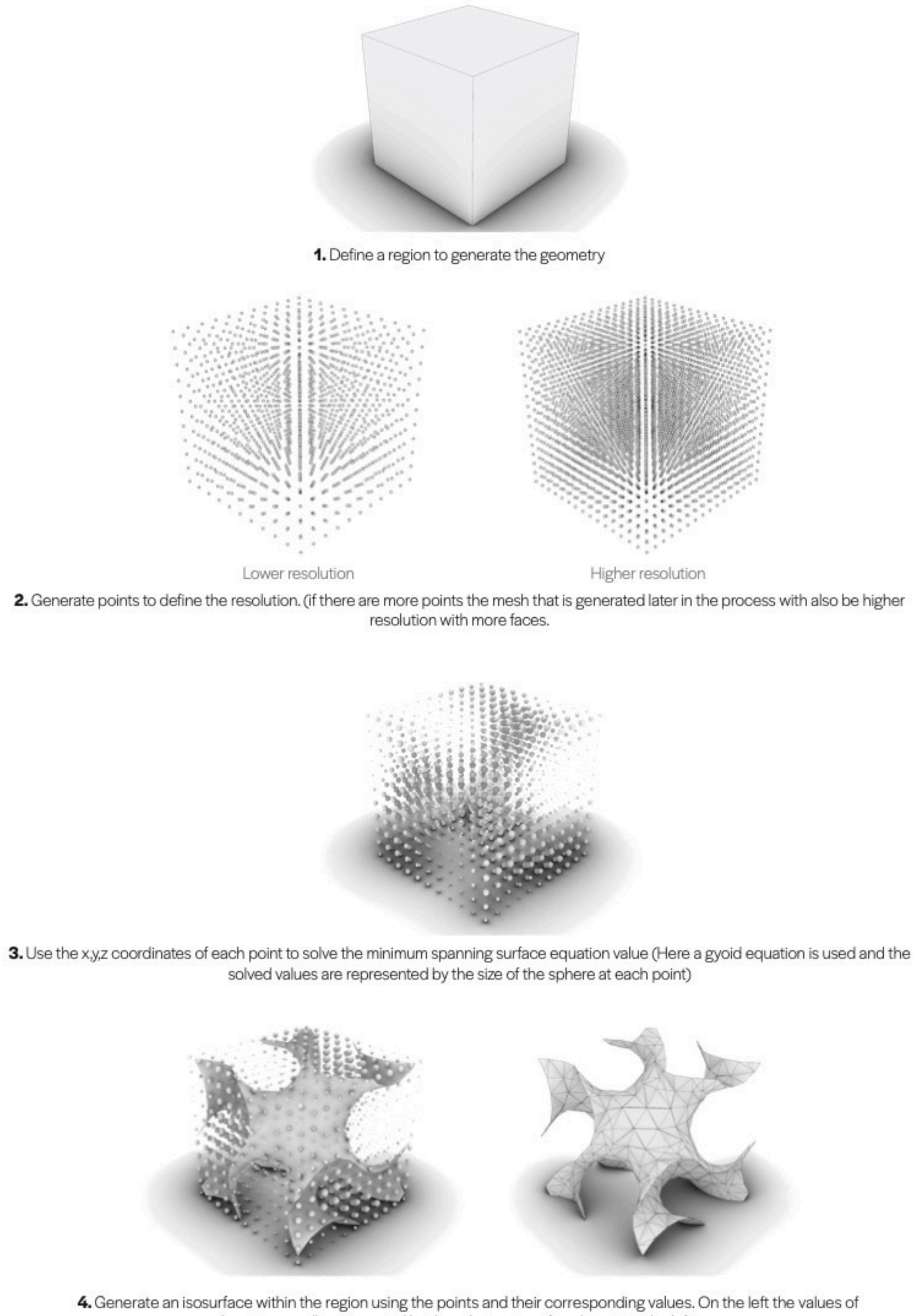

Figure 7.30.1. The process for generating minimal surface Gyroid geometry

7.5. Material selection for additive manufacturing

7.5.1. PloyJet material selection

The literature shows the appropriate material properties of insert for low arch or flatfoot are required high hardness (shore hardness between 55 to 70), high strain and stress and low compression set and compression fatigue (Healy et al., 2010) in traditional manufacturing approach. For traditional manufacturing, the initial foot cast is made by plaster casting and the material sheet is placed on the plantar of the cast. Through heating and vacuuming process, the shell of insert is form by the material sheet. In order to meet the requirements of the material properties mentioned by Healy et al. (2010), the most suitable materials are polyurethane (PU) and ethylene vinyl acetate (EVA) for traditional manufacturing. According to BASF performance footwear standards, the material properties of PU at midsole are 330 to 380 kg/m^3 for density, 50 to 54 for shore A hardness, 3.6 to 4.5 N/mm^2 for tensile strength, and 200 to 230% Elongation at break (BASF, 2018).

In current study, our insert prototypes were produced by addictive manufacturing (AM), PloyJet material jetting. As the manufacturing process of AM is different than traditional approach, the specific AM material for insert needs to be selected. According to Stratasys materials data sheet, Agilus30 (FLX2040) / Agilus30 Black (FLX9840), TANGOBLACKPLUS (FLX980) / TANGOPLUS FLX930 were selected as the primary materials and VERO / VEROWHITEPLUS RGD835 are selected as the secondary material for the required properties (figure 7.30.2). The rubber-liked characteristic of Agulis30 and TANGOBLACKPLUS provide the elasticity when loaded and unloaded, which may be used to mimic the elastic recoil of the foot arch in locomotion. The combination of Agilus30 and Vero (Figure 7.30.2a) and TangoPlus and Vero (Figure 7.30.2b) provides twelves different ranges of mechanical properties that may meet our purpose of novel insert design.

(a)

PRIMARY MATERIAL: AGILUS30 (FLX2040) / AGILUS30 BLACK (FLX9840) SECONDARY MATERIAL: VERO								
PROPERTY	ASTM	UNIT	FLX9740 FLX9840	FLX9750 FLX9850	FLX9760 FLX9860	FLX9770 FLX9870	FLX9785 FLX9885	FLX9795 FLX9895
Tensile strength	D-412	MPa	3-4	3-4	3.5-4.5	4-6	6-10	10-14
Elongation at break	D-412	%	190-210	170-210	150-170	120-140	70-90	50-70
Shore hardness	D-2240	Scale A	40-50	50-55	55-60	60-70	80-85	85-90
Tensile tear resistance	D-624	Kg/cm	6.0-8.0	7.0-9.0	7.0-10.0	12.0-14.0	22.0-26.0	26.0-30.0

(b)

PRIMARY MATERIAL: TANGOBLACKPLUS FLX980 / TANGOPLUS FLX930 SECONDARY MATERIAL: VEROWHITEPLUS RGD835								
PROPERTY	ASTM	UNITS	FLX9840-DM FLX9740-DM	FLX9850-DM FLX9750-DM	FLX9860-DM FLX9760-DM	FLX9870-DM FLX9770-DM	FLX9885-DM FLX9785-DM	FLX9895-DM FLX9795-DM
Tensile strength	D-412	MPa	1.3-1.8	1.9-3.0	2.5-4.0	3.5-5.0	5.0-7.0	8.5-10.0
Elongation at break	D-412	%	110-130	95-110	75-85	65-80	55-65	35-45
Shore hardness (A)	D-2240	Scale A	35-40	45-50	57-63	68-72	80-85	92-95
Tensile tear resistance	D-624	Kg/cm	5.5-7.5	7.5-9.5	11-13	15.5-17.5	23-25	41-44

Figure 7.30.2 Available material combination from Stratasys Data Sheet. (a) The combination of Agilus30 and Vero (b) The combination of TangoPlus and Vero.

Cambridge Engineering *Selector* (CES) was used to select the appropriate materials that meet our purpose. CES is a highly efficient tool for materials selection and graphical analysis according to their properties. The correlation between tensile strength and elongation, and the comparison of tensile strength between materials are analysed in figure 7.31. We finalized three PloyJet materials— FLX9740, FLX9750, FLX9760, as our potential insert materials as their properties (i.e. tensile strength: 3 to 4MPa; elongation at break 150 to 210% at break; Shore A hardness: 40 to 60; tensile tear resistance: 6.0 to 10.0Kg/cm) are closer to the material properties that mentioned in previous study (Healy et al., 2010).

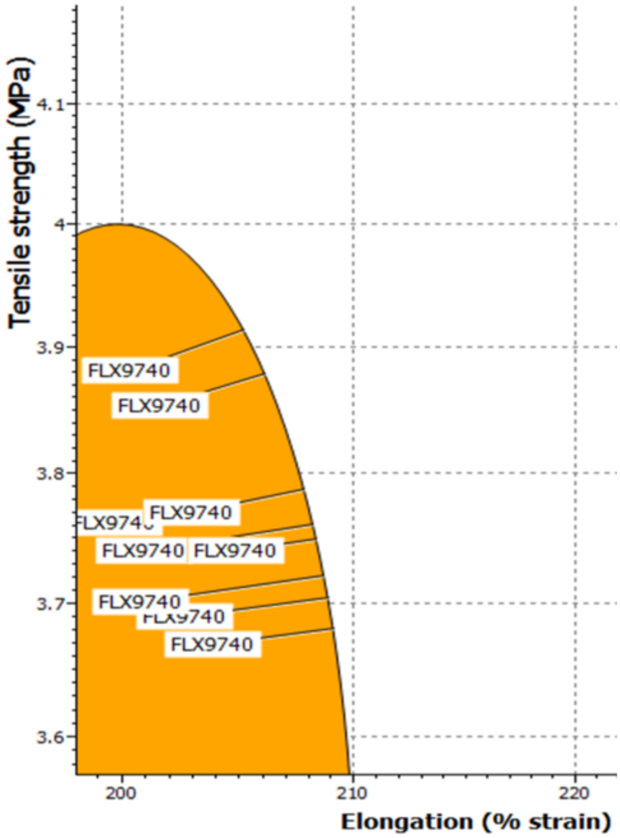

Figure 7.31. Cambridge Engineering *Selector* (CES) was used to select the appropriate materials from the combination of Agilus30 or TangoPlus and Vero

7.5.2. PloyJet material testing

The material properties may be changed in different structures or situations, so the material was tested through the experiments— tensile strength test, compression set test, hardness test and 3D microscopy observation. All the experiments are compliant with ASTM D412 (2016), ASTM D395 (2008) and ASTM D2240 (2005) respectively. FLX9740 was selected for the testing.

- **Tensile strength test**

Five identical test specimens are compliant to the specification from ASTM D412 shown in figure 7.32.a, which is defined as Type-I specimen. The tensile test equipment is a 3kN uniaxial Instron 3365 shown in figure 7.32.b, and the test pieces were tested at a uniform strain rate of 100 mm/min.

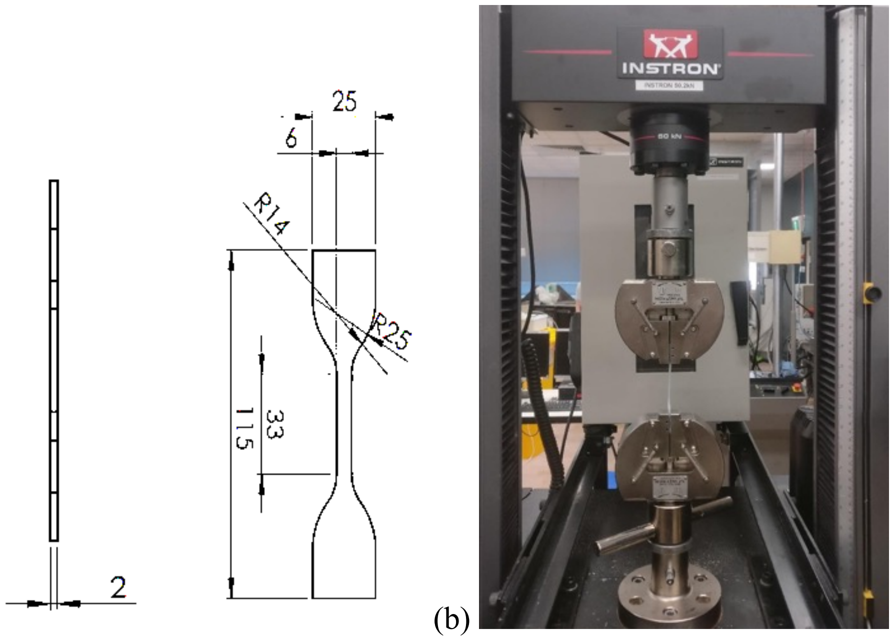

Figure 7.32. (a) Tensile test piece for ASTM D412 (b) tensile test equipment

The results of tensile test were listed in Table 7.1, and the stress strain curve was established showing uniaxial behaviors of the material under tension in Figure 7.33. The average tensile strength is 2.34 MPa and the elongation at break is 331.38% from five specimens (Table 7.1). The variance of the specimens was less than 10%, which is the acceptable variance because the coefficients of variation for tensile strength are commonly within the range of 1 to 10% (Gulzar, 2012). Substantial inconsistency of the specimen or experimental error may be indicated when values are above 10% (Gulzar, 2012). Compare to the Stratasys data sheet (tensile strength is 3 to 4MPa and elongation at break is 190 to 210%), the actual tensile strength decreased 22 to 42% and elongation at break increased 58 to 74%. Other studies reported different tensile stress and elongation of insole materials altered the peak vertical ground reaction force and energy absorption in long duration running (Cheng et al., 2019) and in gait (Palhano et al., 2013) but no difference in step length, stride length and cadence. Moreover, materials with different tensile strength may affect sustainability (Hasan et al., 2015). Lower tensile strength reaches failure at a lower strain that would suggest an increase of wear and tear and it may result in poorer durability of insole.

Table 7.1. Tensile stress and elongation of five specimens of FLX9740

	Sample	Average

	1	2	3	4	5	
Tensile stress at break (MPa)	1.77	2.26	2.36	2.04	2.21	2.34
Elongation at break (%)	264.57	357.48	321.02	341.60	352.27	331.38

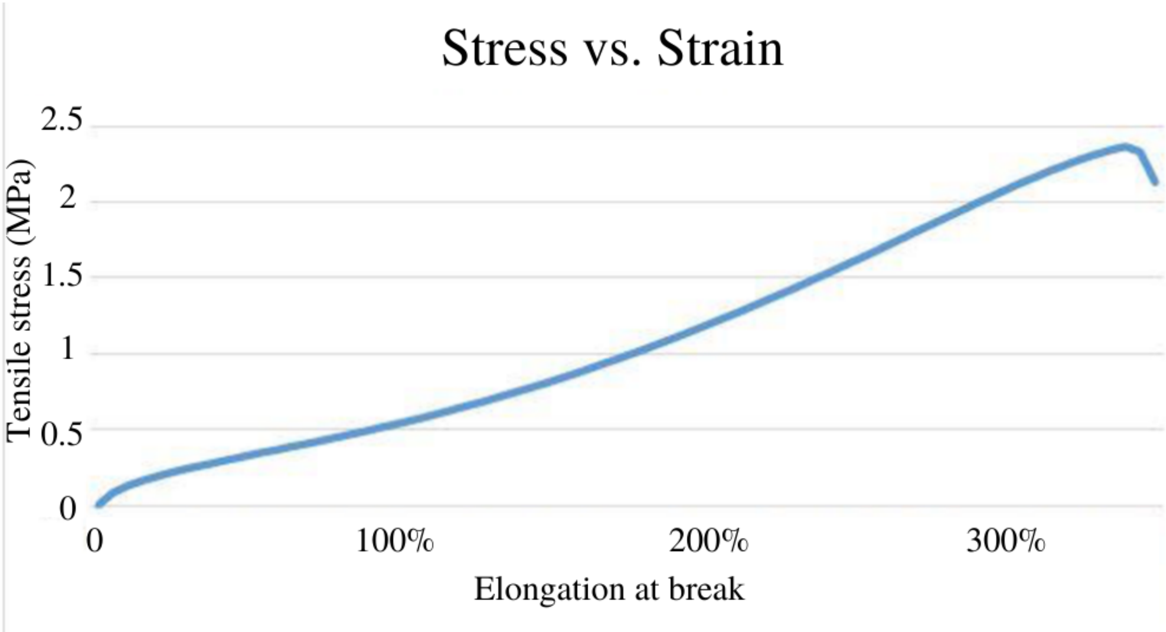

Figure 7.33. The stress and strain curve of FLX9740

Agilus30 was tested in different shore hardness— 40, 50, 60, 70, with five specimens compliant to the specification from ASTM D412 in each hardness. The uniaxial tensile tests were conducted using Instron 3365 series. The results of stress strain curve of the trials of different shore A hardness were presented in Figure 7.34. The elastic property in the linear region of stress-strain curve was evaluated by the “linear regression” analysis. Strain between 0 and 0.25 was selected and the linear regression model was analyzed by SPSS Version 26 (IBM SPSS Inc.). R-squared— the coefficient of determination, is reported to assess the data distribution around the fitted regression line. R-squared indicates the proportion of variance in stress associated with strain which higher R-squared presents the better correlation with linear behavior. As shown in Table 7.2, the slope of the fitted regression line implies elastic modulus of specimen. The specimens of shore 40, 50 and 60 have the relatively higher R-squared values (R^2>.90) showing the higher percentage of data fit the regression model. However, the specimens of shore 40 have the relatively lower R-squared values (.87<R^2<.90) showing the lower correlation with linear behavior. As shown in Table 7.2, the higher mean slope showing higher elastic modulus were found in the specimens with higher hardness. Material with higher shore evidently resulted in higher stiffness at all strain, which agree with the stress strain curve obtained from tensile test. Therefore, the slopes calculated from linear regression are reasonably correlated with elastomer's Young's modulus by a linear relationship.

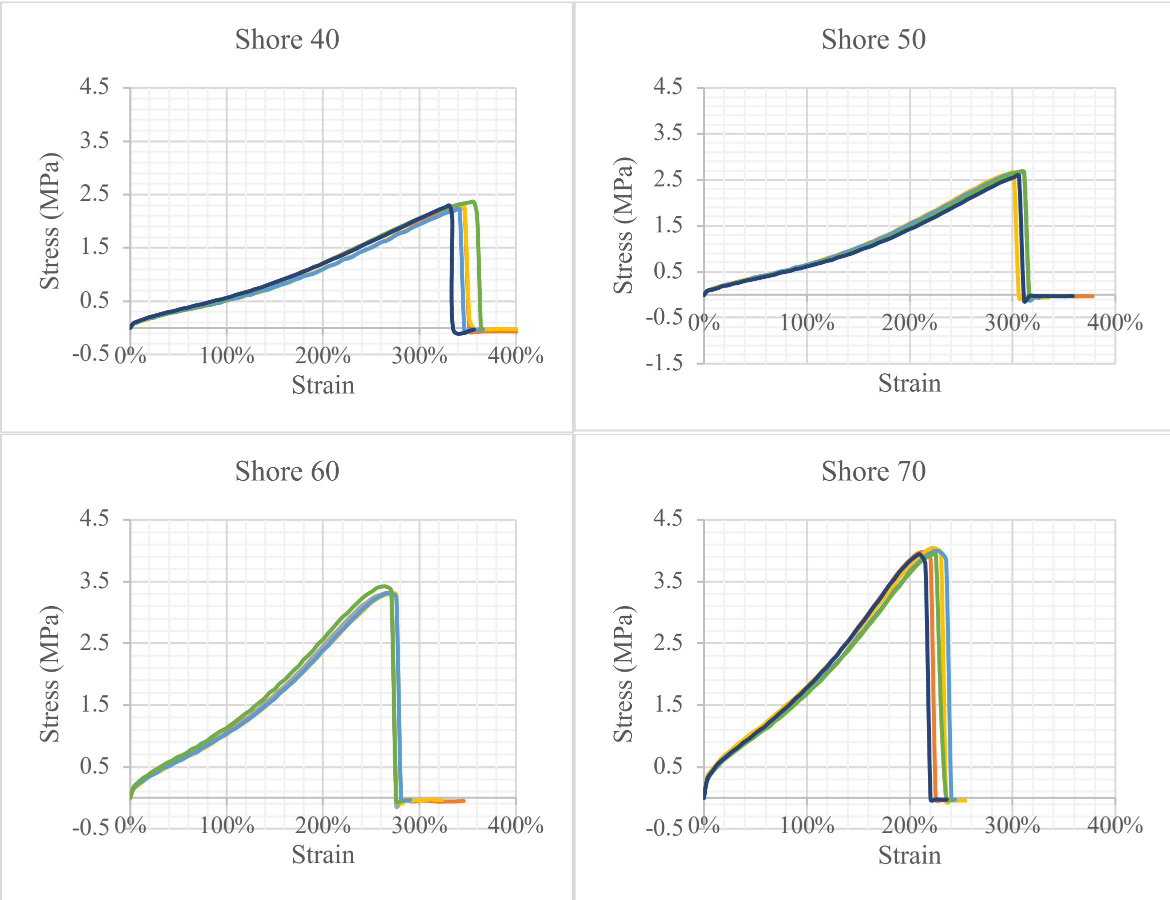

Figure 7.34. The stress strain curve of Agilus30 in different Shore A hardness

Table 7.2. R-squared and slope of linear regression model in each specimen

Shore Hardness	Test specimen										Mean Slope (SD)
	1		2		3		4		5		
	R^2	Slope	R^2	Slope	R^2	Slope	R^2	Slope	R^2	Slope	
40	.921	.757	.929	.773	.940	.724	.957	.810	.869	.750	.763 (.031)
50	.900	.874	.908	.897	.947	.872	.992	.842	.911	.817	.860 (.031)
60	.922	1.500	.910	1.456	.936	1.493	.919	1.439	.906	1.653	1.509 (.085)
70	.872	2.586	.870	2.763	.880	2.664	.896	2.586	.872	2.642	2.648 (.073)

*SD: standard deviation

The homogeneity of variances was used to evaluate the consistency of tensile test for the load at break. The homogeneity of variances was presented by the equality of variances in Levene's test using SPSS Version 26 (IBM SPSS Inc.). One-way ANOVA was employed for statistical analysis and the null hypothesis is set as no difference in the peak load between the same hardness specimens. As the samples are assumed normally distributed in one-way ANOVA, the normality test needs to be carried out beforehand. For normality test, $|z| < 2$ indicates the sample is normally distributed (Kim, 2013) and the z-values were obtained by skewness and kurtosis based on eq. [7.4] and [7.5]:

$$Z_{skewness} = \frac{skewness}{SE_{skewness}} \quad [7.4]$$

$$Z_{kurtosis} = \frac{kurtosis}{SE_{kurtosis}} \quad [7.5]$$

where SE is the standard error.

P-value (Sig.) of Levene's statistic represents the probability that if the null hypothesis were true. As shown in Table 7.3, shore 40, 50, 70 result in the relatively higher probability (p= .227, .206 and .929) while shore 60 has the relatively lower probability (p= .076) to support the null hypothesis were true. All p-values are above .05 showing no statistically significant difference for the peak load at break between the same hardness specimens. Therefore, it can be concluded that the variances of load in the same hardness are equally distributed.

Table 7.3. Levene's test for equality of variance

Sample Hardness	Levene's statistic	
	F	p (Sig.)
Shore 40	2.292	.227
Shore 50	2.593	.206
Shore 60	7.136	.076
Shore 70	.009	.929

- **Compression set test**

As the compression set indicates the resiliency of the material over a period of time, the purpose of the test is to access the recovery ability of the material after a consistent compressed force. It is to simulate the how the material of the insert recovery after the prolonged standing activities. Four FLX9740 test specimens were 12mm in thickness and 29mm in diameter (Figure 7.35). As shown in Figure 7.35, the test equipment is made by three compression plates, four fine hex bolts and six spacers compliant with Test B ASTM D395-16 Standard. The test condition is at room temperature of 23°C for 22 hours. Four specimens are compressed by 25%.

The compression set was calculated according to the thickness before and after the test by the formula listed in eq. [7.6]

$$C_B = \frac{h_0 - h_1}{h_0 - h_s} \times 100\% \qquad [7.6]$$

where h_0 and h_1 are the initial and follow-up thickness of the test piece respectively. h_S is the height of the spacer which is 9.5 mm.

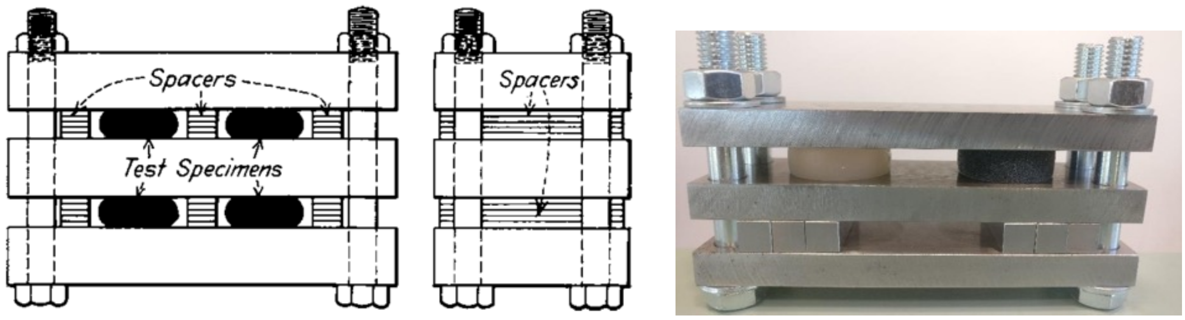

Figure 7.35. Test B apparatus for ASTM D395 for compression set test

The result of compression set is shown in Table 7.5, and the mean compression set for four specimens is 15.49%. The room temperature in our test was 23°C that provide the good characterization of material applying to insert. As compression set is extremely sensitive to the temperature and atmosphere, the strict criteria are needed to be established to conduct the results with high quality. As the compression set of FLX9740 is not shown from Stratasys data sheet, the test result (15.49%) shown in Table 7.4 is similar to the property of PE foam (14.29%) at the similar hardness level (Rome, 1991). According to Figure 7.36, the specimens started to recover after 28th hour and fully recovered to its final thickness until 29th hour. As the purpose of the insert is to correct the abnormal foot position, i.e., the low arch, it is suggested the lower compression set is more suitable such as, rubber, EVA, PE, PU for traditional approach (Healy et al., 2010). However, materials with higher compression set are normally able to absorb more impact to lessen the overall plantar pressure are suggested for accommodative insert (Fauli et al., 2008). The compression set test is crucial for PolyJet additive manufacturing (AM) material because the curing quality of the material can be explored. PolyJet material is highly affected by the curing process that is the adherence between layers during manufacturing process. According to Phillips et al. (1984), stereolithography printing technique depends on UV curing to adhere the layers may not be as strong as polymer chains produced by traditional manufacturing. Therefore, compression set test needs to be carried out for controlling the quality of 3D printed object in terms of curing quality in order to select the appropriate material for insert.

Table 7.4. The results of compression set test of four samples

	Before (mm)	After (mm)	Compression set %
Sample 1	12.28	11.82	16.55
Sample 2	12.17	11.80	13.86
Sample 3	12.36	11.76	20.98
Sample 4	12.05	11.78	10.59
Mean (SD)	12.22 (0.13)	11.79 (0.03)	15.50 (4.39)
Variance	0.0136	0.0005	14.48

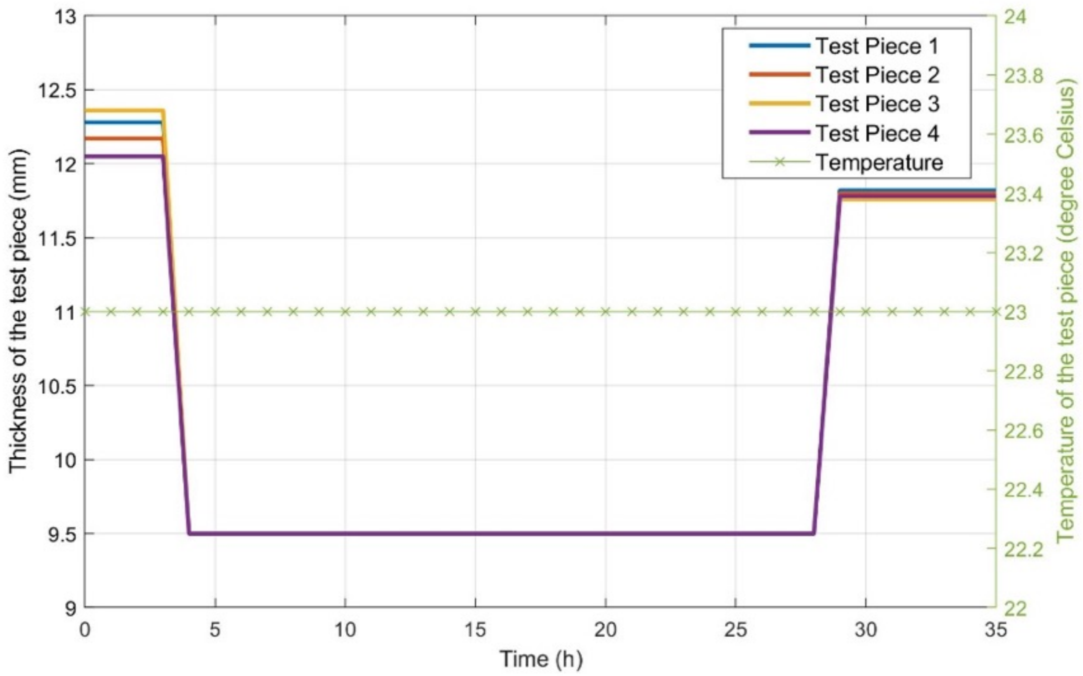

Figure 7.36. The deformation and the recovery of the samples in testing

- **Hardness test**

Shore hardness test measures the resistance of a material to indentation. The testing was set up based on the standard of ASTM D2240, the standard test for rubber property. Shore A was selected as the scale to access the hardness of FLX9740. The testing apparatus was set up as

Figure 7.37 with a test specimen with 6.4mm in thickness under an indenter specified for type A durometer at room temperature. The value of the hardness was presented by the display of durometer.

As the results displayed by durometer, the test piece was in range of 40 to 50 Shore A hardness, which showed a good agreement with the data sheet presented by Stratasys. The hardness of the insert can change the gait pattern in terms of foot and ankle biomechanics. According to Healy et al. (2012), insert with lower hardness may not provide sufficient support to the medial longitudinal arch to prevent the excessive foot pronation and unable to correct the abnormal foot position. However, Su et al. (2017) claim that insert with higher hardness can induce higher stress or pressure on joints and soft tissue, which may increase the risk of acquiring musculoskeletal symptoms. Therefore, the relevent hardness needs to be selected to support the fallen arch and correct the foot position but not increase the unnecessary stress on joints and soft tissue.

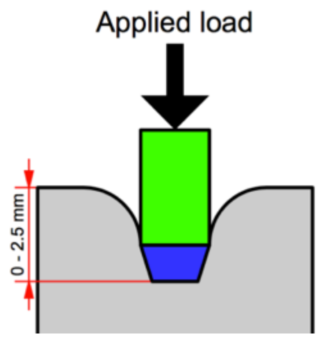

Figure 7.37. The testing specimen and apparatus of the hardness test

- **Microscopy test**

The test piece that underwent tensile testing was examined using Alicona microscope at 100 times magnification. The 2D and 3D image of the test piece were shown in Figure 7.38, which gives us the insight of the internal defect due to the fracture induced by pulling. From the microscopic images, the patterns of voids at the necking (i.e. the fracture point) are different from other regions. Voids at the necking are normally in the scale of 20 microns. The closer view of the patterns of voids allows us to understand the insight of AM material process and it can be a reference to optimize the quality of 3D printed material based on the parameters.

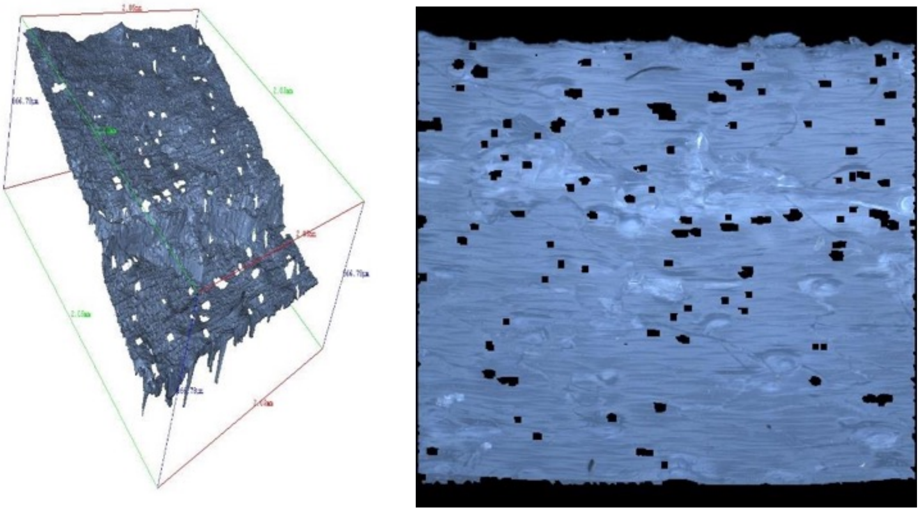

Figure 7.38. 2D (left) and 3D image (right) of the test specimens under microscope at 100 times magnification

7.6. Prototyping

The first prototype was done by stereolithography type 3D printing machine— OBJET Eden260VS (Figure 7.39). One of the advantages of OBJET Eden260VS is to print different materials on a single object. Tangoblackplus plus FLX980 was selected as the AM material. Shore A hardness 80 was selected as we thought thermoplastic polyurethane (TPU) seems the more supportive for the fallen arch. However, we realized that it was not flexible and greatly decreases the comfort level of the users once the prototype was produced. The other drawback of the first prototype is the front part of the insert is too wide so it cannot be put in the shoes.

Figure 7.39. First prototype produced by OBJET Eden260VS using Tangoblackplus plus FLX980

Further prototyping includes the solid traditional insert and Honeycomb novel insert were manufactured by the 3D printer, Stratasys J750 (Figure 7.40). Stratasys J750 is one the PloyJet printing technology which can produce smooth and accurate part and prototypes. Stratasys J750 can print over 360,000 colours in ABS and rubber-like materials in a variety of shore hardness level. Agilus30 FLX935 was selected as the base material and Vero was selected as the secondary material to produce the insert for shore A hardness 60. The inserts produced in the second prototyping were analysed through finite element model and motion analysis in the next two chapters.

Figure 7.40. The second prototyping. The traditional solid and Honeycomb novel inserts were produced by Agilus 30

7.7. Conclusion

In current chapter, a procedure for CAD-generated inserts design is proposed from 3D foot scans, 3D foot image processing, direct modelling of insert in CAD. Moreover, we introduced a parametric modelling of insert design by automatically transferring foot scanned data into parameters that can control the insert geometry through our new-developed algorithms. This parametric modelling method reduced the required time of digital design from 3 hours to 3 minutes. It can be easily operated by medical professionals who may not be experienced to CAD software and to adopt in-house digital insert design. Three novel insoles, Honeycomb, Bubble and Gyroid, were designed using these structures to mimic the foot arch function. Unlike traditional shoe insoles using solid filling to force the foot into the arch shape, the AM materials for the novel insole encompass structural elasticity to actively encourage the foot curvature. Two selected AM materials Agilus30 and Vero were evaluated by compression, tensile and hardness test. Furthermore, the joint's pressure simulation and the motion of midfoot especially the compression and recoil of medial longitudinal arch in locomotion were tested and analysed in the later chapters.

Chapter 8. Finite element analysis of novel insert

8.1. Introduction

Additive manufacturing (AM) is evolving significantly and showing promise in rapid prototyping through its robust capability in producing customized products. AM products are instrumental in various context of research and development processes including the application of insert personalization. The choice of AM material could be broad for insole design as we are looking for the rubber-like material possess the energy absorption and damping capability. The properties of material are usually provided by the manufacturers as a material unit. However, the structure of the object may change the characteristic of the entire insole. The results from the experimental testing of the AM materials used for the novel inserts are in chapter 7. The finite element analysis (FEA) was employed to investigate the characteristic of the entire insole by simulating the interaction of foot and insoles with a view to improve the comfort level of the foot. Although comfort level may be subjective and differs among individuals, it still can be objectively evaluated through physical processes and from a physiological aspect (Putra et al., 2019). Comfort level of foot can be enhanced by mechanically optimizing the insole such as supporting the bodyweight without significant plantar pressure deviations or reducing overall plantar pressure or joint's stress (Antunes et al., 2011). FEA is the powerful tool to simulate the mechanical behavior of foot (e.g. planter pressure, joint's stress) and its implications to human comfort generation (Antunes et al., 2011). The FEA result served as a tool/reference for comfort evaluation directly from the subjects in Chapter 9. In the pilot test, a computer simulation was carried to help us have a better understanding of the whole FEA process. In the second test, the plantar pressure distribution and internal tissue stress for the traditional solid and Honeycomb novel insert were compared. Honeycomb novel insert was reported to reduce the plantar pressure and internal tissue stress. In the third test, the hyper-elastic material and Schwarz family was evaluated in order to simulate the Gyroid novel insert. Gyroid novel insert performed better than Honeycomb novel insert in FEA, which further reduced the plantar pressure and internal tissue stress. In the current chapter, we use FEA to preliminary assess the suitability of the proposed design prior to introducing it to the participants and adapt it accordingly to theoretically enhance the comfort without sacrificing efficiency.

8.2. Pilot FEA Test

8.2.1. Method

Abaqus® was employed for FEA of insert and the procedure includes creating mesh and selecting material, setting the interaction between objects, boundary condition, applying the external load, and generating the FEA report.

- **Create mesh**

The solid mesh can be generated in two independent modules (Caendish et al., 1985). The node point insertion was manually defined on the surface of the object and the node points distribution affect the density of element. For three-dimensional triangulation/ quadrilateral element, the node points were automatically defined and connected to each other to form a mesh as tetrahedral finite elements. Although triangulation is more flexible to create mesh because, the accuracy of the simulation results of triangular elements has been reported lower than the quadrilateral elements (Liu and Quek, 2013). Liu and Quek (2013) also mentioned that the greater number of triangles can result in lower accuracy. Therefore, we used the quadrilateral elements for our mesh for the better accuracy. Moreover, the high aspect ratio such as elongated and skinny element will be ignored in 3D model by the system automatically.

- **Material selection**

Ethylene-vinyl acetate (EVA) properties were used for the insert as linear elastic properties were considered, i.e. 0.923 g/cm^3 density, 60 MPa in Young's modulus and 0.49 Poisson's ratio (Pastina et al., 2012). The values of the Young's modulus and Poisson's ratio are 1.15 MPa and 0.49 respectively for the foot soft tissue that as suggested by Taha et al. (2016) (Table 8.1).

Table 8.1. Element types and material properties of the models.

Components	Element types	Number of elements	Young's Modulus (MPa)	Poisson's ratio
Human foot (soft tissue)	3D-tetrahedral	2763	1.15	0.49
Insert	3D-hexahedral	4385	60	0.49

- **Set the interaction**

The surface-to-surface contact is used to simulate the interaction between foot and the insert. The contact factor between the foot and the insert is set as 0.5 for observing the interaction between foot and the insert once the external load was applied. Values of displacement and rotation at the appropriate nodes (Biggs et al., 2000). Boundary conditions of insert was set as 'pinned' to fix the degrees of freedom of the insert and present the interaction between foot and the insert. In order to present the interaction between two objects, one object need to be fixed in position when the other one is moving. The pressure distribution and the deformation of the insert can be only simulated when the foot is moving over the fixed insert. Therefore, the insert is fixed on its bottom surface (Figure 8.1.a) so no displacement occurs to the insert when the load was applied. The foot model was limited to move on the sagittal plane that is the plane through the foot axis (i.e. the axis through the heel tip and the tip of second toe) and perpendicular to the ground. In the joint motion, the foot/ankle is limited to only dorsiflex and plantarflex in the sagittal plane. We fixed the foot in the middle of the ankle, which is the place between medial and lateral malleolus (Figure 8.1.b), to allow the rotation to occur on the sagittal plane. The foot model rotates in the sagittal plane along with the foot axis to simulate the ankle motion—plantarflexion and dorsiflexion in gait. To simulate the interaction between foot and insert, we "unpinned" the fixed point on foot and allowed the foot to have subtle vertical displacement on the sagittal plane. Through the displacement of the foot, the pressure distribution and the deformation of the insert were simulated. The boundary condition was set to limit the motion of foot' ankle or the displacement of insert to get the ideal results. It should not be forgotten, in the real-life, the insert is attached on the foot in the shoe and they both move at the same time. Moreover, the motion of foot and ankle does not limit on sagittal plane but moving in frontal and transverse plane. However, based on the current knowledge of computational simulation, the motion and displacement of foot and insert need to be limited in order to get the valid results.

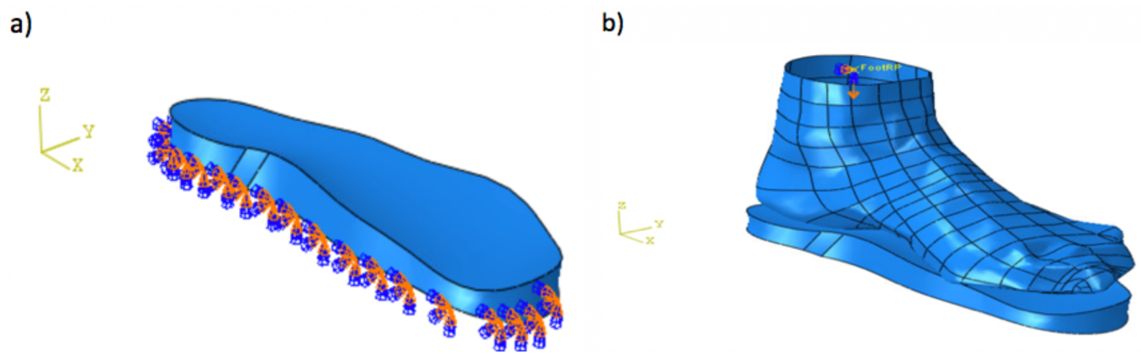

Figure 8.1. (a) Boundary condition of the insert (b) finite element models of insert and foot

The time-dependent motion and load were setup according to movement we intended to simulate. Standing and walking are two major weightbearing activities in cooperate with foot and insert in daily living.

For standing i.e. static simulation, half of the body mass was applied to the foot and vertical displacement toward the insert was naturally occur. In the pilot test, 70kg was the body mass of the subject so the half body mass, 350N, was input on the top of the foot towards the insert. No additional displacement was applied to the foot model.

For the dynamic gait simulation, we applied the foot motion in sagittal plane from heel strike to toe off as the contact phase of the gait cycle. The analysis can be divided in two phases because the rotational center during heel strike and toe off are different. The first phase is from heel strike to foot flat, which is the motion of the foot started from the toe's incline tilted 5 to 0 degrees and the rotational center of the foot model is at the heel (i.e. the contact point of heel and insert) as the 'heel rocker' mentioned by Perry & Burnfield (2010). The second phase is from foot flat to toe off, which the motion of the foot started from horizontal to the toe's declined 15 degrees and the rotational center was set at the metatarsophalangeal joints (MPJ) as the 'toe rocker' mentioned by Perry & Burnfield (2010). Perry & Burnfield (2010) described three rockers of gait— heel, ankle, and toe referred by different rotational centres. 'Ankle rocker' occurs when the lower leg travels over the foot (i.e. lower leg rotate around the ankle joint) while the whole foot is on the ground and it was not included to current study for FE simulation as the 3D image of lower leg was not taken.

Time-dependent load/pressure was applied according to finding reported from Hallemans et al. (2003) of healthy adult subjects. As shown in figure 8.2, the pressure of heel reaches its peak before 10% of gait and it gradually decreases to 0 after the footflat when the heel starts to lift from the ground. The pressure of forefoot including metatarsals joint, and hallux reaches the peak later of the stance phase when the heel lifts from the ground. The middle foot has the relatively smaller pressure than other foot areas according to Hallemans et al. (2003).

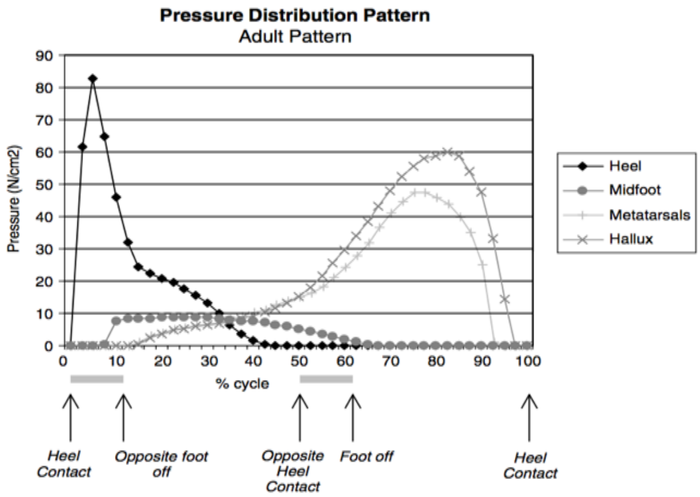

Figure 8.2. The pressure distribution of different foot area in gait reported by Hallemans et al. (2003)

8.2.2. Result and Discussion

The insole stress intensity levels are presented by the equivalent stress (von Mises stress) in standing and in different phases of gait. During bilateral standing, the deformation of insole and over 50% of stress distribution (peak: 0.42MPa) was concentrated on the first metatarsophalangeal joint (MPJ) as shown in Figure 8.3. In gait, during the early stance phase— heel strike, the greater stress was found in rearfoot compared to forefoot (Figure 8.3). The compression of the insole can be clearly observed on the posterior and lateral side of the insole and the peak stress was 0.72MPa (Figure 8.3). During the midstance phase, greater stress distributed on both medial and lateral aspect of the insole with the peak value 0.71MPa at 1st MPJ region (Figure 8.4). During the late stance phase at heel off, greater stress shifted to the anterior aspect of the insole and the peak stress was reported 0.73MPa and the compression can be clearly observed (Figure 8.4).

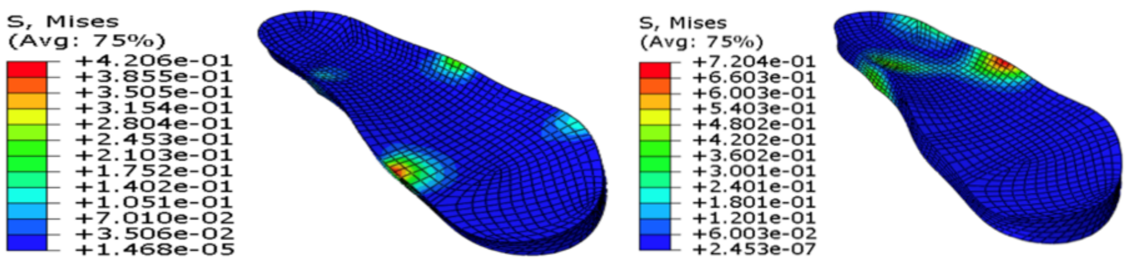

Figure 8.3. The deformation of insole presented by von Mises stress (MPa) at standing (left) and initial foot contact phase— heel strike (right)

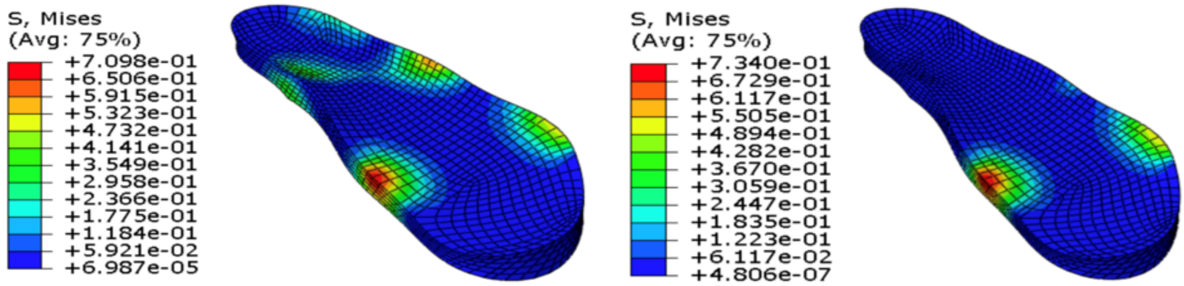

Figure 8.4. The deformation of insole presented by von Mises stress (MPa) at mid stance phase (left) and late stance phase from heel-off to toe-off (right)

As shown in Figure 8.3 and 8.4, the FE model displays the stress distribution in standing and different phases of gait on insole indicating deformation of insole concentrated on the heel cup, and 1st and 5th MPJ region. Greater von Mises stress was found on the posterior edge of the insole indicating the heel cup is required to stabilize the rearfoot in movement. Yung-Hui and Wei-Hsien (2005) claimed the heel cup works as a dampener at heel strike to absorb the impact. In fact, shoe insole is normal a highly nonlinear viscoelastic material and its stiffness is easily affected by rate and level of its deformation. However, insole FE model was assumed homogeneous, isotropic, and linear elastic for analyzing in an ideal scenario, so the result could be slightly deviated from the reality. The generate friction induced by the subtle displacement in the footwear was also cast off to reduce the complexity of FE analysis. The FE simulation assist us to optimize the prototype before manufacturing (i.e. 3D printing), and motion analysis is carried out in the later stage for the obtaining the outcome closer to real human motion.

As shown in Figure 8.3 and 8.4, the peak Von Mises stress is 50% greater in walking compared to standing indicating the insole deformation was two times greater. Yarnitzky et al. (2006) reported the similar result as Von Mises stress and insole deformation was double in the real-time walking compared to standing. gait when compared to standing. As shown in Table 8.2, the peak Von Mises stress reported by the simulation of current study is 0.42 MPa in standing and 0.74 MPa in walking respectively. The values are close to the real-time results reported by Yarnitzky et al. (2006)— 0.31 MPa in standing and 0.80 MPa in walking. The greatest insole deformation is 0.6mm in standing and 1.1mm in walking for our simulation and is 1.2mm in standing and 2.7mm in walking reported by Yarnitzky et al. (2006). Although the magnitudes of the insole deformation are slightly different, the deformation is nearly double in walking compared to standing in both studies.

Table 8.2. Compare the outcome of simulation and real-time experiment in the study of Yarnitzky et al. (2006)

	Simulation in current study		Real-time experiment of Yarnitzky et al. (2006)	
	Standing	Gait	Standing	Gait
Peak von Mises stress (MPa)	0.42	0.74	0.31	0.80
Greatest insole deformation (mm)	0.6	1.1	1.2	2.7

8.3. Traditional solid and Honeycomb novel insole FEA test

In the second test, the pressure distribution between Honeycomb novel insole design and the solid insole were compared through FE model. The skeletons of foot and lower leg were added to the FE model to investigate the internal stresses of foot-ankle complex.

8.3.1. Method

- **FE model and material properties**

The three-dimensional preliminary FE model comprises of three different parts: skeleton, plantar soft tissue and insole. Skeletons are generated based on approximated features of the foot anatomy. In order to simplify the model and facilitate time constraint, ligaments and plantar fascia were defined within soft tissue with bulk properties, and cartilage is defined within bony structure. Plantar soft tissue was extracted from the 3D scanned image and the whole FE model incorporated the nonlinearity of plantar soft tissue by adopting of a second order hyperelastic model. Solid skeletal and foot model were assembled in Autodesk Fusion360 with Boolean operation enable close contact of solid bone structure with soft tissue part. The assembly was then imported into ABAQUS for analysis.

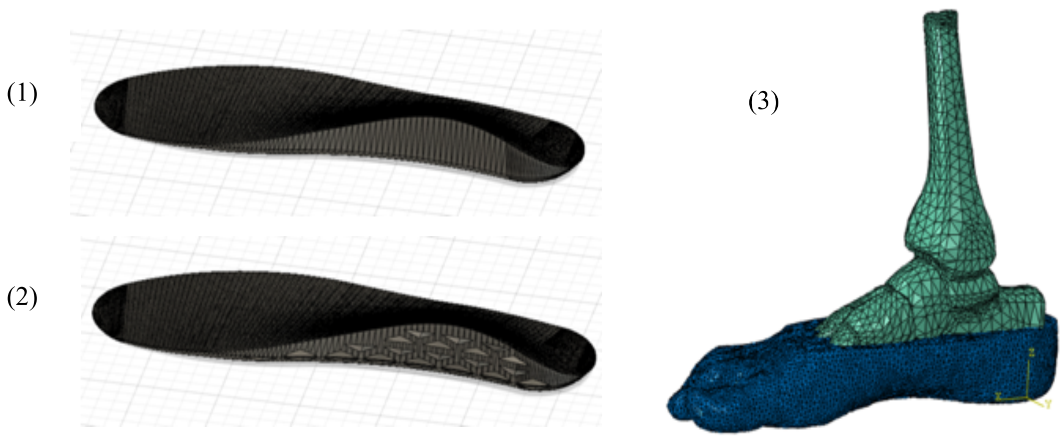

Figure 8.5. (1) Traditional solid insole (2) Our Honeycomb design (3) Entities and assembly of Foot FE models.

The material properties of skeletal model were applied as the elastic material with Young's Modulus of 10 GPa following Chen et al. (2003). The nonlinear material behavior of the plantar soft tissue was modelled by an isotropic, incompressible, hyperelastic second-order polynomial function proposed by Chen et al. (2009).

The nonlinear function describes plantar soft tissue stress-strain relation was achieved through *in vivo* ultrasound-combined study according to Lemmon et al. (1997). Insole was made by thermoelastic material with Shore A hardness 60. Shore A hardness is converted to bulk modulus and C_{10} is calculated by eq. [8.1] and [8.2] suggested by Kunz et al. (2006) and Shi et al. (2017).

$$E = \frac{1-\nu^2}{2 \cdot R \cdot C_3} \cdot \frac{C_1 + C_2 \cdot Sh_A}{100 - Sh_A} \cdot (2.6 - 0.02 \cdot Sh_A) \quad MPa \tag{8.1}$$

$$K_{Neo-Hookean} = \frac{4(\nu+1)C_{10}}{3(1-2\nu)} \; MPa \tag{8.2}$$

E is elastic Young's Modulus while K is material bulk modulus, and their relationship is as eq. [8.3]:

$$K = \frac{E}{3(1-2\nu)} \tag{8.3}$$

As the results shown in Table 8.3, Neo-Hookean with C_{10} hyperelastic model was 1.143 and Poisson ratio was 0.49. The constants R, C_1, C_2, C_3 are respectively 0.395 mm, 0.549 N, 0.07516 N, 0.025 mm as estimated in experimental tests of Kunz et al. (2006).

Table 8.3. Material properties for both designs of insole

Shore A Hardness	Poisson Ratio	Young's Modulus E	Bulk Modulus K	Neo-Hookean C_{10}
60	0.49	6.8122	113.537	1.143

The material of traditional solid and Honeycomb novel insoles are both elastomers and the hardness can be characterized from Shore 40 to 80 as shown in Figure 8.6. For the Shore 60 used in the FE model, Poisson Ratio ν = 0.49 was assumed. In industrial applications, different values of Poisson Ratio and its relationship of material strain are reported in different types of elastomers. Base on the strain to Poisson ratio curve shown in Figure 8.6, the material with appropriate hardness and Poisson Ratio values can be selected for specific insoles. The high strain materials may not be suitable for shock absorption and the low strain material may not be suitable for the movement correction purpose.

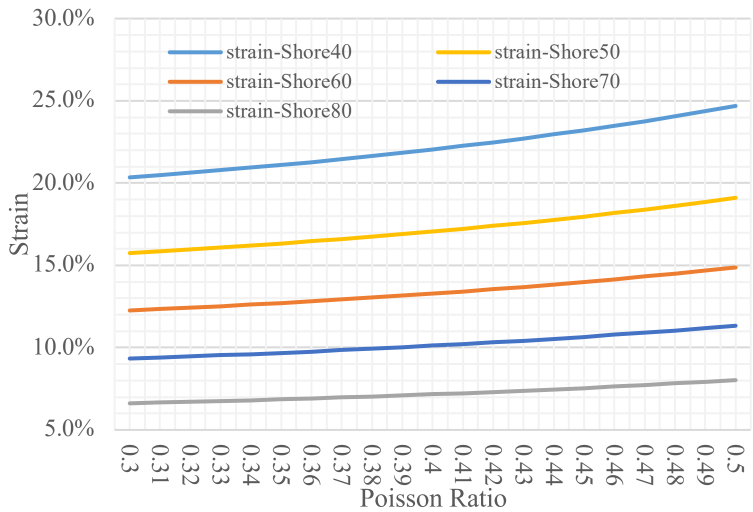

Figure 8.6. Relationship of Poisson ratio and strain

- **Meshing**

There are four basic meshing types for three-dimensional element— tetrahedron, pyramid, triangular prism, and hexahedron. Hexahedral meshing is generally more reliable and accurate than the others, with less computational cost especially when the structure undergoes the large deformation (Tadepadlli et al., 2011). However, processing hexahedron required substantial manual task in partitioning and defining parts of irregular shaped structure. Therefore, we decided to use tetrahedral element for the meshing our FE models.

Geometric order of the elements enables the quadratic elements to capture nonlinear and incompressible material in modelling soft tissue (Tadepadlli et al., 2011), which is significant for getting more accurate results. Both tetrahedral and hexahedral allow different modes, such as hybrid, reduced integrated and incompatible mode, to use different integrated formulations. As the element types shown in Table 8.4, linear tetrahedral C3D4 was used for skeletal model, and hybrid linear tetrahedral element C3D4H was used for soft tissue and Honeycomb insole due to their mechanical definitions of hyperelastic material. 8-node linear brick, hybrid, linear pressure, incompatible modes C3D8IH was used for solid insole, which may improve the performance in FEA process.

Table 8.4. Meshing properties of Foot FE models

Part	*Element type*	*No. of elements*	*No. of nodes*
Bone	C3D4 – 4-node linear tetrahedron	37337	8592
Soft tissue	C3D4H – 4-node linear tetrahedron, hybrid, linear pressure	387825	73498
Solid insole	C3D8IH – 8-node linear brick, hybrid, linear pressure, incompatible modes	18536	23720
Honeycomb insole	C3D4H – 4-node linear tetrahedron, hybrid, linear pressure	24053	6319

- **Interaction, Boundary and Loading conditions**

As there are three objects in an assembly (i.e. bone, soft tissue and insole), two 'contacts' were defined through the 'Interaction' function in Abaqus®. 'Contact' is the place where two objects have 'Interaction'. One contact is between bone and soft tissue and the other between the soft tissue and insole. Both interactions were defined as 'surface-to-surface' interaction with small sliding formulation in the system. 'Node-to-surface' interaction is not suitable in this case due to the potentially high deformation nature of the model. Hence, we assumed no friction between bone and soft tissue. As the friction coefficient for the contact of soft tissue and insole was set at 0.5, we define they are 'normal properties' using the non-linear softened penalty contact. The parts of bone and insole was assigned as 'master surfaces' because soft tissue acted as 'slave' in between the bone and insole.

The analysis was done in two conditions— bilateral standing barefooted and with the different insoles. A single vertical point load was applied to the specific point on midfoot bone structure by the equivalent load 350N – half of subject's body mass 70kg. For boundary condition of barefoot standing, we restricted the movement on plantar surface of soft tissue model with fixed 6 DOFs. For boundary condition of standing in insole, we restricted any movement at the bottom of insole. Furthermore, as we concerned about the geometry of Honeycomb could substantially affect the movement of foot, additional boundary conditions were added to restrict U1, U2, UR1, UR3 of a y-parallel line in bone model. Hence, the bone model can only move in Z-axis and rotate around the defined line. The defined line located in foot-ankle complex was to simulate the movement when foot contacts to insole in standing.

- **Material selection**

Stereolithography technique was selected for the customized insole because of its robustness and availability in producing high detailed parts. Therefore, material selection was based on data sheet provided by material manufacturer Stratasys. Once the correlations were identified, the desired properties were used as parameters to find the respective photopolymer that produces similar properties. The properties of interest are tensile strength and strain at failure and the desired parameters of each property were predefined or achieved by doing research on individuals' needs and conditions. Appropriate material on datasheet that matches the desired parameters is chosen for production. The process of selecting was done by Cambridge engineering selector (CES) by Granta (Granta Design Limited, 2017). FLX9730 was the selected material as the desired tensile strength was ranges from 3.0 to 4.5 Mpa and strain at failure was from 2 to 3.5 and the Shore A hardness was from 40 to 60 (Stratasys, 2017). The correlating properties in focus were tensile strength and strain at failure of material.

- **Building hyperelastic-elastic contact model**

A contact model between a hyperelastic part (i.e. soft tissue) and an elastic part (i.e. bone) was developed, Figure 8.7, bone model is the vertical spherical-ended cylinder and soft tissue encloses side and bottom surface of the bone. For the meshing setup, continuum linear hexahedral, reduced integrated element C3D8R is used for bone model and continuum, hybrid, linear hexahedral, incompatible mode element C3D8IH for soft tissue (Table 8.6). C3D8R was used for the bone rather than C3D4 (as we used it earlier) because the low requirement of computational resources and its rigid-like potential behavior. C3D8IH was selected as soft tissue instead of C3D4H (as we used it earlier) because its capacity of representing bending-like behavior of elements. Moreover, C3D8IH can avoid shear locking phenomenon may potentially yield inaccuracy. Therefore, C3D8IH was considered more suitable than C3D8RH or C3D8H in our model. The materials properties and interaction between the objects (i.e. bone, soft tissue and insole) remain the same as the FEA models. In hyperelastic-elastic contact model, a single point load was applied at the center of top surface on the bone model. As the model is to analyze the maximum internal stress in soft tissue in different radius of spherical ends, the boundary condition restricted all the displacement except for horizontal displacements (U1, U3) at the bottom surface of soft tissue.

Table 8.5. Meshing properties of hyperelastic-elastic contact model

Part	*Element type*

Bone representation	C3D8R – 8-node linear brick, reduced integration, hourglass control
Soft-tissue representation	C3D8IH – 8-node linear brick, hybrid, linear pressure, incompatible modes

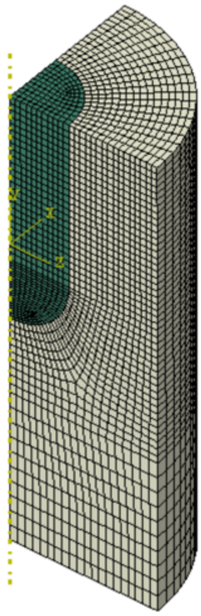

Figure 8.7. Hyperelastic-elastic contact model

Table 8.6. Material Properties for different model entities

Part	*Strain Energy function of Hyperelastic*	*Parameters*		*Value*
Soft Tissue (Chen et al., 2009).	$U = \sum_{i+j=1}^{N} C_{ij}(\bar{I}_1 - 3)^i(\bar{I}_2 - 3)^j + \sum_{i=1}^{N} \frac{1}{D_i}(J_{e1} - 1)^{2i}$ Where U is the strain potential energy; C_{ij}, N, D_i are material coefficients;	Order	N	2
		C_{ij} represents behavior of materials (N/mm^2)	C_{10}	0.08556
			C_{01}	-0.05841
			C_{20}	0.03900
			C_{11}	-0.02319
			C_{02}	0.00851
		D_i represents compressibility (mm^2/N^-)	D_1	3.65273
			D_2	0

	$\overline{I_1}$ and $\overline{I_2}$ are measurements of material distortion; J_{e1} is elastic volume ratio			
Insole	$U = C_{10}(I_c - 3)$ Neo-Hookean hyperelastic model for incompressible materials	Order C_{ij} D_i Poisson Ratio	N C_{10} D_1 N	1 1.142987 0 0.49
	Material properties for Elastic			
Bone		Young's modulus (Mpa) Poisson Ratio	E ν	10E6 0.3

8.3.2. Result

- **Barefoot bilateral standing**

In figure 8.8, the plantar pressure distribution on soft tissue and the internal stress of the joints in barefoot bilateral standing were shown. The peak plantar pressure is 0.155 MPa in heel region and the highest internal stress was 0.187 MPa at the ankle. Taha et al. as to Wafai et al. (2015), Cheung et al. (2005) and Natali et al. (2010) reported the plantar pressure in vivo experiment measured by the in-shoe sensor and 0.23 MPa is the highest plantar pressure at 'foot strike' in heel region. The second highest plantar pressure was found in metatarsal (Wafai et al., 2015; Cheung et al., 2005; Natali et al., 2010). Taha et al. (2016) used the similar FE method that incorporated foot skeletal and soft tissue to the model reported the high agreement of peak pressure 0.160 MPa with current study.

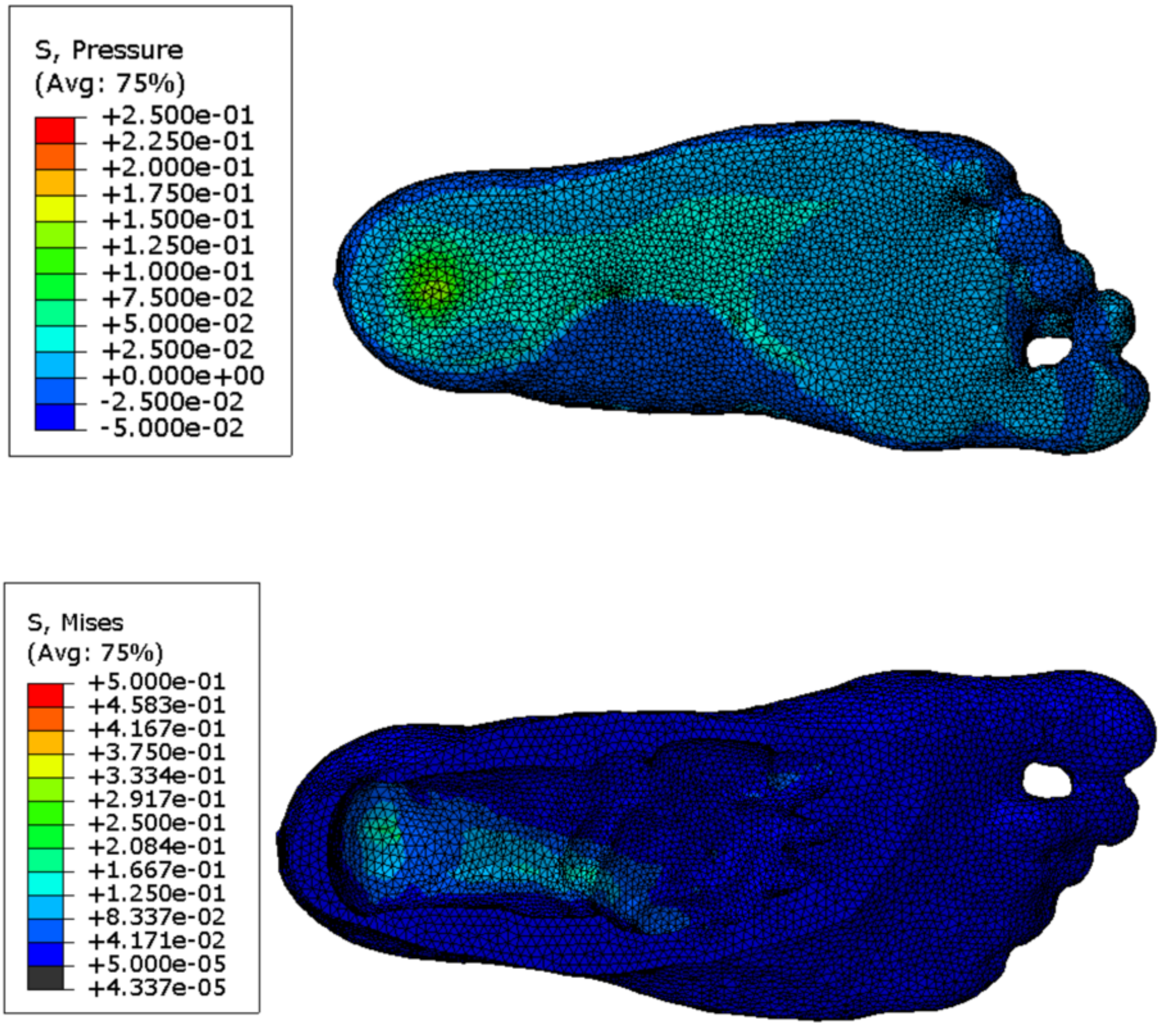

Figure 8.8. Plantar pressure distribution (top) and internal stress (bottom) of barefoot bilateral standing

- **Traditional solid insole and Honeycomb novel insole**

As shown in figure 8.9, the peak plantar pressure was 0.156 MPa and 0.141 MPa for solid and honeycomb insole, respectively. Honeycomb insole has reduced 9.6% of peak pressure from solid insole and the peak pressure was found at different locations. Peak pressure was found in the middle heel when solid insole was applied while peak pressure occurred on the medial side of rearfoot when honeycomb was applied. In the comparison of figure 8.8 and 8.9, solid insole greatly reduced both the peak and average plantar pressure. The place where the peak pressure is found is similar between barefoot and solid insole, which explains the solid insole provide shock absorption to the foot and attenuates the impact to the foot in weightbearing. As shown in Figure 8.9 (right), the peak pressure shifted anteriorly and medially when Honeycomb was applied. The heel region where the peak pressure was found in solid insole has reduced to 0.0119 MPa after honeycomb insole was applied. It should be also noted that higher pressure was found along with foot axis in solid insole, and it shifted medially toward the medial longitudinal arch after honeycomb insole was applied. The range (i.e. from the lowest to the greatest) of pressure distribution has reduced means the pressure is more evenly distributed to the whole plantar area when honeycomb insole was applied.

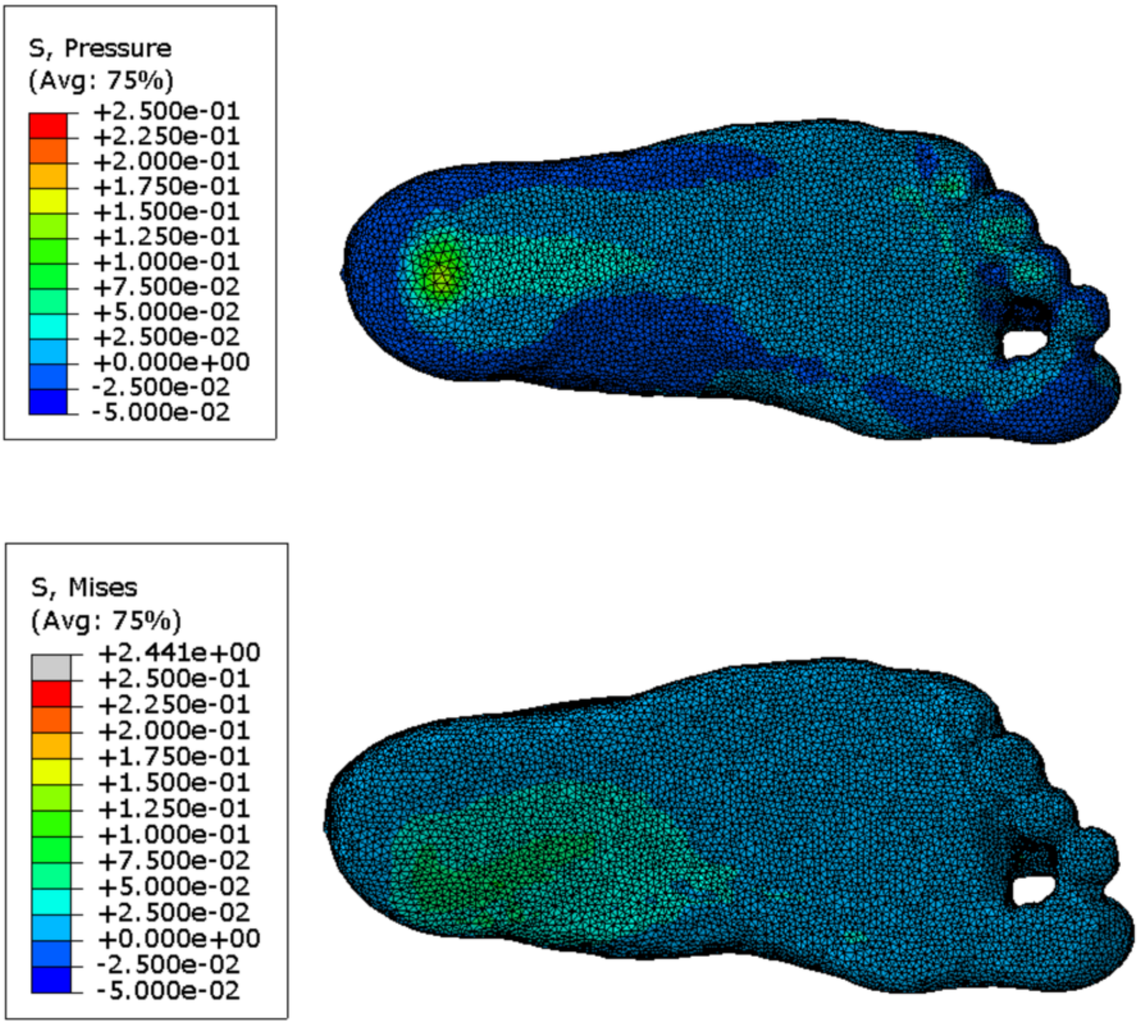

Figure 8.9. Plantar pressure distribution from the case of solid insole (top) and Honeycomb insole (bottom)

As shown in Figure 8.10, the internal stress was compared between solid insole and honeycomb insole. The peak stress was found at the middle of ankle joint for 0.387MPa when solid insole was applied while it substantially reduced 36.8% to 0.244 MPa when the honeycomb insole was applied. The peak stress shifted anteriorly toward midfoot and was found on the articulation of talar and navicular bone. The variance of internal stress distribution was found smaller in Honeycomb insole compared to solid insole. It indicates

Honeycomb novel insole was more evenly distributed the internal stress to foot and ankle complex. As the simulation outcome, Honeycomb insole reduced the peak and average internal stress may attenuate the excessive mechanical load and shock absorption.

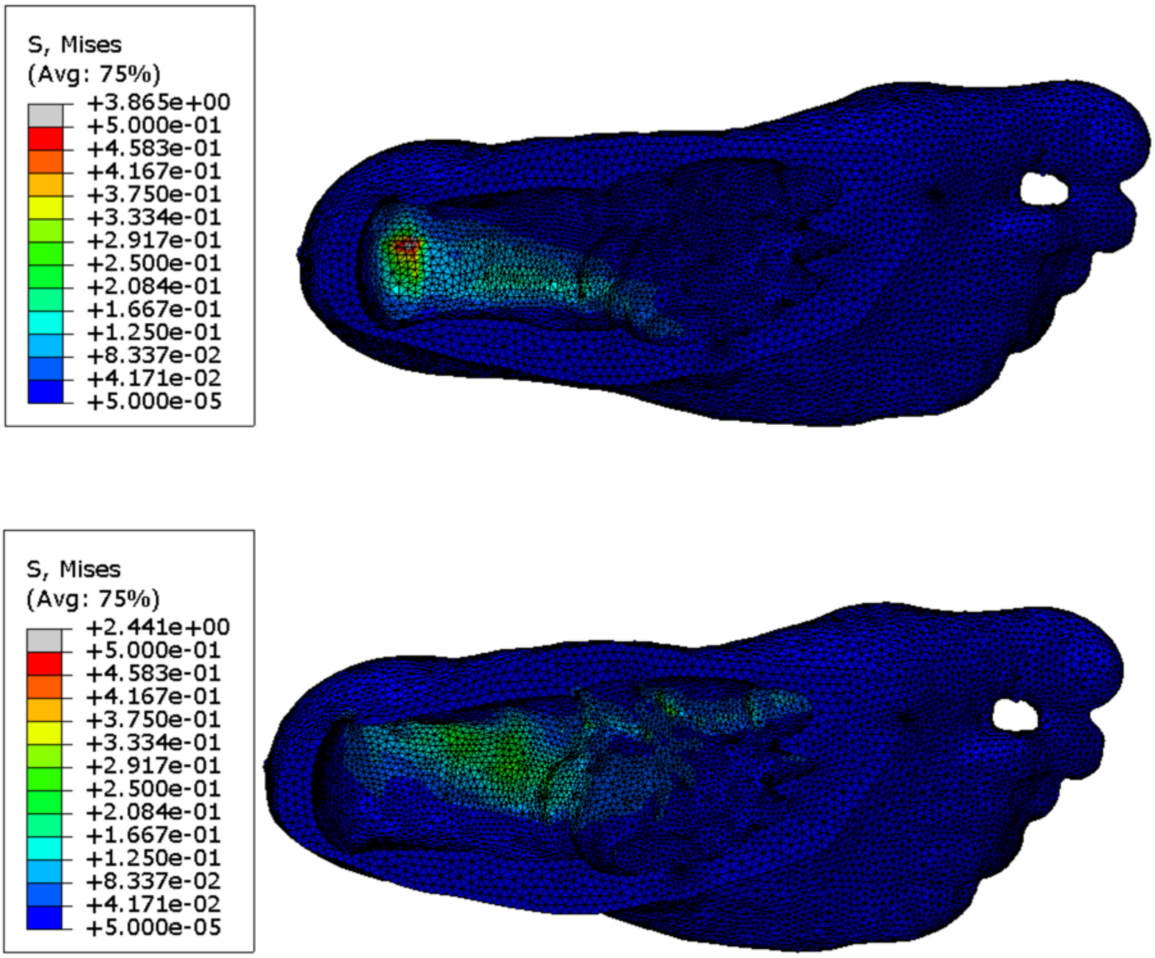

Figure 8.10. Internal stress of joints from the case of solid insole (top) and honeycomb insole (bottom)

- **Hyperelastic-elastic contact model**

As the hyperelastic-elastic contact model was created as Figure 8.7, Hertz's contact theory was used to predict the location of peak stress, contact pressure and pressure distribution in an elastic material. Moreover, the contact mechanics of elastic materials can be also verified by Hertz's contact theory. The contact stress based on different radius of the model (spherical cylinder) and the external force was calculated through eq. [8.4]. The values of internal stresses are assumed as a linear polynomial function of radius (x) and force (y). Force is range from 10 to 30 N and radius is from 10 to 30 mm.

$$f(x,y) = C_{00} + C_{10}x + C_{01}y + C_{20}x^2 + C_{11}xy + C_{02}y^2 + C_{30}x^3 + C_{21}x^2y + C_{12}xy^2 + C_{03}y^3 + C_{40}x^4 + C_{31}x^3y + C_{22}x^2y^2 + C_{13}xy^3 + C_{04}y^4 \qquad [8.4]$$

The values of coefficients are displayed as following.

C_{00} = 0.09943 C_{10} = -0.07338 C_{01} = 0.03853 C_{20} = 0.043

C_{11} = -0.02821 C_{02} = 0.001498 C_{30} = -0.02305 C_{21} = 0.02312

C_{12} = -0.002227 C_{03} = 0.0008955 C_{40} = 0.0098 C_{31} = -0.00755

C_{22} = -0.002653 C_{13} = 0.001006 C_{04} = 0.0008632

As shown in Table 8.7, the maximum internal stress of the model is displayed based on different radius of the model and external force. According to the maximum stress, the fit surface of maximum stress, radius and force of hyperelastic-elastic contact model is drawn as Figure 8.11. The fit surface was used to estimate the local internal stress when different loads applied on different places of tissue. The hyperelastic-elastic contact model was used to simplifies the process of simulating the internal stress between bone and soft tissue, which enable us to accelerate the process of simulating the internal stress for the given bone structure.

Table 8.7. Maximum internal stress (MPa) when different radius and force applied to hyperelastic-elastic model

		Force (N)				
Radius (mm)		10	15	20	25	30
	10	0.1898	0.2863	0.3816	0.4754	0.5768
	15	0.0956	0.1379	0.1747	0.2330	0.2782
	20	0.0527	0.0606	0.1064	0.1327	0.1588
	25	0.0309	0.0464	0.0627	0.0803	0.0992
	30	0.0084	0.0387	0.0549	0.0662	0.0820

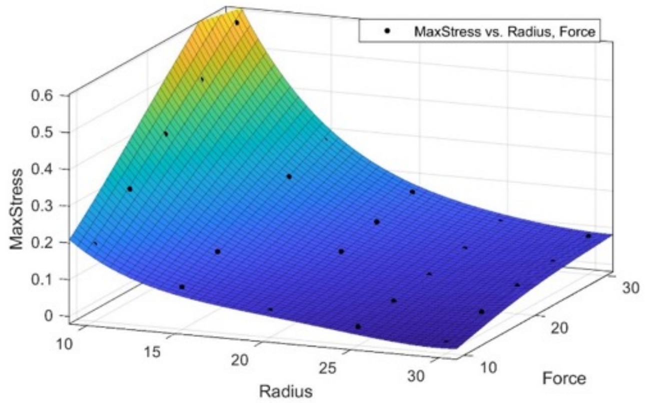

Figure 8.11. Fit surface of maximum stress, radius and force of hyperelastic-elastic contact model

8.3.3. Discussion

Similar FEA finding was reported by Antunes et al. (2008) during barefoot bilateral standing as the peak joint's stress and plantar contact pressure was found on anterior aspect of talus and posterior calcaneus, respectively. The increase of peak pressure may reduce the comfort level (Antunes et al., 2008). Khodaei et al. (2017) measured plantar pressure on flatfoot subjects by PEDAR® system. The peak pressure is 0.22MPa and 0.18MPa at heel region for no insole and with EVA insole (with shore 40) respectively, which is slightly higher than our no insole (0.155MPa) solid insole (0.156 MPa) and Honeycomb insole (0.141 MPa) FEA result. The plantar contact pressure can be also influenced by the height of arch support as Peng et al. (2021) found the higher arch support increased the plantar contact pressures on the medial midfoot region. Therefore, the excessive high arch support may increase discomfort under repeated loading, that need to be avoided in insole design (Su et al., 2017).

8.4. Mechanical performance test of Gyroid (Schwarz P)

Schwarz P, D and G are three members of the unique non-trivial embedded family (Figure 8.12) and their 3D printed viscoelastic/hyperelastic structure performs elastic energy absorption and return when the external force is applied. In order to characterize the properties of Schwarz's structure, the uniaxial tensile and compression test was simulated through FE model on a unit (i.e. 30x30x30 mm^3) cube. The quasi-static problem of virtual uniaxial testing can be modelled using either Implicit or Explicit Solver in ABAQUS®. Explicit Solver normally performs better computational efficiency than Implicit Solver, but it requires more assumptions of unknown to deliver a reliable outcome. Therefore, Implicit Solver was selected to carry out the virtual uniaxial testing. Compared to the structure of

Schwarz D and G, Schwarz P is more symmetric and repetitive in a unit cell. Therefore, Schwarz P for mechanical performance simulation was selected as the iso-stress and iso-strain was assumed in the unit structure.

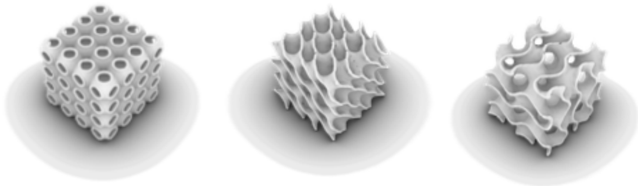

Figure 8.12. Schwarz P (left); Schwarz D (middle); Schwarz G (i.e. Gyroid) (right) (Rossi & Buratti, 2017)

8.4.1. Method

- **Define the geometry**

An arbitrary RUC of Schwarz P was used, and the dimension of a unit cube is 30x30x30 mm^3, which contains 27-unit cells. A unit cell was 10x10x10 mm^3 with 2 mm thickness (Figure 8.13). Theoretically, by analyzing a single unit cell can deliver its distinctive structural characteristic. However, the smaller structure may be stiffer than its real property when boundary condition and contact is applied. Therefore, 27 repetitive unit cells (RUC) were used as a unit cube for the simulation to address this issue. Thus, the more realistic results can be reported once the stiffening factors were minimized.

- **Material property**

For material properties, Odgen hyperelastic strain energy function with N = 2 was used to numerically describe the fundamental behaviors of Schwarz P. Odgen energy (U) was obtained as eq. [8.5].

$$U = \sum_{i=1}^{N} \frac{2\mu_i}{\alpha_i^2}\left(\bar{\lambda}_1^{\alpha_i} + \bar{\lambda}_2^{\alpha_i} + \bar{\lambda}_3^{\alpha_i}\right) + \sum_{i=1}^{N} \frac{1}{D}\left(J_{el} - 1\right)^{2i} \qquad [8.5]$$

Where $\bar{\lambda}_i = J^{-\frac{1}{3}}\lambda_i$ and constants μ and α are responsible for shear behavior whereas D describes compressibility. As shown in Table 8.8, the material parameters for N = 1 and 2, are displayed. The uniaxial stress and strain were analyzed when shore A hardness was 40.

Table 8.8. Material parameters for Odgen model when N = 2

i	μ_i	α_i	D_i	error

1	7.553624461E-03	4.83950201	0	0.4371
2	0.548562283	-4.73537875	0	

- **Meshing**

The geometry of Schwarz P cube was presented as adaptive triangular facets in Abaqus® as the native the unit cells. Tetrahedral mesh with free meshing control was selected as the better option than hexahedral meshing (Figure 8.13). According to the material properties of hyperelastic, hybrid linear tetrahedral element C3D4H was used to reduce the computational cost. Element count was 113419 elements for Schwarz P cube.

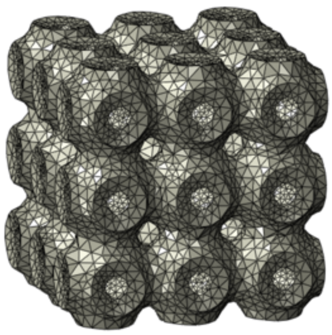

Figure 8.13. Tetrahedral mesh was applied for Schwarz P cube

- **Interaction**

The plates at the top and bottom of the specimen were created to simulate the uniaxial tensile and compression (Figure 8.14). The 'contact' between specimen and plates was set 'tied constraint' for saving the processing time. During uniaxial compression simulation, the self-contact was found between internal and external surfaces as shown in Figure 8.15. The interaction property of self-contact was set as 'tangentially frictionless'.

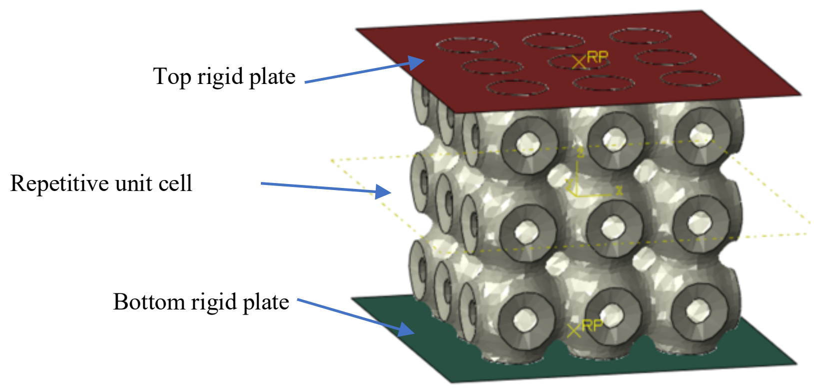

Figure 8.14. Two rigid plates were added at the top and bottom of Schwarz P cube for uniaxial tensile and compression simulation

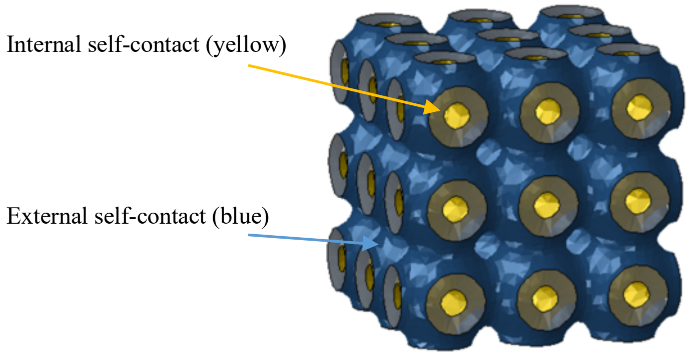

Figure 8.15. Internal and external self-contact were found during compression

- **Loading conditions**

The uniaxial loading conditions were applied on the reference points for controlling the rigid plates. The bottom plate was set as 'constrain' in all degrees of freedom in both tensile and compression simulation. The top plate was limited to displace vertically on z-axis. Accordingly, the loads were applied on the top plate along with z-axis.

- **Multiscale approach**

One of the novel insoles was designed with open cell Schwarz P substructure with external geometries previously in Chapter 7 (figure 8.16). For simulating the high complexity of the substructure, it can be extremely time consuming and not efficiently use of computational work. Multiscale modelling approach has been established in used extensively in composite sectors to improve the efficiency of simulation. Firstly, the behavior of a unit cell of Schwarz P obtained from previous procedure was applied to the whole insole model. The properties were mapped to the solid external geometry of the insole as shown in Figure 8.16. Moreover, the results of multiscale approach should be in the acceptable margin of errors as it has simplified the process of the full-scale modelling.

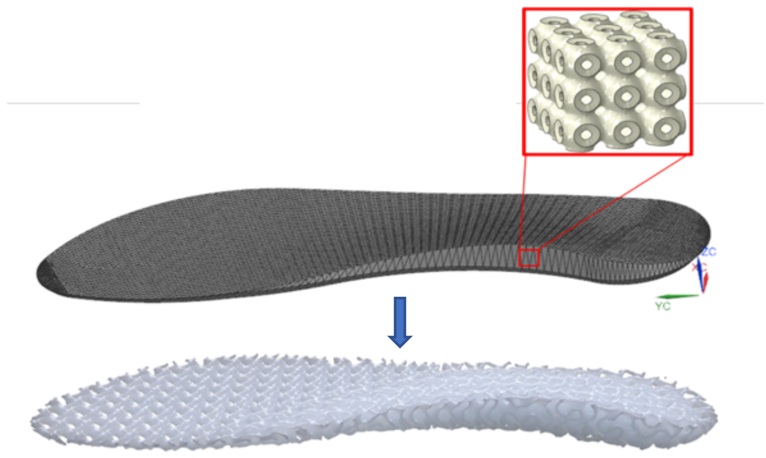

Figure 8.16. Multiscale approach was used to apply the property of a Schwarz P cube to the entire insole

8.4.2. Results and discussion

- **RUC of Schwarz P**

As shown in Figure 8.17, the relationship of stress and strain of Schwarz P cube during compression and tensile test is presented. When the strain level was lower than -0.5, the slope of stress/strain significantly increases showing Schwarz P cube has the linear behavior in this range. Schwarz P cube has the non-linear elastic behavior when the strain level is above -0.5 as the slope has decreased. In compression process, the response of the RUC can be divided in three phases of deformation— linear elastic, plateau, and densification. However, the transition from the linear elastic to plateau is hard to recognized in our case (Figure 8.17).

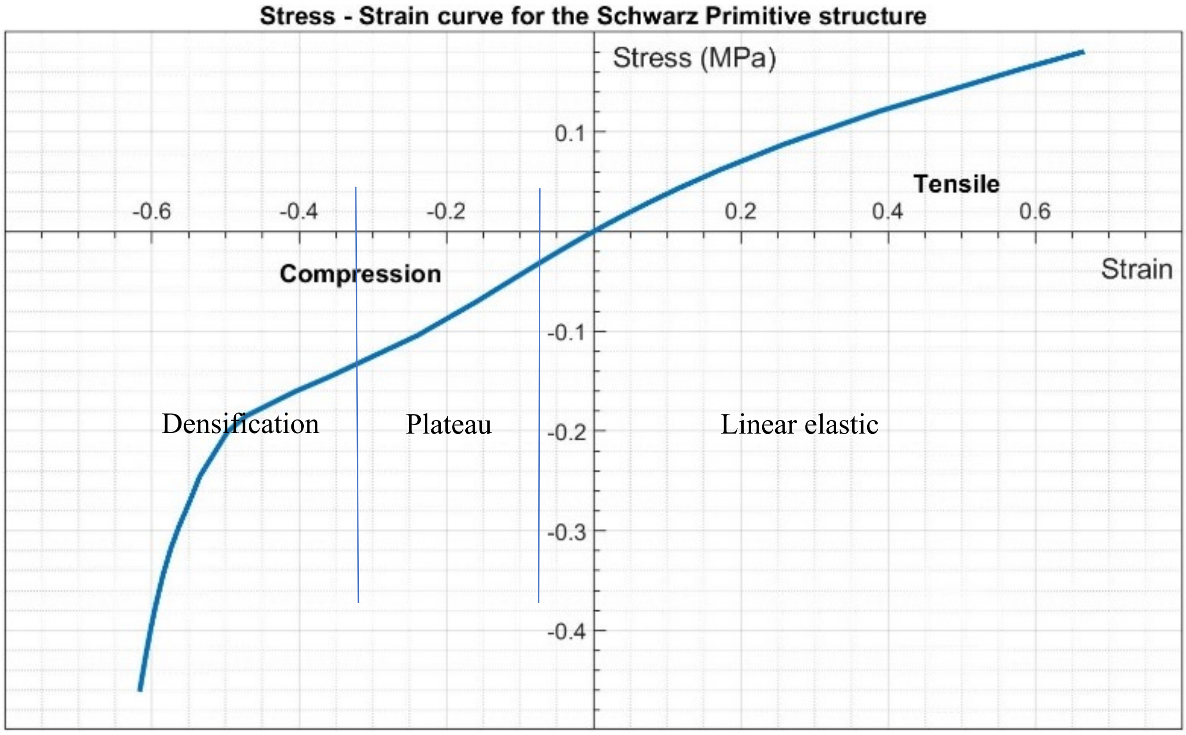

Densification	Plateau/Linear elastic	Tensile
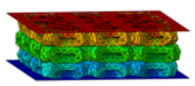	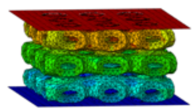	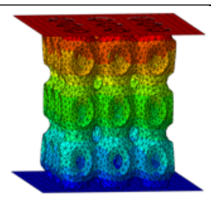

Figure 8.17. Strain stress curve and the structural behaviour of Schwarz P cube under uniaxial compression and tensile loading

As shown in Figure 8.18, the energy absorption of Schwarz P cube is presented by the relationship between stress and energy per unit. As our novel insole aims to mimic the function of foot arch to have the ability of energy absorption and return in gait, Schwarz P cube could be the most suitable material. The energy absorption capacity of Schwarz P drastically declines in densification phase and the shoulder point occurs at $5x10^{-2}$ mJ/mm^3 (Figure 8.18). The shoulder point is the reference to indicate the absorption capacity of the material as the higher the shoulder point, the better the absorption capacity.

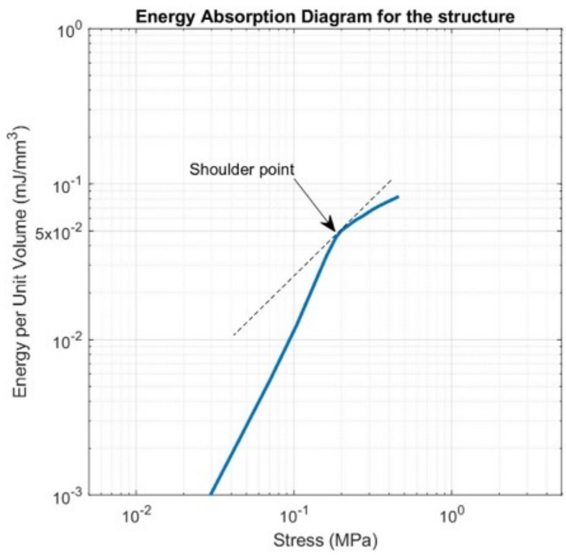

Figure 8.18. Energy absorption capacity of the structure

- **Schwarz P Insole**

As shown in Figure 8.19, the peak plantar pressure was 0.076 MPa at the heel region and the peak internal stress was 0.325 MPa located at midfoot region. The peak pressure of barefoot, solid and honeycomb insole are 0.155, 0.156 and 0.141 MPa respectively. Moreover, the overall pressure is distributed more evenly as the range of variance is smaller for Schwarz P insole. The peak internal stress was found lower than solid insole (0.387 MPa) but higher than honeycomb insole (0.244 MPa). The highest internal stress was reported 0.225MPa if we neglect the highest value, which is slightly lower than honeycomb insole. The range of variance was also more evenly distributed compared to the other insoles. The resultant stress from contact between skeletal loading and soft tissue ranged from 0.05 MPa to 0.15 MPa. We would point out that multiscale approach was used to apply the property of the Schwarz P cube to the entire insole to improve the efficiency of processing FEA.

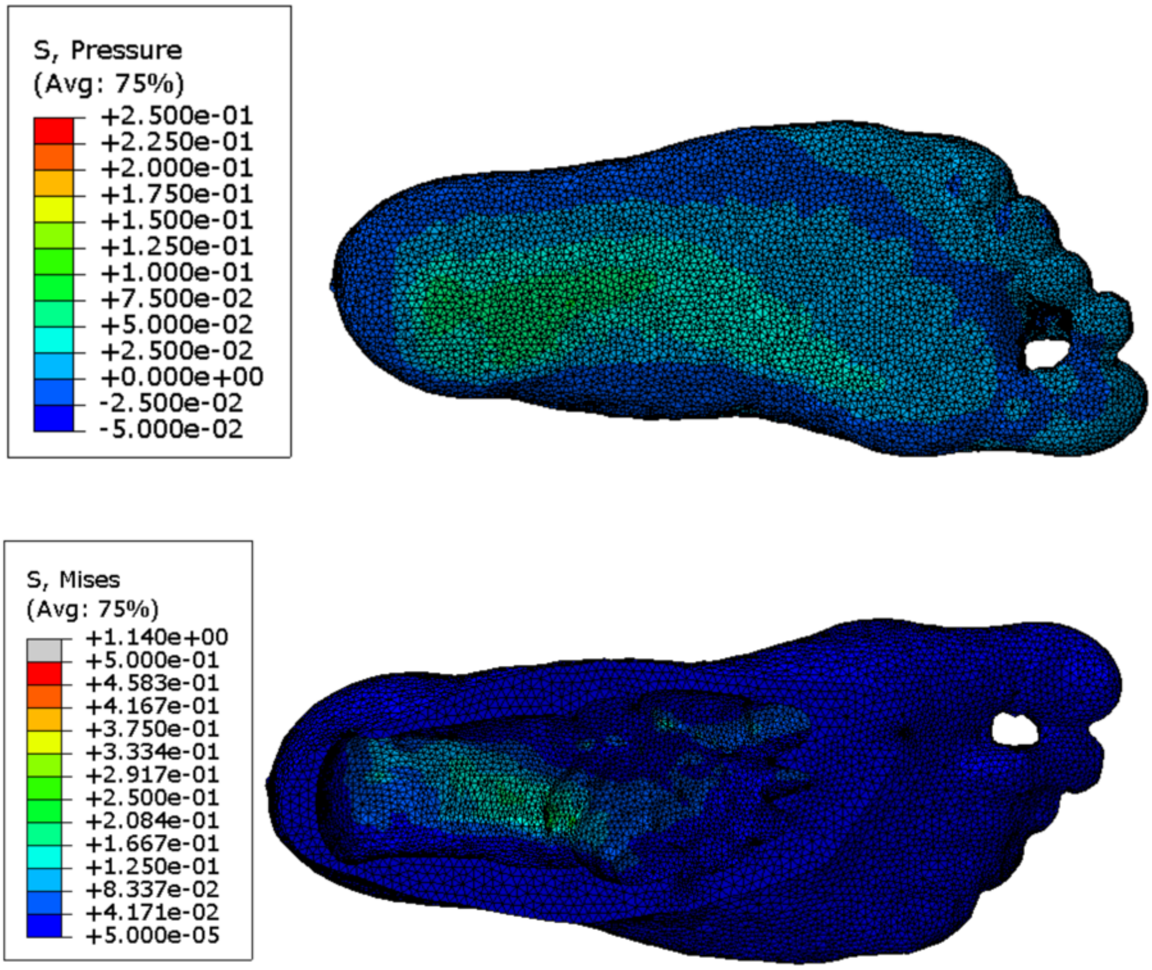

Figure 8.19. The pressure distribution of plantar surface (top) and internal skeletal stress (bottom)

Table 8.9. The peak plantar pressure and joint stress for different insoles.

	Peak plantar pressure (MPa)	**Peak joint stress (MPa)**
No insole	0.147	0.187
Solid insole	0.156	0.387
Honeycomb insole	0.141	0.244
Gyroid insole	0.076	0.225

8.5. Conclusion

The plantar pressure and internal stress at four different conditions— no insole, solid, Honeycomb novel and Gyroid novel insoles, were simulated in bilateral standing position through FEA. A comparison between the solid and Honeycomb insoles shows that Honeycomb reduces the peak plantar pressure and internal stress by 9.6% and 36%

respectively. The variance of the plantar pressure and internal stress was also smaller when honeycomb insole was modelled. The results indicate honeycomb insole has better performance in terms of shock absorption and distribution of plantar pressure and internal joint stress throughout the and ankle. Although traditional solid insole reduces the plantar pressure compared to barefoot, it drastically increases the peak internal stress. Excessive internal stress may cause adverse effect on the foot's tissue (Su et al., 2017). The peak plantar pressure of Gyroid insole was found lowest at 0.076 MPa. However, higher internal stress was found in Gyroid insole compared to Honeycomb novel insole. Therefore, it can be concluded that Honeycomb novel insole displayed the best performance from material point of view. FEA is the powerful tool to investigate the foot mechanical behavior and its implications to perceptive foot comfort. Chapter 8 has shown the novel insoles have reduced the overall plantar pressure and joint's stress compared to solid insoles, which may result in comfort enhancement. FEA result shall serve as a reference for further comfort evaluation directly from the participant as the comfort questionnaire was done by three participants in Chapter 9. As FEA results may not provide full insight on how insole change the foot motion in the better way, detailed motion analysis was conducted to investigate these dynamic affects as outlined in the next chapter.

Chapter 9: Foot and ankle motion analysis

9.1. Introduction

The purpose of the work overall is to develop a Honeycomb insole that not only supports the fallen arch but also facilitates normal foot motion during walking, i.e. compression and recoil of the foot arch. In this chapter, the motion capture system was employed to investigate the kinematic of foot and ankle when different orthoses were applied. A pilot test was carried out to properly set up laboratory environment and to minimize the potential errors that may affect the result. For the motion analysis, the low arched participants were tested in three different conditions— no insole, customized solid insole, Honeycomb insole.

9.2. Method

9.2.1. Participant

As reported in Chapter 4 the NNHt (normalized navicular height truncated) thresholds for low arch is < 0.169 for right foot and < 0.167 for left foot. NNHt is NH (navicular height) divided by tFL (truncated foot length). In Chapter 4, we used foot scanning to obtain the NNHt but for practical purposes and in the absence of a scan, a manual approach could be adopted that involves the following steps.

- Navicular Height Measurement

The participant is asked to stand in shoulder width on a solid ground and to distribute the body weight equally to both feet. Find the medial malleolus at the most prominent bone on the medial side of the ankle. The navicular tuberosity can be palpated 2-3cm anteriorly and inferiorly from the medial malleolus. Mark the navicular tuberosity and use the steel ruler to measure the vertical height of navicular from ground. Then, the participant was asked to relax, and move around. The same measurement was repeated three times to take the average NH value.

- Truncated Foot Length Measurement

Truncated foot length (tFL) is the horizontal distance from the tip of the heel to the first MPJ (metatarsophalangeal joints). The first MPJ can be found at the medial side of the foot on the between the first phalange and first metatarsal. Draw the foot contour on a paper and mark the first MPJ and heel. Draw the foot axis from the heel and the tip of the second toe. Draw a line perpendicular to the foot axis and first MPJ and another line perpendicular to the foot axis and through the heel. Therefore, tFL is the distance between these two lines. Once the

measurement is done, the participant is asked to relax and move around. It is recommended that measurement is repeated three times and the average tFL value was record.
Three low arch participants were selected after NNHt values (Table 9.1) were measured respectively according to the threshold (NNHt is < 0.177 for the right foot and < 0.175 for the left foot) proposed in Chapter 4. Participant 1 is a male, age of 28, 200 cm in height and 115kg in body mass. Participant 2 is a male, age of 26, 188cm in height and 88kg body mass. Participant 3 is a male, age of 35, 173 in height and 68 in body mass. All participants had no leg injury, operations, or other medical condition such as osteoarthritis within the last six months. Participants were asked to not participate no moderate or vigorously intense physical activity, e.g. running, jogging, dancing, any sports activity, etc., prior to the test. They were briefed about the purpose of the study and potential risks and signed the consent statements.

Table 9.1. The value of NH, tFL and NNHt of the participants

Participant	Foot	NH (mm)	tFL (mm)	NNHt
1	Right	37	242	0.152
	Left	39	245	0.159
2	Right	32	226	0.141
	Left	25	231	0.108
3	Right	25	200	0.125
	Left	23	200	0.115

9.2.2. Insole design

- **Capture foot shape**

The traditional method— foot foam impression, was used to capture the foot shapes of the participants as there was no foot scanner available in University of Vienna (Figure 9.1). The procedure is as following.
(1) Participants were asked to sit on a chair with knee bending 90 degrees. Tester was facing the participant and placed the foam impression under the foot without placing the weight on it.
(2) The tester puts the thumb on participant’s medial malleolus and the index finger on the lateral malleolus. Move the fingers anteriorly and inferiorly 2 to 3 cm. Until the next prominent bone is touched, the medial head of talus bone is on tester’s thumb and lateral head

of talus bone is on the index finger. By turning the talus bone, the foot can be everted or inverted. The tester should find the talus neutral position when the calcaneus bone is aligned with the lower leg from the posterior view of the foot.
(3) The plantar fascia was tightened up, so the curve of the foot arch is present. Participant should apply the weight on the heel and push it into the foam impression.
(4) Participant was then standing up and with heel fully pushed into the impression box. He was then asked to step forward with the other leg and walk through the box by maintaining the hallux dorsiflexion.
(5) The same procedure was repeated to capture the foot shape of the other foot.

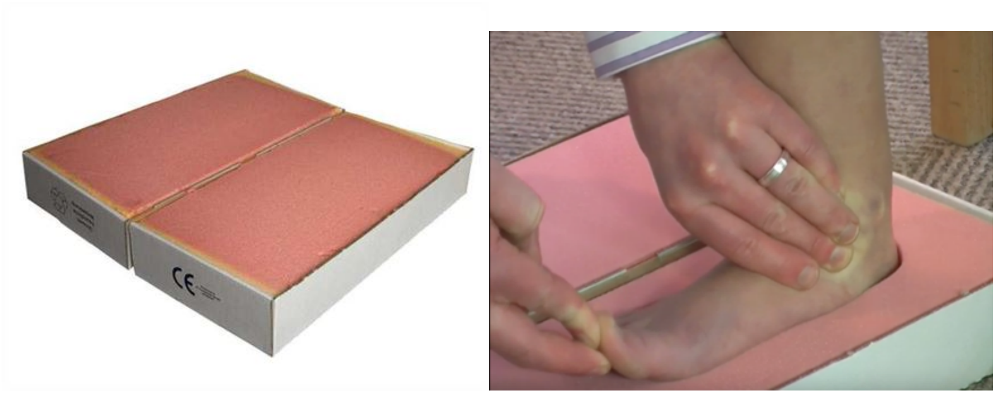

Figure 9.1. The traditional method—foam impression was used for capturing the foot shape.

- **3D foot model and insole design**

Once the foot shape of the participants was captured in University of Vienna, the foam boxes were shipped to RMIT University, Melbourne for insole customization including 3D scanning, CAD design, prototyping and additive manufacturing (AM). Infoot® scanner was used to scan the foot impression and CAD design software (i.e. Fusion 360, 3D experience) was used to reconstruct the original foot shape in 3D image (figure 9.2). However, as the CAD software failed to recognize the scanned foam impression as a solid object in the system, the 3D image of foot model cannot be reconstructed by this method. Alternatively, we decided to use the traditional method created the plaster foot model from foot impression for scanning and the procedure is outlined below.
(1) Plaster liquid needs to be prepared for building the model. A 10L disposable container was used to accommodate the amount of mixture in the ratio of 2:1 for plaster to water. Put one cup of water into the container first and put two cups of plaster powder. Spread the plaster powder to cover all the area and use the stick to disperse the powder into water and remove any air bubble. Stir with the stick to mix the water and powder until the bubble become smaller and disappear. Repeat the previous steps until the container is full.

(2) Pour the plaster liquid into each foam impression box until it covers the top of the foam. Place them at indoor and wait 12 hours for the plaster liquid to become solid model.
(3) Remove all the foam surrounds the plaster model by using the brush. Remove all the foam carefully without damage the plaster. The final plaster foot models were shown as figure 9.3. The plaster foot models were scanned by Infoot® scanner to create the 3D foot image of the participants.
Once the 3D foot model was completed, the same methods as in 7.3 and 7.4 — parametric modelling, Honeycomb insole design and additive manufacturing, were applied to customize a pair of solid and Honeycomb insole for each participant (Figure 9.4). Both solid and Honeycomb insole (figure 4) was produced by J750 PloyJet printer (Stratasys Ltd., US). Two AM materials— Agilus30 FLX935 and Vero, were used to produce a Shore 60A, rubber-like material for solid and Honeycomb insole. Once the insoles were completed, they were shipped to University of Vienna for motion experiment.

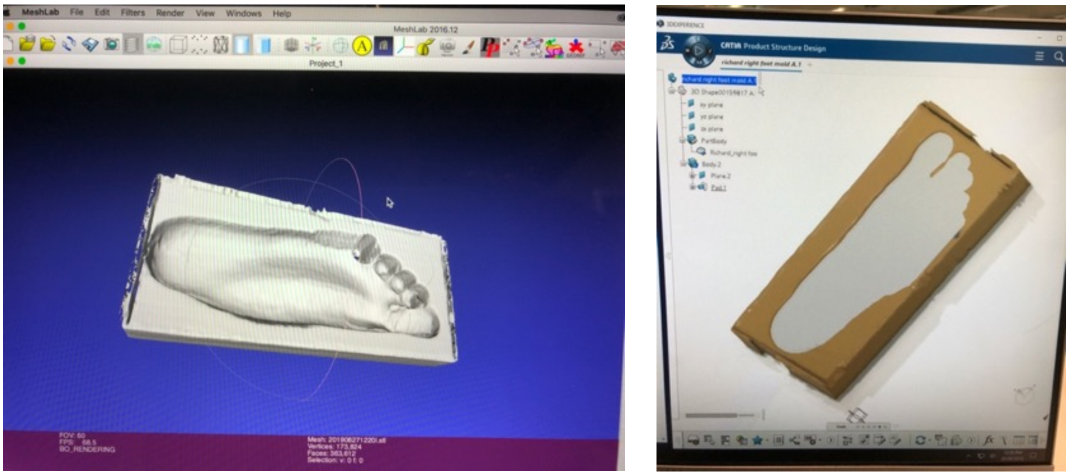

Figure 9.2. Foot impression of the foam box used scanned (left). CAD software was used to create a foot model from the scanned negative foot contour (right).

Figure 9.3. Building plaster foot model using foot impression of foam box.

Figure 9.4. The participants were given a pair of solid and Honeycomb insoles

9.2.3. Motion analysis system setup

Vicon® motion capture system in University of Vienna was employed to analyse the customized orthoses for low-arched participants. Twelve high speed cameras— Vicon Vantage (model V16), were used and the specification is shown as in Table 9.1.1. Eight cameras hanged on the ceiling (3 meters from the ground) and four cameras were set up on the ground with the stand (1.5 meters height from the ground). As shown in Figure 9.5, the grey circles are the cameras on the ceiling and the red triangles are the cameras on the ground. The distance between the grey circle cameras is approximate 4 meters on the long side of big, dark grey rectangle and 3 meters on the shorter side. The red triangle, the standing cameras were place in middle of two ceiling, grey cameras. The white rectangle is the 7 meters walkway and the orange rectangle in the middle represents the force plates.

Table 9.1.1. The specification of Vicon camera

	Vicon Vantage
Model	V8
Resolution (MP)	8
Max Frame Rate (Hz)	260 @ 8MP
Max Frame Rate (Hz)	2000 @ 1MP 1000 @ 2MP
On-Board Marker Processing	Yes
Standard Lens	18 mm
Wide Lens	12.5 mm
Minimum Standard FOV (H x V)°	61.4 x 47
Minimum Wide FOV (H x V)°	47.3

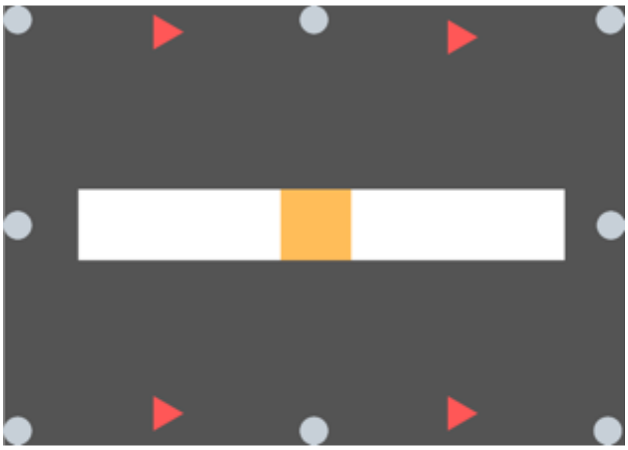

Figure 9.5. The motion capture laboratory setup. Red triangle: cameras on the ground. Grey circle: cameras on the ceiling. White rectangle: walkway. Orange square: force plates

- **Camera calibration**

. The cameras on the ceiling were used to record the gait throughout the walkway so we zoomed out the lens to get the wider picture of the gait. The standing cameras were used to capture those markers in a more horizontal perspective, which is to focus on the 26 markers on the feet. As shown in figure 9.6, the calibration wand was used for the camera calibration in Nexus system (software system of Vicon®). The calibration wand is a T bar with five lights as the markers need to be detected by the cameras. The calibration is as following procedures.

- Strat the software Nexus and click “go live” and click “start calibration”.
- Turn on the wand so the red light on the wand is shown and wave the wand in the workspace until every camera finish the calibration (The display on every camera has the circular block to show the progress of the calibration).
- Once the camera calibration is done, put the calibration wand in the middle of the workspace on the force plate. Click “set the volume origin” on Nexus system to define the origin point and axis on the Nexus coordination system. As shown in Figure 9.5, +X direction is toward the right, +Y direction is toward the top, +Z direction is toward the ceiling in the lab.

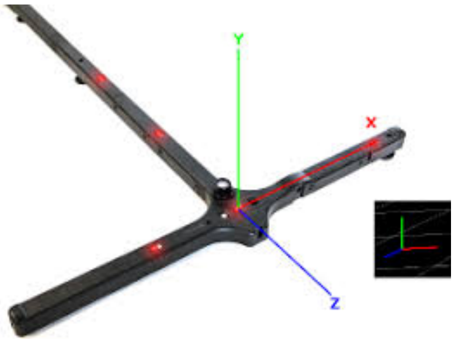

Figure 9.6. The calibration wand was used to calibrate the cameras and the origin

- **Anthropometric measurements**

The indices of upper extremities were not taken because we only focused on lower extremities and foot/ankle in the following experiments. As shown in Table 9.3, the anthropometric indices include body mass, height, inter ASIS distance, leg length, ASIS-trochanter distance, knee width, ankle width, tibial torsion (only needed if using a knee align device), sole thickness delta (only needed if testing the footwear or insoles). The sole thickness delta subject measurement is used if the subject wears the high-heeled footwear or shoe insoles that create a vertical distance between the heel and big toe. In this case, the vertical distance between toe and heel needs to be measured. All the anthropometric measurement were obtained by digital calliper and body tape measure.

Table 9.3. The lists and the description of anthropometric indices of conventional gait analysis

Name	**Description**	**Measure Left**	**Measure Right**
Body Mass	Patient mass.	_____kg	
Height	Patient height.	_____ mm	
Inter ASIS distance	ASIS-ASIS distance is the distance between the left ASIS and right ASIS. This measurement is only needed when markers cannot be placed directly on the ASIS, for example, on obese patients.	_____ mm	
Leg Length	Full leg length measured between the ASIS marker and the medial malleolus, via the knee joint. Measure with patient standing, if possible. If the patient is standing in the crouch position, this measurement is NOT the shortest distance between the ASIS and medial malleoli, but rather the measure of the skeletal leg length.	_____ mm	_____ mm
ASIS-Trochanter Distance	ASIS-greater trochanter distance is the vertical distance, in the sagittal plane, between the ASIS and greater trochanter when the patient is lying supine. Measure this distance with the femur rotated such that the greater trochanter is positioned as lateral as possible.	_____ mm	_____ mm
Knee Width	The medio-lateral width of the knee across the line of the knee axis. Measure with patient standing, if possible.	_____ mm	_____ mm
Ankle Width	The medio-lateral distance across the malleoli. Measure with patient standing, if possible.	_____ mm	_____ mm

Name	Description	Measure Left	Measure Right
Tibial Torsion	The angle between the knee flexion and the ankle dorsi-plantar axes. The ankle is usually externally rotated with respect to the knee flexion axis. The tibial torsion measurement is only needed if you are using a knee alignment device, and the medial malleoli markers are attached to the patient, Plug-in Gait calculates the tibial torsion automatically.	_____ deg	_____ deg
Sole Thickness Delta	The difference in the thickness of the sole at the toe and the heel. A positive sole delta indicates that the patient's heel is raised compared with the toe.	_____ mm	_____ mm

- **Marker placement**

As we focused on the analysis of lower extremities and foot/ankle, Oxford foot model and plug-in gait model were used in Nexus system.

Figure 9.7 shows the markers' placement on the low extremity of plug-in gait are displayed. The standard marker that is 14mm in diameter is too large for the foot as 13 markers were required for each side. Therefore, the smaller markers of 9mm in diameters were selected. The lower body of the conventional plug-in gait markers is in Figure 9.8.

Oxford foot model was used as 40 retro-reflective markers (radius 3mm) were placed on the feet and legs of the participants following by Vicon User Manual (Oxford Metrics Ltd., Oxford, UK). The markers on the medial side of the foot are the major markers for determining medial longitudinal arch— 1st metatarsal distal medial (LD1M/RD1M), Sustentaculum tali (LSTL/RSTL), Heel (LHEE/RHEE). Two extra markers were added on the navicular tuberosity of both feet and named as RNAV and LNAV. The prominence bone of navicular tuberosity can be found 2 to 3cm from Sustentaculum tali along with the bone toward 1st metatarsal joint. The other two newly defined markers are medial talus (LMT/RMT) and lateral talus (LLT/RLT) to indicate the displacement of talus bone because it is important for the eversion and inversion of the rearfoot. LPCA/RPCA markers are only for the static trial and need to be removed in the dynamic trial.

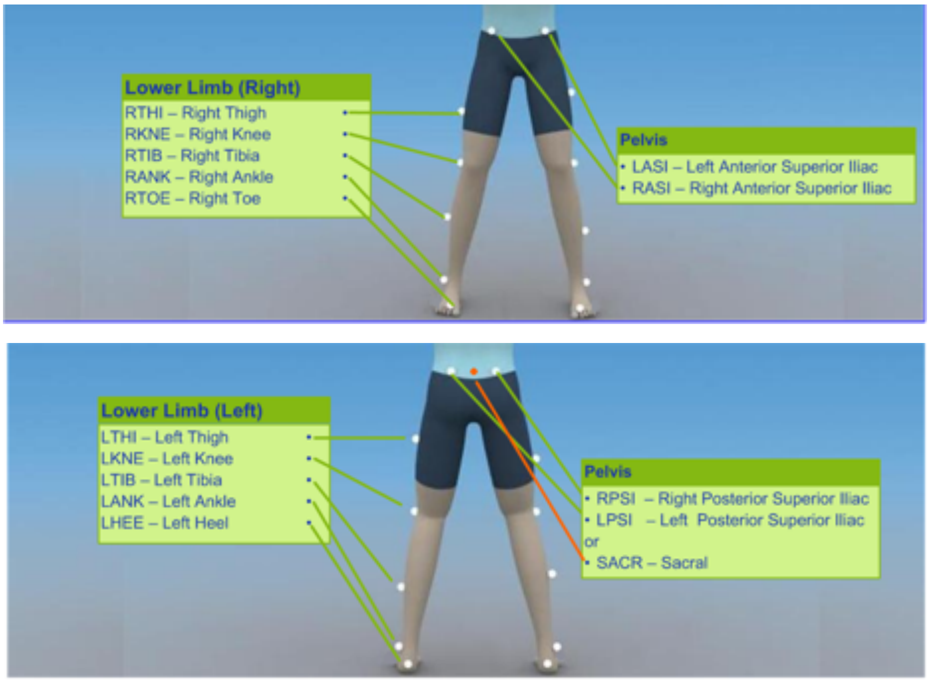

Figure 9.7. The markers placement of the lower leg of plug-in gait model

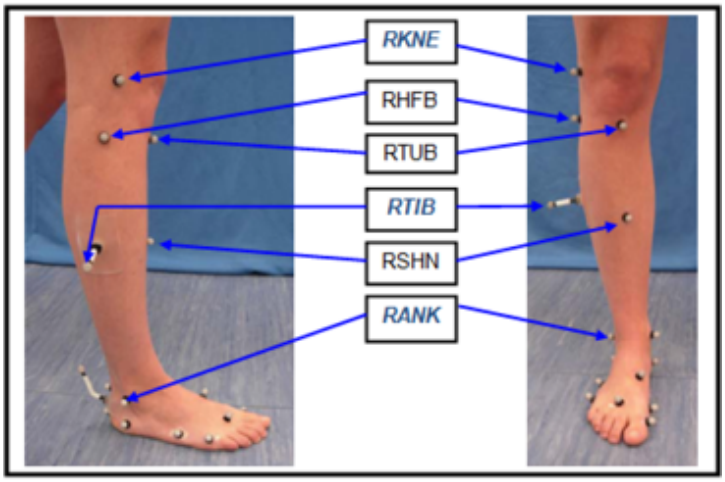

Figure 9.8. Maker placement of lower leg and the lateral aspect of foot in Oxford foot model

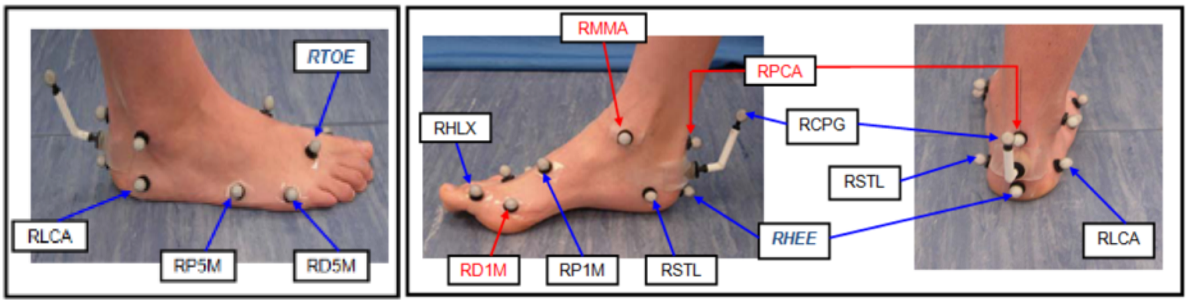

Figure 9.9. The markers placement of the foot in Oxford foot model

Table 9.4. The name and position of the markers in plug-in gait and Oxford foot model

	Marker	Position
Plug-in-gait model	LASI/RASI	Anterior superior iliac spine
	LPASI/RPASI	Posterior superior iliac spine
	SACR	Midway between the LPASI and RPASI
	LTHI/RTHI	Thigh
	LKNE/RKNE	Lateral knee
	LTIB/RTIB	Tibialis
	LTUB/RTUB	Tibial tuberosity
	LHFB/RHFB	Lateral head of fibula
	LSHN/RSHN	Anterior aspect of the shin
	LANK/RANK	Ankle
	LTOE/RTOE	2nd toe between phalanges and metatarsals
Oxford foot model	LCPG/RCPG	Posterior end of calcaneus
	LHEE/RHEE	Heel (on the bisecting line of calcaneus)
	LPCA/RPCA	Posterior calcaneus proximal
	LSTL/RSTL	Sustentaculum tali
	LP1M/RP1M	1st metatarsal, proximal dorsal
	LD1M/RD1M	1st metatarsal, distal medial
	LLCA/RLCA	Lateral calcaneus
	LP5M/RP5M	5st metatarsal, proximal dorsal
	LD5M/RD5M	5st metatarsal, distal medial
	LHLX/RHLX	Hallux
New-defined marker	LNAV/RNAV	Navicular tuberosity
	LMT/RMT	Medial talus
	LLT/RLT	Lateral talus

9.2.4. Gait test

Three different conditions were tested for each participant—no insole, customized solid insole and customized Honeycomb insole (Figure 9.10) to compare the performance of solid and Honeycomb insole and to see how they change the walking pattern and joint’s motion to low arch. As shown in Figure 9.11, the alteration of the footwear allows every marker detected by the cameras in the testing. More importantly, we can change the insoles without moving the markers to reduce unnecessary errors induced by the marker displacement.

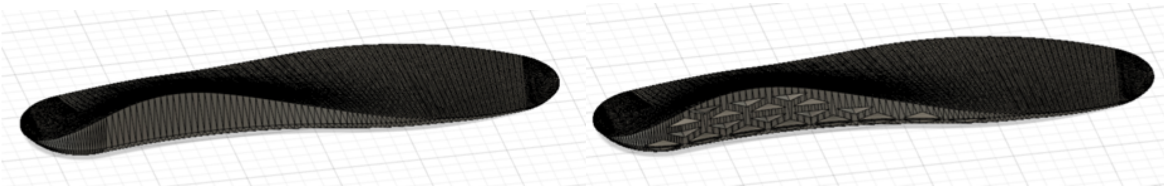

Figure 9.10. Each participant was given a pair of solid insoles (left) and Honeycomb insole (right)

Figure 9.11. The alteration of the footwear allows us to change the insole without replacing the markers

- **Static trial**

After the testing environment and subject have been prepared, the static trial allows the system to define the markers in space. The subject was asked to stand in "T pose" with arms raise at the horizontal level and feet stand slightly wider than shoulder width. Click "start" on the system to ensure that every marker can be detected by the system. It should be aware that all the markers appeared at the same time at least in one frame for building the static kinematic model in Nexus system. The static trial was recorded for 10 seconds to obtain the static unlabelled trajectories as figure 9.12.1. Once the static configuration was recorded, the kinematic model was built by the default label in Nexus system. 'Oxford foot model' was imported in the system to label the markers on foot, lower limbs, and pelvis. As shown in figure 9.12.2, the pelvic was in blue, right leg and foot were in green and left leg and foot were in red. After every marker was labelled, the process called 'fill the gap' was carried out to define the marker that may disappeared in some frames. The 'gap' was defined by the surrounding markers that has been successfully labelled. Once all the gaps were filled, select the 'Plug-in Gait Static pipeline' and tick the check box for 'Process Static Plug-in Gait

Model' in the 'Current Pipeline' to process the static model. Then, tick the check box for 'Processing Static Subject Calibration' and the subject calibration was finished as figure 9.12.2.

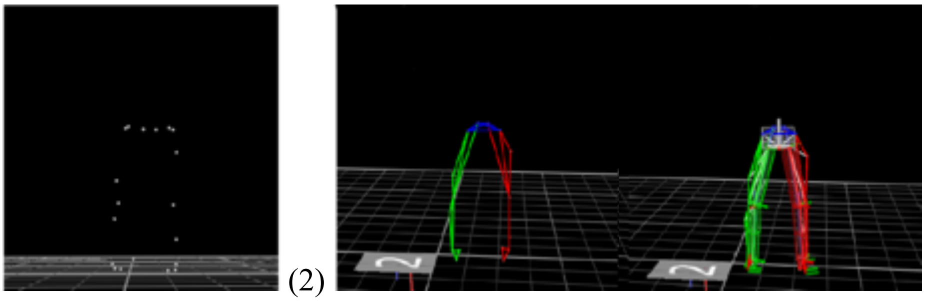

(1) (2)

Figure 9.12. (1) Unlabelled trajectory (2) Labelled trajectory for subject calibration

- **Dynamic trial**

The cadence was guided by a metronome set at 120 BPM (beat per minute), i.e. 0.5s per step. Participants were asked to complete 7m walk as the time was checked to be 5±0.25s, so the speed is approximately 1.4m/s. The gait was recorded in the same walking direction and 30 gait cycles were recorded for each trial. The subject was asked to walk along with the +X direction of the walkway and return to the starting point behind the cameras. Approximate eight to ten steps (i.e., four to five gait cycles) were recorded in each trial and thirty gait cycles were recorded in total. The subject was asked to walk as natural as possible to present the predetermined cadence in testing. The subject was allowed to practice few times before the test started. Each subject was asked to repeat the walking six to eight times to collect thirty gait cycles in total (Figure 9.13). Click "Stop" to finish recording the trial and the trajectory of unlabelled marker in dynamic trial was presented in Nexus system. The kinematic model that has been built in the static trial can be automatically apply to dynamic trial. Go to "tool" and select "Reconstruct and label" in the pipeline pan to run the pipeline. The markers were labelled automatically, and the kinematic model of dynamic trial was reconstructed. The 'fill the gap' function was applied to label the missing markers in some frame. After the 'gap' was filled, click on 'Combined Processing' in the list of current operations to run the pipeline. Once the model was successfully reconstructed, the animation of dynamic trial was shown in 3D perspective as Figure 9.14. Finally, the trajectories of each marker and the force plate data can be exported to XLS file for statistical analysis. The dynamic trial sequences were repeated three times with different insoles— no insole, solid insole and Honeycomb insole. Each trial was saved in *.enf files for Nexus system.

Figure 9.13. Dynamic trial of motion capture

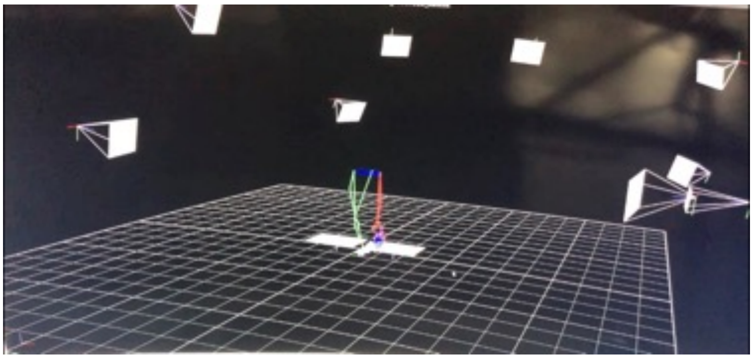

Figure 9.14. The animation of the dynamic trial in 3D perspective view in Nexus system

- **Data analysis— dynamic arch height calculation**

Dynamic arch height refers to the dynamic Normalized Navicular Height truncated (dNNHt), which is the instantaneous navicular height normalized by the instantaneous truncated foot length in a time frame. A similar method has been proposed by Eichelberger et al. (2018). Four markers— NAV, D1M, D5M and HEE, were chosen from the Oxford foot model to calculate dNNHt as in eq. 9.1 below.

$$dNNHt = {}^{A}\!/_{B} \qquad [9.1]$$

A: instantaneous navicular height: the distance from the point NAV to the plane defined by D1M, D5M and HEE in a time frame (Figure 9.15).
B: instantaneous truncated foot length: the distance between D1M and HEE in a time frame (Figure 9.15).

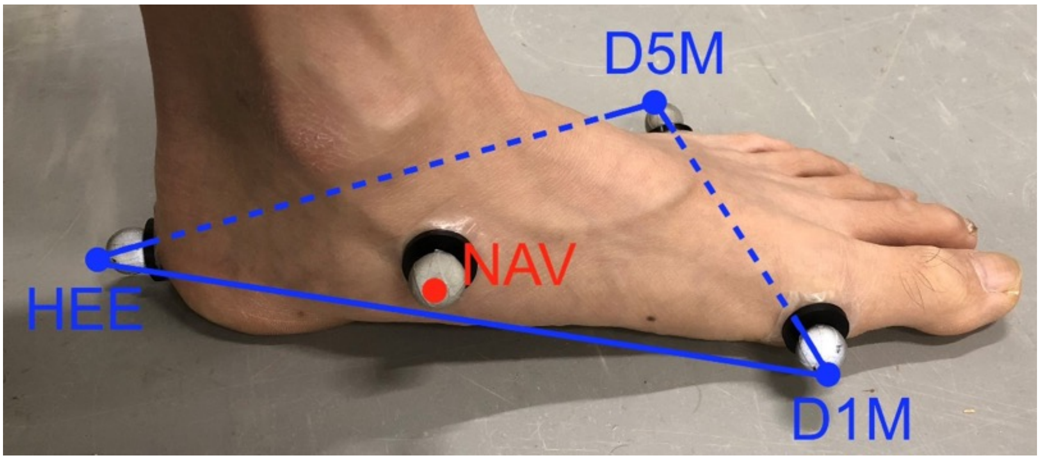

Figure 9.15. Four markers— NAV, D1M, D5M and HEE, were chosen from the Oxford foot model to calculate dynamic Normalized Navicular Height truncated (dNNHt). NAV: Navicular tuberosity, most medial aspect of the navicular bone. D1M: 1st metatarsal phalangeal joint, distal medial aspect. D5M: 5th metatarsal phalangeal joint, distal lateral aspect. HEE: Calcaneal tuberosity, Posterior calcaneus distal aspect.

Three dNNHt values— $dNNHt_{Start}$, $dNNHt_{Min}$ and $dNNHt_{MAX}$, were derived from the three main gait events— heel strike, late foot-flat, and late heel-off, in a single step respectively (Figure 11). The $dNNHt_{Start}$ value was derived at heel strike when HEE reaches its lowest value on z-axis. The $dNNHt_{Min}$ value was derived at late foot-flat as the minimum dNNHt value between heel strike and early heel-off. The $dNNHt_{Max}$ was derived at late heel-off as the maximum dNNHt value between heel-off and early toe-off. Early toe-off was defined when D1M started to increase by more than 0.2mm per time frame on z-axis.
For the dynamic arch height between two gait events, arch compression (ARCOM) was calculated as the differences between $dNNHt_{Start}$ and $dNNHt_{Min}$ in a single step (Eq. 9.2), and arch recoil (ARRE) was calculated as the differences between $dNNHt_{Min}$ and $dNNHt_{Max}$ in a single step (Eq. 9.3). Greater arch compression or arch recoil indicating the better performance of the insole.

$$ARCOM = dNNHt_{Start} - dNNHt_{Min} \quad [9.2]$$

$$ARRE = dNNHt_{Max} - dNNHt_{Min} \quad [9.3]$$

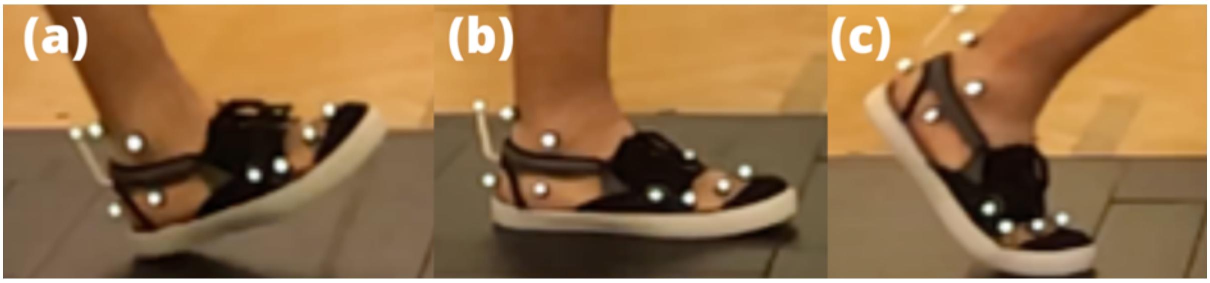

Figure 9.16. Start dNNHt, low dNNHt and peak dNNHt, were derived from three gait events— (a) heel strike, (b) late foot-flat and (c) late heel-off, in a single step respectively.

9.4.5. Statistical analysis

Statistical analysis was performed using SPSS Version 28 (IBM SPSS Inc.). Tukey's Honest Significant Difference (HSD), the post hoc test with ANOVA method, was performed to compare the specific difference for 'arch compression' and 'arch recoil' between the three different trials— without insoles, with customized solid insoles, and with customized novel insoles. The measurements of each participant and their left and right feet were treated separately. The level of statistical significance was set as $p < 0.05$. All variables were tested for normal distribution by the z-value of skewness (eq. 9.4) and kurtosis (eq. 9.5) (Kim, 2013).

$$Z_{skewness} = {}^{Skewness}/_{SE_{skewness}} \quad [9.4]$$

$$Z_{kurtosis} = {}^{Skewness}/_{SE_{kurtosis}} \quad [9.5]$$

9.4.6. User's feedback

- **Instant feedback**

The following questionnaire was given to the participants after the gait test for a feedback regarding balance, comfort level, and arch support with different insoles. 10-point Likert scale (Joshi et al., 2015) was used as participants were asked to score blind from 1 to 10 for each question, i.e. they were not told which insoles they wearing in a given trial until questionnaires were completed. The customized novel shoe insoles were then given to the participants for a prolonged period. Participants were asked to wear the insoles for at least 4 hours daily for two months and to provide their observations and recommendations.

Insole questionnaire

1) Please score 1 to 10 for the balance when you stand on single leg (1 means poorest balance and 10 the greatest balance)
    1. no insole ______
    2. Insole 1 ______
    3. Insole 2 ______

2) Please score 1 to 10 for the comfort level of the middle foot area (1 means least comfortable and 10 means most comfortable)
    1. no insole ______
    2. Insole 1 ______
    3. Insole 2 ______

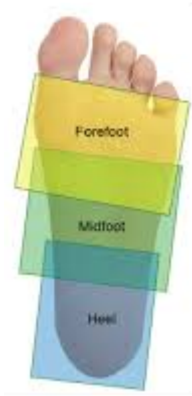

3) Please score 1 to 10 for the dynamic balance and arch support provide by the insoles during walking (1 means no balance and support and 10 the greatest balance and support)
    1. no insole ______
    2. Insole 1 ______
    3. Insole 2 ______

- **Prolonged period feedback**

As the mesh design of novel insole was concerned to be deformed overtime, the customized novel shoe insoles were given to the participants for collecting user's feedback for a prolonged period. The participants were asked to wear the novel insoles in their own shoes as much as possible for a 14-day period. Participants were instructed to abort trials if they experienced foot pain.

9.3. Results

- **Dynamic arch height measurement**

Due to the COVID-19 restriction and the closure of laboratory, only two participants were able to take part in the gait test. At all testing sessions, the distinct differences between no insole, solid insole and novel insole in arch compression and arch recoil were reported through ANOVA test for multiple comparison (Table 9.5 and 9.6). Variables with the absolute z-value of skewness or kurtosis less than 2 indicating normal distribution (Table 9.5). As shown in Table 9.6, novel insole delivered greater arch recoil than no insole for both feet of both participants. Although no insole has shown greater arch recoil than solid insole for the right foot of participant 1, no statistically significant difference was found between them in other trials. Novel and solid insoles have brought greater arch compression than no insole in most trial except for the left foot of participant 1 as no statistically significant difference was found between different insoles (Table 9.6). Although novel insole has shown greater arch compression than solid insole for the left foot of participant 2, no statistically significant difference was found between them in other trials.

Table 9.5. Descriptive statistics of arch compression and recoil for each participant

	Participant	Foot	Insole	N	Mean	Standard Deviation	Standard Error	$Z_{skewness}$	$Z_{kurtosis}$
Arch compression	1	Right	Novel	27	.436*	.019	.004	1.333	-.174
			Solid	25	.444*	.028	.006	-1.407	.714
			No insole	29	.350*	.024	.004	2.046	.822
		Left	Novel	25	.450*	.027	.005	-1.567	-.954
			Solid	26	.439	.058	.011	-2.228	2.089
			No insole	26	.444*	.029	.006	-1.846	.404
	2	Right	Novel	29	.295*	.058	.011	.681	-1.141
			Solid	25	.265*	.072	.014	-1.682	.573
			No insole	26	.165*	.068	.013	-2.173	1.594
		Left	Novel	24	.217*	.024	.005	-.459	-1.312
			Solid	24	.181*	.019	.004	-1.467	-.962
			No insole	26	.158*	.024	.005	.092	-.825
Arch Recoil	1	Right	Novel	27	.496	.043	.008	-5.376	6.347
			Solid	25	.419*	.030	.006	-.448	-1.598
			No insole	29	.444*	.040	.008	.695	-.744
		Left	Novel	25	.506*	.044	.009	-3.009	1.219
			Solid	26	.412*	.113	.022	.875	-1.221
			No insole	26	.362*	.087	.017	.947	-1.879
	2	Right	Novel	29	.452*	.051	.010	-.006	-1.040
			Solid	25	.362*	.079	.016	1.917	2.649
			No insole	26	.380*	.098	.019	-.827	.517
		Left	Novel	24	.366	.048	.010	-3.064	2.464
			Solid	24	.268*	.050	.010	1.176	-0.854

		No insole	26	.279*	.027	.005	.833	.282

*$|Z_{skewness}|$ or $|Z_{kurtosis}|$ < 2 indicates the variable is normally distributed

Table 9.6. ANOVA multiple comparisons test—Tukey HSD Post Hoc Tests, between no insole, customized solid insole, and customized novel insole.

	Participant	Foot	(I) Classification	(J) Classification	Mean Difference (I-J)	Standard Error	Sig. (P-value)
Arch Compression	1	Right	Novel	Solid	-.008	.007	.419
			Novel	No insole	.085*	.006	<.001
			Solid	No insole	.094*	.006	<.001
		Left	Novel	Solid	.011	.011	.577
			Novel	No insole	.006	.011	.854
			Solid	No insole	-.005	.011	.884
	2	Right	Novel	Solid	.030	.018	.224
			Novel	No insole	.130*	.018	<.001
			Solid	No insole	.100*	.018	<.001
		Left	Novel	Solid	.036*	.006	<.001
			Novel	No insole	.059*	.006	<.001
			Solid	No insole	.023*	.006	.002
Arch Recoil	1	Right	Novel	Solid	.078*	.011	<.001
			Novel	No insole	.052*	.010	<.001
			Solid	No insole	-.025*	.010	.048
		Left	Novel	Solid	.094*	.024	<.001
			Novel	No insole	.144*	.024	<.001
			Solid	No insole	.050	g.024	.100
	2	Right	Novel	Solid	.090*	.021	<.001
			Novel	No insole	.072*	.021	.003
			Solid	No insole	-.018	.022	.687
		Left	Novel	Solid	.098*	.012	<.001
			Novel	No insole	.086*	.012	<.001
			Solid	No insole	-.011	.012	.615

*The mean difference is statistically significant as the P < .05

- **Users' instant feedback**

As shown in Table 9.7, participant 1 and 2 stated that novel insoles have provided the best stability (balance) while participant 3 felt no insole is the best. For comfort level, the participants found novel insoles were better than solid insoles that in turn were better than no insole. For arch support, novel insoles provided better support for participant 1 and 2 than solid and no insole, while participant 3 felt novel and solid provided the similar support but better than no insole. In summary, the novel insole achieved the highest total (average) scores, followed by solid insole that was slightly higher than no insole (Table 9.7).

Table 9.7. Questionnaire regarding on balance, comfort level, and arch support

Classification	Participant	Q1: Balance	Q2: Comfort level	Q3: Arch support	Total score	Average score
No insole	1	5	4	5	14	15
	2	6	4	4	14	
	3	8	4	5	17	
Solid	1	5	6	5	16	17
	2	4	5	5	14	
	3	6	6	9	21	
Novel	1	8	9	9	26	25
	2	9	9	8	26	
	3	6	8	9	23	

- **Users' prolonged period feedback**

Participant 1, 2, and 3 wore the novel insoles for an average of 11, 4, and 8 hours a day respectively. All participants were having sedentary lifestyle, which less than 10,000 steps/day. As shown in Figure 18, slight deformation was observed on the mesh pad for participant 1 but no deformation for participant 2 and 3. Participant 1 and 3 both experienced the soreness on the midfoot (i.e. medial longitudinal arch) in the first three days, but it went away after the feet adapted to the insoles. However, participant 2 did not experience any muscle soreness of the foot when he wore the novel insoles. Participant 1 said, 'Other than the insoles I had before, I can feel my feet were working on the insoles rather than passively supported by the insoles. The insoles are very comfortable once my feet adapt to them, and I will continue to wear them.' Participant 2 also said, 'The novel insoles have greatly alleviated the discomfort he had while standing and walking.' Participant 3 said, 'My arch feels very supportive by the novel insoles, and when the feet hit the ground while I am walking, I can feel the insoles absorb the impact on my heels.'

9.4. Discussion

- **Arch compression and arch recoil in gait**

As shown in Table 9.8 (detailed in Table 9.6), the best performance in arch compression was found in novel insole and solid insole generally had higher arch compression than no insole. As shown in Table 9.6, novel and solid insoles performed greater arch compression than no insole in most cases. However, previous study (Stearne et al., 2016) reported a contradictory result as a reduction in arch compression with a solid full-arch insole compared to no insole. The reason for the higher arch compression with solid insoles in the current study could be that the elastic AM materials deforms more when loaded and contributed to more arch height reduction from heel-strike to foot-flat. Arch compression may be increased by a more compressible material as the insole is compressed substantially to attenuate the impact force after heel-strike (Walker et al., 2006). As arch compression can contribute to elastic energy storage and reuse by the human foot, i.e. better energetic function of the foot during locomotion (Kelly et al., 2019; Riddick et al., 2019), greater arch compression was expected to result in greater arch recoil. However, although solid insoles performed similar arch compression as novel insoles, they showed poorer performance in arch recoil compared to novel insole (Table 9.6). For arch recoil, novel insoles displayed the best performance compared to solid and no insole showing the mesh pad design was able to facilitate the arch elevation for people with low arch. A noticeable discrepancy was found between the feet of participant 2 as the arch compression and arch recoil was significantly greater on the right foot (Table 9.6). It could be caused by the distinct arch height differences as the right foot was 0.141 in NNHt and left foot 0.108 for participant 2 (Table 9.1). Previous studies also have the similar finding of the significant asymmetric arch height in flatfooted people (Murley et al., 2009; Zifchock et al., 2006). We interpret these results cautiously and consider the indicative as the relative error in marker reconstruction is bound to affect the reliability and a lot larger result sample is needed (Dabnichki, 1998; Dabnichki et al., 1997). Based upon the results on a small number of participants, we hypothesize that the arch compression and arch recoil increase by the developed novel insoles as per the results of the current preliminary study.

Table 9.8. The summary of arch compression and recoil between no insole, solid and novel insole

Participant	Foot	Arch Compression Mean	Arch Recoil Mean
1	Right	solid > novel > no insert .444(.028). >436(.019) >.350(.024)	novel > no insert > solid .496(.043) >.444(.040) >.419(.030)
	Left	novel ≥ no insert ≥ solid .450(.027) ≥.444(.029) ≥.439(.058)	novel > solid ≥ no insert .506 (.044) >.412(.113) ≥.363(.087)
2	Right	novel ≥ solid > no insert .295(.058) ≥.265(.072) >.165(.068)	novel > no insert ≥ solid .452(.051) >.380(.098) ≥.362(.079)
	Left	novel > solid > no insert .217(.024) > .181(.019) >.158(.024)	novel > no insert ≥ solid .366(.048) >.279(.027) ≥.268(.050)

If the comparison sign shows without the equal sign, it means there is statistically significant differences ($p<0.05$) between two groups. If the comparison sign shows with the equal sign, it means there is no statistically significant differences ($p>0.05$) between two groups

- **Users' feedback**

Participants provided contradictory responses to question 1 as the novel insoles were perceived to improve single leg balance for participant 1 and 2 (Table 9.7) because they did not feel the balance was compromised despite the removed arch support of the mesh pad. However, participant 3 felt the single leg balance was negatively influenced by both the solid and novel insoles. Moreover, novel insoles were more comfortable for all participants who scored 8 or 9 out of ten (Table 9.7 Q2). All participants have all agreed that the novel insoles provided the best arch support during walking in (Table 9.7 Q3). Furthermore, light muscle soreness was also sensed at midfoot after the gait test. Participant 1 detected foot muscle contraction during walking with the novel insoles causing some degree of difficulty in walking. Although perceived as discomfort, this could be a good sign as the elastic mesh pad of the novel insole was created not to passively support the fallen arch but to activate the foot muscle and this way increase the arch height and elastic return of the external force during locomotion.

- **Other models for dynamic arch height measurement**

For the motion analysis regarding arch motion, Dicharry et al. (2009) used five markers to calculate dynamic navicular height (NH) to determine arch compression and recoil. They calculated the vertical distance between navicular marker (NAV) and a plane constructed by other four markers— the first metatarsal head (D1M), the medial aspect of the calcaneus (LCA), and the bisector of the fifth metatarsal head (D5M) and the lateral aspect of the calcaneus (STL) (Figure 9.20). Dicharry et al. (2009) extracted the lowest NH at the swing phase prior to foot contact and the lowest NH at the stance phase to determine the arch compression. However, as their study does not mention how to define four points in space as a plane but not the curved surface. Therefore, the same method was not used in current study. It is important to define D1M, D5M, LCA and STL as a plane for calculating NH. Otherwise, the distance between NAV to the plane cannot accurately present the height of the arch.

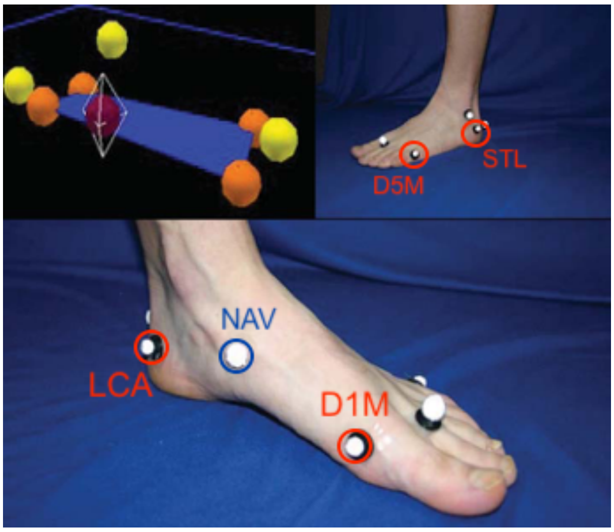

Figure 9.17. Navicular height is the distance between NAV and the plane constructed D1M, D5M, STL and LCA

9.5. Conclusion

Customized novel inserts were designed, manufactured, and preliminary tested on a small number of participants. The proposed design has aimed to improve the longitudinal tensile elasticity and replace solid support with a facilitated arch recoil. The conducted tests confirmed that the proposed design showed best performance in arch compression and recoil showing that the newly developed mesh pad has successfully facilitated the arch elasticity. The greater arch compression and recoil improved the mechanical efficiency of gait, which in turn led to better comfort perception and superior performance as indicated by the participants' scores. At the same time the customized solid insert showed the least arch recoil indicating the arch movement was restricted further confirming the benefits of the newly proposed design feature. Future work will include larger scale testing that would also gyroid insoles already developed.

Chapter 10. Conclusion

The current thesis has addressed the study aims, knowledge gaps and research questions mentioned in Chapter 2 and 3. The main contribution is to successfully design and manufacture the novel insole Honeycomb for low arch people (Chapter 7) and the insole has improved the arch compression and arch recoil according to the preliminary motion analysis (Chapter 9), which addressed the limitations of current solid insole. Moreover, the low arch assessment protocol and thresholds using 3D foot scans has also developed as the quantitative foot arch assessment was devised to automatically identify low arch in a simpler, quicker, and more accurate manner (Chapter 4 to 6). The protocol of insole customization has been developed in current study as the parametric modelling method was introduced (Chapter 7). Through the newly developed algorithms, foot scanned data can be automatically transferred into design parameters to generate the insole geometry in three minutes (it takes over three hours by direct modelling method). From the FEA results (Chapter 8), Honeycomb insoles reduced the peak plantar pressure and joint's internal stress compared to solid insole, which may lead to the better comfort level, balance, and arch support according to the users' instant and prolonged period feedback (Chapter 9). From the result of the preliminary motion analysis (Chapter 9), it is encouraging that Honeycomb insoles tend to improve the arch compression and arch recoil compared to solid and no insole and the movement efficiency is also expected to be improved accordingly.

However, there are few limitations that may lead to the future work of current study. Due to COVID-19 and the closure of the lab, we only recruit three participants for the testing of Honeycomb insoles. We are also unable to test our other novel design, Bubble and Gyroid insole, through in vivo experiment. It is believed the Gyroid insole can provide the better spring effect to the foot and better user's experience due to its lighter weight and better elasticity. Therefore, the future work is to recruit more participants for insole customization using the protocol proposed in current thesis and test our novel insoles through motion analysis in order to deliver the statistic results with larger data base (i.e. subjects). As the novel insoles were reported to induce the instantaneously 'biomechanical change' in gait by increasing the arch compression and recoil. The future study is required to observe whether the novel insoles induce the physiological change for surrounding musculature and connective tissue (e.g. Calves, Achilles tendon) or the change of neuromuscular connection (e.g. proprioceptor) in long term due to the better loading and explode (i.e. eccentric and concentric contraction) in gait.

Reference

Abayazid, F. F., & Ghajari, M. (2020). Material characterisation of additively manufactured elastomers at different strain rates and build orientations. *Additive Manufacturing*, 33, 101160.

Abdel Fattah, M. M., Hassanin, M. M., Felembane, F. A., & Nassaane, M. T. (2006). Flat foot among Saudi Arabian army recruits: prevalence and risk factors. *EMHJ-Eastern Mediterranean Health Journal, 12(1-2),* 211-217

Aboutorabi, A., Saeedi, H., Kamali, M., Farahmand, B., Eshraghi, A., & Dolagh, R. S. (2014). Immediate effect of orthopedic shoe and functional foot orthosis on center of pressure displacement and gait parameters in juvenile flexible flat foot. *Prosthetics and orthotics international*, *38*(3), 218-223.

Aboutorabi, A., Arazpour, M., Hutchins, S.W., Curran, S. and Maleki, M. (2015). The efficacy of shoe inserts on alteration to center of pressure displacement in subjects with flat and normal feet: a literature review. *Disability and Rehabilitation: Assistive Technology*, *10*(6), 439-444.

Abu-Faraj, Z. O., Harris, G. F., Smith, P. A., & Hassani, S. (1999). Human gait and clinical movement analysis. Wiley Encyclopedia of Electrical and Electronics Engineering, 1-34.

Accuthotix, 2017, photograph, viewed 30 April 2020, <http://www.accuthotix.com/index.php/functional-vs-accommodative-inserts/>

Adams, R. J., Appleton, S. L., Taylor, A. W., Gill, T. K., Lang, C., McEvoy, R. D., & Antic, N. A. (2017). Sleep health of Australian adults in 2016: results of the 2016 Sleep Health Foundation national survey. *Sleep Health*, *3*(1), 35-42.

Adelaide pediatrist centre. (n.d.) Inserts process and design. Retrieved from: https://adelaidepodiatrist.net.au/inserts-process-and-design/ [Accessed on 18 May, 2020]

Alexander, R. M. (1991). Energy-saving mechanisms in walking and running. *Journal of Experimental Biology,* 160**,** 55-69.

Allen D.G., Lamb G.D., Westerblad H. (2008) Skeletal muscle fatigue: cellular mechanisms. Physiological reviews, 88(1):287-332.

Anggoro, P. W., Tauviqirrahman, M., Jamari, J., Bayuseno, A. P., Bawono, B., & Avelina, M. M. (2018). Computer-aided reverse engineering system in the design and production of insert insole shoes for patients with diabetes. *Cogent Engineering*, *5*(1), 1470916.

Antunes, P. J., Dias, G. R., Coelho, A. T., Rebelo, F., & Pereira, T. (2011). Nonlinear 3D foot FEA modeling from CT scan medical images.

Arif, M., & Kattan, A. (2015). Physical activities monitoring using wearable acceleration sensors attached to the body. *PloS one*, *10*(7), e0130851.

ASTM D395-18, Standard Test Methods for Rubber Property — Compression Set, Annu. B. ASTM Stand. (2008).

ASTM D412-16, Standard Test Methods for Vulcanized Rubber and Thermoplastic Elastomers—Tension, ASTM Int. West Conshohocken, PA. (2016).

ASTM, D2240-05-Standard Test Method for Rubber Property — Durometer Hardness 1, Standard. (2005).

Ataee, A., Li, Y., Fraser, D., Song, G., & Wen, C. (2018). Anisotropic Ti-6Al-4V gyroid scaffolds manufactured by electron beam melting (EBM) for bone implant applications. *Materials & Design*, *137*, 345-354.

Avin, K. G., Bloomfield, S. A., Gross, T. S., & Warden, S. J. (2015). Biomechanical aspects of the muscle-bone interaction. *Current osteoporosis reports*, *13*(1), 1-8.

Baldassin, V., Gomes, C. R., & Beraldo, P. S. (2009). Effectiveness of prefabricated and customized shoe inserts made from low-cost foam for noncomplicated plantar fasciitis: a randomized controlled trial. *Archives of physical medicine and rehabilitation*, *90*(4), 701-706.

Balsdon, M., Dombroski, C., Bushey, K., & Jenkyn, T. R. (2019). Hard, soft and off-the-shelf shoe inserts and their effect on the angle of the medial longitudinal arch: A biplane fluoroscopy study. *Prosthetics and inserts international*, *43*(3), 331-338.

Banwell, H. A., Mackintosh, S., & Thewlis, D. (2014). Foot orthoses for adults with flexible flatfoot: a systematic review. *Journal of foot and ankle research*, *7*(1), 23.

Banwell, H. A., Mackintosh, S., Thewlis, D., & Landorf, K. B. (2014). Consensus-based recommendations of Australian podiatrists for the prescription of shoe inserts for symptomatic flexible flatfoot in adults. *Journal of foot and ankle research*, *7*(1), 49-66.

Bao, S., Lin, J.H. (2018). An investigation into four different sit–stand workstation uses schedules. Ergonomics, 61(2), 243-254.

Barani, Z., Haghpanahi, M., Katoozian, H. (2005). Three-dimensional stress analysis of diabetic insole: a finite element approach. Technology and Health Care, 13, 185-192

BASF. (2018, October 15). BASF Performance Footwear. Retrieved from: http://www.performancematerials.basf.us/files /pdf/FootWear_bk_en.pdf

Baum, I. M. (2000). *U.S. Patent No. 6,141,889*. Washington, DC: U.S. Patent and Trademark Office.

Baxi, O., Yeranosian, M., Lin, A., Munoz, M., & Lin, S. (2019). Insert management of neuropathic and dysvascular feet. In *Atlas of Inserts and Assistive Devices*, 268-276.

Berrar, D., & Flach, P. (2012). Caveats and pitfalls of ROC analysis in clinical microarray research (and how to avoid them). *Briefings in bioinformatics*, *13*(1), 83-97.

Bert Reld. (1977). Amfit. Retrieved from: http://www.amfit.com/products/contact-digitizer [accessed on 19 May, 2020]

Bertani, A., Cappello, A., Benedetti, M. G., Simoncini, L., & Catani, F. (1999). Flat foot functional evaluation using pattern recognition of ground reaction data. Clinical Biomechanics, 14(7), 484-493

Barton, F. W., Biggs, R. M., Gomez, J. P., Massarelli, P. J., & McKeel Jr, W. T. (2000). *Finite element modeling and analysis of reinforced-concrete bridge* (No. VTRC 01-R4). United States. Federal Highway Administration.

Birtane, M., & Tuna, H. (2004). The evaluation of plantar pressure distribution in obese and non-obese adults. *Clinical Biomechanics*, *19*(10), 1055-1059.

Bishop, C., Paul, G., & Thewlis, D. (2012). Recommendations for the reporting of foot and ankle models. *Journal of biomechanics*, *45*(13), 2185-2194.

Bishop, D. (2003). Warm up I. Sports medicine, 33(6), pp.439-454.

Blackburn, R., & Dennis, C. (2005). U.S. Patent Application No. 11/033,011.

Bok, S. K., Lee, H., Kim, B. O., Ahn, S., Song, Y., & Park, I. (2016). The effect of different foot orthosis inverted angles on plantar pressure in children with flexible flatfeet. *PLoS One*, *11*(7), e0159831.

Bonita, R., Beaglehole, R., & Kjellström, T. (2006). *Basic epidemiology*. World Health Organization.

Braun, B., & Baritz, M. (2017). FEM modelling of shoes insoles components for standing and walking simulation. In *MATEC Web of Conferences* (Vol. 94, p. 01002). EDP Sciences.

Bucki M, Luboz V, Perrier A, Champion E, Diot B, Vuillerme N., Payan Y. Clinical workflow for personalized foot pressure ulcer prevention. Medical engineering & physics. 2016;38(9):845-53.

Budiman-Mak, E., Conrad, K. J., Roach, K. E., Moore, J. W., Lertratanakul, Y., Koch, A. E., ... & Joyce-Clark, N. (1995). Can shoe inserts prevent hallux valgus deformity in rheumatoid arthritis? A randomized clinical trial. *Journal of clinical rheumatology: practical reports on rheumatic & musculoskeletal diseases*, *1*(6), 313-322.

Buldt, A. K., Murley, G. S., Butterworth, P., Levinger, P., Menz, H. B., & Landorf, K. B. (2013). The relationship between foot posture and lower limb kinematics during walking: A systematic review. Gait & posture, 38(3), 363-372.

Buldt, A. K., Levinger, P., Murley, G. S., Menz, H. B., Nester, C. J., & Landorf, K. B. (2015). Foot posture is associated with kinematics of the foot during gait: A comparison of normal, planus and cavus feet. *Gait & posture*, *42*(1), 42-48.

Butler, R. J., Hillstrom, H., Song, J., Richards, C. J., & Davis, I. S. (2008). Arch height index measurement system: establishment of reliability and normative values. *Journal of the American Podiatric Medical Association*, *98*(2), 102-106.

Cavendish, J. C., Field, D. A., & Frey, W. H. (1985). An approach to automatic three-dimensional finite element mesh generation. *International journal for numerical methods in engineering*, *21*(2), 329-347.

Camacho, D. L., Ledoux, W. R., Rohr, E. S., Sangeorzan, B. J., & Ching, R. P. (2002). A three-dimensional, anatomically detailed foot model: a foundation for a finite element simulation and means of quantifying foot-bone position. *Journal of rehabilitation research and development*, *39*(3), 401-410.

Canseco, K., Long, J., Marks, R., Khazzam, M., & Harris, G. (2008). Quantitative characterization of gait kinematics in patients with hallux rigidus using the Milwaukee foot model. *Journal of Orthopaedic Research*, *26*(4), 419-427.

Carroll, M., Annabell, M. E., & Rome, K. (2011). Reliability of capturing foot parameters using digital scanning and the neutral suspension casting technique. Journal of foot and ankle research, 4(1), 9-15

Cascade. (2018). Carboplast. Retrieved from: https://www.cascade-usa.com/footcare/foot-inserts/carboplast/carboplast-foot-plates.html [accessed on 12 May, 2020]

Chalmers, A. C., Busby, C. A. T. H. E. R. I. N. E., Goyert, J. I. L. L., Porter, B. A. R. B. A. R. A., & Schulzer, M. I. C. H. A. E. L. (2000). Metatarsalgia and rheumatoid arthritis--a randomized, single blind, sequential trial comparing 2 types of foot orthoses and supportive shoes. *The Journal of rheumatology*, *27*(7), 1643-1647.

Chang, B. C., Liu, D. H., Chang, J. L., Lee, S. H., & Wang, J. Y. (2014). Plantar pressure analysis of accommodative insole in older people with metatarsalgia. *Gait & posture*, *39*(1), 449-454.

Chang, H. W., Lin, C. J., Kuo, L. C., Tsai, M. J., Chieh, H. F., & Su, F. C. (2012). Three-dimensional measurement of foot arch in preschool children. *Biomedical engineering online*, *11*(1), 76-88.

Chang, J. S., Kwon, Y. H., Kim, C. S., Ahn, S. H., & Park, S. H. (2012). Differences of ground reaction forces and kinematics of lower extremity according to landing height between flat and normal feet. *Journal of back and musculoskeletal rehabilitation*, *25*(1), 21-26.

Chen, R. K., Jin, Y. A., Wensman, J., & Shih, A. (2016). Additive manufacturing of custom orthoses and prostheses—a review. *Additive Manufacturing*, *12*, 77-89.

Chen, T.H., Chou, L.W., Tsai, M.W., Lo, M.J. and Kao, M.J. (2014). Effectiveness of a heel cup with an arch support insole on the standing balance of the elderly. *Clinical interventions in aging*, *9*, 351-356.

Chen, W. M., Lee, T., Lee, P. V. S., Lee, J. W., & Lee, S. J. (2010). Effects of internal stress concentrations in plantar soft-tissue—a preliminary three-dimensional finite element analysis. *Medical engineering & physics*, *32*(4), 324-331.

Chen, W. P., Ju, C. W., & Tang, F. T. (2003). Effects of total contact insoles on the plantar stress redistribution: a finite element analysis. *Clinical Biomechanics*, *18*(6), 17-24.

Cheng, C. S., Tan, J. P., & Qing, T. Y. (2019). The Effect of Material Characteristic of Shoe Soles during Long Duration Running. In *Journal of Physics: Conference Series* (Vol. 1372, No. 1, p. 012040). IOP Publishing.

Chen, Y.C., Lou, S.Z., Huang, C.Y. and Su, F.C. (2010). Effects of shoe inserts on gait patterns of flat feet patients. *Clinical biomechanics*, *25*(3), 265-270.

Cheung, J. T. M., & Zhang, M. (2008). Parametric design of pressure-relieving foot orthosis using statistics-based finite element method. *Medical engineering & physics*, *30*(3), 269-277.

Cheung, J. T. M., & Zhang, M. (2005). A 3-dimensional finite element model of the human foot and ankle for insole design. *Archives of physical medicine and rehabilitation*, *86*(2), 353-358.

Cheung, J. T. M., Zhang, M., Leung, A. K. L., & Fan, Y. B. (2005). Three-dimensional finite element analysis of the foot during standing—a material sensitivity study. *Journal of biomechanics*, *38*(5), 1045-1054.

Cheung, J.T., Zhang, M. (2006). Finite Element Modeling of the Human Foot and Footwear. ABAQUS Users’ Conference, 145-159

Chikofsky, E. J. & Cross, J. H., II (1990). "Reverse Engineering and Design Recovery: A Taxonomy". IEEE Software, 7(1), 13-17.

Chu, W. C., Lee, S. H., Chu, W., Wang, T. J., & Lee, M. C. (1995). The use of arch index to characterize arch height: a digital image processing approach. *IEEE Transactions on Biomedical Engineering*, *42*(11), 1088-1093.

Chuckpaiwong, B., Nunley, J.A., Mall, N.A. and Queen, R.M. (2008). The effect of foot type on in-shoe plantar pressure during walking and running. Gait & posture, 28(3), 405-411.

Çilli, F., Pehlivan, Ö., Keklikçi, K., Mahiroğulları, M., & Kuşkucu, M. (2009). Prevalence of flatfoot in Turkish male adolescents. *Joint Diseases and Related Surgery*, *20*(2), 90-92.

Ciobanu, O. (2012). The use of CAD/CAM and rapid fabrication technologies in prosthesis and inserts manufacturing. Revista medico-chirurgicala a Societatii de Medici si Naturalisti din Iasi, 116(2), 642-648.

Ciobanu, O., Soydan, Y., & Hizal, S. (2012, September). Customized foot orthosis manufactured with 3D printers. In *Proceedings of IMS* (pp. 91-98).

Clinical specialties in inserts and prosthetics. (n.d.) Retrieved from https://www.aopa.org.au/publications/foot-inserts [Accessed 4 May. 2020],

Cody, E. A., Williamson, E. R., Burket, J. C., Deland, J. T. & Ellis, S. J. 2016. Correlation of Talar Anatomy and Subtalar Joint Alignment on Weightbearing Computed Tomography with Radiographic Flatfoot Parameters. *Foot & ankle international*, 1-8.

Collins, N., Crossley, K., Beller, E., Darnell, R., McPoil, T. and Vicenzino, B. (2008). Shoe inserts and physiotherapy in the treatment of patellofemoral pain syndrome: randomised clinical trial. *Bmj*, *337*, 1735-1742.

Corazza, S., Muendermann, L., Chaudhari, A. M., Demattio, T., Cobelli, C., & Andriacchi, T. P. (2006). A markerless motion capture system to study musculoskeletal biomechanics: visual hull and simulated annealing approach. *Annals of biomedical engineering*, *34*(6), 1019-1029.

Cornwall, M. W., & McPoil, T. G. (1997). Effect of shoe inserts on the initiation of plantar surface loading. *The Foot*, *7*(3), 148-152.

Cornwall, M. W., & McPoil, T. G. (1999). Relative movement of the navicular bone during normal walking. *Foot & ankle international*, *20*(8), 507-512.

Cowan, D. N., Jones, B. H., & Robinson, J. R. (1993). Foot morphologic characteristics and risk of exercise-related injury. *Archives of family medicine*, *2*(7), 773-777.

Cowley, E., & Marsden, J. (2013). The effects of prolonged running on foot posture: a repeated measures study of half marathon runners using the foot posture index and navicular height. *Journal of Foot and Ankle Research*, *6*(1), 20.

Creaby, M., May, K. and Bennell, K. (2011). Insole effects on impact loading during walking. Ergonomics, 54(7), 665-671.

Dabnichki, P., Lauder, M., Aritan, S. E. R. D. A. R., & Tsirakos, D. (1997). Accuracy evaluation of an on-line kinematic system via dynamic tests. Journal of medical engineering & technology, 21(2), 53-66.

Dabnichki, P. (1998). Biomechanical testing and sport equipment design. Sports Engineering, 1(2), 93-105.

Dabnichki P (2005) Fast Mesh generator for Boundary Element Analysis of static and dynamic problems forces, Adv. Bound. Elem. VI, EC Publ. pp. 261-266.

Dabnichki, P., & Zhivkov, A. (2005). Analytical Approach to cell geometry reconstruction. *Computer, Materials and Continua*, *2*(2), 97-104.

Dabnichki, P., & Zhivkov, A. (2010). An analytical method for reconstruction of biological objects from discrete noisy data. *Mathematical and Computer Modelling of Dynamical Systems*, *16*(5), 431-442.

Dahle, L. K., Mueller, M., Delitto, A., & Diamond, J. E. (1991). Visual assessment of foot type and relationship of foot type to lower extremity injury. *Journal of Orthopaedic & Sports Physical Therapy*, *14*(2), 70-74.

Dars, S., Uden, H., Banwell, H. A., & Kumar, S. (2018). The effectiveness of non-surgical intervention (shoe inserts) for paediatric flexible flatfoot: a systematic review: update. *PloS one*, *13*(2), e0193060

Das, S. C., Ranganathan, R., & Murugan, N. (2018). Effect of build orientation on the strength and cost of PolyJet 3D printed parts. *Rapid Prototyping Journal*.

Davia-Aracil, M., Hinojo-Pérez, J. J., Jimeno-Morenilla, A., & Mora-Mora, H. (2018). 3D printing of functional anatomical insoles. *Computers in Industry*, *95*, 38-53.

David P. & David R.T. (2005). Clinical Skills in Treating the Foot (Second Edition), 211-229. https://doi.org/10.1016/B978-0-443-07113-3.50014-7 (Available online 15 May 2009)

Davidson, C. (2012). Investigating the suitability of laser sintered elastomers for running footwear applications (Doctoral dissertation, © Craig Davidson).

De Mits S, Coorevits P, De Clercq D, Elewaut D, Woodburn J, Roosen P. (2010). Reliability and validity of the Infoot 3D foot digitizer for normal healthy adults. Footwear Science, 2(2), 65-75.

De Vet, H. C., & Terwee, C. B. (2010). The minimal detectable change should not replace the minimal important difference. *Journal of clinical epidemiology*, *63*(7), 804.

Deland, J. T., de Asla, R. J., Sung, I.-H., Ernberg, L. A., Potter, H. G. (2005). Posterior tibial tendon insu ciency: which ligaments are involved? Foot & ankle international, 26(6), 427-435.

DeToro, W. A. (2012). Risks associated with the use of PVC-based plastics in Inserts. Retrieved from: https://www.anatomicalconceptsinc.com/risks-with-pvc-based-plastics [Accessed 8 May. 2020]

Desmyttere, G., Hajizadeh, M., Bleau, J., & Begon, M. (2018). Effect of foot orthosis design on lower limb joint kinematics and kinetics during walking in flexible pes planovalgus: A systematic review and meta-analysis. *Clinical Biomechanics*, *59*, 117-129.

Dias, R. B., Coto, N. P., Batalha, G. F., & Driemeier, L. (2017). Systematic study of ethylene-vinyl acetate (EVA) in the manufacturing of protector devices for the orofacial system. *Archives of Materials Science and Engineering*, *86*(1).

Dicharry, J. M., Franz, J. R., Croce, U. D., Wilder, R. P., Riley, P. O., & Kerrigan, D. C. (2009). Differences in static and dynamic measures in evaluation of talonavicular mobility in gait. *journal of orthopaedic & sports physical therapy*, *39*(8), 628-634.

Dombroski, C. E., Balsdon, M. E., & Froats, A. (2014). The use of a low cost 3D scanning and printing tool in the manufacture of custom-made shoe inserts: a preliminary study. *BMC research notes*, *7*(1), 443-446.

Eichelberger P, Blasimann A, Lutz N, Krause F, Baur H. (2018). A minimal markerset for three-dimensional foot function assessment: measuring navicular drop and drift under dynamic conditions. Journal of foot and ankle research, 11(1), 1-10.

Eilam, E. (2011). Reversing: secrets of reverse engineering. John Wiley & Sons.

Elite inserts, 2015, photograph, viewed 30 April 2020, <https://www.eliteinserts.com.au/elitesemirigid.html>

Engineering ToolBox. (2001). Thermoplastics - Physical Properties. Retrieved from: https://www.engineeringtoolbox.com [Accessed 5 May. 2020]

Erdemir, A., Hamel, A. J., Fauth, A. R., Piazza, S. J., & Sharkey, N. A. (2004). Dynamic loading of the plantar aponeurosis in walking. *JBJS*, *86*(3), 546-552.

Esfandiari, E., Kamyab, M., Yazdi, H. R., Foroughi, N., & Sanjari, M. A. (2013). The immediate effect of lateral wedge insoles, with and without a subtalar strap, on the lateral trunk lean motion in patients with knee osteoarthritis. *Geriatric orthopaedic surgery & rehabilitation*, *4*(4), 127-132.

Eslami, M., & Ferber, R. (2013). Can inserts and navicular drop affect foot motion patterns during running?. Journal of science and medicine in sport, 16(4), 377-381.

Esteves, J., Luz, A., Fidalgo, R., Briôa, M., & Matos, J. P. (2019). Influence of functional shoe inserts on the plantar pressure of 5 handball athletes: analysis using a novel system during 3 athletic tasks. *Academic Journal of Electronics Telecommunications and Computers.*

Faulí, A. C., Andrés, C. L., Rosas, N. P., Fernández, M. J., Parreño, E. M., & Barceló, C. O. (2008). Physical evaluation of insole materials used to treat the diabetic foot. *Journal of the American Podiatric Medical Association*, *98*(3), 229-238.

Ferguson, H., Raskowsky, M., Blake, R. L., & Denton, J. A. (1991). TL-61 versus Rohadur inserts in heel spur syndrome. Journal of the American Podiatric Medical Association, 81(8), 439-442.

Ferri, M., Scharfenberger, A. V., Goplen, G., Daniels, T. R., & Pearce, D. (2008). Weightbearing CT scan of severe flexible flatfoot deformities. *Foot & ankle international*, *29*(2), 199-204.

Field, A. (2009). Discovering statistics using SPSS. Sage publications.

Fiolkowski, P., Brunt, D., Bishop, M., Woo, R., Horodyski, M. (2003). Intrinsic pedal musculature support of the medial longitudinal arch: an electromyography study. The Journal of foot and ankle surgery, 42(6), 327-333.

Fong, D.T., Lam, M.H., Lao, M.L., Chan, C.W., Yung, P.S., Fung, K.Y., Lui, P.P. and Chan, K.M. (2008). Effect of medial arch-heel support in inserts on reducing ankle eversion: a biomechanics study. *Journal of orthopaedic surgery and research*, *3*(1), 7-13.

Franco, A. H. (1987). Pes cavus and flatfoot: analyses and treatment. *Physical therapy*, *67*(5), 688-694.

Fuchioka, S., Iwata, A., Higuchi, Y., Miyake, M., Kanda, S., & Nishiyama, T. (2015). The forward velocity of the center of pressure in the midfoot is a major predictor of gait speed in older adults. *International Journal of Gerontology*, *9*(2), 119-122.

Genova, J. M., & Gross, M. T. (2000). Effect of shoe inserts on calcaneal eversion during standing and treadmill walking for subjects with abnormal pronation. *Journal of Orthopaedic & Sports Physical Therapy*, *30*(11), 664-675.

Gensole. (2018). [online] Available at: http://gensole.com/ [Accessed 30 Sep. 2018].

Gibson, I., Rosen, D.W. and Stucker, B. (2010). Design for additive manufacturing. In *Additive Manufacturing Technologies,* 299-332

Giddings, V. L., Beaupre, G. S., Whalen, R. T., & Carter, D. R. (2000). Calcaneal loading during walking and running. *Medicine & Science in Sports & Exercise*, *32*(3), 627-634.

Granta Design Limited. (2017). *Granta Design Home.* Retrieved Ocrober 15, 2018, from Granta Material Inelligence: https://www.grantadesign.com/products/ces/

Gulzar, M. (2012). Linear Analysis of Crack Propagation in a Solid Rocket Propellant. In Applied Mechanics and Materials (Vol. 229, pp. 742-746). Trans Tech Publications Ltd.

Gyrobot. (2016). Gensole®. Retrieved from: http://gensole.com/ [accessed on 22 May 2020]

Hallemans, A., D'Août, K., De Clercq, D., & Aerts, P. (2003). Pressure distribution patterns under the feet of new walkers: the first two months of independent walking. *Foot & ankle international*, *24*(5), 444-453.

Halstead, J., Keenan, A. M., Chapman, G. J., & Redmond, A. C. (2016). The feasibility of a modified shoe for multi-segment foot motion analysis: a preliminary study. *Journal of foot and ankle research*, *9*(1), 1-8.

Hamill, J. and Knutzen, K.M. (2006). Biomechanical basis of human movement. Lippincott Williams & Wilkins.

Hamzah, H. H., Shafiee, S. A., Abdalla, A., & Patel, B. A. (2018). 3D printable conductive materials for the fabrication of electrochemical sensors: A mini review. *Electrochemistry Communications*, *96*, 27-31.

Han, K., Bae, K., Levine, N., Yang, J., & Lee, J. S. (2019). Biomechanical effect of foot orthoses on rearfoot motions and joint moment parameters in patients with flexible flatfoot. *Medical science monitor: international medical journal of experimental and clinical research*, *25*, 5920.

Harris, G. F., & Wertsch, J. J. (1994). Procedures for gait analysis. Archives of Physical Medicine and Rehabilitation, 75(2), 216-225.

Hasan, M. I., Taufiq Rashid, M., & Arefin, S. An Analysis on the Sustainability of Different Outsole Materials During Shoe Flexing Using FEA Method. *International Conference on Mechanical, Industrial and Materials Engineering 2015 (ICMIME2015)*

He, M., Zhao, Y., Wang, B., Xi, Q., Zhou, J., & Liang, Z. (2015). 3D printing fabrication of amorphous thermoelectric materials with ultralow thermal conductivity. *Small*, *11*(44), 5889-5894.

Headlee, D. L., Leonard, J. L., Hart, J. M., Ingersoll, C. D., & Hertel, J. (2008). Fatigue of the plantar intrinsic foot muscles increases navicular drop. *Journal of Electromyography and Kinesiology*, *18*(3), 420-425.

Healy, A., Dunning, D. N., & Chockalingam, N. (2010). Materials used for footwear inserts: a review. *Footwear Science*, *2*(2), 93-110.

Healy, A., Dunning, D. N., & Chockalingam, N. (2012). Effect of insole material on lower limb kinematics and plantar pressures during treadmill walking. *Prosthetics and inserts international*, *36*(1), 53-62.

Hessert, M. J., Vyas, M., Leach, J., Hu, K., Lipsitz, L. A., & Novak, V. (2005). Foot pressure distribution during walking in young and old adults. BMC geriatrics, 5(1), 1-8.

Hill, M., Naemi, R., Branthwaite, H., & Chockalingam, N. (2017). The relationship between arch height and foot length: Implications for size grading. *Applied ergonomics*, *59*, 243-250.

Hodge, M. C., Bach, T. M., & Carter, G. M. (1999). Insert management of plantar pressure and pain in rheumatoid arthritis. *Clinical biomechanics*, *14*(8), 567-575.

Hösl, M., Böhm, H., Multerer, C., & Döderlein, L. (2014). Does excessive flatfoot deformity affect function? A comparison between symptomatic and asymptomatic flatfeet using the Oxford Foot Model. Gait & posture, 39(1), 23-28.

Hu, C. W., Baca, A., Groeber, M., & Dabnichki, P. (2018). Geometrical Model for Characterization of Foot Deformity using 3D imaging. *IFAC-PapersOnLine*, *51*(2), 373-378.

Hu, C. W., Dabnichki, P., Baca, A., Nguyen, C. T., & Pang, T. Y. (2021). Preventive strategy of flatfoot deformity using fully automated procedure. Medical Engineering & Physics, 95, 15-24.

Huang, C. K., Kitaoka, H. B., An, K. N., & Chao, E. Y. (1993). Biomechanical evaluation of longitudinal arch stability. *Foot & ankle*, *14*(6), 353-357.

Huang, C. N., Lee, M. Y., & Chang, C. C. (2011). Computer-aided design and manufacturing of customized insoles. *IEEE computer graphics and applications*, *31*(2), 74-79.

Hunt, A. E., & Smith, R. M. (2004). Mechanics and control of the flat versus normal foot during the stance phase of walking. *Clinical biomechanics*, *19*(4), 391-397.

Ibuki, A., Cornoiu, A., Clarke, A., Unglik, R., & Beischer, A. (2010). The effect of insert treatment on midfoot osteoarthritis assessed using specifically designed patient evaluation questionnaires. *Prosthetics and inserts international*, *34*(4), 461-471

International Organization for Standardization. (1977). Prosthetics and inserts. (ISO Standard No. TC 168). Retrieved from https://www.iso.org/committee/53630.html

International Organization for Standardization. (1998). Footwear (ISO Standard No. TC 216). Retrieved from https://www.iso.org/committee/54972.html

International Organization for Standardization. (2017). Prosthetics and inserts-Shoe inserts-Uses, functions classification and description (ISO Standard No. 21064:2017). Retrieved from https://www.iso.org/standard/69813.html?browse=tc

International Organization for Standardization. ISO 20685:2010 3-D scanning methodologies for internationally compatible anthropometric databases. [cited 2010 June]. Avaliable from: International Organization for Standardization.

Janisse, D. J., & Janisse, E. (2008). Shoe modification and the use of orthoses in the treatment of foot and ankle pathology. *JAAOS-Journal of the American Academy of Orthopaedic Surgeons,* 16(3), 152-158.

Janisse, D., & Janisse, E. (2015). Pedorthic management of the diabetic foot. *Prosthetics and inserts international*, *39*(1), 40-47.

Jeffrey Root (n.d.). Casting guide: neutral position suspension casting technique. Retrieved from: http://www.pedorthic.ca/wp-content/uploads/2015/04/Casting-Guide.pdf [accessed on 19 May, 2020]

Jennings, M. M., Christensen, J. C. (2008). The effects of sectioning the spring ligament on rearfoot stability and posterior tibial tendon efficiency. The Journal of Foot and Ankle Surgery, 47(3), 219-224.

Jonson, L. S. R., & Gross, M. T. (1997). Intraexaminer reliability, interexaminer reliability, and mean values for nine lower extremity skeletal measures in healthy naval midshipmen. *Journal of Orthopaedic & Sports Physical Therapy*, *25*(4), 253-263.

Joshi, A., Kale, S., Chandel, S., & Pal, D. K. (2015). Likert scale: Explored and explained. *Current Journal of Applied Science and Technology*, 396-403.

Jumani, M. S., Shaikh, S., & Shah, S. A. (2014). Fused deposition modelling technique (fdm) for fabrication of custom-made foot orthoses: a cost and benefit analysis. *Science International*, *26*(5).

Jumani, S., Memon, Z.A. and Larik, J. (2013). Process Modelling of Rapid Manufacturing Based Mass Customisation System for Fabrication of Custom Shoe inserts— Review Paper. *Mehran University Research Journal of Engineering and Technology*, *32*(2), 183-196.

Kao, K. C., & Perell, K. L. (2006). Effects of footwear on medial compartment knee osteoarthritis. *Journal of rehabilitation research and development*, *43*(4), 427-434.

Karimi, M. T., Fereshtehnejad, N., & Pool, F. (2013). The impact of foot insole on the energy consumption of flat-footed individuals during walking. *Foot & ankle specialist*, *6*(1), 21-26.

Karvonen, J. (1992). Importance of warm-up and cool down on exercise performance. *In Medicine in Sports Training and Coaching,* 35, 189-214

Kelikian, A. S., & Sarrafian, S. K. (Eds.). (2011). *Sarrafian's anatomy of the foot and ankle: descriptive, topographic, functional*. Lippincott Williams & Wilkins.

Kelly, L. A., lichtwark, G. & cresswell, A. G. (2015). Active regulation of longitudinal arch compression and recoil during walking and running. *Journal of The Royal Society Interface,* 12, 1076-1083.

Kelly, L. A., Lichtwark, G. A., Farris, D. J., Cresswell A. (2016). Shoes alter the spring-like function of the human foot during running. Journal of The Royal Society Interface, 13(119), 20160174.

Kelly, L. A., Farris, D. J., Cresswell, A. G., Lichtwark, G.A. (2019). Intrinsic foot muscles contribute to elastic energy storage and return in the human foot. Journal of Applied Physiology, 126(1), 231-238.

Kennedy, S. (2004). Casting for shoe inserts. Retrieved from: <http://www.oandp.com/articles/2004-08_08.asp> [accessed on 19 May, 2020]

Ker, R.F., Bennett, M.B., Bibby, S.R., Kester, R.C. and Alexander, R.M. (1987). The spring in the arch of the human foot. *Nature*, *325*(6100), pp.147-149.

Kersten, T. P., Przybilla, H. J., & Lindstaedt, M. (2016). Investigations of the geometrical accuracy of handheld 3D scanning systems. *Photogrammetrie-Fernerkundung-Geoinformation*, *2016*(5-6), 271-283.

Kevin Orthopedic. (n.d.). Frame Attributes: Heel Cup Depth. Retrieved from: https://kevin-orthopedic.myshopify.com/pages/clinic-guide-heel-cup-depth [Accessed 11 May. 2020]

Khaderi, S. N., Deshpande, V. S., & Fleck, N. A. (2014). The stiffness and strength of the gyroid lattice. *International Journal of Solids and Structures*, *51*(23-24), 3866-3877.

Khodaei, B., Saeedi, H., Farzadi, M., & Norouzi, E. (2017). Comparison of plantar pressure distribution in CAD–CAM and prefabricated foot orthoses in patients with flexible flatfeet. *The Foot*, *33*, 76-80.

Kim, H. Y. (2013). Statistical notes for clinical researchers: assessing normal distribution (2) using skewness and kurtosis. *Restorative dentistry & endodontics*, *38*(1), 52-54.

Kim, H. Y., Shin, H. S., Ko, J. H., Cha, Y. H., Ahn, J. H., & Hwang, J. Y. (2017). Gait analysis of symptomatic flatfoot in children: an observational study. Clinics in orthopedic surgery, 9(3), 363-373.

Kim, K., Park, J., Suh, J.H., Kim, M., Jeong, Y. and Park, I. (2017). 3D printing of multiaxial force sensors using carbon nanotube (CNT)/thermoplastic polyurethane (TPU) filaments. *Sensors and Actuators A: Physical*, *263*, 493-500.

Koo, T. K., & Li, M. Y. (2016). A guideline of selecting and reporting intraclass correlation coefficients for reliability research. *Journal of chiropractic medicine*, *15*(2), 155-163.

Kothari, A., Dixon, P. C., Stebbins, J., Zavatsky, A. B., & Theologis, T. (2016). Are flexible flat feet associated with proximal joint problems in children?. *Gait & posture*, *45*, 204-210.

Kunz, J., & Studer, M. (2006). Determining the modulus of elasticity in compression via Shore-A hardness. *Kunststoffe international*, *96*(6), 92-94.

Lai, P. P., Leung, A. K., Li, A. N., & Zhang, M. (2008). Three-dimensional gait analysis of obese adults. *Clinical biomechanics*, *23*, S2-S6.

Landers, R. N. (2015). Computing intraclass correlations (ICC) as estimates of interrater reliability in SPSS. *The Winnower*, *2*, e143518.

Leardini, A., Caravaggi, P., Theologis, T., & Stebbins, J. (2019). Multi-segment foot models and their use in clinical populations. *Gait & posture*, *69*, 50-59.

Leber, C., & Evanski, P. M. (1986). A comparison of shoe insole materials in plantar pressure relief. *Prosthetics and Inserts International*, *10*(3), 135-138.

Leber, C., & Evanski, P. M. (1986). A comparison of shoe insole materials in plantar pressure relief. Prosthetics and Inserts International, 10(3), 135-138.

Ledoux, W. R., & Hillstrom, H. J. (2002). The distributed plantar vertical force of neutrally aligned and flatfoot feet. *Gait & posture*, *15*(1), pp.1-9.

Lee, Y. C., Lin, G., & Wang, M. J. J. (2014). Comparing 3D foot scanning with conventional measurement methods. *Journal of foot and ankle research*, *7*(1), 44.

Lee, H. J., Lim, K. B., Yoo, J., Yoon, S. W., Yun, H. J., & Jeong, T. H. (2015). Effect of custom-molded shoe inserts on foot pain and balance in children with symptomatic flexible flat feet. Annals of rehabilitation medicine, 39(6), 905-913.

Lee, I. M., & Paffenbarger Jr, R. S. (2000). Associations of light, moderate, and vigorous intensity physical activity with longevity: the Harvard Alumni Health Study. *American journal of epidemiology*, *151*(3), 293-299.

Lee, P., Liu, C. H., Fan, C. W., Lu, C. P., Lu, W. S., & Hsieh, C. L. (2013). The test–retest reliability and the minimal detectable change of the Purdue Pegboard Test in schizophrenia. *Journal of the Formosan Medical Association*, *112*(6), 332-337.

Lee, W., Lee, C., Leung, A., & Hutchins, S. W. (2012a). Is it important to position foot in subtalar joint neutral position during non-weight-bearing molding for foot orthoses?. Journal of rehabilitation research and development, 49(3), 459-466

Lee, W., Wong, W. Y., Kung, E., & Leung, A. (2012b). Effectiveness of adjustable dorsiflexion night splint in combination with accommodative foot orthosis on plantar fasciitis. Journal of Rehabilitation Research & Development, 49(10), 1557-1564

Lee, Y.C. and Wang, M.J. (2015). Taiwanese adult foot shape classification using 3D scanning data. *Ergonomics*, 58(3), 513-523.

Lemmon, D., Shiang, T. Y., Hashmi, A., Ulbrecht, J. S., & Cavanagh, P. R. (1997). The effect of insoles in therapeutic footwear—a finite element approach. *Journal of biomechanics*, *30*(6), 615-620.

Levinger, P., Murley, G. S., Barton, C. J., Cotchett, M. P., McSweeney, S. R., & Menz, H. B. (2010). A comparison of foot kinematics in people with normal-and flat-arched feet using the Oxford Foot Model. *Gait & posture*, *32*(4), 519-523.

Levitz, S. J., & Sobel, E. (2002). Prescribing Shoe inserts. *Podiatry Management*, 103-116.

Li, F., Li, Y., Wang, M., & Wu, J. (2009, November). Research on computer aided design of customized insoles. In *2009 IEEE 10th International Conference on Computer-Aided Industrial Design & Conceptual Design* (pp. 1430-1433). IEEE.

Li, J., & Tanaka, H. (2018). Feasibility study applying a parametric model as the design generator for 3D–printed orthosis for fracture immobilization. 3D printing in medicine, 4(1), 1-15.

Liu, G. R., & Quek, S. S. (2013). *The finite element method: a practical course*. Butterworth-Heinemann.

Liu, X., Kim, W., & Drerup, B. (2004). 3D characterization and localization of anatomical landmarks of the foot by FastSCAN. Real-time imaging, 10(4), 217-228.

Lochner, S. J., Huissoon, J. P., & Bedi, S. S. (2012). Parametric design of custom shoe insert model. *Computer-Aided Design and Applications*, *9*(1), 1-11.

Lockard MA. (1998), Shoe inserts, Physical therapy, 68(12), 1866-1873.

MacLean, C.L., Davis, I.S. and Hamill, J. (2008). Short-and long-term influences of a custom shoe insert intervention on lower extremity dynamics. *Clinical Journal of Sport Medicine*, *18*(4), 338-343.

MacSween, A., Brydson, G., & Hamilton, J. (1999). The effect of custom moulded ethyl vinyl acetate shoe inserts on the gait of patients with rheumatoid arthritis. *The Foot*, *9*(3), 128-133.

Macy, B. (2013). Reverse Engineering for Additive Manufacturing. *Handbook of Manufacturing Engineering and Technology*, 1-17.

Manter, J. T. (1941). Movements of the subtalar and transverse tarsal joints. *The anatomical record*, *80*(4), 397-410.

Mayich, D. J., Novak, A., Vena, D., Daniels, T. R., & Brodsky, J. W. (2014). Gait analysis in orthopedic foot and ankle surgery—topical review, part 1: principles and uses of gait analysis. Foot & ankle international, 35(1), 80-90.

McCahill, J., Stebbins, J., Koning, B., Harlaar, J., & Theologis, T. (2018). Repeatability of the Oxford Foot Model in children with foot deformity. *Gait & posture*, *61*, 86-89.

McCrory, J.L., Young, M.J., Boulton, A.J.M. and Cavanagh, P.R. (1997). Arch index as a predictor of arch height. The Foot, 7(2),79-81.

Mckenzie, D. C. (1987). The role of the shoe and inserts. In *Foot and Ankle in Sport and Exercise,* 23, 30-38.

McKeon, P. O., Hertel, J., Bramble, D., & Davis, I. (2015). The foot core system: a new paradigm for understanding intrinsic foot muscle function. *British journal of sports medicine*, *49*(5), 290-290.

McPoil, T. G., & Cornwall, M. W. (2000). The effect of foot orthoses on transverse tibial rotation during walking. *Journal of the American Podiatric Medical Association*, *90*(1), 2-11.

McPoil, T. G., Cornwall, M. W., Vicenzino, B., Teyhen, D. S., Molloy, J. M., Christie, D. S., & Collins, N. (2008). Effect of using truncated versus total foot length to calculate the arch height ratio. *The Foot*, *18*(4), 220-227.

Meneses, J., Gharbi, T. and Cornu, J.Y. (2002). Three-dimensional optical high-resolution profiler with a large observation field: foot arch behavior under low static charge studies. *Applied optics,* 41(25), 5267-5274.

Menz, H. B. (2004). Two feet, or one person? Problems associated with statistical analysis of paired data in foot and ankle medicine. *The foot*, *14*, 2-5.

Menz, H. B., Morris, M. E., & Lord, S. R. (2005a). Foot and ankle characteristics associated with impaired balance and functional ability in older people. *The Journals of Gerontology Series A: Biological Sciences and Medical Sciences*, *60*(12), 1546-1552.

Menz, H. B., & Munteanu, S. E. (2005b). Validity of 3 clinical techniques for the measurement of static foot posture in older people. *Journal of orthopaedic & sports physical therapy*, *35*(8), 479-486.

Menz, H. B., Allan, J. J., Bonanno, D. R., Landorf, K. B., & Murley, G. S. (2017). Custom-made shoe inserts: an analysis of prescription characteristics from an Australian commercial insert laboratory. *Journal of foot and ankle research*, *10*(1), 23.

Michelson, J. D., Durant, D. M., & McFarland, E. (2002). The injury risk associated with flatfoot in athletes. *Foot & ankle international*, *23*(7), 629-633.

Miller, C. D., Laskowski, E. R., & Suman, V. J. (1996, August). Effect of corrective rearfoot orthotic devices on ground reaction forces during ambulation. In *Mayo Clinic Proceedings* (Vol. 71, No. 8, pp. 757-762). Elsevier.

Mitra G. K., P. De and B. B. Paira (1987), Effective utilization of polymeric materials in process industry, Proc. National Sem. on Modern Plastics and Polymers, 61-68.

Mittlböck, M. (2008). Critical Appraisal of Randomized Clinical Trials: Can We Have Faith in the Conclusions?. *Breast Care*, *3*(5), 341-346.

Morales-Orcajo, E., Souza, T. R., Bayod, J., & de Las Casas, E. B. (2017). Non-linear finite element model to assess the effect of tendon forces on the foot-ankle complex. *Medical Engineering & Physics*, *49*, 71-78.

Mosher, M. R. (1980). *U.S. Patent No. 4,232,457*. Washington, DC: U.S. Patent and Trademark Office.

Mündermann, A., Nigg, B. M., Humble, R. N., & Stefanyshyn, D. J. (2003). Shoe inserts affect lower extremity kinematics and kinetics during running. *Clinical biomechanics*, *18*(3), 254-262.

Mündermann, L., Corazza, S., & Andriacchi, T. P. (2006). The evolution of methods for the capture of human movement leading to markerless motion capture for biomechanical applications. *Journal of neuroengineering and rehabilitation*, *3*(1), 1-11.

Murley, G. S., Menz, H. B., & Landorf, K. B. (2009a). A protocol for classifying normal-and flat-arched foot posture for research studies using clinical and radiographic measurements. *Journal of foot and ankle research*, *2*(1), 22-34.

Murley, G. S., Menz, H. B., & Landorf, K. B. (2009b). Foot posture influences the electromyographic activity of selected lower limb muscles during gait. *Journal of foot and ankle research*, *2*(1), pp.1-9.

Murley, G. S., Landorf, K. B., Menz, H. B., & Bird, A. R. (2009c). Effect of foot posture, foot orthoses and footwear on lower limb muscle activity during walking and running: a systematic review. *Gait & posture*, *29*(2), 172-187.

Murley, G.S., Landorf, K.B. and Menz, H.B. (2010). Do shoe inserts change lower limb muscle activity in flat-arched feet towards a pattern observed in normal-arched feet? Clinical Biomechanics, 25(7), 728-736.

Myers, T. (2014). Anatomy trains: Myofascial meridians for manual and movement therapists (Third ed.). Edinburgh: Churchill Livingstone/Elsevier.

Natali, A. N., Forestiero, A., Carniel, E. L., Pavan, P. G., & Dal Zovo, C. (2010). Investigation of foot plantar pressure: experimental and numerical analysis. *Medical & biological engineering & computing*, *48*(12), 1167-1174.

Nester, C. J., Van Der Linden, M. L., & Bowker, P. (2003). Effect of foot orthoses on the kinematics and kinetics of normal walking gait. *Gait & posture*, *17*(2), 180-187.

Nester, C., Jones, R. K., Liu, A., Howard, D., Lundberg, A., Arndt, A., ... & Wolf, P. (2007). Foot kinematics during walking measured using bone and surface mounted markers. *Journal of biomechanics*, *40*(15), 3412-3423.

Nielsen, R. G., Rathleff, M. S., Simonsen, O. H., & Langberg, H. (2009). Determination of normal values for navicular drop during walking: a new model correcting for foot length and gender. *Journal of foot and ankle research*, *2*(1), 12-18.

Nilsson, M. K., Friis, R., Michaelsen, M. S., Jakobsen, P. A., & Nielsen, R. O. (2012). Classification of the height and flexibility of the medial longitudinal arch of the foot. *Journal of foot and ankle research*, *5*(1), 3-11.

Noddeland, H., & Winkel, J. (1988). Effects of leg activity and ambient barometric pressure on foot swelling and lower-limb skin temperature during 8 h of sitting. *European journal of applied physiology and occupational physiology*, *57*(4), 409-414.

Noll, K.H. (2001). The use of insert devices in adult acquired flatfoot deformity. Foot and Ankle Clinics of North America, 6, 25-36

Norušis, MJ 2006, SPSS 14.0 guide to data analysis, Prentice Hall Upper Saddle River, NJ.

Okamura, K., Kanai, S., Oki, S., Tanaka, S., Hirata, N., Sakamura, Y., ... & Otsuka, A. (2017). Does the weakening of intrinsic foot muscles cause the decrease of medial longitudinal arch height?. *Journal of Physical Therapy Science*, *29*(6), 1001-1005.

Orr, J. D., Nunley, J. A. (2013). Isolated spring ligament failure as a cause of adult-acquired flatfoot deformity. Foot & ankle international, 34(6), 818-823.

Otman, S., Basgöze, O. and Gökce-Kutsal, Y. (1988). Energy cost of walking with flat feet. Prosthetics and inserts international, 12(2), 73-76.

Palhano, R., Antonio Zaro, M., Vargas Avila, A., & Roberto Strohaecker, T. (2013). Analysis impact in shoes with different material soles. *Footwear Science*, *5*(sup1), S34-S36.

Park, K., & Seo, K. (2015). Effects of a functional foot orthosis on the knee angle in the sagittal plane of college students in their 20s with flatfoot. *Journal of physical therapy science*, *27*(4), 1211-1213.

Pastina, M., Mihai, A. and Bilalis, N. (2012). Finite Element Analysis for Insole-Sole Prototypes. ICAMS– 4th International Conference on Advanced Materials and Systems

Peng, Y., Wong, D. W. C., Chen, T. L. W., Wang, Y., Zhang, G., Yan, F., & Zhang, M. (2021). Influence of arch support heights on the internal foot mechanics of flatfoot during walking: A muscle-driven finite element analysis. *Computers in Biology and Medicine*, *132*, 104355.

Perry, J. (1992). Gait analysis systems in gait analysis: normal and pathological function. Thorofare, NJ: Slack, 353-411.

Perry J. & Burnfield, M. (2010). Gait analysis: normal and pathological function. *Journal of Sports Science and Medicine*, *9*(2), 353.

Plott, J., & Shih, A. (2017). The extrusion-based additive manufacturing of moisture-cured silicone elastomer with minimal void for pneumatic actuators. Additive Manufacturing, 17, 1-14.

Pohl, M. B., Rabbito, M., & Ferber, R. (2010). The role of tibialis posterior fatigue on foot kinematics during walking. *Journal of foot and ankle research*, *3*(1), 1-8.

Pollo FE. (1998). Bracing and heel wedging for unicompartmental osteoarthritis of the knee. Am J Knee Surg, 11, 47–50.

Prachgosin, T., Chong, D. Y., Leelasamran, W., Smithmaitrie, P., & Chatpun, S. (2015). Medial longitudinal arch biomechanics evaluation during gait in subjects with flexible flatfoot. *Acta of bioengineering and biomechanics*, *17*(4).

Pratt, D.J. (1995). Functional shoe inserts. *The Foot*, *5*(3), 101-110.

Prolab inserts, 2009, photograph, viewed 30 April 2020, <https://www.prolabinserts.com/Products/tabid/68/Default.aspx>

Puszczalowska-Lizis, E., Bujas, P., Omorczyk, J., Jandzis, S., & Zak, M. (2017). Feet deformities are correlated with impaired balance and postural stability in seniors over 75. *PloS one*, *12*(9), e0183227.

Putra, Y. E. A., Anggoro, P. W., Yuniarto, T., Bayuseno, A. P., Jamari, J., & Bawono, B. (2019, October). Optimization of Mechanical Parameters on Outsole Shoes Orthotic Comfort Using Finite Element Analysis. In *2019 International Biomedical Instrumentation and Technology Conference (IBITeC)* (Vol. 1, pp. 31-36). IEEE.

Queen, R. M., Mall, N. A., Nunley, J. A., Chuckpaiwong, B. (2009). Differences in plantar loading between flat and normal feet during different athletic tasks. Gait & posture 29(4), 582-586.

Rankine, L., Long, J. T., Canseco, K., & Harris, G. F. (2008). Multisegmental foot modeling: a review. *Critical Reviews™ in Biomedical Engineering*, *36*(2), 127-181

Razavi Ratki, S. K., Forooghnia, M., Abrisham, S. M. J., & Nafisi Moghadam, R. (2017). The Usefulness of Therapeutic Diabetic Footwear and Insoles in Diabetic Foot Treatment-A Narrative Review. *Iranian Journal of Diabetes and Obesity*, *9*(3), 132-135.

Razeghi, M., & Batt, M. E. (2002). Foot type classification: a critical review of current methods. *Gait & posture*, *15*(3), 282-291.

Robert W. Keller. (2003). Plastazote: pratitioners' choice for diabetic inserts. Retrieved from: https://opedge.com/Articles/ViewArticle/2003-11_12 [accessed 5 May 2020]

Rodrigo-Carranza, V., González-Mohíno, F., Santos-Concejero, J., & González-Ravé, J. M. (2020). Influence of Shoe Mass on Performance and Running Economy in Trained Runners. *Frontiers in Physiology*, *11*, 1178.

Rogers, K., Otter, S. J., & Birch, I. (2006). The effect of PORON® and Plastazote® insoles on forefoot plantar pressures. *British Journal of Podiatry*, *9*(4), 111.

Rome, K. (1991). A study of the properties of materials used in podiatry. *J Am Podiatr Med Assoc*, *81*(2), 73-83.

Rosenbloom, K. B. (2011). Pathology-designed custom molded shoe inserts. *Clinics in podiatric medicine and surgery*, *28*(1), 171-187.

Rossi, M., & Buratti, G. (2017). Form is matter. Triply periodic minimal surfaces structures by digital design tools. In *ShoCK!-Sharing Computational Knowledge!* (pp. 259-268)

Rossi, M., & Schettler, T. (2000). PVC & healthcare. In *Setting Healthcare's Environmental Agenda: Papers and Proceedings from the October 16, 2000 Conference in San Francisco, California, USA*.

Sachithanandam, V. and Joseph, B. (1995). The influence of footwear on the prevalence of flat foot. A survey of 1846 skeletally mature persons. *The Journal of bone and joint surgery,* 77(2), 254-257.

Saghazadeh, M., Kitano, N., & Okura, T. (2015). Gender differences of foot characteristics in older Japanese adults using a 3D foot scanner. *Journal of foot and ankle research*, *8*(1), 29.

Saltzman, C. L., Nawoczenski, D. A., & Talbot, K. D. (1995). Measurement of the medial longitudinal arch. *Archives of physical medicine and rehabilitation*, *76*(1), 45-49.

Saraswat, P., MacWilliams, B. A., & Davis, R. B. (2012). A multi-segment foot model based on anatomically registered technical coordinate systems: method repeatability in pediatric feet. *Gait & Posture*, *35*(4), 547-555.

Savic, S. P., Lukic, N., Prodanovic, N., & Devedzic, G. (2019, June). A Comparative FE Analysis of a Flat Foot with and without a Custom-made Insert Insole. In *2019 8th Mediterranean Conference on Embedded Computing (MECO)* (pp. 1-4). IEEE.

Schmalz, T., Blumentritt, S., Drewitz, H., & Freslier, M. (2006). The influence of sole wedges on frontal plane knee kinetics, in isolation and in combination with representative rigid and semi-rigid ankle–foot-inserts. *Clinical Biomechanics*, *21*(6), 631-639.

Schoen, A. H. (1970). *Infinite periodic minimal surfaces without self-intersections*. National Aeronautics and Space Administration.

Séamus, K. (2008). Material choices in shoe insert design. Retrieved from: https://opedge.com/Articles/ViewArticle/2008-02_13 [accessed 11 May 2020]

Shi, W., Liu, G., & Chen, Z. (2017). Effects of the bulk compressibility on rubber isolator's compressive behaviors. *Advances in Mechanical Engineering*, *9*(5), 1687814017699352.

Shih, Y. F., Chen, C. Y., Chen, W. Y., & Lin, H. C. (2012). Lower extremity kinematics in children with and without flexible flatfoot: a comparative study. BMC musculoskeletal disorders, 13(1), 1-9.

Shorten, M.R. (1987). Muscle elasticity and human performance. In *Current research in sports biomechanics*, 25, 1-18

Shrout, P. E., & Fleiss, J. L. (1979). Intraclass correlations: uses in assessing rater reliability. *Psychological bulletin*, *86*(2), 420.

Slattery, M., & Tinley, P. (2001). The efficacy of functional shoe inserts in the control of pain in ankle joint disintegration in hemophilia. Journal of the American Podiatric Medical Association, 91(5), 240-244.

Silder, A., Heiderscheit, B., & Thelen, D. G. (2008). Active and passive contributions to joint kinetics during walking in older adults. Journal of biomechanics, 41(7), 1520-1527.

Soames, R. (1985). Foot pressure patterns during gait. Journal of Biomedical Engineering, 7(2), pp.120-126.

Stearne, S. M., McDonald, K. A., Alderson, J. A., North, I., Oxnard, C. E., & Rubenson, J. (2016). The foot's arch and the energetics of human locomotion. Scientific reports, 6(1), 1-10.

Stratasys (2018). Objet Eden260VS | Stratasys. [online] Available at: http://www.stratasys.com/3d-printers/objet-eden260vs [Accessed 4 Oct. 2018].

Stratasys. (2017). *PolyJet Material Data Sheet*. Retrieved October 8, 2018, from Stratasys: http://usglobalimages.stratasys.com/Main/Files/Material_Spec_Sheets/MSS_PJ_PJMaterialsDataSheet.pdf?v=635785205440671440

Su, S., Mo, Z., Guo, J., & Fan, Y. (2017). The Effect of Arch Height and Material Hardness of Personalized Insole on Correction and Tissues of Flatfoot. *Journal of healthcare engineering*, *1-9*.

Sundman, A., & Davis, J. (2011). *U.S. Patent No. 7,952,727*. Washington, DC: U.S. Patent and Trademark Office.

Swedler, D. I., Knapik, J. J., Grier, T., & Jones, B. H. (2010). Validity of plantar surface visual assessment as an estimate of foot arch height. *Medicine and science in sports and exercise*, *42*(2), 375-380.

Tadepalli, S. C., Erdemir, A., & Cavanagh, P. R. (2011). Comparison of hexahedral and tetrahedral elements in finite element analysis of the foot and footwear. *Journal of biomechanics*, *44*(12), 2337-2343.

Taha, Z., Norman, M. S., Omar, S. F. S., & Suwarganda, E. (2016). A finite element analysis of a human foot model to simulate neutral standing on ground. *Procedia engineering*, *147*, 240-245.

Taniguchi, A., Tanaka, Y., Takakura, Y., Kadono, K., Maeda, M., Yamamoto, H. (2003). Anatomy of the spring ligament. JBJS 85(11), 2174-2178.

Tao, W., Liu, T., Zheng, R., & Feng, H. (2012). Gait analysis using wearable sensors. *Sensors*, *12*(2), 2255-2283.

Taylor, M. J. D., Strike, S. C., & Dabnichki, P. (2006). Strategies used for unconstrained direction change during walking. *Perceptual and motor skills*, *102*(2), 576-588.

Telfer, S., & Woodburn, J. (2010). The use of 3D surface scanning for the measurement and assessment of the human foot. *Journal of foot and ankle research*, *3*(1), 1-9.

Telfer, S., Abbott, M., Steultjens, M. P., & Woodburn, J. (2013). Dose–response effects of customised foot orthoses on lower limb kinematics and kinetics in pronated foot type. Journal of biomechanics, 46(9), 1489-1495.

Telfer, S., Gibson, K. S., Hennessy, K., Steultjens, M. P., & Woodburn, J. (2012a). Computer-aided design of customized shoe inserts: reproducibility and effect of method used to obtain foot shape. *Archives of physical medicine and rehabilitation*, *93*(5), 863-870.

Telfer, S., Pallari, J., Munguia, J., Dalgarno, K., McGeough, M., & Woodburn, J. (2012b). Embracing additive manufacture: implications for foot and ankle orthosis design. *BMC musculoskeletal disorders*, *13*(1), 84.

Tenenbaum, S., Hershkovich, O., Gordon, B., Bruck, N., Thein, R., Derazne, E., Tzur, D., Shamiss, A., and Afek, A. (2013). Flexible flatfoot in adolescents: body mass index, body height, and gender—an epidemiological study, Foot & Ankle International, vol. 34, no. 6, pp. 811-7.

Tickner, J. A., Schettler, T., Guidotti, T., McCally, M., & Rossi, M. (2001). Health risks posed by use of Di-2-ethylhexyl phthalate (DEHP) in PVC medical devices: A critical review. *American journal of industrial medicine*, *39*(1), 100-111.

Tomaro J, Burdett RG. (1993). The Effects of Shoe inserts on the EMG Activity of Selected Leg Muscles during Gait. The Journal of Orthopaedic and Sports Physical Therapy, 18(4), 532-536

Tong, J.W. and Kong, P.W. (2013). Association between foot type and lower extremity injuries: systematic literature review with meta-analysis. journal of orthopaedic & sports physical therapy, 43(10), 700-714.

Toshev, Y. E., Hieu, L. C., Stefanova, L. P., Tosheva, E. Y., Zlatov, N. B., & Dimov, S. (2005). Reverse engineering and rapid prototyping for new insert devices. Intelligent Production Machines and Systems", 567-571.

Tsung, B. Y. S., Zhang, M., Fan, Y. B., & Boone, D. A. (2003). Quantitative comparison of plantar foot shapes under different weight-bearing conditions. *Journal of rehabilitation research and development*, 517-526

Tudor-Locke, C., & Bassett, D. R. (2004). How many steps/day are enough?. *Sports medicine*, *34*(1), 1-8.

Urabe, Y., Maeda, N., Kato, S., Shinohara, H., Sasadai, J. (2014). Effect of shoe insole for prevention and treatment of lower extremity injuries. The Journal of Physical Fitness and Sports Medicine, 3(4) 385-398.

Varady, T., Martin, R. R., & Cox, J. (1997). Reverse engineering of geometric models—an introduction. Computer-aided design, 29(4), 255-268.

Villarroya, M. A., Esquivel, J. M., Tomás, C., Moreno, L. A., Buenafé, A., & Bueno, G. (2009). Assessment of the medial longitudinal arch in children and adolescents with obesity: footprints and radiographic study. *European journal of pediatrics*, *168*(5), 559-567.

Villwock, M.R., Meyer, E.G., Powell, J.W., Fouty, A.J. and Haut, R.C. (2009). The effects of various infills, fibre structures, and shoe designs on generating rotational traction on an artificial surface. *Proceedings of the Institution of Mechanical Engineers, Part P: Journal of Sports Engineering and Technology*, *223*(1), 11-19.

Wafai, L., Zayegh, A., Woulfe, J., Aziz, S. M., & Begg, R. (2015). Identification of foot pathologies based on plantar pressure asymmetry. *Sensors*, *15*(8), 20392-20408.

Wagner, A., & Luna, S. (2018). Effect of footwear on joint pain and function in older adults with lower extremity osteoarthritis. *Journal of Geriatric Physical Therapy*, *41*(2), 85-101.

Walker C. The effect of cyclic loading on the stiffness and damping factors in the midsoles of running shoes. Proceedings of the Institution of Mechanical Engineers, Part L: Journal of Materials: Design and Applications, 2006; 220(1): 41-47.

Walther, M., Kratschmer, B., Verschl, J., Volkering, C., Altenberger, S., Kriegelstein, S., & Hilgers, M. (2013). Effect of different insert concepts as first line treatment of plantar fasciitis. Foot and Ankle Surgery, 19(2), 103-107.

Wang, X., Jiang, M., Zhou, Z., Gou, J. and Hui, D. (2017). 3D printing of polymer matrix composites: A review and prospective. *Composites Part B: Engineering*, *110*, 442-458.

Waters, R.L. and Mulroy, S. (1999). The energy expenditure of normal and pathologic gait. *Gait & posture*, *9*(3), 207-231.

Weatherwax, R. J. (1981). The plaster slipper cast. Clinical orthopaedics and related research, (154), 327-329.

Weir, J. P. (2005). Quantifying test-retest reliability using the intraclass correlation coefficient and the SEM. *The Journal of Strength & Conditioning Research*, *19*(1), 231-240.

Whiting, W. C., Zernicke, R. F., 2008. Biomechanics of musculoskeletal injury. Human Kinetics

Williams, D. S., & McClay, I. S. (2000). Measurements used to characterize the foot and the medial longitudinal arch: reliability and validity. *Physical therapy*, *80*(9), 864-871.

Williams, D. S., McClay, I. S., & Hamill, J. (2001a). Arch structure and injury patterns in runners. Clinical biomechanics, 16(4), 341-347.

Williams, D. S., McClay, I. S., Hamill, J., & Buchanan, T. S. (2001b). Lower extremity kinematic and kinetic differences in runners with high and low arches. *Journal of applied biomechanics*, *17*(2), pp.153-163.

Winkel, J., & Jørgensen, K. (1991). Significance of skin temperature changes in surface electromyography. *European journal of applied physiology and occupational physiology*, *63*(5), 345-348.

Winkel, J., Jørgensen, K. (1986). Swelling of the foot, its vascular volume and systemic hemoconcentration during long-term constrained sitting. European journal of applied physiology and occupational physiology, 55(2), 162-166.

Witana, C.P., Xiong, S., Zhao, J. and Goonetilleke, R.S. (2006). Foot measurements from three-dimensional scans: A comparison and evaluation of different methods. *International Journal of Industrial Ergonomics,* 36(9), 789-807.

Wong, L., Hunt, A., Burns, J., & Crosbie, J. (2008). Effect of foot morphology on center-of-pressure excursion during barefoot walking. *Journal of the American Podiatric Medical Association*, *98*(2), 112-117.

Woodburn, J., Barker, S., & Helliwell, P. S. (2002). A randomized controlled trial of foot orthoses in rheumatoid arthritis. *The Journal of rheumatology*, *29*(7), 1377-1383.

Xiong, S., Goonetilleke, R. S., Witana, C. P., Weerasinghe, T. W., & Au, E. Y. L. (2010). Foot arch characterization: a review, a new metric, and a comparison. *Journal of the American Podiatric Medical Association*, *100*(1), 14-24.

Yánez, A., Cuadrado, A., Martel, O., Afonso, H., & Monopoli, D. (2018). Gyroid porous titanium structures: a versatile solution to be used as scaffolds in bone defect reconstruction. *Materials & Design*, *140*, 21-29.

Yánez, A., Herrera, A., Martel, O., Monopoli, D., & Afonso, H. (2016). Compressive behaviour of gyroid lattice structures for human cancellous bone implant applications. *Materials Science and Engineering: C*, *68*, 445-448.

Yarnitzky, G., Yizhar, Z., & Gefen, A. (2006). Real-time subject-specific monitoring of internal deformations and stresses in the soft tissues of the foot: a new approach in gait analysis. *Journal of biomechanics*, *39*(14), 2673-2689.

Yarwindran, M., Ibrahim, M., & Raveverma, P. (2017, April). The feasibility study on fabrication customized insert insole using fused deposition modelling (FDM). In AIP Conference Proceedings (Vol. 1831, No. 1, p. 020001). AIP Publishing LLC.

Yarwindran, M., Sa'aban, N. A., Ibrahim, M., & Periyasamy, R. (2016). Thermoplastic elastomer infill pattern impact on mechanical properties 3D printed customized insert insole. *ARPN Journal of Engineering and Applied Sciences*, *11*(10), 6519-6524.

Young, J., & Jackson, S. (2019). Improved motor function in a pre-ambulatory child with spastic bilateral cerebral palsy, using a custom rigid ankle-foot orthosis–footwear combination: A case report. *Prosthetics and inserts international*, *43*(4), 453-458.

Younger, A. S., Sawatzky, B., & Dryden, P. (2005). Radiographic assessment of adult flatfoot. *Foot & ankle international*, *26*(10), 820-825.

Yung-Hui, L., & Wei-Hsien, H. (2005). Effects of shoe inserts and heel height on foot pressure, impact force, and perceived comfort during walking. *Applied ergonomics*, *36*(3), 355-362.

Zhai, J. N., Qiu, Y. S., & Wang, J. (2016). Effects of insert insoles on adults with flexible flatfoot under different walking conditions. *Journal of physical therapy science*, *28*(11), 3078-3083.

Zhang, M., Cheung, J. T. M., & Li, Y. (2007). Computational modeling the foot-insole interface. In *Computational Textile* (pp. 311-321). Springer, Berlin, Heidelberg.

Zheng, S., Zlatin, M., Selvaganapathy, P. R., & Brook, M. A. (2018). Multiple modulus silicone elastomers using 3D extrusion printing of low viscosity inks. Additive Manufacturing, 24, 86-92.

Zifchock, R. A., Davis, I., Hillstrom, H., & Song, J. (2006). The effect of gender, age, and lateral dominance on arch height and arch stiffness. *Foot & Ankle International*, *27*(5), 367-372.

Zotefoams. (1981). Plastazote®. Retrieved from: https://www.zotefoams.com/ [Accessed 5 May. 2020]

Appendix I: Abstract

Adult-acquired flatfoot deformity alters the biomechanics of human's lower extremities, which increases the risk of injury and causing musculoskeletal disorder. Foot orthotic is a current intervention for flatfoot that increases the arch height and alleviate symptoms. However, conventional corrective insoles utilize the solid full arch support that restricts midfoot motion and compromises elastic recoil function of the foot arch. This can result in reducing the elastic energy return and decreasing the gait efficiency. In our study, the novel customized design insoles were designed using subject-specific 3D foot scans image and manufactured by 3D printing technology. A novel elastic mesh pad was implemented in the mid-insole to replace the conventional solid arch support. The new insoles were tested in standard straight gait laboratory trials. The kinematic analysis showed that the novel insoles improved foot arch compression and recoil in stance phase with flatfooted individuals.

Zusammenfassung

Ein im Erwachsenenalter erworbener Plattfuß (*adult-acquired flatfoot deformity*) verändert die Biomechanik der unteren Extremitäten des Menschen, was das Verletzungsrisiko erhöht und muskuloskelettale Erkrankungen verursacht. Der Einsatz von Fußorthesen ist eine aktuelle Interventionsmöglichkeit für Plattfüße, um das Fußgewölbe anzuheben und Symptome zu lindern. Herkömmliche Korrektureinlagen setzen jedoch auf eine feste Stützung des gesamten Fußgewölbes, was die Bewegung des Mittelfußes einschränkt und die stoßdämpfende Funktion des Fußgewölbes beeinträchtigt. Dies kann zu einer Verringerung der elastischen Energierückgabe und der Effizienz des Gangs führen. In unserer Studie wurden neuartige, individuell gestaltete Einlegesohlen unter Verwendung von personenspezifischen 3D-Scans des Fußes entworfen und mittels 3D-Druck hergestellt. Als Ersatz für die übliche feste Stütze für das Fußgewölbe wurde in der Mitte der Einlage ein neuartiges elastisches Netzpolster eingesetzt. Die neuen Einlegesohlen wurden in standardmäßigen Laborversuchen mit geradem Gang getestet. Die kinematische Analyse zeigte, dass die neuartigen Einlegesohlen die Kompression des Fußgewölbes und den Rückstoß in der Standphase bei Personen mit Plattfuß verbesserten.

Appendix II: List of Figure

Appendix III: List of Table

Appendix IV: Ethics approval letter

RMIT UNIVERSITY

College Human Ethics Advisory Network (CHEAN)
College of Science, Engineering and Health

Email: seh-human-ethics@rmit.edu.au
Phone: [61 3] 9925 4620
Building 91, Level 2, City Campus/Building 215, Level 2, Bundoora West Campus

18 April 2018

Professor Peter Dabnichki
School of Engineering
RMIT University

Dear Professor Dabnichki

SEHAPP 10-18 Temporary change in foot morphology due to individual activity level

Thank you for submitting your amended application for review.

I am pleased to inform you that the CHEAN has approved your application from the date of this letter to **2 August 2018** and your research may now proceed.

The CHEAN would like to remind you that:

All data should be stored on University Network systems. These systems provide high levels of manageable security and data integrity, can provide secure remote access, are backed up on a regular basis and can provide Disaster Recover processes should a large scale incident occur. The use of portable devices such as CDs and memory sticks is valid for archiving; data transport where necessary and for some works in progress. The authoritative copy of all current data should reside on appropriate network systems; and the Principal Investigator is responsible for the retention and storage of the original data pertaining to the project for a minimum period of five years.

Please Note: Annual reports are due on the anniversary of the commencement date for all research projects that have been approved by the CHEAN. Ongoing approval is conditional upon the submission of annual reports failure to provide an annual report may result in Ethics approval being withdrawn.

Final reports are due within six months of the project expiring or as soon as possible after your research project has concluded.

The annual/final reports forms can be found at:
www.rmit.edu.au/staff/research/human-research-ethics

Yours faithfully,

Associate Professor Barbara Polus
Chair, Science Engineering & Health
College Human Ethics Advisory Network

Cc	Student Investigator/s:	Mr Che-Wei Hu, s3584609, School of Engineering Mr Raymond Tran, s3674382, School of Engineering
	Other Investigator/s:	Dr Toh Yen Pang, School of Engineering Dr Amit Jadhav, School of Fashion and Textiles

RMIT UNIVERSITY

RMIT University

Science Engineering and Health

College Human Ethics Advisory Network (CHEAN)

Plenty Road
Bundoora VIC 3083

PO Box 71
Bundoora VIC 3083
Australia

Tel. +61 3 9925 7096
Fax +61 3 9925 6506
• www.rmit.edu.au

23rd December 2015

Dr Toh Yen Pang
Building 251 Level 3, Room 62
School of Aerospace & Mechanical
Manufacturing Engineering
RMIT University

Dear Dr Pang

ASEHAPP 57-15 PANG Digital design of customized shoes using 3D algorithms

Thank you for submitting your amended application for review.

I am pleased to inform you that the CHEAN has approved your application for a period of **3 Years** from the date of this letter to **23rd December 2018** and your research may now proceed.

The CHEAN would like to remind you that:

All data should be stored on University Network systems. These systems provide high levels of manageable security and data integrity, can provide secure remote access, are backed up on a regular basis and can provide Disaster Recover processes should a large scale incident occur. The use of portable devices such as CDs and memory sticks is valid for archiving; data transport where necessary and for some works in progress. The authoritative copy of all current data should reside on appropriate network systems; and the Principal Investigator is responsible for the retention and storage of the original data pertaining to the project for a minimum period of five years.

Please Note: Annual reports are due on the anniversary of the commencement date for all research projects that have been approved by the CHEAN. Ongoing approval is conditional upon the submission of annual reports failure to provide an annual report may result in Ethics approval being withdrawn.

Final reports are due within six months of the project expiring or as soon as possible after your research project has concluded.

The annual/final reports forms can be found at:
www.rmit.edu.au/staff/research/human-research-ethics

Yours faithfully,

Dr Linda Jones
Chair, Science Engineering & Health
College Human Ethics Advisory Network

Cc CHEAN Member: Dr Amanda Kimpton School of Health Sciences RMIT University
Other Investigator/s: Dr Amit Jadhav Centre for Advanced Materials and Performance Textiles